Fatigue Behaviour of RC beams Strengthened with CFRP

Analytical and Experimental investigations

Mohammed Salih Mohammed Mahal

LULEÅ
UNIVERSITY
OF TECHNOLOGY

DOCTORAL THESIS

Fatigue Behaviour of RC beams Strengthened with CFRP

Analytical and Experimental investigations

Mohammed Salih Mohammed Mahal

Submitted in Partial Fulfilment of the Requirements for the Degree of
Doctor of Philosophy in Structural Engineering

To the ones who were
and will always be
in my mind…
in my heart…
'my mother and my father'
Mohammed

Fatigue Behaviour of RC beams Strengthened with CFRP
Mohammed Salih Mohammed Mahal

Division of Structural and Construction Engineering
Department of Civil, Environmental and Natural Resources Engineering
Luleå University of Technology

Dissertation

For the degree of Doctor of Philosophy (PhD) in subject area of Structural Engineering, which with the due permission of Faculty Board at Luleå University of Technology will be defended in public at
Luleå University of Technology, Luleå, on Friday the 27th of March 2015, at 10:00 in room F1031

Opponent /Examiner:	Professor Pilate Moyo, Department of Civil Engineering, University of Cape Town, South Africa
Examining Committee:	Professor Timo Aho, Department of Construction Technology, Oulu University, Finland.
	Associate Professor Kjell Eriksson , Division of Solid Mechanics, Luleå university of technology , Luleå, Sweden.
	Associate Professor Mohammad Al Emrani , Department of Structural Engineering, Chalmers University, Gothenburg,Sweden.
Supervisor:	Professor Björn Täljsten, Division of Structural and Construction Engineering, Luleå university of technology, Luleå, Sweden.
Assistant supervisor:	Dr. Thomas Blanksvärd, Division of Structural and Construction Engineering, Luleå university of technology, Luleå, Sweden.

Preface

First of all, all praise to Allah (God) for giving me the strength and patience to complete this work. I gratefully acknowledge the Swedish construction industry's organization for research and development (SBUF) for their financial support and I am grateful to Mosul University and the Ministry of Higher Education in Iraq for offering me the opportunity to conduct my PhD studies at Luleå University of Technology.

I give my sincerest gratitude to my supervisors, Professor Björn Täljsten and Dr. Thomas Blanksvärd, who have supported me throughout my thesis work with their patience and knowledge whilst allowing me space to work under my own direction. Their expertise and understanding added considerable value to my graduate experience. I am very grateful for the time and effort they dedicated to me. Their technical and editorial advice was essential to the completion of this thesis and they have given me innumerable lessons on and insights into the workings of academic research in general.

Special thanks go to Professor Jan-Erik Jonasson, who guided me at the beginning of my studies. I am especially grateful to him for the time, effort, and patience he dedicated to me. Many thanks go to Professor Nadhir Al-Ansari for helping me with some aspects of my scholarship.

My thanks also go to the staff at TESTLAB, the structural laboratory at LTU. All of you have been involved in my work, but I would in particular want to thank Mr. Georg Danielsson, Mr. Mats Petersson, Mr. Roger Lindfors and Mr. Lars Åström for all of their advice and help during the laboratory tests.

I would also like to send a special thought to my colleagues and friends in the research group "Innovative Materials and Structures" at the division of Structural Engineering, Gabriel, Jonny, Jens, Cosmin and Niklas for all their help and support. I am also personally grateful to the staff in the division of Structural Engineering and its head, Dr. Martin Nilsson, for exposing me to such a wide range of conversations and festivities.

I am also hugely grateful to all of the Iraqi PhD students at Ltu, whose company helped me cope with feelings of being away from home – thank you all!

Finally, writing a thesis is not possible without an extremely understanding family, so I must thank my mother for her limitless and devoted care, my father for his unbounded confidence in me, and my brother and sisters for helping us all out while I was studying. I cannot express in words how grateful I am to my wife Am Amen for her support and patience during my work. My kids, Amen, Abdulmalek and Maryam – your smiles kept me going! Love you all!

Mohammed
Luleå, March 2015

I

Summary

Repeated cyclic loading of reinforced concrete (RC) structures such as bridges can cause reduced service life and structure failure due to fatigue even when the stress ranges applied to the structural components are very low. These problems can be mitigated by using fibre-reinforced polymer (FRP) composites to increase the structures' load carrying capacity and fatigue life or service life. Strengthening of this sort may be a suitable way to prolong the service life of concrete structures.

FRP strengthening involves externally bonding a plate, sheet or rod of the strengthening material to the surface of the concrete member or placing the strengthening element in grooves cut into the member's surface. The bonding of plates or sheets to the surface is often referred to as EBR (externally bonded reinforcement) whereas the placement of strengthening bars in grooves carved into the member's surface is referred to as NSM (Near Surface Mounted) reinforcement. When this research project was initiated, it was not clear whether EBR or NSM strengthening was more effective at alleviating the effects of fatigue loading, and there were many aspects of their use that warranted further investigation.

The main objectives of the work presented in this thesis were to study the behaviour of materials and structures under fatigue loading, to assess the structural challenges presented by fatigue loading of members strengthened with EBR plates or NSM bars, and to identify analytical models suitable for the design and analysis of FRP-strengthening elements and strengthened concrete members.

The scientific approach adopted in this work is based on experimental fatigue loading tests of RC beams strengthened with EBR plates and NSM bars together with the development and assessment of analytical methods for describing the fatigue behaviour of tested strengthened beams and numerical models for predicting the behaviour of bond joints under fatigue loading. The analytical models were then verified against experimental results. The theoretical and experimental studies were supported by a state-of-the-art literature review that was conducted to gather existing knowledge concerning FRP strengthening of RC members and their fatigue behaviour at the material and structural levels.

This work is a summary thesis based on five appended papers. The first paper is a state-of-the-art review covering existing knowledge of various material combinations and applications of mineral-based and epoxy-based bonded FRP systems used for repair and strengthening of concrete structures subjected to fatigue loading. The review also covers existing models for predicting the fatigue life at the material and structural levels. Particular emphasis was placed on publications reporting studies on the mechanical behaviour of FRP materials, surface bonding behaviour and concrete beams strengthened with different FRP systems (including systems bonded with epoxy- or mineral-based bonding agents) under fatigue loading. The review presents existing knowledge concerning the relationship between the fatigue life of strengthened RC beams and the applied load, time dependent effects, the nature of the applied strengthening (shear, flexural or combined), the strengthening technique (EBR or NSM) and the configuration of the FRP sheets or plates. In addition, the requirements of building codes and the recommendations of researchers concerning the design of FRP strengthening is discussed. Overall, the review provides a detailed overview of current knowledge concerning the selection of materials and methods for strengthening structures

subject to fatigue loading based on their estimated fatigue life values and the level of stress to which the structure will be subjected.

The second paper presents four-point bending experiments using strengthened RC beams under monotonic and fatigue loading. All of the tested beams were tested with the same level of stress at the tension steel bars so as to ensure that all of the observed differences were solely due to the effects of the EBR plates and NSM bars. The influence of the strengthening materials' properties and the effects of pre-cracking of the concrete before the attachment of the FRP strengthening element were investigated by analysing the failure mechanism, load-deflection pattern, and measured strain in the reinforcing steel bars and CFRP elements. The results obtained indicate that the efficiency of strengthening is primarily determined by the relief of local stress in the member's reinforcing steel bars before they rupture, and the fatigue life of the reinforcing steel after its initial fracturing. The latter of these quantities is related to the strengthened member's ability to absorb the energy released at the moment the reinforcing bar fractures.

The third paper reports the use of a digital image correlation (DIC) technique to investigate the fatigue cracks behaviour of reinforced concrete beams externally strengthened with EBR plates and NSM bars. Displacement fields obtained from digital images recorded during specific loading cycles in fatigue tests are analysed to determine crack widths, beam deflections and curvatures, and major principle strains in order to support crack detection. The DIC method was found to provide very accurate and detailed information about the strain fields.

The fourth paper describes an analytical model for simulating the fatigue behaviour of reinforced concrete beams strengthened with EBR plates and NSM bars. The fatigue calculations are performed using a fibre section model that accounts for the fatigue behaviour of the concrete and CFRP. The beam deflection and strain in each material could be calculated with sufficient accuracy to allow reliable prediction of the fatigue behaviour of FRP-strengthened beams.

The fifth and final paper presents a new two-scale damage model that describes the behaviour of the fibre-reinforced polymer (FRP)-concrete bond under high-cycle fatigue. An accurate model of this sort is required for the development of robust procedures for simulating strengthened RC beams by three dimensional finite element modelling (FEM). The bond is treated as being elastic-plastic and capable of sustaining damage on the micro-scale, and as being elastic on the meso-scale. A new damage law for the interface joint is described. The two-scale damage model was implemented as a material model in conjunction with a three dimensional eight-node interface element of zero thickness and used to simulate a double shear joint specimen under high cycle fatigue. Numerical calculations were performed using both a full incremental cyclical solution method and a faster cycle jump approach. The model efficiently computed the damage to the FRP-concrete bond under high-cycle fatigue loading before the fracture stage was reached.

Sammanfattning (Swedish)

Upprepad cyklisk belastning på armerade betongkonstruktioner, exempelvis broar, kan leda till begränsad livslängd och brott på grund av utmatning. Detta kan förekomma även om spänningsnivåerna i konstruktionen är relativt låga. Fiberkompositer (FRP – fibre reinforced polymers) kan användas för att öka dessa konstruktioners bärförmåga samt förlänga dess livslängd med avseende på utmatning. Den här tekniken kan således användas för att på ett lämpligt sätt förlänga livslängden med avseende på utmatning.

Metoden går ut på att plattor, väv eller stavar limmas mot konstruktionen – antingen utanpåliggande eller i uppfrästa eller uppsågade spår i det täckande betongskiktet. Tekniken med plattor och väv kallas ofta EBR (Externally Bounded Reinforcement) medan metoden med stavar betecknas som NSM (Near Surface Mounted).

Vid början av den aktuella forskningen var det utifrån litteraturstudien inte klart vilken av dessa metoder; EBR eller NSM som var att föredra med avseende på utmatning och det finns fortfarande många aspekter att utreda. Det viktigaste målet med denna avhandlingen är att erhålla utökad kunskap om beteendet hos material och konstruktioner under utmattningsbelastning. Utöver detta var det även intressant att försöka utveckla en lämplig analytisk modell för analys och dimensionering som beaktar utmaningarna med utmattningsbelastning efter förstärkning med EBR eller NSM.

Det vetenskapliga förhållningssättet i den här avhandlingen omfattar experimentella utmattningsförsök av armerade betongbalkar förstärkta med EBR-plattor och NSM-stavar. Studien inkluderar även analytiska metoder för att beskriva beteendet hos förstärkta betongbalkar samt numerisk modellering av vidhäftningen mellan materialen under utmattningsbelastning. De analytiska resultaten är verifierade jämtemot experimentella mätningar. Utöver det teoretiska och experimentella arbetet har en litteraturstudie (state of the art) genomförts för att kunna identifiera forskningsfronten inom området samt förstå utmattning på såväl materialnivå samt strukturnivå.

I avhandling finns fem stycken artiklar bifogade. Den första artikeln presenterar en "state of the art" översyn av olika materialkombinationer och tillämpningar av mineral- och epoxibaserade FRP-system vid tillämpning för reparation och förstärkning av betongkonstruktioner utsatta för utmattningsbelastning. I denna undersökning presenteras modeller för utmattningslivslängd på både materialnivå såväl som stukturnivå. Studien undersöker de mekaniska egenskaperna hos FRP-materialet, vidhäftningens beteende samt betongbalkar förstärkta med olika typer av FRP-system (epoxi- eller mineralbaserade system). Studerade parameterar är; påförd last, tidsberoende effekter, typ av förstärkning (skjuvning, böjning eller en kombination av dessa), typ av förstärkningsteknik (plattor eller NSM) och konfigurationen av väv eller plattor. Byggnadsnormer såväl som andra forskares rekommendationer diskuteras också. Genom översynen får läsaren en genomgång av lämpliga material och metoder för förstärkning av utmattningsbelastade konstruktioner.

Den andra artikeln beskriver en försöksserie med förstärkta betongbalkar belastade med utmattningslast, där förstärkta balkar utsätts för samma spänningsnivå i armeringen som oförstärkta för att kunna jämföra effektiviteten mellan EBR plattor och NSM stavar.

Inverkan av förstärkningsmaterialets egenskaper för uppsprucken betong utreds och diskuteras genom att analysera brottmoden, last-deformation och töjningsmätningar i armeringen samt

förstärkningsmaterialet (CFRP). Baserat på mätresultaten så är reduktionen av lokala spänningar samt förmågan att absorbera den energi som frigörs då ett armeringsjärn går i brott de avgörande faktorerna för förstärkningsåtgärdens effektivitet.

Den tredje artikeln beskriver utmattningsbeteendet av armerade betongbalkar med utanpåliggande förstärkning bestående av EBR plattor och NSM stavar genom att använda fotometrisk töjningsmätning (DIC-digital image correlation). Förskjutningsfält erhålls genom digitala bilder som registreras under utmattningsförsöken vid specifika cykler, dessa analyseras med avseende på sprickvidd, nedböjning och krökning samt huvudtöjningar med avseende på att upptäcka sprickor. Det observerades att DIC-tekniken kunde leverera mycket exakt och detaljerad information om töjningsfälten.

Den fjärde artikeln beskriver en analytisk modell för simulering av utmattningsbeteendet av testade betongbalkar förstärkta med EBR plattor och NSM-stavar. Utmattningsberäkningarna utförs genom en sektionsanalys som tar hänsyn till både betongen och förstärkningsmaterialets egenskaper med avseende på utmattning. Resultaten visar på att balkens nedböjning och töjningarna i båda materialen kunde beräknas med tillräckligt god noggrannhet. Utmattningsbeteendet kan således uppskattas med hjälp av den typen av analys.

Den femte och sista artikeln beskriver en ny tvåskalig skademodell av vidhäftningen FRP och betong under hög cyklisk utmattning/belastning. Detta tar hänsyn till det viktigaste steget för en korrekt analys av förstärkta armerade betongbalkar genom en tredimensionell FEM. Materialet modelleras som elasto-plastiskt kombinerat med skador för analysen i mikroskala samt elastiskt för analysen i mesoskala. Ett nytt skadevillkor för förbandet beskrivs. De tvåskaliga skademodellerna har implementerats som materialmodeller för ett tredimensionellt åtta-nod-gränssnitt element med noll tjocklek och används för att simulera en provkropp med dubbel skjuvyta under hög cyklisk utmattning/belastning. De numeriska beräkningarna utfördes med inkrementell lösning och en metod har föreslagits. Resultaten visar på att modellen beräknar skadorna på förbandet mellan FRP och betong under hög cykel belastning på ett effektivt sätt.

Notations and symbols

Upper case letters

A_{CFl}	Area of fibre l of CFRP	$[mm^2]$
A_{cj}	Area of fibre j of concrete	$[mm^2]$
A_{si}	Area of fibre i of steel reinforcement	$[mm^2]$
D_j	Damage variable	$[-]$
E	Elastic stiffness matrix for the interface element	$[-]$
EE	Normalized concrete strain	$[-]$
E_B	Elastic stiffness matrix of the element	$[-]$
E_e	Elastic modulus of elasticity	$[N/mm^2]$
$E_{e,N}$	Secant modulus of elasticity of concrete in the nth load cycle	$[N/mm^2]$
E_f	Young's modulus of continuous fibres	$[N/mm^2]$
E_{f_N}	Modulus of elasticity of strengthening CFRP in the n:th load cycle	$[N/mm^2]$
F	Applied axial load	$[N]$
G_f	Interfacial fracture energy	$[N/mm]$
K_n	Normal component of interface elastic stiffness in n direction	$[N/mm^2]$
K_s	Shear component of interface elastic stiffness in s direction	$[N/mm^2]$
K_t	Shear component of interface elastic stiffness in t direction	$[N/mm^2]$
L	Span length	$[mm]$
$L_{e,j}$	Total length of the elastic stage	$[mm]$
M	Applied bending moment	$[N.m]$
N	Number of loading cycles	$[-]$
N_f	Number of cycles to failure	$[-]$
N_i	Shape function at the ith node	$[-]$
$\dot{P}$	Accumulated plastic strain rate	$[-]$
P_{th}	Damage threshold	$[-]$
S_r	Steel stress range	$[N/mm^2]$

$V_n, V_s, , V_t$	Direction cosines of the local coordinate system	$[-]$
Tol	Acceptable tolerance	$[-]$

Lower case letters

c	Neutral axis position	$[mm]$
f	Loading cycle frequency	$[Hz]$
$\acute{f}_c$	Compressive strength of concrete	$[N/mm^2]$
f_c	Stress in concrete	$[N/mm^2]$
ff	Normalized concrete stress	$[-]$
f_{fu}	Ultimate capacity of CFRP	$[N/mm^2]$
f_{sy}	Reinforcing steel yield stress	$[N/mm^2]$
f^μ	Micro yield criterion function	$[-]$
m	Initial Young's modulus	$[N/mm^2]$
$m\,m,nn,kk$	Total number of section fibres	$[-]$
n	Number of plies of continuous fibre sheets	$[-]$
t_f	Thickness of one layer of continuous fibresheet	$[mm]$
u_i, v_i , w_i	Corresponding nodal displacements	$[mm]$
y_i, y_j ,y_l	Distance between centroid of fibres i,j,l and top of section	$[mm]$

Greek letters

ε_c	Strain in concrete	$[-]$
ε_{CF}	Strain of the strengthening CFRP element	$[-]$
ε_{CFu}	Ultimate strain of the strengthening CFRP element	$[-]$
ε_{cu}	Ultimate concrete strain	$[-]$
ε_s	Reinforcing steel strain	$[-]$
ε_{su}	Reinforcing steel ultimate strain	$[-]$
ε_{sy}	Reinforcing steel yield strain	$[-]$
$\varepsilon_{cN,max}$	Total maximum strain at any time and at any number of cycles	$[-]$
ε_{cN}	Concrete compressive strain	$[-]$

ε_B^e	Strain tensor	$[-]$
ε_{ce}	Elastic components strain	$[-]$
ε^e	Elastic strain in the interface element	$[-]$
ε_i	Concrete fibre strains at layer i	$[-]$
ε_{j3}	Current total strain in normal and shear directions(j)	$[-]$
ε_{j3}^μ	Micro strain	$[-]$
$\varepsilon_{j3}^{\mu e}$	Microelastic strain	$[-]$
$\varepsilon_{j3}^{\mu p}$	Microplastic strain	$[-]$
$\varepsilon_{top,N}$	Strain at the extreme top fibre	$[-]$
$\varepsilon_{top,N}$	Strain at the extreme top fibre	$[-]$
ε_u^μ	Ultimate static strain	$[-]$
$\dot{\lambda}$	Plastic multiplier	$[-]$
σ_{CF}	Strengthening CFRP stress	$[N/mm^2]$
σ_s	Reinforcing steel stress	$[N/mm^2]$
σ_B	Stress strain tensor	$[N/mm^2]$
σ_c^m	Mean applied stress	$[N/mm^2]$
σ_c^r	Stress range	$[N/mm^2]$
σ_f	Normal fatigue stress limit	$[N/mm^2]$
σ_{max}	Maximum applied compressive stress	$[N/mm^2]$
σ_{min}	Minimum applied compressive stress	$[N/mm^2]$
σ_u	Ultimate static stress	$[-]$
$\tau_{f_{j,3}}$	Shear fatigue stress limit	$[N/mm^2]$
ΔM	Moment difference between two load stages	$[N.m]$
$\Delta\varphi$	Curvature difference between two load stages	$[1/mm]$
μ	Reduction factor	$[-]$
α	Damage exponent parameter	$[-]$
δ	Deflection	$[mm]$

η	Long-term conversion factor	$[-]$
ν	Poisson's ratio	$[-]$
ξ, η, ζ	Local element coordinates system	$[-]$
φ	Beam curvature	$[1/mm]$

Table of Contents

Paper I-V

Part I

1 Introduction

1.1 Background

Rehabilitation and strengthening of reinforced concrete structures are major challenges faced by structural engineers. When considering the rehabilitation of an RC structure such as a bridge that has been subjected to cyclic loading, the deleterious effects of fatigue over its life must be evaluated. When such evaluation indicates that the structure or structural component is approaching the end of its fatigue life, its fatigue life must be extended via some form of rehabilitation. Furthermore, structures that have been built more than several decades ago may require upgrading to meet current service load requirements. Several methods for strengthening reinforced concrete (RC) structures using various approaches and materials have been developed and use for rehabilitation (Romualdi,1987; Täljsten,1994; Diab,1998). One such method that was introduced quite recently involves the use of strengthening Fibre Reinforced Polymer (FRP) elements. FRP has proven to be an excellent strengthening material for rehabilitation or upgrading of RC structures compared to traditional alternatives because it has a low weight to volume ratio, which makes its application easier, together with a high strength to weight ratio and non-corrosive properties, which enhance the strengthened structure's durability. In addition, FRP elements have high fatigue strength under repeated loading (fatigue); this is particularly true for carbon fibre reinforced polymers (CFRP). FRP elements can be used as internal reinforcements for new constructions in a similar way to conventional steel reinforcement. Alternatively, they may be used to strengthen existing reinforced concrete (RC) structures, in the form of externally bonded reinforcement (EBR) plates or near surface mounted (NSM) rods/strips.

When using FRP to rehabilitate or strengthen existing structures, it is important to consider the fatigue characteristics of the FRP-concrete bond. While many tests have been conducted to assess the strengthening effects of EBR and NSM systems on RC members, many aspects of the behaviour of such systems remain unclear, particularly in terms of their fatigue behaviour. In particular, before this work was conducted, it was not clear whether NSM bars or EBR plates offered better overall strengthening performance. New studies were therefore required to better understand the behaviour of EBR and NSM systems under fatigue loading and to support the identification and development of models for the design and analysis of strengthened structures under fatigue loading.

1.2 Hypothesis and research questions

At the beginning of this PhD program, a key hypothesis was stated:

"The fatigue life of an EBR- or NSM-strengthened RC beam is governed by the fatigue life of its reinforcing steel bars."

The work in this thesis has aimed to answer the following main research questions:

-What is the most important factor that determines the impact of a strengthening material on the fatigue life of strengthened beams subject to fatigue loads?

-Are EBR plates better or worse than NSM bars for keeping the fatigue life of RC beams?

-How can the fatigue life and behaviour of EBR- and NSM-strengthened RC beams be estimated accurately?

1.3 Objective

The main objective of this thesis work was to investigate the effectiveness and feasibility of using CFRP EBR plates and NSM rods for flexural strengthening of reinforced concrete (RC) members under fatigue loading. Two main lines of investigation – analytical and experimental – were pursued to achieve this objective. The specific objectives of the analytical and experimental studies were:

- To develop an analytical model that describes the nonlinear behaviour of strengthened beams and accounts for the effects of progressively more severe damage to the concrete.
- To develop a constitutive model that can describe the behaviour of FRP-to-concrete bonding interfaces under high cyclic fatigue, and to integrate this model into finite element models for predicting the behaviour of FRP-strengthened RC beams.
- To determine how fatigue affects the behaviour of RC beams strengthened with EBR plates or NSM rods;
- To characterize the influence of the modulus of elasticity of the strengthening CFRP element on the behaviour of EBR- and NSM-strengthened RC beams under fatigue loading;
- To determine how prior cracking affects the response of EBR- and NSM-strengthened RC beams to fatigue loading.

A final objective of the experimental studies was:

- To verify the developed analytical models by comparing predicted and experimental cycle-deflection and cycle-strain diagrams for EBR- and NSM-strengthened beams.

1.4 Limitations

The subject of these investigations is complex, and only a few of the parameters affecting the behaviour of strengthened beams have been possible to investigate in laboratory fatigue loading tests. Parameters that have been studied include the applied strengthening method, the modulus of elasticity of the CFRP element, and the extent of cracking in the strengthened beams prior to strengthening. The experimental studies thus focused exclusively on RC members with rectangular geometries strengthened with non-prestressed FRP elements and subjected to fatigue loading at a single constant frequency. In addition, only one type of epoxy was used to bond the FRP elements to the beams, and all of the tested beams were tested with the same level of stress at the tension steel bars and same amount of steel reinforcement.

During the analytical work of strengthened beams, no attempt was made to account for the effects of damage to the bonding between the FRP elements and the RC member, for the effect of the positioning of NSM bars within the width of the member's soffit, or for events after the first rupture of the reinforcing steel. An additional limitation is that the numerical

model was only developed to model the behaviour of FRP-concrete interfaces subjected to high-cycle fatigue.

1.5 Scientific approach and methods

The research in this work was conducted in a conventional way, starting with an extensive literature study and then proceeding to laboratory tests, evaluations, theoretical derivations, and comparisons between experimental data and theoretical predictions.

The results obtained are presented in a summary thesis consisting of an extended summary of the work followed by a series of journal and conference publications. This is the standard format for Swedish PhD theses in the field of Civil Engineering. In brief, the work involved the following processes: stating of hypotheses; conduct of a literature review; defining research questions; planning, performing and evaluating experiments; drawing conclusions; and finally, writing the thesis and answering the research questions.

In the beginning of the PhD studies, it was considered necessary to understand fatigue behaviour at the material and structural levels. Therefore a state-of-the-art review of different material combinations and applications of mineral-based and epoxy-based bonded Fibre Reinforced Polymers (FRP), used for the strengthening of concrete structures subjected to fatigue loading was conducted. The findings of this review are presented in Chapter 2 and *Paper I. Paper I* deals with literature models of the fatigue life of FRP-strengthened RC beams at the material and structural levels. Particular emphasis is placed on the mechanical behaviour of the FRP-material, surface bonding behaviour and concrete beams strengthened under fatigue loading with different types of FRP systems. The literature search focused on the effects of the applied load on fatigue life, time-dependent effects, the effects of different types of strengthening (shear strengthening, flexural strengthening, or combined strengthening), and the effects of altering the configuration of the strengthening sheets or plates. Existing building codes and recommendations made by the authors of the identified studies were also discussed. The review provides an overview of current knowledge concerning the selection of materials and methods for strengthening structures subjected to fatigue loading based on estimated fatigue life values for materials and structures at various applied stress levels.

An important finding from the literature review was that it was not clear which of EBR or NSM strengthening is most effective for extending the fatigue life of RC beams subject to fatigue loading in case good bond quality of EBR. To address this knowledge gap, experiments were conducted to investigate the response of unstrengthened RC beams and beams strengthened with either EBR plates or NSM bars under monotonic and fatigue loading, with all tested beams having the same level of stress in their reinforcing steel. The results of these investigations are presented in *Paper II*, and the experimental work is briefly discussed in Chapter 3 of this thesis. This experimental work also examined the impact of varying the properties of the CFRP material, and the effect of prior cracking of the RC beams. In addition, the cracking patterns of the tested beams and the widths of the resulting cracks were studied using a digital image correlation (DIC) technique; the results of this investigation are presented in *Paper III*. In general, the experimental work improved our

understanding of FRP-strengthened RC beams under fatigue loading conditions and provided key insights into the relative advantages and drawbacks of the EBR and NSM approaches.

The experimental studies were complemented by a theory-based effort to develop predictive models that describe the flexural behaviour of strengthened beams under fatigue loading using a fibre section technique. This work is presented in *Paper IV*. The resulting models accurately predict the overall response of strengthened reinforced concrete beams and the evolution of strains during fatigue loading when their output is compared to experimental data.

Finally, in an initial step towards the development of robust three-dimensional finite element models for the accurate analysis and simulation of strengthened RC beams, a new two-scale damage model describing the behaviour of the bond between fibre-reinforced polymer elements and reinforced concrete during high-cycle fatigue was developed. This model is detailed in *Paper V*. The two-scale damage model was implemented as a material model for a three dimensional eight-node interface element of zero thickness and used to simulate a double shear joint specimen under high cycle fatigue. This approach proved to be effective at modelling the bond between the CFRP and concrete under fatigue loading, making it possible to link micro-scale phenomena to meso-scale outcomes. On the basis of this promising result, future studies will aim to develop similar models for the other components of strengthened RC beams (steel and concrete) under fatigue.

1.6 Thesis guide

This section describes briefly the structure of the thesis in order for the reader to obtain a clear overview of the content and ease the reading of this thesis. The chapters of part I are briefly described below.

Chapter 1 provides a general overview of the research conducted, including the research questions that were answered and the methods used to answer them.

Chapter 2 gives an introduction to fatigue in general, with particular emphasis on the fatigue behaviour of the component materials of strengthened beams, the fatigue of FRP-strengthened RC beams, and the fatigue of FRP-to-concrete bonding materials. Existing building codes and researchers' recommendations concerning the strengthened reinforced concrete beams subject to fatigue loading are discussed, and an overview of the theoretical modelling of FRP-strengthened RC beams and bond joints is presented.

Chapter 3 describes experimental studies on concrete beams strengthened with EBR plates and NSM rods. The testing matrix, including information on the test specimens and the properties of their constituent materials, is presented. The chapter also provides details of the instrumentations used as well as the strengthening and testing procedures. Finally, the key results of their experimental studies are presented and discussed.

Chapter 4 describes the analytical approach used to develop models describing the fatigue behaviour of the tested strengthened beams and joint bonds. The assumptions made in

developing the models are presented, and models for predicting the fatigue life of strengthened RC beams are elaborated.

Chapter 5 provides an integrated discussion of the results of the experimental and theoretical studies, presents some conclusions, and offers some suggestions for future studies.

Part II consists of the six appended papers, briefly described below.

Paper I, Ex*amination at a Material and Structural Level of the Fatigue Life of Beams Strengthened with Mineral or Epoxy Bonded FRPs: The State of the Art*. Published in the Advances in Structural Engineering (2013). Authors are Mohammed Mahal, Thomas Blanksvärd and Björn Täljsten. My contribution to this paper consisted of formulating the fundamental idea of the study in collaboration with the co-authors, performing the literature study, collecting and analysing data, and writing the paper under the co-authors' supervision.

Paper II, *Experimental performance of RC beams strengthened with FRP materials under monotonic and fatigue loads*. Submitted to Journal of Composites for Construction (2015). Authors are Mohammed Mahal, Björn Täljsten and Thomas Blanksvärd. My contribution to this paper consisted of planning the test series in collaboration with the co-authors, performing the experimental tests, analysing and evaluating their results, and writing the paper under the co-authors' supervision.

Paper III, *Using digital image correlation to evaluate fatigue behaviour of strengthened reinforced concrete beams*. Submitted to Engineering Structures (2015). Authors are Mohammed Mahal, Thomas Blanksvärd, Björn Täljsten and Gabriel Sas. My contribution to this paper consisted of planning the test series in collaboration with the co-authors, performing the experimental tests, analysing and evaluating their results, and writing the paper under the co-authors' supervision.

Paper IV, *Fatigue analysis of reinforced concrete beams strengthened in flexure using CFRP*. Submitted to Composite Structures (2015). Authors are Mohammed Mahal, Björn Täljsten and Thomas Blanksvärd. My contribution to this paper consisted of formulating the fundamental idea of the study in the collaboration with the co-authors, developing the analytical models, writing the program code, analysing and evaluating the results obtained, and writing the paper under the co-authors' supervision.

Paper V, *A two-scale damage model for high-cycle fatigue at the fibre-reinforced polymer-concrete interface*. Submitted to Computers and Concrete (2015). Authors are Mohammed Mahal, Björn Täljsten and Thomas Blanksvärd. My contribution to this paper consisted of formulating the fundamental idea of the study in collaboration with the co-authors, deriving the equations, developing and implementing the finite element models, writing code, analysing and evaluating the results, and writing the paper under the co-authors' supervision.

Paper VI, *FE Modelling of FRP-concrete Interface for Very High Cycle Fatigue Behavior*. Published in Key Engineering Materials (2013). Authors are Mohammed Mahal, Thomas Blanksvärd and Björn Täljsten. My contribution to this paper consisted of formulating the

fundamental idea of the study in collaboration with the co-authors, deriving the equations, developing and implementing the finite element models, writing code, analysing and evaluating the results, and writing the paper under the co-authors' supervision.

1.7 Additional publications

The following report has been produced by the author, related to scope of the thesis.

Report

Mahal, Mohammed (2015) Experimental investigations of RC beams strengthened with FRP materials under monotonic and fatigue loads. Research report 2015, Luleå University of Technology, Division of Structural and Construction Engineering, Department of Civil, Environmental and Natural Resources Engineering, ISBN 978-91-7583-211-1, pp. 150.

2 Background and literature review

2.1 Fatigue

In general, fatigue is related to the distinctive behaviours exhibited by materials in response to cyclic loading. The first symptom of fatigue damage is micro cracking, and the ultimate result is fatigue failure (fracture). The most important aspect of such behaviour is that the failures occur under cyclic loading where the peak stress is considerably lower than that required to cause rupture by a single application of a static load. Fatigue cracks can form even when the cyclic stresses are below the yield strength of the material studied.

Fatigue loading is usually classified into two categories, i.e. low-cycle and high-cycle loading. Low-cycle loading involves the application of a few load cycles at high stress levels, with the maximum applied stress being greater than the yield stress of the loaded materials. In contrast, high-cycle loading is characterized by a large number of cycles at stress levels that are lower than the yield stress of the loaded materials. Lee and Barr (2004) presented a more detailed system for classifying fatigue loading regimes, including a new class of "super-high cycle loading" as shown in Table 2.1.

In general, high-cycle fatigue behaviour may be divided into three stages that are associated with increasing levels of maximum strain. In the first stage, which is known as the initiation stage, the strain increases rapidly but at a rate that decreases progressively as the number of cycles increases. The second stage is known as the stability state, during which the strain increases linearly with the number of cycles. The final stage is unstable; strain increases progressively with the number of cycles until failure occurs.

Table 2.1. Classes of fatigue loading regimes (Lee and Barr, 2004).

Low-cycle fatigue		High-cycle fatigue				Super-high-cycle fatigue		
1	10^1	10^2	10^3	10^4	10^5	10^6	10^7	10^8	10^9
Structures subjected to earthquake		Airport pavements and bridges		Highway and railway bridges, highway pavements		Mass rapid transit structures		Sea structures

The most common method of relating the fatigue life of a material to the applied stress is the stress-life (S-N) approach, in which the number of cycles to failure is plotted against the applied stress range. The fatigue life of a component is defined by the total number of stress cycles required to cause failure. The actual fatigue life can be divided into three stages: crack initiation, crack growth, and rapid fracture. The rapid fracture stage is not usually accounted for in expressions designed to predict fatigue life. When attempting to predict the fatigue life of CFRP-strengthened beams, it is important to consider the effects of fatigue on the concrete, the reinforcing steel, and the strengthening composite. The fatigue life of the strengthened beam is usually equal to that of whichever one of its component materials has the shortest fatigue life; usually, if one component fails to withstand the applied fatigue load, the entire structural element will fail (El Refai, 2007). The fatigue limit stress of a structural element is defined as the maximum stress it can tolerate without undergoing fatigue failure after an

arbitrarily large number of fatigue loading cycles. Figure 2.1 shows a plot of stress against time for a fatigue test, illustrating some of the key terms used in the analysis of fatigue data.
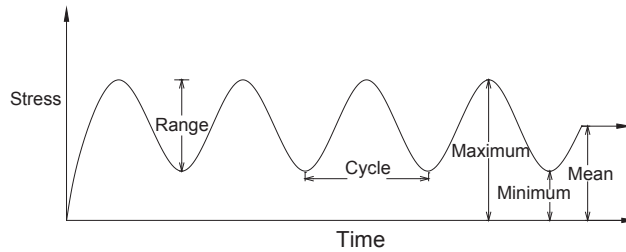
Figure 2.1. Terms used in the analysis of fatigue.

The following sections describe the fatigue behaviour of components in a typical strengthened reinforced concrete structure.

2.1.1 Concrete

Under fatigue loads, the strain of concrete increases significantly beyond the value observed after the first load cycle, which is similar to the behaviour of concrete under sustained stress. In addition, concrete usually shows a softening in its stress-strain behaviour under repeated loading, causing the slope of the stress-strain curve to change as the number of cycles increases (ACI 215, 1997). Multiple hypotheses concerning the initiation and propagation of cracks in concrete under fatigue loading have been presented (Lloyd et al., 1968 and Antrim, 1965). In general, it seems that fatigue in concrete is caused by micro cracks, which are formed by shrinkage during the hardening period. These micro cracks probably grow both within the cement matrix and the aggregate interface, weakening the section until it can no longer sustain the applied load. It is common to compare experimentally determined fatigue strength values to static strengths measured for equivalent concrete structures so that the fatigue strength can be defined as a fraction of static strength for a given number of cycles (ACI Committee 215, 1997). Fatigue strength is influenced by many different factors. Most previously reported experiments on the fatigue behaviour of concrete were conducted to characterize the effects of different loading regimes and environmental conditions on the fatigue strength. The fatigue strength of concrete structures is primarily determined by the stress range to which they are subjected. Other important factors include the cement content, water to cement ratio, stress gradient, and the rate of loading. However, at maximum stress levels (up to 75% of the static strength), increasing the loading frequency from 1 Hz to 15 Hz has no significant effect on the fatigue strength of concrete (ACI 215, 1997).

2.1.2 Steel

Many experiments have been conducted to assess the fatigue strength of reinforcing steel bars (ACI 215, 1997). In most of these experiments, the relationship between stress range and fatigue life of reinforcing bar was characterized by performing a series of cycled load tests on bars which were either embedded in concrete or tested in air. The first sign of fatigue damage in reinforcing steel is the formation of microcracks at points where stress is concentrated on the bar's surface. The cracks gradually propagate as the number of load cycles increases,

growing until the cross section of the reinforcing steel becomes too small to carry the applied load, at which point a fast fracture takes place. Crack initiation typically occurs at the location of the largest stress concentration, usually at the intersection of transverse lugs and longitudinal ribs (Papakonstantinou et al., 2001). The fatigue strength of reinforcing bars depends mainly on their microstructure, inclusions, minimum stress, bar size, type of beam, the geometry of their deformations, and their yield and tensile strengths (ACI 215, 1997). Many experiments showed that reinforcing steel has a fatigue limit, i.e. a stress threshold below which no fatigue failure occurs. In contrast, concrete has no such limiting value. This difference exists because steel is a strain hardening material whereas concrete is strain softening material (Gylltoft, 1983).

2.1.3 FRP

A Fibre Reinforced Polymer (FRP) is a linear elastic composite material that consists of a polymer matrix reinforced with a fibrous material. Three types of fibre are widely used in the construction of FRPs: aramid, glass and carbon. All three have higher ultimate strengths than normal reinforcing steel. Thermosets such as vinyl esters, polyesters and epoxies are often used as the matrix material because they have a higher strain to fracture than the fibres and because they bind to the fibres, thereby transferring stresses between them. In addition, the matrix material protects the fibres from mechanical and environmental damage (Jones, 1998). FRP elements can be constructed and applied in several different configurations including 1) rods with circular or rectangular cross-sections, which are used as internal reinforcements or for near-surface mounted reinforcement (NSM); 2) composite plates and sheets; 3) FRP grids, which are typically multidirectional prefabricated composites; and 4) impregnated textiles, which provide a variety of textile structures that are used as reinforcement. FRP rods and plates are often bonded to the member to be strengthened using epoxy-based bonding agents whereas grids and textiles are more commonly bonded using mineral-based bonding agents. FRP elements are normally more fatigue resistant than the reinforcing steel of RC members, especially when fibres with a high modulus of elasticity such as carbon fibres are used. However, the fatigue strength of glass fibre composites is lower than that of steel with a low stress ratio (Badawi, 2007). The fatigue failure mechanism of FRP composites is more complex than those of plain concrete or steel. Composite materials often have a much greater fatigue life than other homogenous materials (Papakonstantinou et al., 2001), in which cracks are formed by fatigue at weak points and then grow progressively with each load cycle. Conversely, if an individual fibres within an FRP composite develops a defect, this defect will not propagate across to the other fibres, reducing the extent to which cracks can grow. Once the FRP composite has been damaged, the damage propagates along the matrix between unidirectional fibres and does not pass through adjacent fibres (Kim and Heffernan, 2008). A failure of an FRP composite therefore involves a combination of different degradation mechanisms including matrix cracking, fibre breakage, fibre-matrix debonding and delamination (Adimi et al., 2000). If the surface fibres fail under repeated loading, the remaining fibres continue to support the redistributed load and this behaviour continues until a total failure occurs. There are four stages that the FRP composites go through before failure due to fatigue (Ramakrishnan and Jayaraman, 1993; Curtis, 1989; Newaz, 1985; Salvia et al., 1997). The first and second stages are matrix cracking combined with interfacial debonding.

9

The third stage involves the delamination of the matrix and the fibres, and the final stage involves the failure of the remaining fibres due to tensile stress. It is important to note that FRP composites are incapable of supporting compressive loads, which cause local layer instability and failure-inducing layer buckling, possibly even before resin and interfacial damage occurs within individual layers. Consequently, reversed axial fatigue or tension-compression loading is considered to be extremely detrimental to FRP composites. For this reason, the most suitable use for FRP composites is to strengthen structures that are subject to tension-tension fatigue loading. Gorty (1994) showed that the modulus of elasticity of a CFRP rod did not change when the material was subjected to high cyclic loading. Similarly, Ferrier et al. (2011) found that cyclic loading caused a negligible decrease in the ultimate strength of carbon/epoxy composites but reduced the stiffness of FRP laminates.

2.1.4 Fatigue of FRP-strengthened RC beams

The most common methods of strengthening RC beams with CFRP elements involve the attachment of EBR sheets or plates to the girder soffit surface, or the insertion of NSM laminate strips or rods into slots carved into the soffit surface of the RC member. For a more detailed discussion of these approaches, see the review written by Täljsten (2002).Several recent studies have investigated the effects of strengthening FRP laminates on the fatigue strength of reinforced concrete beams (Meier et al., 1992; Shahawy and Beitelman, 1999; Heffernan and Erki, 2004;Barnes and Mays,1999;Masoud et al., 2001;Papakonstantinou et al.,2001; Breña et al., 2005; Aidoo et al., 2004; Aidoo et al., 2006;Gussenhoven and Breña, 2005;Toutanji et al., 2006, Harries et al., 2007 and Dong et al., 2011) and limited studies dealing with NSM bars (Aidoo et al., 2006; Badawi and Soudki, 2009; Oudah and El-Hacha, 2012; Yost et al., 2007; Rosenboom and Rizkalla, 2006; Quattlebaum et al., 2005 and Wahab et al., 2012).

Most of these studies indicated that FRP-strengthened beams under fatigue loading generally exhibit an initial change in stiffness and an increase of deflection due to a redistribution of cracks in the beams. The stiffness then remains constant while the deflection increases slowly due to cyclic creep, i.e. the gradual evolution of the plastic strain of the concrete, FRP, steel reinforcement and the FRP-concrete bond under cyclic load. Finally, there is a sudden increase in deflection immediately prior to failure. The behaviour of strengthened beams under fatigue loading depends mainly on the maximum stress generated in the main tension reinforcement, the strength of the bond between the FRP and the concrete, and the configuration of the FRP. If the bonding strength between the concrete and the FRP is sufficient, the initial failure will be due to steel rupture followed by rupture of the FRP, debonding of the FRP from the concrete substrate, or delamination of the concrete cover caused by flexural-shear cracking. FRP debonding is rare because both the tensile and shear strengths of epoxy adhesive are at least twice as large as those of the concrete cover (Derkowski, 2006). Moreover, if the bonding between the FRP and concrete substrate is defective, either because of sub-standard workmanship or design problems with the anchorage, the fatigue life of beam will obviously be impaired because the FRP will not help the beam and steel rebar resist the applied stress, accelerating the rupture of the steel rebar.

Several studies have been conducted on the effects of fatigue on structures strengthened with FRP bonded using epoxy-based materials. These studies investigated the relationship between fatigue life and the nature of the strengthening material (i.e. the fibres used in its construction), the applied load, the type of strengthening applied (i.e. flexural, shear, or combined), and the configuration of the strengthening FRP element (EBR or NSM). In addition, the impact of time-dependent variables and processes such as the temperature, relative humidity, and freeze/thaw has been examined. In order to evaluate the fatigue performance of EBR and NSM, this section presents test results of beams subjected to fatigue loading under different conditions, drawn from the literature. Among them, Yu *et al.* (2011) carried out fatigue testing of RC beams strengthened with GFRP sheets, which were shown to reduce the stress in the reinforcing steel and increase the fatigue life of the strengthened beams under fatigue loading. In addition, the fatigue failure of beams strengthened with GFRP was shown to resemble that for beams strengthened with CFRP. The fatigue behaviour of concrete beams strengthened in flexure with NSM CFRP was investigated by Yost *et al.* (2007), whose results suggested that the bond between the NSM CFRP and the concrete was not affected by fatigue loading. The responses of CFRP-strengthened beams under fatigue loading with different load amplitudes were studied by Gheorghiu *et al.* (2007), who found that increasing the fatigue load amplitude significantly increased the cracking strain of the CFRP-concrete joint. The fatigue performance of RC beams shear strengthened with CFRP fabrics was investigated by Chaallal *et al.* (2010), who discovered that the fatigue life of beams strengthened with two layers of CFRP was lower than that for beams strengthened with a single layer. This counterintuitive result was attributed to the greater rigidity of the dual-layer strengthening elements, which changed the stress distribution in the concrete and caused it to be crushed rather than allowing the steel stirrups to yield. Ekenel and Myers (2009) exposed test beams to severe environments and defects caused by delamination in order to study the durability of RC beams strengthened with CFRP. By using cycles of continuous freeze and thaw, prolonged exposure to extreme temperatures, continuous relative humidity cycles and ultraviolet light, they showed that fatigue loads combined with harsh environmental conditions significantly affected the flexural stiffness of the beams because they reduced the strength of the adhesive binding the FRP strengthening element to the beam. Gussenhoven and Breña (2005) discovered that wider laminates are more effective than narrower laminates at increasing the fatigue life of strengthened beams because wider laminates reduce shear lag effects and restrain crack opening more effectively than narrower laminates. Al-Rousan and Issa (2011) studied the effect of various parameters on the fatigue life of RC beams strengthened in flexure with CFRP elements. The parameters examined in this work included the configuration of the CFRP sheets, the number of CFRP layers, the size of the CFRP-concrete contact area, the applied stress range, the frequency and number of fatigue cycles, and the extent of salt water exposure. The applied stress range had the strongest effect on the fatigue life, but the frequency of fatigue loading had no effect provided that it was kept within the range of 1 – 4 Hz. The latter finding was used to expedite the fatigue testing: all subsequent fatigue tests were conducted using loading frequencies at the upper end of this range. The fatigue life also increased with the number of layers in the CFRP strengthening element and the size of the CFRP-concrete contact area, both of which facilitate the transfer of stress from the tensioning steel to the CFRP element. Barnes and Mays (1999)

investigated the effects of different types of load on the fatigue behaviour of RC beams. When they applied the same stress range to the rebar of the strengthened and unstrengthened beams, they found that the fatigue life of the strengthened beams was greater than that of the unstrengthened beams. However, when the strengthened and unstrengthened beams were subjected to fatigue loading using the same percentage of their ultimate static load capacity, the strengthened beams had shorter fatigue lives. This was because the ultimate load value for the strengthened beams was much greater than that for the unstrengthened beams. Consequently, when the beams were loaded to the same percentage of their ultimate load capacity, the reinforcing steel bars of the strengthened beams were subjected to a much greater stress range. Masoud *et al.* (2001) showed that the fatigue life of a corroded beam improved using transverse CFRP wrapping and flexural sheet causing reduction of stress level in the corroded tension steel bars. Khan *et al.* (2011) reported that shear end anchorages enhanced the fatigue performance of flexurally strengthened RC beams. This was attributed to the ability of the end anchorages to reduce the high interfacial shear and peeling stresses at the point of plate cut-off, which cause debonding of CFRP laminates. Huang *et al.* (2011) studied the effects of temperature on the fatigue behaviour of strengthened beams. Their results showed that the fatigue life decreased with increasing temperature, and that the failure modes of strengthened beams shifted from steel yielding to interface debonding of the laminate as the temperature rose. However, Senthilnath *et al.* (2001) showed that even when the extent of delamination exceeded the limits defined as acceptable by the ACI, there were only very minor effects on the fatigue performance of CFRP-strengthened RC beams. Minnaugh and Harries (2009) examined the fatigue behaviour of RC beams strengthened with steel fibre-reinforced polymers (SFRP) and CFRP; their results suggested that SFRP strengthening elements outperformed CFRP, significantly improving the fatigue behaviour of RC beams and showing no evidence of debonding even at relatively high stress ranges. Derkowski (2006) tested beams under fatigue loading strengthened in flexure using one or two CFRP strips on the soffit surface. The fatigue lives of beams strengthened with two strips were greater than those strengthened with single strips because the dual strips were more effective at restraining crack opening. Wang *et al.* (2007) discovered that T-beams with excellent behaviour under fatigue loading could be repaired by strengthening with a hybrid FRP consisting of CFRP plates for flexural strength and a GFRP strip for shear strength. Harries *et al.* (2007) studied the effect of adhesive stiffness on the fatigue life of FRP-strengthened RC beams, showing that the use of a more flexible adhesive increased the stress on the tensile steel because the flexible adhesive was less effective at transferring stress to the strengthening material.

There have been few comparative studies on the relative efficiency of strengthening with NSM bars and EBR plates as means of increasing fatigue life. Aidoo et al. (2006) studied the fatigue performance of full-scale Interstate bridge girders strengthened with three different CFRP composite strengthening systems: surface-bonded CFRP strips, NSM strips in grooves carved into the girders' soffit surfaces, and hybrid strips fixed using powder-actuated fasteners. Under monotonic loading, all three methods increased the girders' load-carrying capacity. However, it was not clear whether EBR or NSM strengthening offered the best performance under fatigue loading because the CFRP strips exhibited a certain degree of relative slippage or debonding. A similar study was conducted by Quattlebaum et al. (2005)

using small-scale specimens strengthened with three different CFRP strengthening methods. Their test results showed that CFRP strips were unable to bridge cracks resulting from the failure of the primary reinforcing steel, in contrast to the report of Meier et al. (1992). Consequently, they found that NSM CFRP strips performed better than EBR CFRP strips and hybrid strips fixed using powder-actuated fasteners. Sena-Cruz et al. (2012) conducted a similar comparison to Quattlebaum et al. (2005) and Aidoo et al. (2006) by tested reinforced concrete beams strengthened with the same three methods under monotonic and fatigue loads. There was no fatigue failure. The post-fatigue monotonic behaviour showed that the greatest decrease in stiffness due to fatigue loading was observed for beams strengthened with NSM strips.

2.1.5 Fatigue of FRP-To-Concrete bonds

The strength of bonded joints depends on the cohesive strength of the adhesive (O'Neill *et al*., 2007), the degree of adhesion to the bonding surface (Täljsten, 2006), and the type of FRP being used (Ko and Sato, 2007). For these reasons, the fatigue life of epoxy material is not representative of the fatigue life of the whole epoxy bond system even if the failure is only in the epoxy layer. Test methods used to evaluate the bonding behaviour of externally-bonded FRP composite sheets and plates under fatigue loading include the single shear (single lap joint) test (Bizindavyi *et al*., 2003; Mazzotti and Savoia, 2009), the double lap joint test (Ferrier *et al*., 2005), the pull-out specimen method for measuring peeling stresses (Khan *et al*., 2011) and the partially bonded beam test (Gheorghiu *et al*., 2004). The single lap joint test gives inaccurate results because it creates undesirable flexural loading. Overall, the available experimental data indicate that the local slippage of FRP-concrete joints increases gradually with cyclic loading (Dai *et al*., 2005; Bizindavyi *et al*., 2003; Yun *et al*., 2008; Nigro *et al*., 2010; Diab *et al*., 2007; Ko and Sato, 2007).

There are three distinct phases in the behaviour of FRP-concrete bonded joints under fatigue loading, as shown in Figure 2.2. During the first phase, the bond mainly sustains damage in the form of micro cracks that cause residual plastic strain with negligible stiffness degradation. In the second phase, macro cracks start to cause stiffness degradation but the joint retains its ability to resist the applied load. Finally, debonding and fracture occur when the cracks propagate to the extent that the joint loses both its stiffness and its capacity to resist the load. The duration of any one phase is dependent on the maximum applied stress and the joint's fatigue limit stress, which determine the fatigue type (high or low fatigue). Where, the first phase be prevalent of the joints behaviour when the applied maximum stress is somewhat greater than the fatigue limit stress.
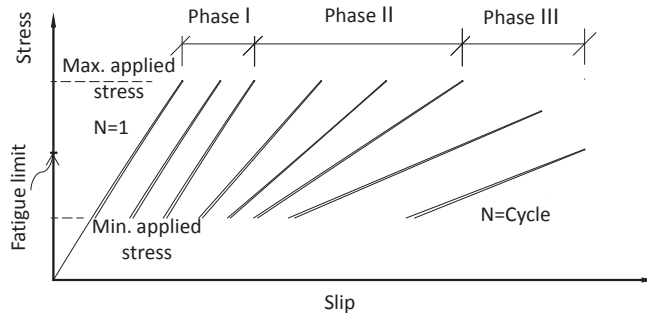
Figure 2.2. Typical bond stress-slip relationship in FRP-concrete joints under high-cycle fatigue.

The general behaviour is similar to that observed under monotonic loading except for the rate of debonding propagation. The stress-slip slope (stiffness degradation) increases with increasing stress amplitude (Dai *et al.*, 2005; Bizindavyi *et al.*, 2003; Yun *et al.*, 2008). Debonding can cause multiple different types of failure; debonding between the epoxy adhesive and epoxy primer, debonding into the coarse aggregate (splitting of the concrete cover) and debonding between the plies for joints with multiple plies (Bizindavyi *et al.*, 2003).

Dai *et al.* (2005) and Bizindavyi *et al.* (2003) showed that an increase in bond length under cyclic fatigue loading led to an increase in fatigue life unlike under static loading, where an increase in length beyond the effective length made no difference. Nigro *et al.* (2011) found that under cyclic loading with 70% of the maximum debonding static load, the fatigue loading was negligible even when the bond length was less than 50% of the theoretical effective bond length for carbon fibre sheets and plates. Diab *et al.* (2007) showed that the fatigue endurance limit (2 million cycles) is reached when the stress level is below 30% of the maximum debonding static load.

2.2 Building codes and researchers' recommendations

Analysis of various building codes and the primary research literature revealed the following recommendations concerning epoxy-based methods:

1. The ACI 440.2R-08 (2008) code recommends that in order to prevent fatigue and creep failure, epoxies used with GFRP, AFRP and CFRP materials should have a total stress to FRP ultimate strength ratios of less than 0.2, 0.3 and 0.55, respectively. Diab and Wu (2008), Breña et al. (2005) and Harries and Aidoo (2006) considered this recommendation to be inadequate and impossible to achieve. Additionally, it has been shown (Harries and Aidoo, 2006) that the bond is also affected by fatigue loading. The author considers the ACI recommendation adequate to ensure that the FRP itself does not fail under fatigue load.

2. The Japanese Society of Civil Engineers (JSCE, 2001) recommended a reduction factor of $\mu = 0.7$ for the interfacial fracture energy relating to the bonding of fibre-

reinforced polymer sheets to concrete under fatigue loading to mitigate peeling failures of the FRP as shown in Eq. 2.1, which can be used to check that the FRP stress is below a threshold value which ensures that its failure will occur only after the rupture of the reinforcing steel. Peeling failure will not occur if the stress in the FRP, σ_f (N/mm^2), satisfies Eq. 2.1:

$$\sigma_f \leq \sqrt{\frac{2\mu G_f E_f}{n t_f}} \qquad\qquad (2.1)$$

Here, G_f is the interfacial fracture energy corresponding to debonding of the continuous FRP sheet and the concrete (N/mm), E_f is the Young's modulus of continuous fibres (N/mm^2), n the number of plies of continuous fibre sheets, and t_f is the thickness of one layer of continuous fibre sheet (mm).

Harries and Aidoo (2006) considered this reduction factor too small compared to the recommended reduction factor for a monotonic load to prevent debonding. In the author's opinion, this recommendation is suitable for cases involving high cyclic fatigue, where the load is less than the beam's static yield load.

3. The Italian design guide CNR-DT200 (NRC, 2004) recommends a long-term conversion factor, $\eta = 0.5$, which is multiplied by selected properties of the FRP composite to define thresholds that should not be exceeded in order to avoid fatigue failure. However, this approach does not account for the stress range of the fatigue loading or the properties of the concrete.

4. The ISIS Canadian design manual (ISIS Canada, 2008) only recommends a reduction factor to account for the effect of creep on FRP composites without fatigue load.

5. The 2010 model code suggests different stress ranges for different types of FRP bar that can be used as reinforcement bars in concrete members. These values are unsuitable for use with NSM systems due to the different bonding materials used in such cases.

6. The Concrete Society: Technical Report No. 55 also recommends limits on the permissible stress range in the FRP for fatigue applications. These limits are 80%, 30%, and 70% of the ultimate capacity of the FRP element for CFRP, GFRP and AFRP materials, respectively. The resulting thresholds are intended to control the fatigue behaviour of the FRP plates or strips bonding application by limiting the cyclic stresses applied to the FRP material. In a realistic plate bonding application of CFRP, it would be nearly impossible to achieve a stress equal to 80% of the ultimate capacity of the CFRP because the strengthened beam would fail by some other means first: either the CFRP element would delaminate from the concrete substrate or the reinforcing steel would fail followed by CFRP delamination.

Kim and Heffernan (2008), as well as Barnes and Mays (1999) recommended that the conventional approach of using unstrengthened reinforced concrete to prevent fatigue failure should be used for FRP-strengthened structures; in the author's opinion, this suggestion is reasonable. Ferrier et al. (2011) did not account for the stress range in the reinforcing steel and instead suggested that the shear stress between the concrete and CFRP should be limited to 0.8 MPa to prevent fatigue failure over 1×10^6 cycles. Yao et al. (2006) proposed that in order to prevent fatigue failure of the CFRP, the fatigue strength of a carbon fibre laminate strengthened reinforced concrete beam should be 0.58 times its ultimate static loading strength. Breña et al. (2005) indicated that the maximum tolerable composite stress in CFRP laminates is 15 to 25% of the CFRP element's ultimate strength, which is lower than the threshold suggested by the ACI 440.2R-08 (2008). Senthilnath et al. (2001) performed fatigue tests on CFRP-strengthened beams with differing degrees of CFRP delamination and showed that even when the extent of delamination was 16000 mm², corresponding to the upper limit defined as tolerable by the ACI 440.2R-08 (2008), the flexural fatigue behaviour of the beam was largely unaffected. These authors also argued that a lap length of 50 mm is insufficient for CFRP sheets under fatigue loading despite this value being recommended when using the MBrace composite strengthening system (2002) under a static load. Yang and Nanni (2002) recommended a lap splice length of 101.6 mm, if the maximum applied stress does not exceed 40% of the ultimate static strength. Diab et al. (2007) recommended that the FRP fatigue stress for FRP strengthened beams should not exceed 30% of the static bond capacity of the FRP-concrete interface. Gunes et al. (2006) recommended that a minimum bond anchorage be provided on the end regions of the FRP flexural reinforcement, at a distance equal to the beam depth to ensure improved cyclic load performance. By combining these recommendations, it is possible to establish robust criteria for designing strengthened beams subject to fatigue loading in terms of the properties of the bonding material, FRP element, and reinforcing steel.

2.3 Theoretical modelling of FRP-strengthened RC beams under fatigue loading

The mechanical and deformation properties of RC beam components change significantly over time under fatigue loading, thus causing residual strains (Holmen, 1982).However, fatigue rupture of the internal reinforcement appears to govern the failure of RC members strengthened with CFRP materials in flexure. Even under high initial compressive stresses where fatigue of concrete might be expected, reinforced members fail systematically due to the brittle fatigue fracture of the steel reinforcing bars (Johansson, 2004). This is due to concrete's high capacity for redistributing stresses. It is therefore recommended (Barnes and Mays, 1999) that the stress ranges in the rebars of strengthened members should not exceed those permitted for unstrengthened RC members.

Theoretical models for describing the effects of fatigue on strengthened reinforced concrete beams have been developed based on several different approaches. Most existing models are based on S-N curves and the static stress state (Mahal et al., 2011; Breña et al., 2005; Al-Hammoud et al., 2010). This approach focuses exclusively on the number of cycles to failure without considering the redistribution process or the evolution of strain, and the influence of the fatigue process on the response of reinforced concrete is not completely understood.

The damage theory approach assumes that the rate of damage accumulation is independent of the level of applied stress. This is a poor assumption because materials' responses are greatly influenced by the levels of applied load. Additionally, the linear damage rule ignores the effects of loading sequence. Predictions obtained using such models deviate widely from experimental results (Lin et al., 2008; Zheng et al., 2008 and Yao et al., 2006).

The fibre section technique approach describes the fatigue of strengthened reinforced concrete beam using fatigue uniaxial material models of their separate components. The effect of fatigue on the structural response is evaluated by implementing a sectional method whereby the beam's cross section is divided into a number of discrete fibres or segments. This approach is easy to understand and produces accurate predictions that are consistent with diverse experimental measurements of structural concrete elements. In addition, fibre section models can be used to study the evolution of stresses and strains during fatigue loading, and to predict the final type of failure based on the component materials' capacity to redistribute stresses (El-Tawil et al., 2001 and Papakonstantinou et al., 2002).

2.4 Theoretical modelling of the FRP-concrete bond

A number of fatigue life models for FRP-concrete bonds have been developed (Mahal et al., 2011; Bizindavyi et al., 2003; Ferrier et al., 2005 and Ferrier et al., 2011). However, as discussed in the preceding sections, none of these models account for the actual degradation mechanisms and damage processes that occur within the CFRP-concrete joint. Few numerical models have been developed for predicting the behaviour of FRP-concrete interfaces under fatigue loading, and most researchers analysing FRP-strengthened RC beams subjected to fatigue loads have simulated the FRP-concrete bond as a perfect bond with full composite action (El-Tawil et al., 2001; Papakonstantinou et al., 2002 and Al-Rousan and Issa, 2011). The models described in the literature are mainly based on the fracture mechanism, which is unsuitable for simulating high-cycle fatigue, especially in the first phase. Loo et al. (2012) developed a model of the interface bond under fatigue loading based on the degradation of the joint stiffness cycle, but this model did not produce good results when used to analyse joint behaviour during high-cycle fatigue. Diab et al. (2009) presented a model for predicting the bonding fatigue behaviour of the FRP-concrete interface. This model's description of the joint before the initiation of debonding and subsequent fatigue crack growth is based on the creep-fatigue interaction, which was represented by the degradation of the interfacial stiffness. Unfortunately, this approach is also inaccurate when considering the first phase of high cycle fatigue.

3 Experimental Program, results and discussion

3.1 General

Twelve large-scale, simply supported, RC beams were prepared and tested to investigate the fatigue of RC beams strengthened with EBR plates or NSM bars under monotonic and fatigue loading. All of the RC beams had longitudinal steel reinforcements with applied the same steel stress levels. In addition, experiments were conducted to determine how the fatigue life of the beams was affected by varying the properties of the CFRP strengthening element and by pre-cracking of the beam prior to the application of the CFRP element. This section first describes the fabrication of the beams, their strengthening with EBR plates and NSM rods, and the properties of the materials used. It then presents the experimental setup and the instrumentation used to monitor the state of the beams during loading, and finally presents and discusses the results obtained.

3.2 Details of specimens

All beams used in this work were 4000 mm long with a rectangular cross section of 200 x 300 mm as shown in Figure 3.1. Longitudinal reinforcement in tension and compression was provided by two steel bars with nominal diameters of 16 mm. The shear reinforcement, designed to ensure that flexural failure would occur in the strengthened beams, consisted of 10 mm stirrups spaced at 75 mm intervals. Of the 12 tested beams, 5 were strengthened with NSM bars, 5 with EBR plates and two non-strengthened RC beams were prepared for use as controls in static and fatigue loading tests. The cross-sectional area of the FRP materials used in the EBR-strengthened beams was equal to that used in the NSM beams. For beams using EBR plates, strengthening was provided by laminates with a cross sectional area of 1.4 x (100+43) mm, prepared from one 100 mm wide strip of laminate and one 43 mm wide strip, which was prepared by cutting a wider strip to the desired size. A 300 mm wide two-layer U-jacket made from CFRP sheets was wrapped around the EBR-strengthened beams on one side of the mid-span to ensure that failure would occur on the other end of the beam. The NSM beams were strengthened with two 10x10mm CFRP rods with square cross sections, which were placed in grooves that were cut into the beams' soffit surface with a width and depth of 15 and 17 mm, respectively. The plates and rods used in the strengthened test beams were all 3200 mm in length.

Figure 3.2 outlines the procedure used to fabricate the RC beams, which was based on standard building practices. Plastic spacers were placed underneath the steel reinforcement at several points to provide the desired concrete cover (30 mm) at the bottom of the beams. The beams were then prepared using ready-mixed concrete with a specified compressive strength of 65 MPa.
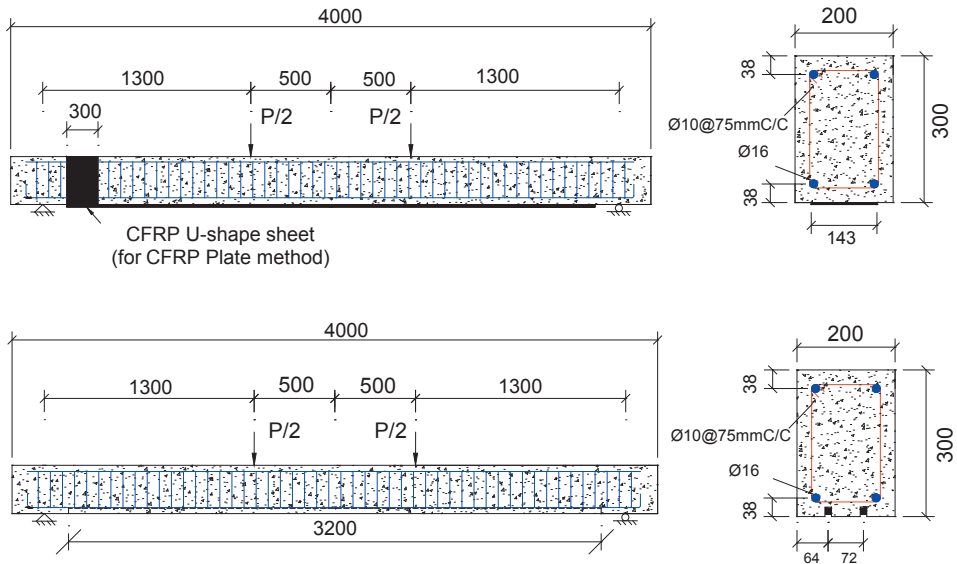
Figure 3.1. Beam geometry and reinforcement details.

Steel cage construction

Forms and cages

Concrete casting

Concrete vibration
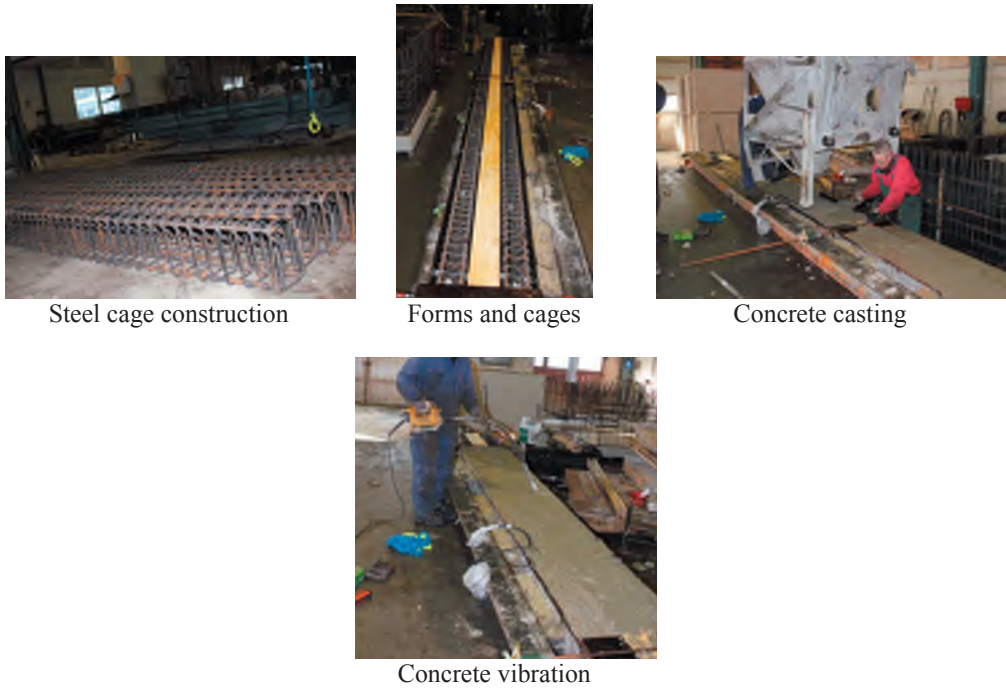
Figure 3.2. Construction of the RC beams.

3.2.1 Strengthening of RC beams with CFRP plate

Before any CFRP could be applied to the concrete surface of the beams, the bottom surface of the concrete beams had to prepare by grinding to provide a rough surface to improve its bonding capacity, as shown in Figure 3.3 (a). The concrete surface was grinded until aggregates with a diameter of approximately 5 mm became visible. The ground surface was then cleaned by airbrushing to remove dust or debris and fine particles. After this surface preparation, a primer was mixed according to the supplier's instructions and applied to the concrete surface, see Figure 3.3 (b). After the primer had cured (around 6 hours after its application), the two-component epoxy adhesive was mixed, and a uniform 2 mm thin layer of the epoxy adhesive was applied to the CFRP plate using a special applicator. The CFRP plate was placed in position on the concrete surface and pressed onto the plate using a hard rubber roller until the epoxy was forced out on both sides. To ensure a good bond with the concrete, a uniform pressure should be applied along the entire length of the plates. The strengthening of RC beams with CFRP plates was completed by scraping off the excess epoxy, see Figure 3.3 (c). The application of the primer and epoxy, and the hardening, were all conducted at room temperature, i.e. 21 °C.

| (a) Grinding | (b) Priming | (c) CFRP and epoxy |
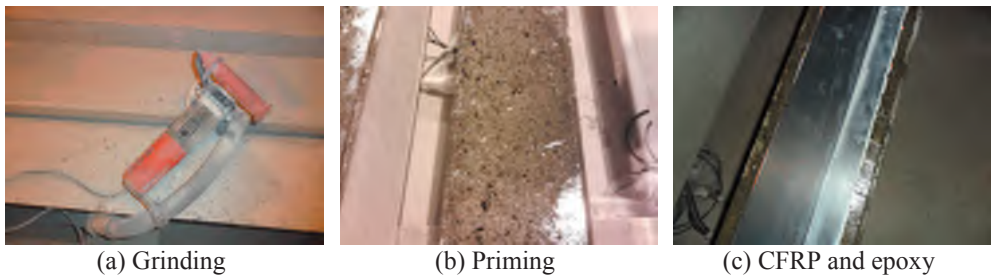
Figure 3.3. CFRP plate installation.

After 7 days of adhesive curing, the beam was U-wrapped at one end with two layers of CFRP sheets (300 mm wide), with the fibre direction being perpendicular to the longitudinal axis of the beam, to ensure that debonding of the EBR plates would occur at the beam's other end (see Figure 3.4). As before, the concrete surface at this location was prepared by grinding and applying primer. The concrete was then coated with the epoxy adhesive and the first CFRP sheet was placed into position and pressed with a roller. Additional epoxy was then applied and pressed with a rubber plate, after which the second CFRP sheet was applied over the top of the first and pressed down using the roller and additional epoxy.
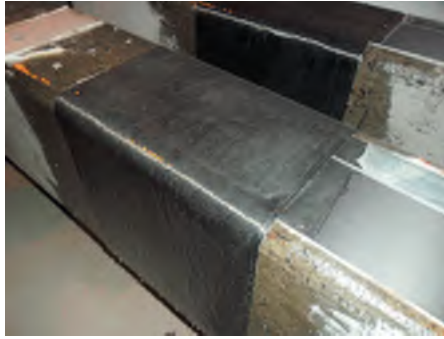
Figure 3.4. CFRP sheet installation.

3.2.2 Strengthening of RC beams with NSM

The installation of the NSM bars began with the cutting of grooves to accommodate them in the tension surfaces of the concrete beams. The grooves were cut using a special concrete saw with a diamond blade. Each groove was approximately 15 mm wide and 17 mm deep to accommodate the 10x10mm quadratic bars, as shown in Figure 3.1. Based on the research of De Lorenzis and Nanni (2002) and Hassan and Rizkalla (2004), larger groove sizes provide greater bond strengths than smaller ones. On the other hand, the depth of the groove is limited by the placement of the steel reinforcement, and the width should not be excessive to limit construction costs. First, the grooves were cleaned and compressed air was used to remove debris and fine particles to ensure proper bond formation between the epoxy adhesive and the concrete, see Figure 3.5 (a). The primer was then applied to the concrete surface as shown in Figure 3.5 (b), after which the groove was half-filled with epoxy adhesive and the CFRP bars were lightly pressed into the epoxy. The grooves were then filled with more paste and the surface was levelled, after which excess adhesive was removed with a spatula, see Figure 3.5 **(c)**. The thickness of the adhesive surrounding the NSM bars was determined to be 2.5 mm on all three bonded sides. As in the EBR case, the bonding and hardening were performed at 21 °C. The adhesive was allowed to harden for at least 7 days before testing.
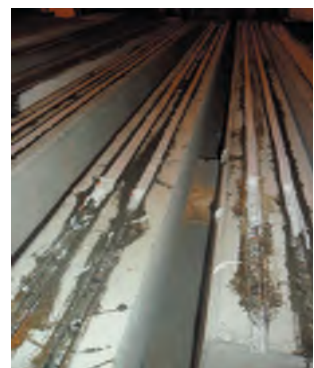
| (a) Groove | (b) Primer | (c) CFRP and filling epoxy |

Figure 3.5. NSM CFRP bar installation.

3.3 Material properties

The mechanical properties of the reinforcing steel bars were determined in experimental tensile tests using 6 of the deformed 16 mm diameter steel bars used as longitudinal reinforcements and 3 of the deformed 10 mm diameter steel bars used as stirrups. The tests were conducted according to international standards (ISO 6892-1:2009). The test setup is shown in Figure 3.6. An extensometer with a 50 mm gage length was installed to measure the bars' strains. The mean yield strength and modulus of elasticity of the longitudinal steel reinforcements were 578 MPa and 208 GPa, respectively, while the corresponding values for the stirrups were 533 MPa and 202 GPa, respectively. Stress-strain curves for one of the tested longitudinal steel reinforcement bars and one tested stirrup are shown in Figures 3.7 and 3.8, respectively. Steel yielding and strain hardening were clearly observed in both types of steel rebar.

Figure 3.6. Apparatus used to determine the steel bars' mechanical properties.
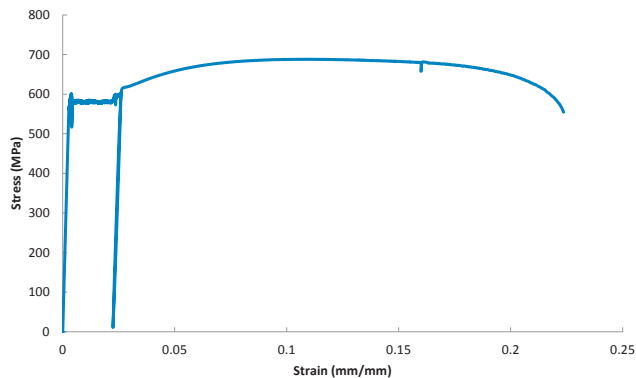
Figure 3.7. Stress-strain curve for a longitudinal steel reinforcement bar (16 mm).
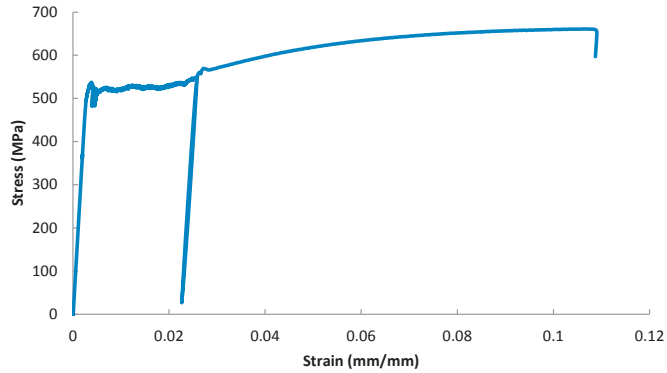
Figure 3.8. Stress-strain curve for a steel stirrup (10 mm).

The compressive and tensile strength of the concrete were determined according to Swedish standards SS 12390-3:2009 (SIS,2009a) and SS 12390-6:2009 (SIS,2009b), respectively, while the reinforced beams were being tested. The test setup is shown in Figure 3.9. The tests were performed using concrete cubes, and each test was performed in triplicate so that average values could be computed. The mean compressive and tensile strengths of the concrete used can be seen in Table 3.1.

Figure 3.9. Apparatus used to determine the tensile and compressive strength of the concrete, and the failure mode of a tested cube during a tensile test.

Three-point bending tests on a twelve-notched beam were performed to determine the fracture energy of the four concrete batches used to prepare the beams. The notches were made using a suitable saw (see Figure 3.10). The procedure followed in these experiments was based on the RILEM recommendations (1991); the test setup is shown in Figure 3.11. The specimens' fracture energy G_F, which represents the energy released during the cracking process, is

24

commonly calculated by dividing the surface under the load–crack mouth opening displacement curve, i.e. the shaded area in Figure 3.12, by the notch thickness. The average fracture energy of the concrete used in this work can be seen in Table 3.1.

Figure 3.10. Manual sawing of the prism.

Figure 3.11. Photograph of set up used to determine the fracture energy of the concrete.
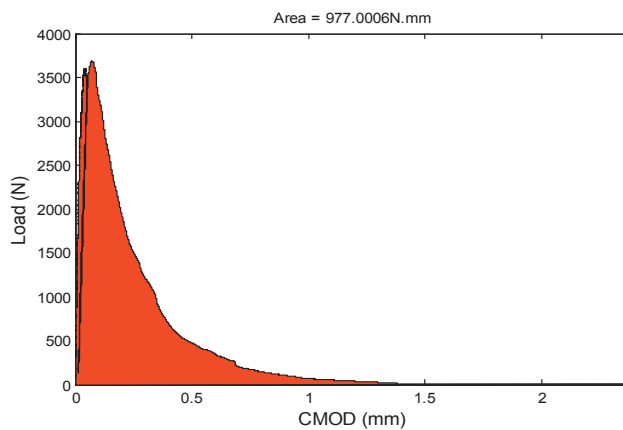
Figure 3.12. Typical of Load-crack mouth opening displacement (CMOD) diagram for the concrete used in this work.

Table 3.1. Beams tested.

Specimen	Type of load	Concrete compressive strength (MPa)	Standard deviation	Concrete Tensile strength (MPa)	Standard deviation	Fracture energy (N/mm)	Young's modulus of CFRP (GPa)
B13-0-F	Fatigue	71	0.71	4.2	0.28	0.1655	-
B10-NE1-F-C	Fatigue	73	1.34	4.3	0.02	0.1714	200
B9 -PE1-F-C	Fatigue	72	2.28	3.9	0.24	0.1714	200
B8-NE2-F	Fatigue						
B7-NE2-S	Static	75	1.47	4.5	0.19	0.1768	150
B3-NE1-F	Fatigue						
B4-NE1-S	Static	71	1.50	4.7	0.26	0.1448	200
B1-PE1-F	Fatigue						
B2-PE1-S	Static	71	2.18	4.2	0.16	0.1448	200
B5-PE2-S	Static						
B6-PE2-F	Fatigue	72	0.26	3.9	0.34	0.1768	150
B11-0-S	Static	64	1.40	4.0	0.51	0.1655	-

Two types of NSM bars and EBR plates were used. NSM strengthening was performed with either StoFRP BAR IM 10C or StoFRP BAR E 10C bars, both of which have cross-sectional areas of 10x10 mm. The IM bars have a modulus of elasticity of 200 GPa while that of the E bars was 150 GPa. EBR strengthening was performed with either StoFRP Plate IM 100C and StoFRP Plate IM 60C or StoFRP Plate E 100C and StoFRP Plate E 50C. All of these plates were 1.4 mm thick. Two different epoxies were used in the tests, StoPox SK41 for EBR plates and NSM bars, and StoPox LH for sheets. The former is a high viscosity adhesive whereas the latter is a low viscosity adhesive that easily wets carbon fibres. The properties of these materials are shown in Table 3.2.

Table 3.2. Properties of the carbon fibre reinforced polymers and adhesives used.

Material	Compressive strength (MPa)	Tensile strength (MPa)	Young's modulus (GPa)	Ultimate strain (‰)
Composite[a]				
StoFRPComposite E	-	1800	150	12
StoFRPComposite IM	-	2900	200	14
Adhesive[a]				
StoPox LH	100	90	3.50	-
StoPox SK 41	82	19	7.87	-

[a] Supplier's data

3.4 Instrumentation

The test instrumentation is shown in Figure 3.13. The beams were equipped with strain gauges on their internal steel bars (Figure 3.14) and FRP composites, as shown in Figures 3.15 (a) and (b). In addition to the strain gauges (SG), the midpoint deflection and support settlement were determined using linear voltage differential transducers (LVDTs), and crack opening displacement (COD) gauges were fitted at the one end of the NSM bar and plate of the each beam as shown in Figures 3.16 (a) and (b).
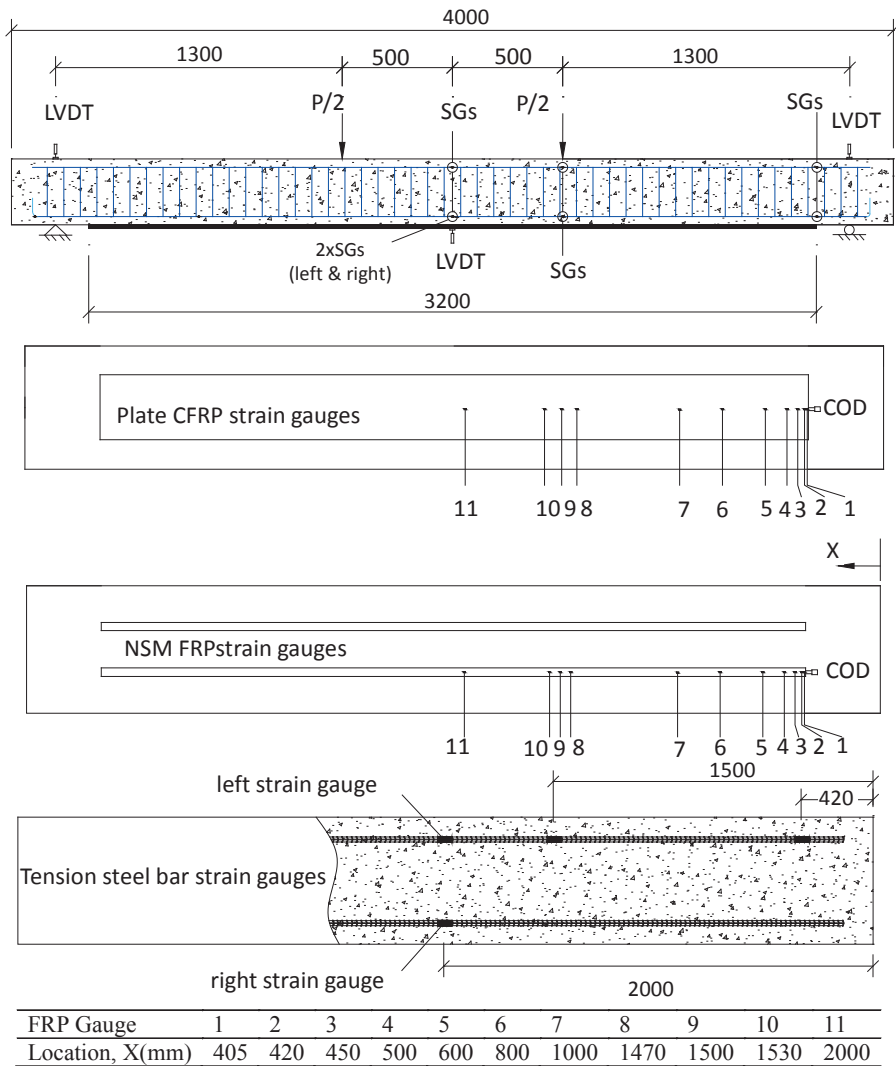
Figure 3.13. Locations at which different instruments were located along the beams' length.

FRP Gauge	1	2	3	4	5	6	7	8	9	10	11
Location, X(mm)	405	420	450	500	600	800	1000	1470	1500	1530	2000

27

Figure 3.14. Installation of steel strain gauges.

(a) Plate   (b) NSM bar

Figure 3.15. Positioning of FRP composite strain gauges.

(a) Plate   (b) NSM bar

Figure 3.16. Positioning of COD gauges.

The ARAMIS optical strain measuring system (GOM-Gesellschaft für Optische Messtechnik GmbH), see Figure 3.17, was used to monitor crack growth during the fatigue and monotonic loading of the beams by monitoring the principle strain distribution within a defined area of each beam's surface. This technique requires a stochastic pattern to be painted onto the specimen's surface as shown in Figure 3.18. The measuring system consists of two high-resolution cameras connected to a computer running the ARAMIS image recognition software, which matches the images from the cameras. ARAMIS can calculate the strain at each point on the monitored surface by using digital image correlation in conjunction with established theories of solid mechanics.

The system was calibrated for a 700 mm × 560 mm field of view using standard calibration panels (see Figure 3.19) as described in the User's Manual for the ARAMIS system (ARAMIS manual, 2007 and Xavier et al., 2012). The calibration process yielded a set of calibration data including camera angles and values for the distance between the object and each camera. After calibration, the measured field of view for all beams other than B3-NE1-F was set to 750×300 mm, for which a field of view of 600×300 mm was chosen. The calibration deviation in all tests was ±0.021 pixels.

In brief, the ARAMIS system works by recording sequential images of the specimen as its load is increased during monotonic loading or while it is under cycle load during fatigue testing. Each recorded image defines a separate stage in the loading process; the number of stages depends on the type of test being conducted and the specimen's behaviour. The first image in all tests is referred to as stage 0 and was used as a reference image of the undeformed specimen for displacement calculations. The stage 0 image for the first load was acquired with no load on the specimen; for all subsequent load cycles, the stage 0 image was acquired with the specimen under the minimum load for that cycle. The region of interest (750 mm × 300 mm) in each of the initial images of each specimen was defined manually within the ARAMIS system. The ARAMIS software can identify points on the specimen surface from the images and divides the surface into facets (pixels). Each facet contains individual greyscale information and can, therefore, be traced throughout the experiment. To determine the surface displacement of the target object, each facet is tracked from the initial stage 0 image to the next, creating a series of data points that are mapped to create the displacement field. This process is discussed at greater length in Paper III.

Figure 3.17. Configuration of the ARAMIS optical strain measuring system.
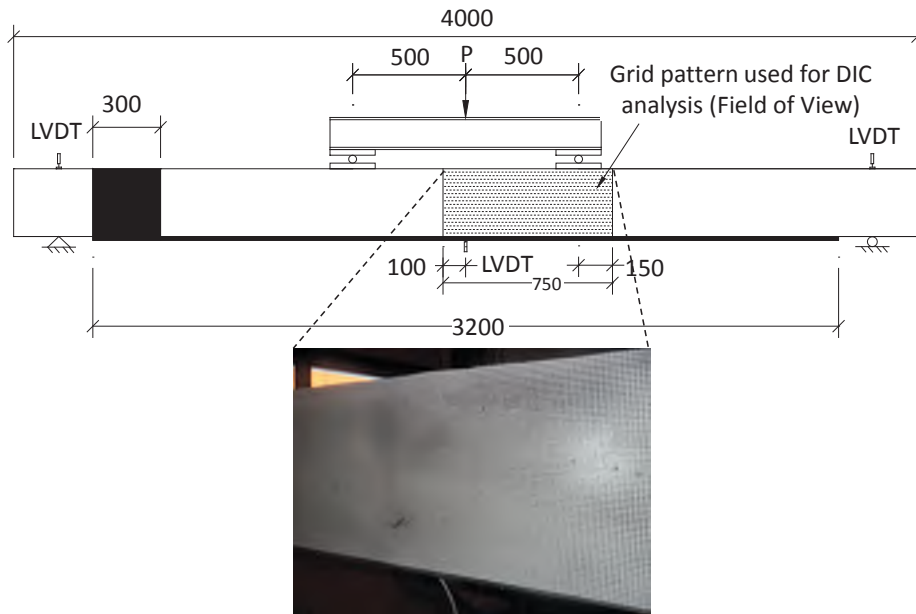
Figure 3.18. Location of the region of interest on the beam, and the stochastic pattern used for photometric strain measurement.

Figure 3.19. Calibration of the ARAMIS optical strain measuring system.

3.5 Test setup and Procedure

The 12 reinforced, simply supported, concrete beams were tested in a four-point bending configuration. The span of each beam was 3600 mm, as shown in Figure 3.20. The beams were named systematically: control specimens are labeled "0" whereas CFRP-strengthened specimens are labelled "N" or "E" corresponding to NSM bar- and EBR plate-strengthening, respectively. The labels E1 or E2 are then used to designate specimens strengthened with CFRP reinforcement having a modulus of elasticity of 200GPa and 150GPa, respectively. The

symbols F or S designate specimens under fatigue and static load, respectively; finally, the label C indicates that the beam was pre-cracked before strengthening. Thus, for example, specimen B10-NE1-F-C is a pre-cracked beam strengthened with NSM bars having a modulus of elasticity of 200 GPa.

One beam of each type (NSM, EBR) was pre-cracked under a load of 24 kN before strengthening with CFRP plates or rods having a 200 GPa modulus of elasticity. Cracking at 24 kN produced main cracks with a width of around 0.25 mm, which is approximately 28 % of the ultimate load of the reference beam. A minimum fatigue load of 6 kN was applied to the strengthened and unstrengthened beams in order to avoid impact loads during cycling. The reinforcing steel in both the strengthened beams and the unstrengthened controls was subjected to the same stress range (258 MPa). This value was chosen to allow for a design fatigue life of 600,000 cycles using the Tilly and Moss model (Barnes and Mays, 1999). Based on this stress range and the minimum applied load, the calculated maximum applied loads for the unstrengthened control beams and their strengthened counterparts were 38.7 kN and 64 kN, respectively. In the fatigue tests, all of the specimens were loaded at a rate of 1.7 Hz. This frequency is within the range imposed by vehicular loads travelling over bridge decks (Masoud et al., 2005). In the first cycle, the load was applied monotonically in order to monitor the cyclic load damage and cracking pattern. Thereafter, a sine wave load was applied. The fatigue loading was terminated after 600,000 fatigue life cycles in all cases. After the $600,000^{th}$ cycle, beams that had not yet failed were loaded monotonically until failure under displacement control.

For photometric strain measurement, the servo/hydraulic load frame was controlled by the ARAMIS software, which can link images to the corresponding maximum and minimum load levels during fatigue testing, or the corresponding monotonic load level for static tests. Therefore, the strains determined by the optical measurements correspond to the difference in strain between the maximum and minimum loads within a cycle for fatigue test. During each fatigue test, the ARAMIS system was used to record images of the beam over the course of the first cycle, starting with a reference image at zero load. The imaging system and beam were then kept in the same place to ensure that the deformations in subsequent cycles could be compared to the first cycle reference data. Additional recordings were performed during the 10,0005th, 100,000th, 200,000th, 300,000th, 400,000th, 500,000th and 600,000th cycles. For each of these cycles, the ARAMIS system recorded two images, one at the minimum and one at the maximum load; the minimum load image was treated as a reference for that cycle.

Figure 3.20. Beam test setup.

3.6 Test Results and Discussion

Table 3.3 summarizes the test results in terms of the failure modes, the number of load cycles, the number of cycles until steel bar rupture, and the load at failure under monotonic loading for those specimens which did not fail under cyclic loading. Table 3.3 also shows the rate of first cycle energy dissipation, which is calculated as the area under the load-deflection curve for the first cycle divided by the maximum applied load for each beam. The curve used to compute this value for the first load cycle of beam B1-EE1-F is shown in Figure 3.21; the corresponding curves for the other beams are presented in Appendix F. Table 3.3 also shows the ratio of the beam's remaining fatigue life after the first rupture of a reinforcing steel bar to its total fatigue life. This section reports the general results of the experimental investigations; the full results are presented in Appendices A, B, C, D, E and G.
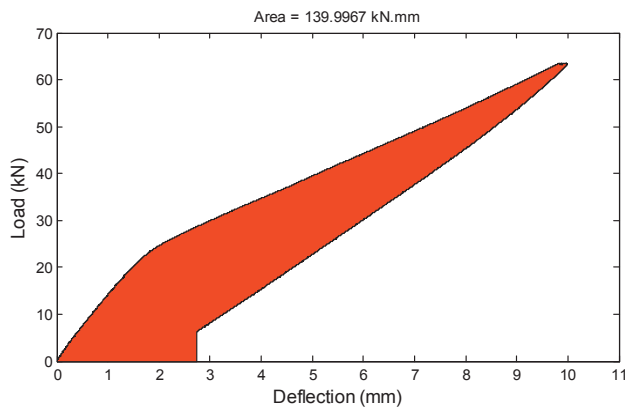
Figure 3.21. Energy dissipation during the first fatigue cycle of beam B1-EE1-F.

Table 3.3. Monotonic and Fatigue loading testing results.

Beam	Load range (kN)	1st cycle dissipation energy (Area/ load)	Total No. cycles	Total deflection during last cycle (mm)	No. of cycles at steel ruptures	Percentage of fatigue life remaining after first rupture	Fatigue Failure mode	Ultimate static load (kN)	Static Failure mode
B3-NE1-F	6-64	2.5	437,222	22.9	408,094	6.6	ID*	-	-
B8-NE2-F	6-64	2.3	599,107	54.9	348,245 373,460 463,394 491,492	41.8	ID	-	-
B1-EE1-F	6-64	2.2	520,733	15.9	456,213	12.4	ID	-	-
B6-EE2-F	6-64	2.6	438,593	14.7	416,866	4.9	ID	-	-
B9-EE1-F-C	6-64	1.7	600,000	11.7	-	-	-	177	ID*
B10-NE1-F-C	6-64	1.6	600,000	23	470,305 503,841	21.6	-	115	ID
B13-0-F	6-38.7	3.1	600,000	12.45	-	-	-	82.7	SY*+CC*
B7-NE2-S	Static	-	-	-	-	-	-	194.4	SY+ID
B4-NE1-S	Static	-	-	-	-	-	-	210.9	SY+ID
B2-EE1-S	Static	-	-	-	-	-	-	177.4	SY+ID
B5-EE2-S	Static	-	-	-	-	-	-	169.5	SY+ID
B11-0-S	Static	-	-	-	-	-	-	86.1	SY+CC

*ID=intermediate debonding, CC=concrete crushing, SY=steel yielding

3.7 Beam behaviour under monotonic loading

The midspan deflections of the monotonically loaded beams are plotted against the applied loads in Figure 3.22. The initial stiffness of the strengthened specimens is essentially equal to that of the unstrengthened control beams before cracking because the laminate has relatively little influence on the second moment of inertia of the uncracked section. The post-cracking stiffness of the strengthened beams is higher than that of the unstrengthened beam. This was attributed to the restraint of crack opening and growth by the external strengthening, which increased the beams' stiffness. The increases in stiffness and ultimate strength are largely dependent upon the properties of the FRP material and method of strengthening beams. In the case of beams B4-NE1-S and B7-NE2-S, the capacity of the strengthened beam increased with the stiffness of the bars. A similar result was observed with the plate-strengthened beams B2-EE1-S and B5-EE2-S, which had capacities of 177kN and 173kN, respectively.

Regardless of the strengthening method used, beams strengthened with FRP elements having the same modulus of elasticity (i.e. B4-NE1-S/B2-EE1-S and B5-EE2-S/B7-NE2-S) exhibited identical stiffnesses (demonstrated by the identical slopes of their load- deflection curves) until the applied load became equal to the beam's maximum capacity. The strengthened beams were also less ductile than the control. In addition, the presence of the CFRP laminate influenced the crack pattern: strengthened beams formed fewer and narrower cracks than the

control, and the cracks were more evenly distributed along the strengthened beams' lengths at a given load level. The average crack spacing in beams strengthened with EBR plates (90mm to 100mm) was greater than in those strengthened with NSM bars (80mm to 90mm). This may be because the contact area between the plate and concrete was greater than that between the bars and the concrete, making the plate-strengthened beams more resistant to crack formation and growth. The load carrying capacity of beams strengthened with NSM bars was greater than that of beams strengthened with EBR plates because of the stronger bonding between the bars and the concrete. The failures of all of the strengthened beams were initiated by intermediate crack interfacial debonding at the midspan which then progressed towards the supports until the force acting on the CFRP could not be sustained by the anchorage length. At this point, a sudden debonding failure occurred. The strains distribution in tensile steel bars and CFRP of all beams are presented in Appendix B.2 and the figures of failure modes for all beams are presented in Appendix E.1.The full details of the monotonic test results are presented in the author's report (Mahal, 2015) and paper II.
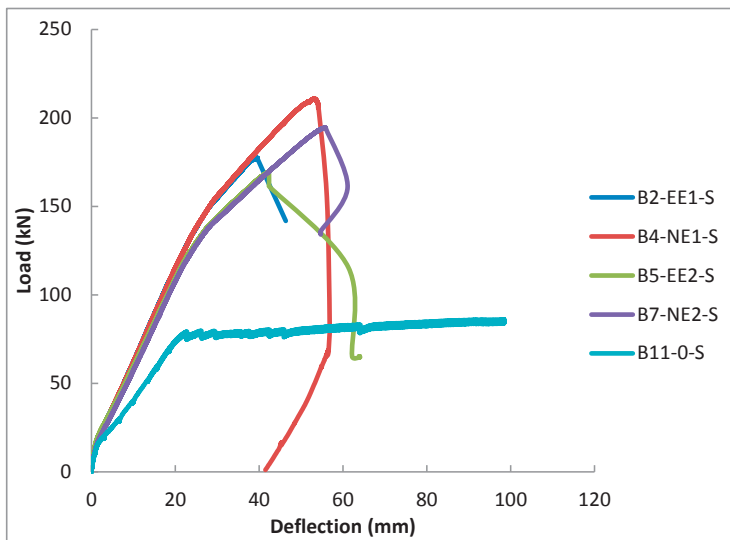
Figure 3.22. Load-midspan deflection under monotonic loading.

3.8 Beam behaviour under fatigue loading

The cracking pattern for the beams tested in fatigue depended on whether the test specimen was a control beam, an un-cracked and strengthened beam, or a pre-cracked and strengthened beam. Both un-cracked and strengthened beams with EBR plates and NSM bars exhibited the same mode of failure under fatigue loading.

Generally, the rate of crack growth and the development of new cracks were rapid during the first cycle of the test but no substantial change in the crack pattern or damage accumulation was observed during subsequent cycles until the tensile steel bars ruptured (see Figure 3.23). The images for the other beams are presented in Appendix D.The crack patterns observed during testing indicated that for the control specimen the distribution of cracks extends over

almost the entire span of the beam. The strengthened beams, however, exhibited a more localized crack distribution within their middle sections. The average crack spacing (150mm) in the unstrengthened beam was higher than in the strengthened beams. In pre-cracked strengthened beams, the presence of CFRP plates or bars reduced the width of existing vertical cracks; new flexural cracks formed between the existing cracks but these new cracks did not extend far beyond the height of the bottom reinforcement layer.
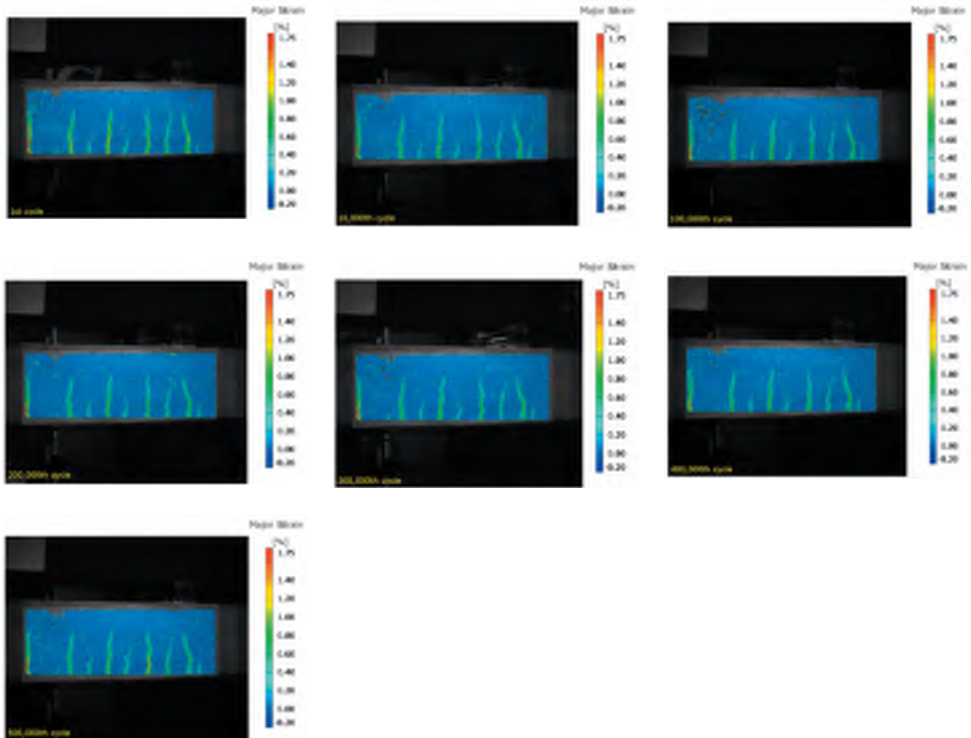
Figure 3.23. Typical principle strain and crack patterns determined using the ARAMIS optical strain measuring system ARAMIS (data shown are for beam B1-EE1-F).

After steel rupture, the fatigue fracture of the reinforcing steel was usually obvious because the fractured bars were visible to the naked eye. The recorded strains also increased sharply when the steel underwent fatigue fracture, as shown in Figure 3.24. However, the CFRP elements continued to carry the applied load. There was no physical sign of debonding in any of the strengthened beams immediately before the rupture of the steel reinforcement.

In every strengthened beam that underwent steel rupture, the first rupture was followed by a sharp increase in the strain of the second reinforcing bar at the point along its length were the first bar ruptured. The second bar therefore ruptured shortly after the first, as shown in Figure 3.24 ; the corresponding curves for the other beams are presented in Appendix B.1.
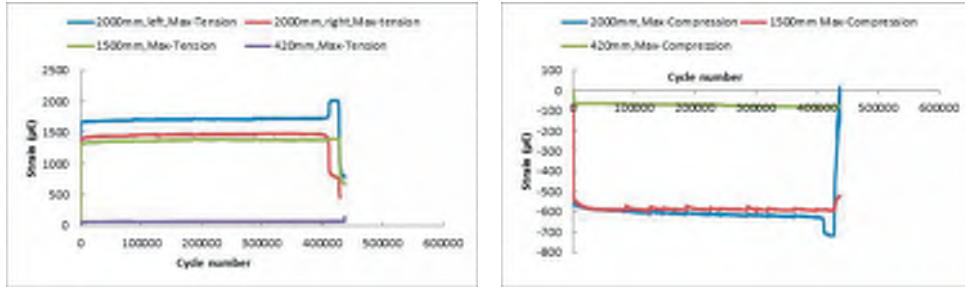
(a) Steel strains
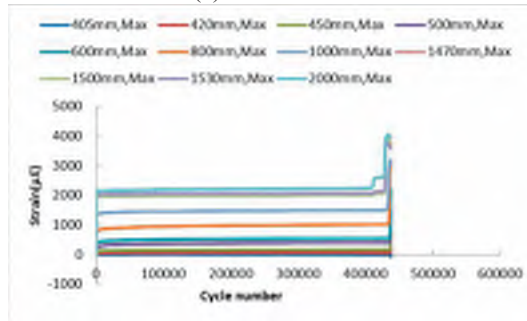
(b)CFRP strains

Figure 3.24. Steel and CFRP strains during fatigue loading of beam B3-NE1-F.

The distributions of the maximum CFRP bond stresses over the half length of the beam at different cycles were determined from the measured maximum strains shown in Appendix B.1 and are plotted in Figures (3.25-3.30). The average shear stress in NSM-strengthened bars between points i and i+1,$\tau_{i,i+1}$ was determined from the strains at these two points using the expression shown below (Carolin et al. 2005):

$$\tau_{i.i+1} = \frac{\varepsilon_{i+1} - \varepsilon_i}{x_{i+1} - x_i} \frac{Et}{3} \tag{3.1}$$

The corresponding values for plate-strengthened beams were obtained using the expression of Nigro et al. (2010):

$$\tau_{i.i+1} = \frac{\varepsilon_{i+1} - \varepsilon_i}{x_{i+1} - x_i} Et \tag{3.2}$$

Here, the strains at points x_i and x_{i+1} are ε_i and ε_{i+1}, E is the Young's modulus of the CFRP element, and t is its thickness.

In general, the shear bond stresses are around zero within the constant moment region for an uncracked section, but varies depending on the external loading and the crack development along the beam depending on the effect of intermediate crack debonding. The calculated bond stresses values oscillate around average levels due to the presence of cracks and the consequent non-uniform transfer of stresses between concrete and FRP. The change of shear stresses directions are clear under applied load directly. High shear bond stresses are seen in the cutoff region as expected and under the applied load point due to formation of a main crack and changing the value of applied shear stress on the beam. Notable increased in shear

stresses in cutoff region and applied load location was occurred during the 10,000 cycles. Then, the shear stresses were almost steady until beams failed or terminated after 600,000 cycles. The shear stresses in beams strengthened with NSM bars (B8-NE2-F and B10-NE1-F-C) at final cycle are increased sharply under the applied load, near location of steel bar rupture, and slightly at cutoff region. These increases indicating intermediate cracks induced debonding failure mode in that beams. Sharply increased of shear bond stresses in both previous locations in beam B3-NE1-F at failure cycle is noticed. These increasing indicating intermediate crack induced debonding failure mode under the load and peeling failure mode in the cutoff region. For beams strengthened with external plate (B1-EE1-F and B6-EE2-F), decreases and increases in shear bond stresses are identified at two locations, under the applied load point and cutoff region, respectively. These data clearly reflect the progression of debonding from intermediate crack to the cutoff point. No sharply increasing in shear bond stresses are noticed in beam B9-EE1-F-C and almost constant shear stress can be noticed until the test was terminated; the corresponding curves for the static beams are presented in Appendix G.
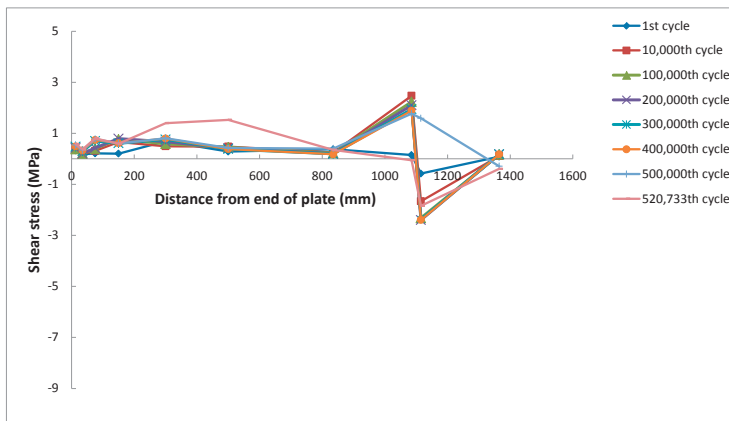
Figure 3.25 Bond stress distributions B1-EE1-F.
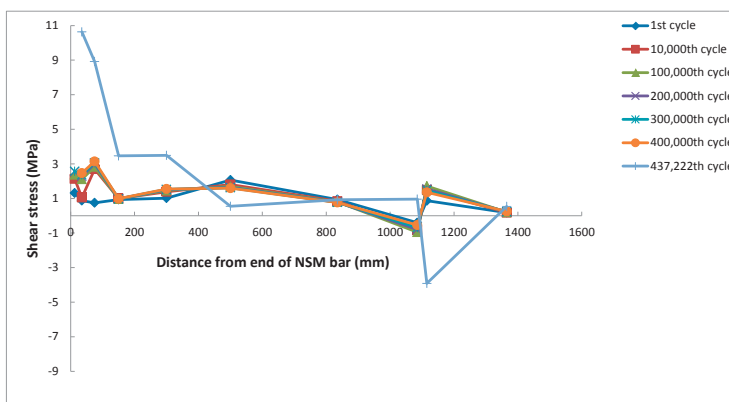
Figure 3.26 Bond stress distributions B3-NE1-F.

37
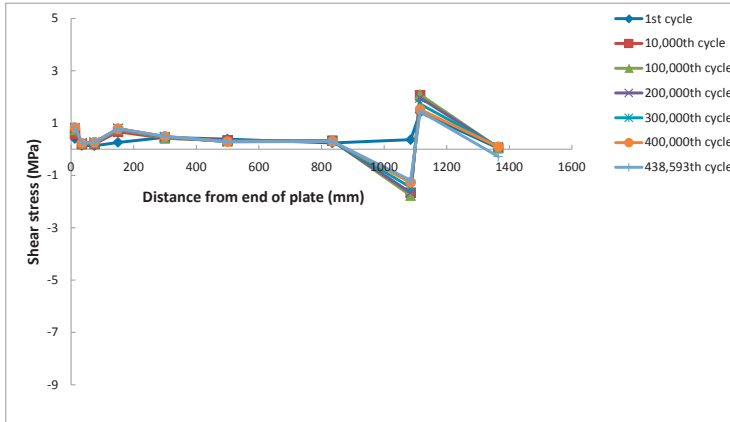
Figure 3.27 Bond stress distributions B6-EE2-F.
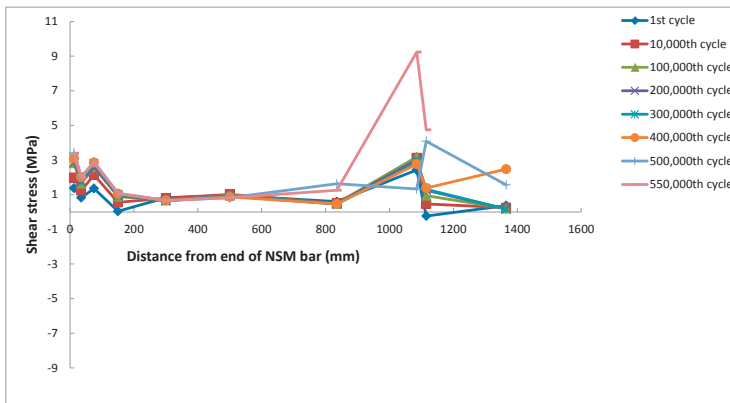
Figure 3.28 Bond stress distributions B8-NE2-F.
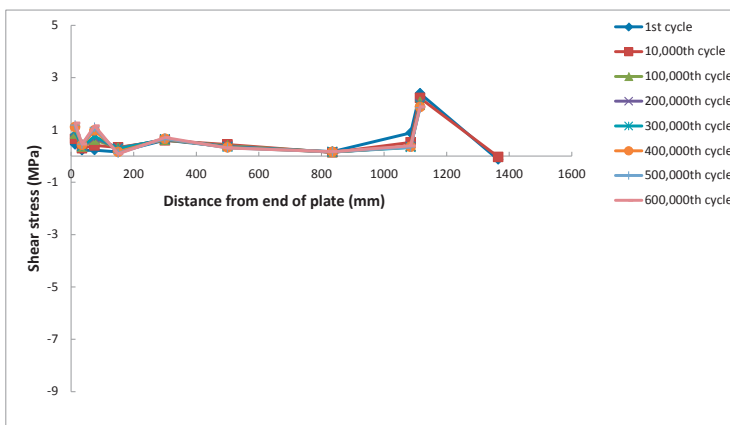
Figure3.29 Bond stress distributions B9-EE1-F-C.
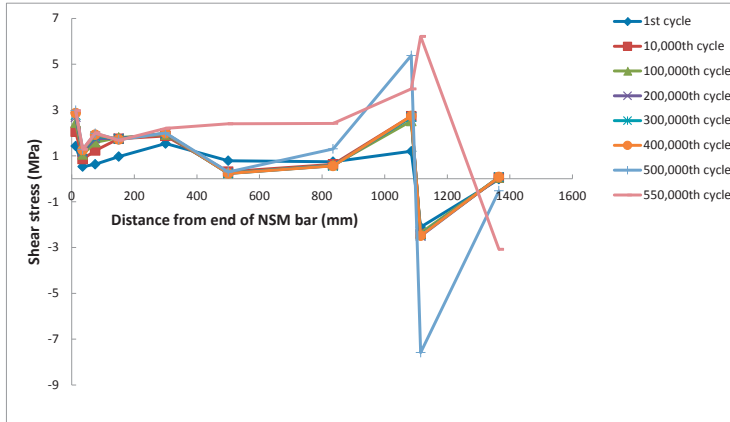
Figure 3.30 Bond stress distributions B10-NE1-F-C.

Beam failure by debonding was initiated when pieces of concrete at the positions where the steel bars had ruptured began to separate from the beam. In all cases, the debonding originated from the position of the steel ruptures and propagated toward the near end of the EBR plate or NSM bar. The delamination failures did not follow the ruptures directly, in contrast to previous reports (Heffernan and Erki, 2004; Barnes and Mays, 1999; Papakonstantinou et al., 2001; and Aidoo, 2004).

Of the 7 beams tested under fatigue loading in this study, 4 failed by debonding of the CFRP reinforcement after the fatigue fracture of one or more of the tensile reinforcing bars. This is the typical mode of fatigue failure for under-reinforced concrete beams. Typical fatigue failure modes of beams strengthened with NSM bars and EBR plates are shown in Figure 3.31 and Figure 3.32; the figures of failure modes for the other beams are presented in Appendix E.2.

Figure 3.31 Fatigue fracture of steel reinforcing bars of NSM strengthened beam (B8-NE2-F).

Figure 3.32. Fatigue fracture of steel reinforcing bars of Plate strengthened beam (B1-EE1-F).

The unstrengthened control beam (B13-0-F) exhibited a much higher rate of energy dissipation during the first cycle than did the strengthened beams because the strengthening elements of the latter limited the extent of crack growth. The rates of energy dissipation in the pre-cracked beams were significantly lower than in the others, suggesting that the presence of pre-existing cracks prevents the dissipation of much energy during the first cycle. Full details of the fatigue test results and discussions of all tested beams can be found in the author's report (Mahal, 2015) and paper II.

3.9 Post-fatigue monotonic behaviour

The specimens that did not fail after 600,000 cycles of fatigue loading (B13-0-F, B9-EE1-F-C and B10-NE1-F-C) were loaded monotonically to failure. Figure 3.33 compares the load-deflection responses of the pre-cracked B9-EE1-F-C and the initially uncracked B2-EE1-S to demonstrate the general effects of fatigue loading. No change in the ultimate load-carrying capacity and stiffness of the member were observed. This is attributed to the fact that the strengthened beams that survived 600,000 fatigue cycles were loaded within their service load levels and thus accumulated little fatigue damage, leaving their ultimate strength unaffected. The overall failure mode observed for this specimen is similar to that for the corresponding monotonically loaded specimens (B2-EE1-S). At 177 kN, debonding was initiated from one of the flexural cracks near the loading point.

Figure 3.34 compares the post-fatigue load-deflection response of the unstrengthened specimen B13-0-F to that of the statically loaded control beam B11-0-S. The post-fatigue monotonic response is almost identical to that of the equivalent statically-loaded beam because once again, the fatigue loading was within the beam's service load levels. The overall failure mode observed for this specimen is similar to that for the monotonically loaded specimens (B11-0-S): after steel yielding, the concrete was crushed at a load level of 82.7 kN. In contrast, Figure 3.35 shows that the ultimate post-fatigue load-carrying capacity of the pre-cracked beam B10-NE1-F-C was substantially lower (by around 45%) than that of the

40

corresponding statically loaded but not pre-cracked beam B4-NE1-S. This was attributed to fractures of the steel bars and accumulated fatigue damage in the fatigued specimen. Debonding was initiated from one of the main flexural cracks near the right loading point at 115kN. This result is interesting because the ultimate load of specimen B10-NE1-F-C was around 33% higher than that of the unstrengthened statically loaded control beam.
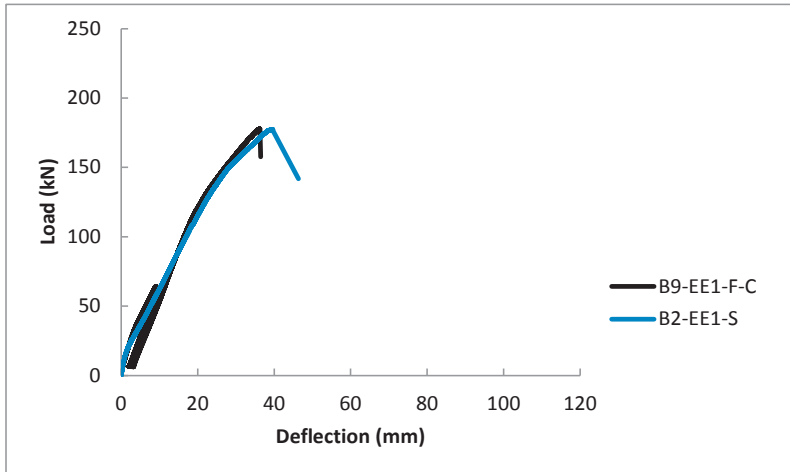
Figure 3.33 Load–deflection curves of beams subjected to post-fatigue monotonic loading: Beams B9-EE1-F-C and B2-EE1-S.
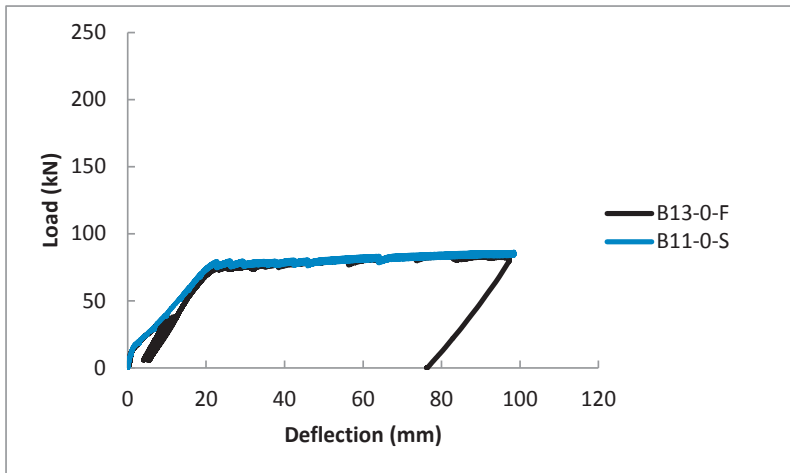
Figure 3.34 Load–deflection curves of beams subjected to post-fatigue monotonic loading: B13-0-F and B11-0-S.
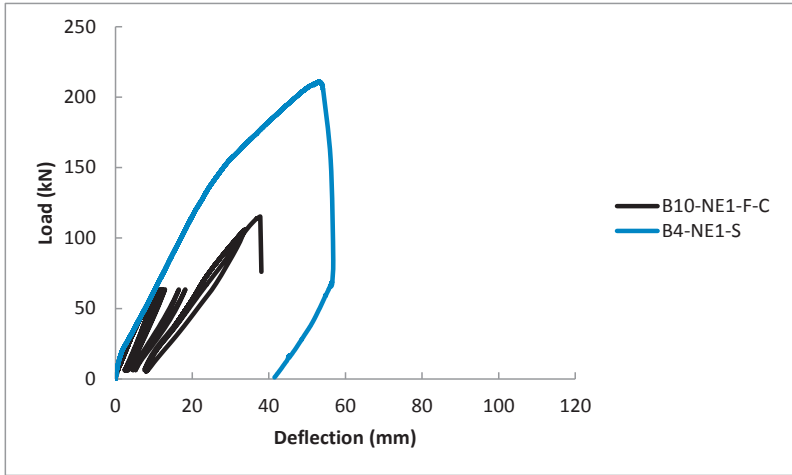
Figure 3.35 Load–deflection curves of beams subjected to post-fatigue monotonic loading: B10-NE1-F-C and B4-NE1-S.

4 Theoretical Analyses

4.1 General

An overall fatigue prediction model should account for both the fatigue life and the fatigue behaviour (deflection and strain). Separating the variables that affect the fatigue life from those which affect the fatigue behaviour would simplify the problem. Therefore, sections 4.2 and 4.6 present fatigue behaviour models of strengthened beams and bonded joints, respectively, while section 4.5 presents fatigue life models for strengthened beams.

4.2 Analyses of strengthened beams

An analytical model was developed to predict the behaviour of reinforced concrete beams strengthened with FRP elements. When RC beams strengthened with FRP are subjected to repetitive cyclical fatigue loading, the stress conditions of the materials are not identical to those experienced during monotonic loading conditions and become significantly different over time. This is because fatigue loading creates residual strains that produce different failure mechanisms to those seen in monotonically loaded beams. This section describes the development of analytical models for predicting the fatigue properties of strengthened RC beam components.

4.2.1 Fatigue of concrete

The fatigue behaviour of concrete under compression stress has been investigated by many researchers. Holmen (1982) proposed that the total maximum strain at any time and at any number of cycles is the sum of two components: the elastic strain, (ε_{ce}), and the concrete compressive strain (ε_{c_N}) with the number of loading cycles (N), knowing the cyclic creep strain:

$$\varepsilon_{c_{N,max}} = \varepsilon_{ce} + \varepsilon_{c_N} \tag{4.1}$$

The evolution of the concrete compressive strain ε_{c_N} with the number of loading cycles (N) is defined by Ferrier et al.(2011) as a function of the mean stress (σ_c^m), stress range (σ_c^r) ,number of cycles (N), loading cycle frequency (f) and the nominal compressive strength of the concrete (f_c'), as shown in Eq. (4.2):

$$\varepsilon_{c_N} = 8.417 \times 10^{-6} \left(\frac{\sigma_c^m}{f_c'}\right) \left[\left(\frac{N}{f}\right)^{\frac{1}{3}} + 3.87 \left(\frac{\sigma_c^r}{f_c'}\right) \left(\frac{N}{9.75}\right)^{\frac{1}{3}}\right] \tag{4.2}$$

Where the mean stress and the stress range are calculated from the maximum (σ_{max})and minimum (σ_{min}) compressive stress applied to the concrete:

$$\sigma_c^m = (\sigma_{max} + \sigma_{min})/2 \tag{4.3}$$

$$\sigma_c^r = (\sigma_{max} - \sigma_{min}) \tag{4.4}$$

The residual strain of concrete (cyclic creep strain) in the compression zone under cyclic loading is known to contribute significantly to the deflection of fatigue loaded beams (Tan

and Saha, 2007). To account for cyclic residual strain, an effective cycle-dependent secant modulus of elasticity of concrete $E_{e,N}$ is considered:

$$E_{e,N} = \frac{\sigma_{max}}{\varepsilon_{c_{N,max}}} \qquad (4.5)$$

Where N is the number of cycles, σ_{max} is the average stress in concrete at the maximum load level and $\varepsilon_{c_{N,max}}$ is total maximum strain at any time.

Knowing the total maximum strain, the cycle-dependent secant modulus of elasticity for concrete in compression ($E_{e,N}$) after N fatigue cycles can be computed.

The material model adopted in the analysis for concrete in compression subjected to fatigue loading is that introduced by Warner and Hulsbos (1966). This model considers the influence of the concrete's modulus of elasticity on the stress-strain relationship; its output is plotted in Figure 4.1 and the corresponding expression for ascending branch is given by equation 4.6:
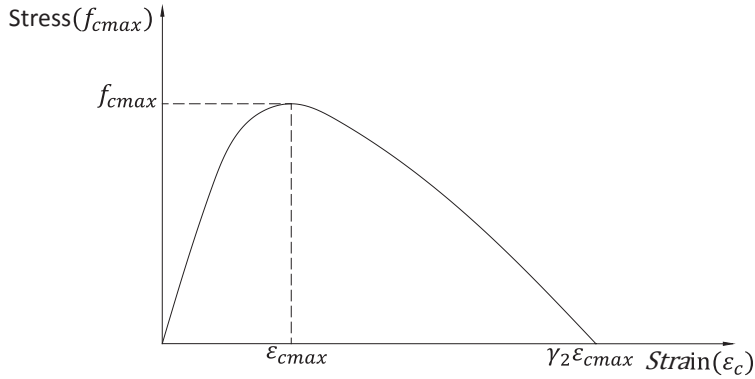
Figure 4.1. Warner's concrete compression model (1966).

$$ff = \gamma EE + (3 - 2\gamma)EE^2 + (\gamma - 2)EE^3 \qquad (4.6)$$

Where

$$ff = f_c / \acute{f}_c$$

$$EE = \varepsilon_c / \varepsilon_{cu}$$

$$\gamma = E_{e,N} \cdot \varepsilon_{cu} / \acute{f}_c$$

Where ff is the normalized concrete stress, EE the normalized strain, γ a dimensionless quantity defining the form of the concrete stress-strain relationship, $E_{e,N}$ the modulus of elasticity of concrete in the nth load cycle, $\acute{f}_c$ the concrete's compressive strength , f_c the stress in the concrete, ε_c the strain in the concrete, and ε_{cu} the ultimate concrete strain.

The concrete's strength is taken to be 0.85 $\acute{f_c}$ instead of $\acute{f_c}$ in the analysis, in line with the ACI 318R-14 (2014). The factor of 0.85 is used to account for differences between concrete in a test cube and reinforced concrete beams, which include their geometry, steel reinforcement, method of load application, and rate of loading, as well as differences in concrete compaction and the water-cement ratio. Concrete under tension is assumed to have no significant tensile strength in cyclic fatigue calculations.

4.2.2 Fatigue of steel

Under high cyclic fatigue conditions (i.e. low fatigue loading), the elastic fatigue mechanism is responsible for the fracture of reinforcing steel because the steel's maximum stress during its fatigue life is below its yield point (Mogami et al., 1990). Fatigue failure of reinforcing steel is caused by a micro-crack that is initiated at a stress concentration on the bar surface. The crack gradually propagates as the stress continues to cycle. Sudden fracture occurs when the crack reaches a critical length at which its propagation becomes unstable. The experimental results of Barsom and Rolfe (1999) suggest that the modulus of elasticity for steel remains unchanged until just before failure during high cycle fatigue. Thus, it is very reasonable to assume that no degradation in residual capacity (strength and stiffness) occurs when reinforcing steel is subjected to service fatigue loading conditions.

The reinforcing steel is therefore assumed to exhibited linear elastic-perfect plastic behaviour, i.e. its unloading and reloading modulus is equal to its initial elastic modulus in the beam's tension and compression zones (see Figure 4.2 and equations 4.7 and 4.8).
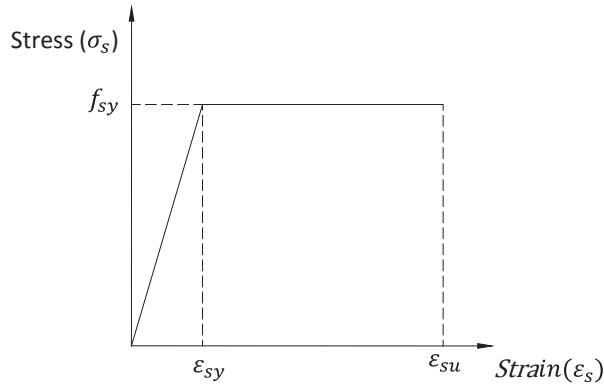
Figure 4.2. Material laws for reinforcing steel.

$\varepsilon_s \leq \varepsilon_{sy}$: $\sigma_s = E_s \varepsilon_s$ (4.7)

$\varepsilon_{sy} < \varepsilon_s < \varepsilon_{su}$: $\sigma_s = f_{sy}$ (4.8)

Where ε_s is the reinforcing steel strain, σ_s the reinforcing steel stress, ε_{sy} the reinforcing steel yield strain, f_{sy} the reinforcing steel yield stress and ε_{su} is the reinforcing steel ultimate strain.

4.2.3 Fatigue of CFRP and epoxy

The fatigue performance of FRP composite materials depends on their matrix composition and, to some extent, on the type of fibre (Curtis, 1989). The fatigue strength is smallest for Glass FRP and greatest for Carbon FRP composite materials. Ferrier et al. (2011) found that the decrease in ultimate strength may be neglected in the case of carbon/epoxy composites, and that cyclic loading degrades the stiffness of FRP laminates according to the following expression:

$$E_{f_N}=m\text{-}n\ log(N) \tag{4.9}$$

Where E_{f_N} is the Young's modulus of the CFRP at cycle (N) , m is the initial Young's modulus, and n is equal to 1100.

The bonding layer between the CFRP laminates and the concrete is assumed to be stiff and not influenced by fatigue loading. This is a reasonable assumption for beams in which failure is initiated in a high moment zone where shear stresses in the epoxy are low (El-Tawil, 2001), and negligible or no slippage or debonding was actually observed between the concrete and CFRP before steel bar rupture during tests.

In the model, the CFRP material is assumed to exhibit linear-brittle failure with the same modulus of elasticity of (E_{f_N}) during unloading and reloading (see Figure 4.3).

$$\varepsilon_{CF}\leq\varepsilon_{CFu}: \ \sigma_{CF}=E_{f_N}\varepsilon_{CF} \tag{4.10}$$
$$\varepsilon_{CF}>\varepsilon_{CFu}: \ \sigma_{CF}=0 \tag{4.11}$$

Where ε_{CF} is the strengthening CFRP strain, σ_{CF} the strengthening CFRP stress, E_{f_N} the modulus of elasticity of strengthening CFRP at cycle (N), and ε_{CFu} is the ultimate strain of the strengthening CFRP.
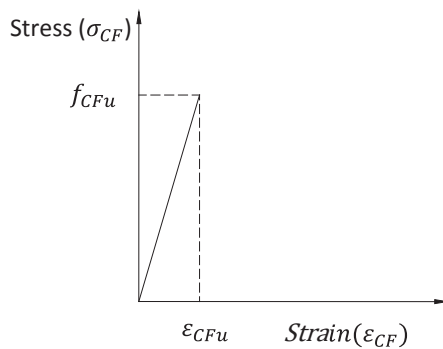
Figure 4.3. Material laws for CFRP.

4.3 Analysis method

The fatigue analyses are based on the fibre section technique with incremental loading during each cycle. The beam's cross section is divided into a number of discrete fibres or segments (see Figure 4.5). The model's output is then obtained by calculating the moment-curvature response for equilibrium axial loads in each fibre during each cycle.

To simulate the fatigue behaviour of a cross section during any cycle, the moment-curvature response is obtained by incrementally increasing the curvature during the cycle and solving for the corresponding value of the applied load. For a given curvature, the moment–curvature response of the section (i.e. the slope of the strain distribution profile) during each cycle can be obtained using an iterative process of adjusting the neutral axis position for a given strain distribution to maintain the horizontal force equilibrium of the section. Based on the assumption that plane sections remain planar after bending, the neutral axis location and the fibre strains are a function of the strain in the topmost fibre, $\varepsilon_{top,N}$, and the curvature, φ.

$$\varepsilon_i = \varepsilon_{top,N} - \varphi y_i \tag{4.12}$$

$$\varphi = \frac{\varepsilon_{top,N}}{c} \tag{4.13}$$

where c is the neutral axis position. The stresses in each fibre are calculated from the fibre strains using the constitutive relationships. The resultant axial force and the bending moment are obtained by summing the results for all of the fibres in the beam's cross-section according to the following equations:

$$\sum_{i=1}^{mm} \sigma_{si} A_{si} + \sum_{j=1}^{nn} \sigma_{cj} A_{cj} + \sum_{l=1}^{kk} \sigma_{CFl} A_{CFl} + Tol = F = 0 \tag{4.14}$$

$$\sum_{i=1}^{mm} \sigma_{si} A_{si} y_i + \sum_{j=1}^{nn} \sigma_{cj} A_{cj} y_j + \sum_{l=1}^{kk} \sigma_{CFl} A_{CFl} y_l + Tol = M \tag{4.15}$$

where F is the axial load; M the major bending moment along the beam; σ_{si}, σ_{cj} and σ_{CFl} the stress of the steel reinforcement, concrete and CFRP at the centroids of fibres $i,j,$ and l, respectively; A_{si}, A_{cj} and A_{CFl} are the areas of fibres $i,j,$ and l of the steel reinforcement, concrete and CFRP, respectively; y_i, y_j and y_l are the distances between the centroids of fibres $i,j,$ and l and the top of the section; mm, nn and kk are the total number of section fibres; and Tol is the acceptable tolerance.

As fatigue loading progresses, the stress-strain responses of the concrete and CFRP change as a function of the number of cycles. Within each layer or segment, the stresses in the concrete, CFRP plate and steel reinforcement are different because each material has a different modulus of elasticity.

New moment-curvature calculations are initiated at the start of each cycle when a pre-specified number of curvature increments have been applied such that the simulated load is equal to the maximum applied load for the cycle in question.

Once the moment curvature relationship of a cross section is determined at the end of a cycle, the load-deflection response of the beam is calculated using a well-known method from beam bending theory (Equation 4.17) and using the flexural stiffness(EI) obtained from the slope of the moment-curvature curve (Figure 4.4)

$$(EI)_N = \frac{\Delta M}{\Delta \varphi} \tag{4.16}$$

Where $(EI)_N$ is the flexural beam stiffness at N cycle, and ΔM and $\Delta \varphi$ are the moment and curvature differences between two load stages during the cycle, respectively.
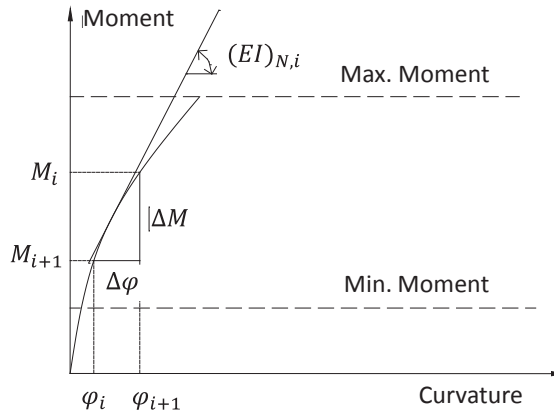
Figure 4.4. Calculation of flexural stiffness from the moment-curvature relationship.

The deflection, δ, at a given load during a cycle is given by:

$$\delta = \frac{23ML^2}{216(EI)_N} \tag{4.17}$$

Where M is the applied moment and L the span length.

Main assumptions

The main assumptions and limitations of the proposed fibre section model are:
1-The strain in each fibre is constant across its thickness.
2- The concrete cannot sustain any additional tensile stress.
3- There is perfect bonding between the concrete and the beam's other constituent materials (steel reinforcement and CFRP laminates or bars).
4- The final failure of the structure is governed by the rupture of the first tensile steel reinforcing bar.
5- Planar sections remain planar after bending.
6- The concrete stress-strain behaviour implemented in this model represents the behaviour of conventional concrete.
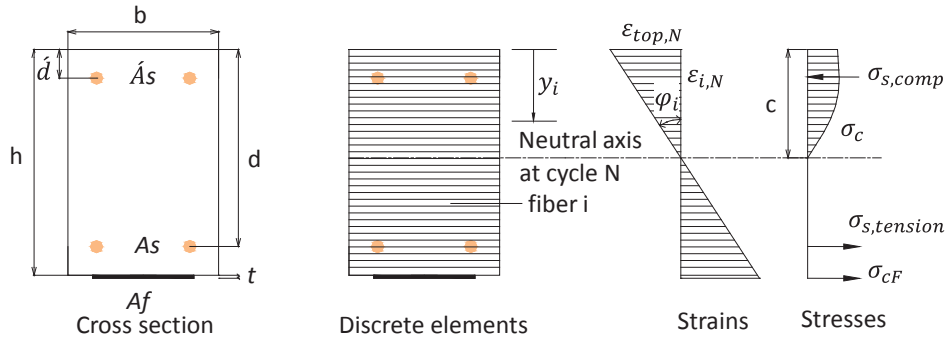
Figure 4.5. Schematics of section discretization of reinforced concrete section strengthened with CFRP plates.

4.4 Model verification

To illustrate the validity of the fatigue model developed in this study, it was used to simulate the behaviour of four of the CFRP-strengthened beams examined during the experimental phase discussed in Chapter 3 of this thesis (B1-EE1-F , B6-EE2-F, B3-NE1-F and B8-NE2-F). Figure 4.6 compares the experimental deflection responses to the output of the analytical fatigue model developed in this study for beams B1-EE1-F and B3-NE1-F. The agreement between model and experiment is reasonably good (although it should be noted that no attempt was made to model the beams' behaviour after the rupture of the first reinforcing bar). However, the predicted deflections for beams strengthened with NSM bars are smaller than those observed experimentally. This may be because the model assumes that the strengthening CFRP is present as a thin layer covering the underside of the beam rather than in near-surface mounted bars, making the real beams less stiff than would be expected according to the model's assumptions. In addition, the model assumes a perfect bond between the concrete and the carbon fibre reinforcement, which may also contribute to the discrepancy.
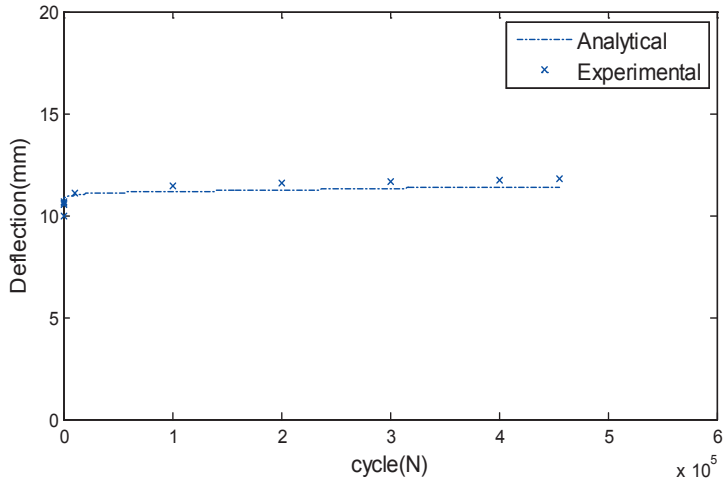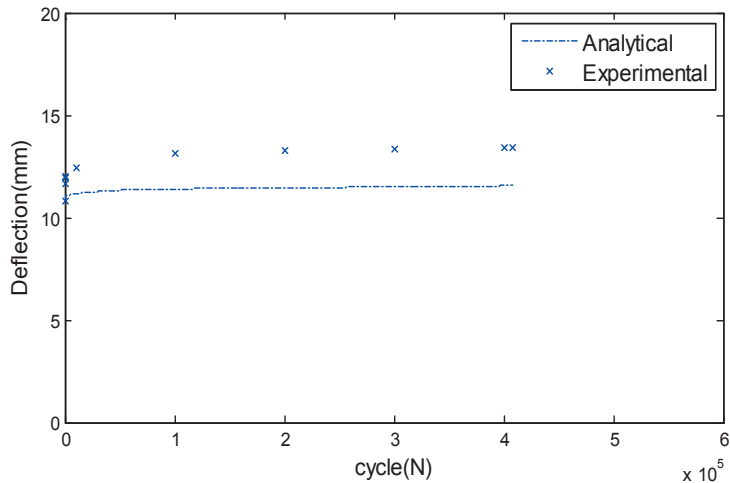
Figure 4.6 Predicted and observed mid-span deflections during fatigue loading: (a) Beam B1-EE1-F; (b) Beam B3-NE1-F.

The predicted and measured strains of the internal tensile steel and CFRP at the beams' mid-spans are compared in Figure 4.7 and Figure 4.8. As was typically observed, the steel and CFRP strains increase rapidly during the initial loading cycles and then flatten out. It is clear from the figures that the computed strains responses correspond well with the measured strains. It is also readily apparent that the calculated CFRP strain for the beams strengthened with NSM bars deviate widely from the experimental results, which is probably due to the use of inaccurate assumptions concerning the bars' positions, as discussed in the preceding section. Comparisons for the other beams examined in the experimental phase are presented in paper IV.
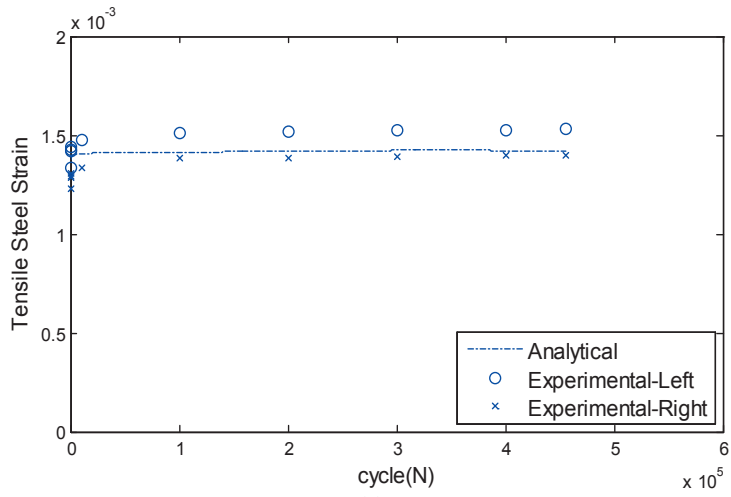
(a)
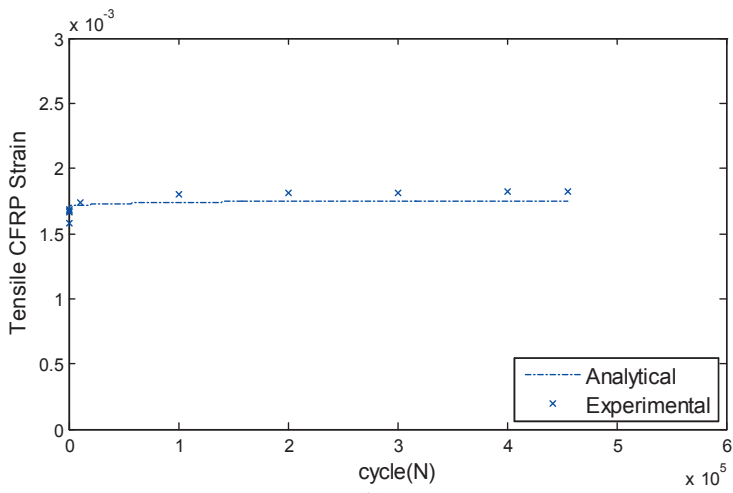
(b)

Figure 4.7 Tensile strains of B1-EE1-F of the mid-span of (a) steel reinforcement and (b) CFRP strain as a function of cycle number.
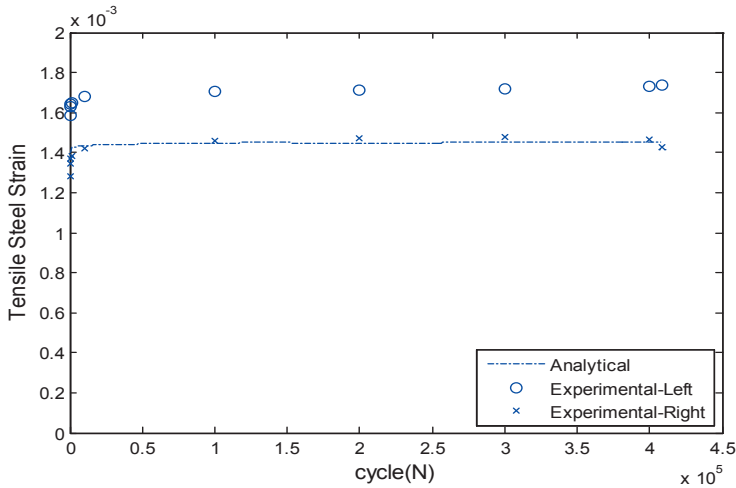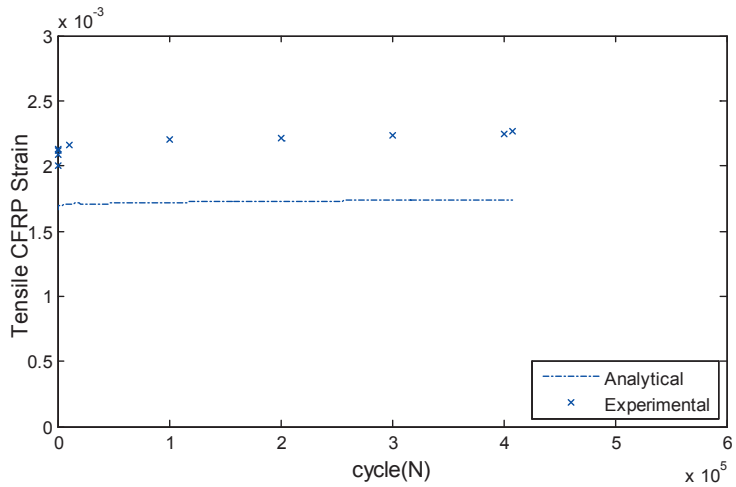
Figure 4.8 Predicted and measured strains of (a) the steel reinforcement and (b) the CFRP at the mid-span of beam B3-NE1-F during fatigue loading.

4.5 Fatigue life models for strengthened beams

An overall fatigue prediction model should account for both the fatigue behaviour in order to predict the fatigue response and the fatigue life of the strengthened beams in order to predict the number of cycles at failure. The previous sections deal with models for predicting the behaviour of FRP-strengthened RC beams during fatigue loading. Moreover, because the fatigue life of FRP composites is generally greater than that of the reinforcing steel (Schütz and Gerharz, 1977), the fatigue life of reinforced concrete beams (whether strengthened or un-strengthened) can be estimated easily using existing steel fatigue life prediction models if the structural members are designed to be under-reinforced (Harries, 2005 and Kim and Heffernan, 2008). Since no delamination occurred before the fatigue fracture of the steel

reinforcement, the fatigue life of the strengthened beam is equal to the life of the beam at tensile steel bar rupture. This is assumed to be equal to the life of crack initiation in the steel rebar plus the life during crack growth.

The most common way of modelling the effect of applied stress on the fatigue life of a material is the stress-life (S-N) approach, which is based on so-called Wöhler curves. Here, S is the stress range. These empirical curves give a graphical representation of the fatigue performance under a certain load. This section presents the development of a fatigue life model for reinforced concrete beams strengthened with CFRP elements.

Figure 4.9 shows S-N data for sheet-strengthened, EBR plated and NSM bar-strengthened RC beams from the literature (Barnes and Mays, 1999; Breña et al., 2005; Dong et al., 2011; Heffernan and Erki ,2004; Papakonstantinou et al., 2001; Yu et al., 2011; Quattlebaum et al., 2005; Badawi, 2007; Wahab, 2011; Gussenhoven and Breña, 2005; Ma et al., 2007; Aidoo et al., 2004; Derkowski, 2006 and Harries et al., 2007). This figure only includes data for beams that failed by steel bar rupture due to fatigue loading. The stress range (S_r) reported is the stress range in the internal reinforcing tension steel during the first cycle. A regression curve for strengthened beams is also shown in Figure 4.9, which has the following equation:

$S_r=1038.5-132.2 \ Log \ N_f$ (4.18)

where S_r is the stress range of the reinforcing steel.
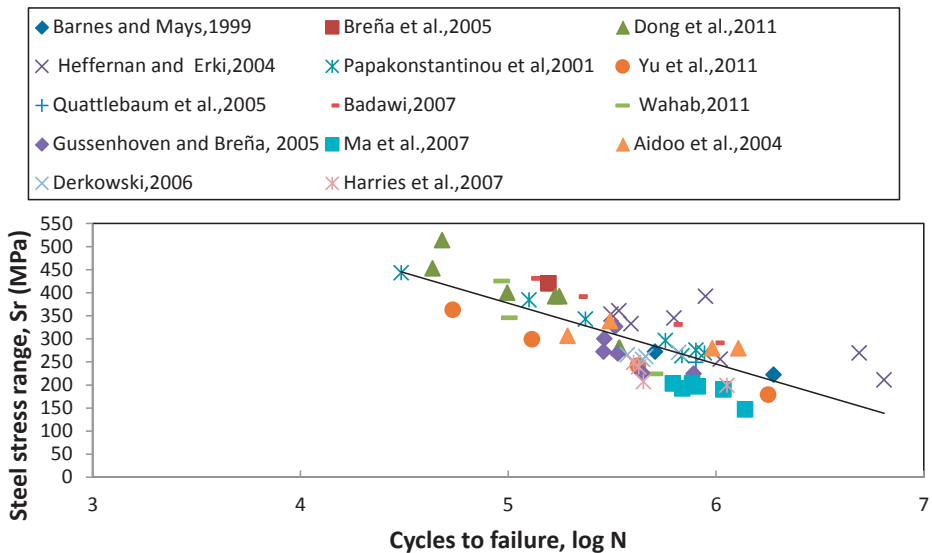
Figure 4.9. S-N curves for FRP laminates, sheets and NSM.

In order to find a model capable of accurately estimating the fatigue life of strengthened beams, the model developed in this work was compared to some developed by other

researcher. These alternative models are shown in Table 4.1, which presents each model's relationship between the steel stress range (S_r) and number of cycles to failure (N_f) .

Table 4.1. Fatigue life models.

Model	Fatigue life model
RC beam ,Tilly and Moss (Barnes and Mays, 1999)	$S_r^9 * N_f = 3.09 * 10^{27}$
RC beam, Model Code (2010)	$S_r^5 * N_f = 4.0841 * 10^{17}$
Helgason and Hanson model of steel under direct tension in air (Zorn, 2006)	$log(N_f) = 6.969 - 0.00555 S_r$

The outputs of the three literature models and the new model outlined above for a steel stress range of 258 MPa (corresponding to the range calculated for the experimental fatigue tests reported in Chapter 3 of this thesis) are presented in Table 4.2. The results obtained suggest that the most accurate and conservative estimate of the fatigue life of CFRP-strengthened RC beams is provided by a model originally developed to estimate the fatigue life of 'naked' steel bars in air. Conversely, the S-N model developed in this work predicts a much longer fatigue life than was achieved experimentally. This indicates a need to develop a more accurate S-N model for strengthened beams under fatigue loads that accounts for the effects of parameters other than the steel stress range, such as the presence or absence of shear strengthening, the number of tensioning steel bars, and the effect of the shear span length.

Table 4.2. S-N models and their predicted fatigue life values for the beams examined in the experimental phase.

Model	Estimated fatigue life
Strengthened beam model proposed in Eq.11	801,555
RC beam ,Tilly and Moss (Barnes and Mays 1999)	600,000
RC beam, Model Code (2010)	353,986
Helgason and Hanson model for steel under direct tension in air (Zorn 2006)	342,336

4.6 Modelling the FRP-concrete bond

A two-scale damage model has been implemented for modelling FRP-concrete joints under high-cycle fatigue in the first phase when the stress level is below the engineering yield stress and the degradation of the bond stiffness is negligible. The development of this model represents an important step towards the establishment of finite element methods for analysing the behaviour of strengthened beams under fatigue loading. The behaviour of the bond between the concrete and CFRP at the first phase of the fatigue bond behaviour had a profound influence on all of the beams examined in the experimental work, as demonstrated by the CFRP slippage plots presented in Figures 4.10 and 4.11; the corresponding curves for the other beams are presented in Appendix C.
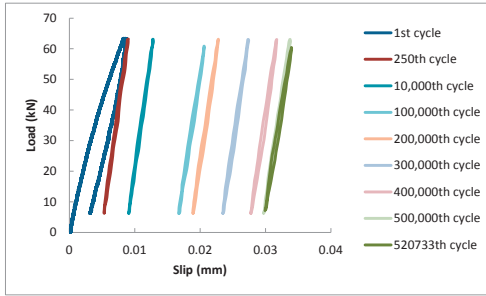
(a) Load-End slip
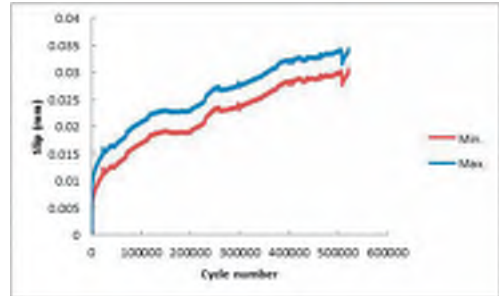
(b) End slip- Cycle Number

Figure 4.10. Slippage of the strengthening plate of beam B1-EE1 during fatigue loading.
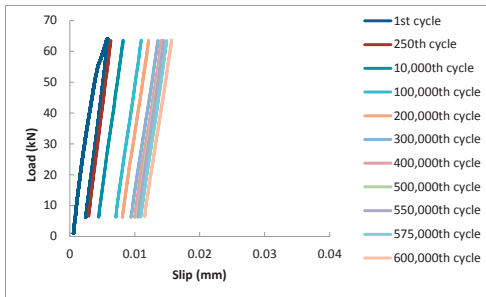
(a) Load-End Slip.
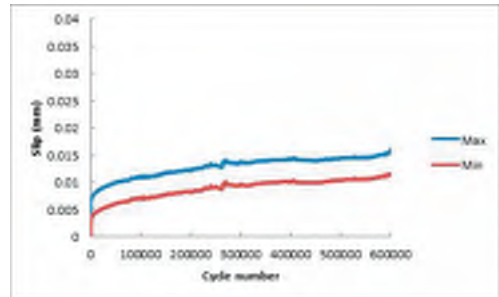
(b) End slip - Cycle Number.

Figure 4.11. Slippage of the strengthening bars of beam B10-NE1-C during fatigue loading.

The general principles of the two-scale damage model for FRP-concrete bonds under high cycle fatigue are outlined in Figure 4.12. Its key assumptions are:

-The bond is assumed to be elastic on the meso-scale, i.e. the scale of the represented volume element. Where, the material engineering yield stress being usually not reached in high cycle fatigue.

-The behaviour at mico-scale is elastic-perfectly plastic coupled with damage, the scale of micro-inclusion. Where, the weakness of the inclusion being represented by a yield stress at micro-scale is taken equal to the fatigue limit of the joint.
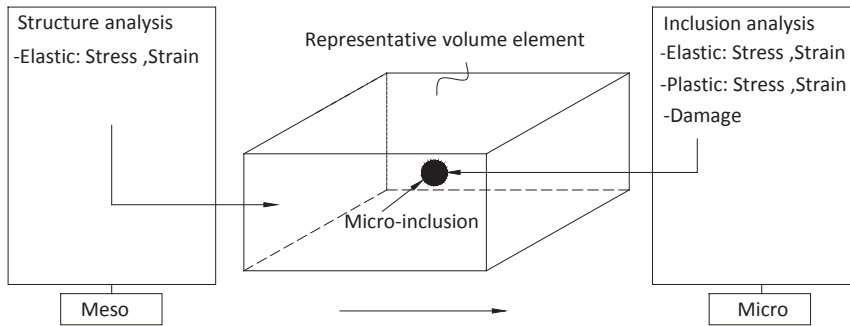
Figure 4.12. Two scale model.

4.6.1 Constitutive damage equation

The deterioration of the mechanical response of most engineering materials can usually be attributed to irreversible energy-dissipating changes in their microstructure. There are at least three different scales on which physical processes can be observed within materials. The micro-scale, or defects scale, is the size at which the elementary processes occur; the macro-scale is the scale of engineering structures whose damage can be described by continuum mechanics; and the meso-scale, which is the size for which homogeneous constitutive equations are written and which is modelled in terms of representative volume elements (RVEs) in the mechanics of materials. So, damage to a material refers to the gradual deterioration of its mechanical strength due to the development of micro-cracks and micro-cavities (Skrzypek and Ganczarski, 1999) and covers the material behaviour from a reference state until the initiation of a meso-crack.

Most damage models introduce a damage variable (Lemaitre and Desmorat, 2005) that is equal to the ratio of the effective area or volume of the intersections of all micro-cracks or micro-cavities to the total undamaged area or volume. The damage model used herein is of this form.

A suitable damage model for the joint interface represented by an interface element under fatigue load must consider the different materials of the joint and must relate directly to the accumulated micro plastic strain. In addition, the parameters must be easy to determine by static testing. To meet these criteria, we must describe the behaviour of the joint under monotonic loading. Figure 4.13 (a) shows a schematic of the general behaviour of the FRP-concrete joint under static load constructed on the basis of an experiment (Täljsten,1997) in which the stress is the applied average bond stress and slip represents the slip of FRP with respect to the concrete block. The joint behaviour has two stages, the elastic stage and the fracture stage. The fracture stage starts after the maximum load is reached, which means that the damage behaviour of the bond occurs only during the elastic stage. Therefore, the first phase of fatigue joint behaviour occurs exclusively during this stage. The fatigue behaviour phases can be represented schematically by considering the model presented in Figure 4.13(b).To describe this damage behaviour, we define the damage variable D_j for the

3-D joint as a function of the total strain (elastic and accumulated plastic strain) within the elastic stage as

$$D_j = (1 - \frac{\varepsilon_{j3}}{L_{ej}})^{(\alpha - \frac{1}{\alpha})} \qquad (4.19)$$

where ε_{j3} is the current total strain (interface slip which has the dimension of length) in the normal and shear directions (j), and $L_{e,j}$ is the total length of the elastic stage obtained from static tests of FRP-concrete joints with different modes. This parameter allows us to account for the state of the stress (mode I, mode II, mode III). α is the damage exponent that determines the shape of the damage evolution curve and should be greater than one.
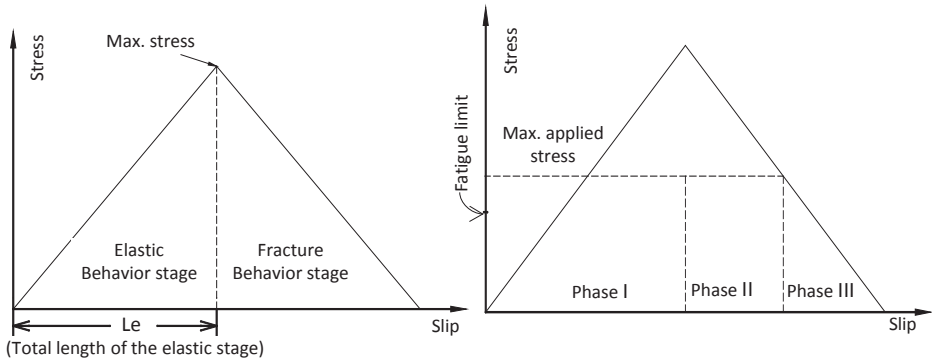
Figure 4.13. Typical FRP-concrete joint behaviour under static loading. (b) Static stages and (a) Fatigue phases as equivalent in static stress-slip space .

4.6.2 Material models

4.6.2.1 Concrete and FRP

The concrete and FRP are modelled at the meso scale only, i.e. the scale of the representative volume element. At this scale, the material exhibits linear elastic behaviour and the standard form of the linear elastic relationship between generalized stress (σ) and strain (ε) for the elements is used:

$$\sigma_B = E_B \varepsilon_B^e \qquad (4.20)$$

where E_B is the elastic stiffness matrix of the element and $\sigma_B, \varepsilon_B^e$ are the stress and strain tensors, which have six components for the 3-D eight-node brick element used to simulate the concrete and FRP .The elastic stiffness is given by:

$$E_B = \frac{E_e}{(1+v)(1-2v)} \begin{bmatrix} 1-v & v & v & 0 & 0 & 0 \\ v & 1-v & v & 0 & 0 & 0 \\ v & v & 1-v & 0 & 0 & 0 \\ 0 & 0 & 0 & \dfrac{1-2v}{2} & 0 & 0 \\ 0 & 0 & 0 & 0 & \dfrac{1-2v}{2} & 0 \\ 0 & 0 & 0 & 0 & 0 & \dfrac{1-2v}{2} \end{bmatrix}$$

Where E_e is the elastic modulus of elasticity and v is Poisson's ratio.

4.6.2.2 The bond

The bond between the concrete and FRP, which is represented by the interface element, is treated with a two-scale damage model. The two scale model is treated as an inclusion within an elastic meso-matrix as shown in Figure 4.12 (Lemaitre et al., 1999). This inclusion is assumed to be elastic-plastic and coupled with damage.

4.6.2.2.1 Elastic meso scale model

The standard form of the linear elastic relationship between the generalized stress (σ) and strain (ε) of the elements is used:

$$\sigma = E\varepsilon^e \tag{4.21}$$

where E is the elastic stiffness matrix for the interface element$\{K_n, K_s, K_t\}$; n denotes the normal components and s and t denote the shear components. The stress and strain tensors have three components for the 3-D eight-node interface element.

4.6.2.2.2 Plasticity and damage microscale model

The principle of Lemaitre model is used here for the discontinuum interface element material model. Lemaitre et al. (1999) developed a micromechanical model of high cycle fatigue that is based on a weak micro-inclusion that exhibits plasticity and is subject to damage, embedded in an elastic meso-element. The developed model is outlined schematically in Figure 4.14. It is assumed that the inclusion exhibits elastic and perfectly plastic behaviour with damage, and that the plastic stress threshold is lower than the mesoscale yield stress and equal to the fatigue limit. This means that there is no microplastic strain below the fatigue limit, and no damage occurs. The damage threshold is the limit above which damage in the form of microstresses (micro crack initiation) starts to occur, as shown in Figure 4.14.
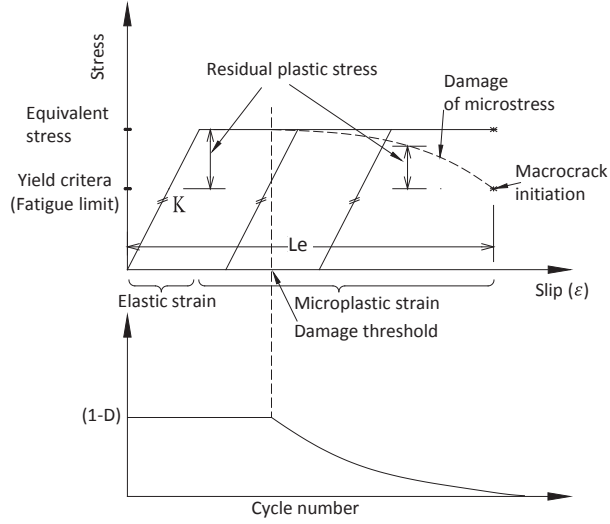
Figure 4.14. Constitutive model for a FRP-concrete bond subjected to fatigue loading.

According to these assumptions, the total strain is divided into a micro elastic ($\varepsilon_{j3}^{\mu e}$) part and a micro plastic ($\varepsilon_{j3}^{\mu p}$) part (recall that the superscripted μ denotes microscale variables):

$$\varepsilon_{j3}^{\mu}=\varepsilon_{j3}^{\mu e}+\varepsilon_{j3}^{\mu p} \tag{4.22}$$

The micro elastic strain is calculated at the meso scale, where the strain is equal to the strain at the micro scale (see Figure 4.14). The micro plastic strain rate is derived from the yield criterion function (Hashin, 1980):

$$f^{\mu}=\frac{1}{(1-D)}\sqrt{\sigma^{\mu T}A\sigma^{\mu}}-1=0 \tag{4.23}$$

where

$$\sigma^{\mu}=\begin{Bmatrix}\sigma_{33}^{\mu}\\\tau_{13}^{\mu}\\\tau_{23}^{\mu}\end{Bmatrix} \quad , \quad A=\begin{bmatrix}\frac{1}{\sigma_{f33}^2} & 0 & 0\\0 & \frac{1}{\tau_{f13}^2} & 0\\0 & 0 & \frac{1}{\tau_{f23}^2}\end{bmatrix} \quad , \quad (1-D)=D_j \quad , \quad \sigma^{\mu T}=\{|\sigma_{33}^{\mu}|\ \tau_{13}^{\mu}\ \tau_{23}^{\mu}\}$$

and σ_f and $\tau_{f_{j,3}}$ are the normal and shear fatigue stress limits of the joint.

By the normality rule, the micro plastic strain is

$$\varepsilon_{ji}^{\mu p}=\frac{\partial f^{\mu}}{\partial\sigma^{\mu}}\dot{\lambda}=\frac{A\sigma^{\mu}}{g(\sigma^{\mu})}\frac{\lambda}{(1-D)} \qquad \text{if} \qquad f^{\mu}=0\ and\ \dot{f}^{\mu}=0 \tag{4.24}$$

$$g(\sigma^{\mu})=\sqrt{\sigma^{\mu T}A\sigma^{\mu}} \tag{4.25}$$

59

where $\dot{\lambda}$ is the plastic multiplier derived from the accumulated plastic strain rate $(\dot{P})$ which must always be positive and increasing. The simplest combination of this kind which is dimensionally correct is defined in accordance with the discontinuity consideration:

$$\dot{P}=\sqrt{(\dot{\varepsilon}_{ji}^{\mu P})^T\dot{\varepsilon}_{ji}^{\mu P}}=\frac{\lambda}{(1-D)}\frac{\sqrt{\sigma^{\mu T}A^TA\sigma^{\mu}}}{g(\sigma^{\mu})} \tag{4.26}$$

which can be arranged as

$$\frac{\lambda}{(1-D)}=\dot{P}\frac{g(\sigma^{\mu})}{\sqrt{\sigma^{\mu T}A^TA\sigma^{\mu}}} \tag{4.27}$$

The micro scale stresses are related to the meso scale stresses as follows:

$$\sigma^{\mu}=\sigma_{j3} \qquad\qquad \text{if} \qquad\qquad f^{\mu}<0 \tag{4.28}$$

$$\sigma^{\mu}=\sigma_{j3}D_j \qquad\qquad \text{if} \qquad\qquad f^{\mu}\geq0, \tag{4.29}$$

where

$$\sigma_{ij}=E(\varepsilon_{j3}\text{-}\varepsilon_{j3}^{\mu p}) \tag{4.30}$$

and

$$D_j=(1\text{-}\frac{\varepsilon_{j3}^{\mu}}{L_{e,j}})^{(\alpha\,\text{-}\frac{1}{\alpha})} \tag{}$$

4.6.3 Integration of the elastic-plastic damage equation

An incremental load procedure for each cycle is used to analyse the structure system under fatigue load as shown in Figure 4.15. The method of integration is strain driven and involves two steps: the calculation of trial elastic stress, also called the elastic predictor, and the return mapping to the yield surface, also called the plastic corrector. For the sake of simplicity during the derivation of the elastic predictor, the plastic effective micro stress is represented as follows in the equations below: $\bar{\sigma}=\frac{\sigma^{\mu}}{(1-D)}$. The following equations must be satisfied to calculate the residual stresses that cause plastic strain for each increment in a cycle:

$$h=\bar{\sigma}\text{-}K_s(\varepsilon_{ji}\text{-}\varepsilon_{ji,n}^{P})+K_s(\frac{A\bar{\sigma}}{\sqrt{\bar{\sigma}^TA^TA\bar{\sigma}}})\Delta\dot{P} \tag{4.31}$$

$$h=\bar{\sigma}\text{-}K_s(\varepsilon_{ji}\text{-}\varepsilon_{ji,n}^{P})+K_s\,S\Delta\dot{P} \tag{4.32}$$

$$f=\sqrt{\bar{\sigma}^TA\bar{\sigma}}\text{-}1=0 \tag{4.33}$$

and

$$D_j=(1\text{-}\frac{\varepsilon_{j3}^{\mu}}{L_{e,j}})^{(\alpha\,\text{-}\frac{1}{\alpha})} \tag{4.34}$$

To solve this nonlinear problem, Newton's iterative method for multiple variables was used:

$$f+\frac{\partial f}{\partial \bar{\sigma}}:C\bar{\sigma}+\frac{\partial f}{\partial \Delta P}:CP=0 \tag{4.35}$$

$$h+\frac{\partial h}{\partial \bar{\sigma}}:C\bar{\sigma}+\frac{\partial h}{\partial \Delta P}:CP=0 \tag{4.36}$$

Taking the derivatives of (4.33) with respect to $\bar{\sigma}$ and ΔP,

$$\frac{\partial f}{\partial \bar{\sigma}}=\frac{A\bar{\sigma}}{\sqrt{\bar{\sigma}^T A\bar{\sigma}}}=\frac{A\bar{\sigma}}{g(\bar{\sigma})} \qquad , \qquad \frac{\partial f}{\partial \Delta P}=0 \tag{4.37}$$

and substituting (4.37) into (4.35) yields

$$C\bar{\sigma}=-\frac{g(\bar{\sigma})}{A\bar{\sigma}}:f \tag{4.38}$$

The derivatives of (4.32) with respect to $\bar{\sigma}$ and ΔP are

$$\frac{\partial h}{\partial \bar{\sigma}}=\left[II+K_s\frac{\partial S}{\partial \bar{\sigma}}\Delta \dot{P}\right] \qquad , \qquad \frac{\partial h}{\partial \Delta P}=K_s\,S \tag{4.39}$$

and (4.36) can be rewritten with (4.39) as

$$h+\left[II+K_s\frac{\partial S}{\partial \bar{\sigma}}\Delta \dot{P}\right]:C\bar{\sigma}+K_s\,S:CP=0 \tag{4.40}$$

Substituting (4.38) into (4.40) yields

$$h-\left[II+K_s\frac{\partial S}{\partial \bar{\sigma}}\Delta \dot{P}\right]\frac{g(\bar{\sigma})}{A\bar{\sigma}}:f+K_s\,S:CP=0 \tag{4.41}$$

where $\quad II = \begin{bmatrix} 1 & 0 & 0 \\ 0 & 1 & 0 \\ 0 & 0 & 1 \end{bmatrix}$.

Eq. (4.41) multiplied by S is

$$S:h-\left[S:II+K_s S\frac{\partial S}{\partial \bar{\sigma}}:\Delta \dot{P}\right]\frac{g(\bar{\sigma})}{A\bar{\sigma}}:f+K_s\,S:S:CP=0 \tag{4.42}$$

where

$$\frac{\partial S}{\partial \bar{\sigma}}=\frac{A}{\sqrt{\bar{\sigma}^T A^T A\bar{\sigma}}}-\frac{(A\bar{\sigma})(\bar{\sigma}^T A^T A)}{(\bar{\sigma}^T A^T A\bar{\sigma})^{3/2}}$$

Because $\frac{\partial S}{\partial \bar{\sigma}}:S=0$, $S:II=S$ and $S:S=1$, (4.42) can be rewritten as

$$S:h-\frac{A\bar{\sigma}}{\sqrt{\bar{\sigma}^T A^T A\bar{\sigma}}}\frac{g(\bar{\sigma})}{A\bar{\sigma}}:f+K_s:CP=0 \tag{4.43}$$

CP (the plastic corrector) can be written as

$$CP=\frac{\frac{g(\bar{\sigma})}{\sqrt{\bar{\sigma}^T A^T A\bar{\sigma}}}f-S:h}{K_s} \tag{4.44}$$

61

By substituting (4.44) into (4.40), we get elastic predictor $C\bar{\sigma}$

$$C\bar{\sigma}=AC^{-1}\left(-h\text{-}S\left(\frac{g(\bar{\sigma})}{\sqrt{\bar{\sigma}^T A^T A\bar{\sigma}}}f\text{-}S\text{:}h\right)\right)$$ (4.45)

where $AC=\left[II+K_s\frac{\partial S}{\partial\bar{\sigma}}\Delta\dot{P}\right]$

The following algorithm is performed at each integration point at any time during the cycles:

1. Compute the mesoscale elastic stress:
   $\sigma=E\varepsilon^e.$

2. Compute a trial elastic micro stress:
   $\sigma^\mu=\sigma^e D.$

3. Check for plastic behaviour:

   If $f^\mu<0$, the integration point is elastic. Update stress and strain.

   If $f^\mu\geq0$, the integration point is plastic.

   For iterations $i=0\ldots\ldots\ldots n$,

   - Update the cumulative plastic strain (P) using the plastic corrector (CP):
     $$\Delta P^\mu_{i+1}=\Delta P^\mu_i+CP^\mu_{i+1},$$

   - Update the stress (σ^μ) using the elastic predictor ($C\sigma$):
     $$\Delta\sigma^\mu_{i+1}=\Delta\sigma^\mu_i+C\sigma_{i+1},$$

   until $f^\mu<Tolerance.$

4. Update the micro plastic strain and total strain, and check and update the damage variables:
   $$\varepsilon^\mu_{j3}=\varepsilon^{\mu e}_{j3}+\varepsilon^{\mu p}_{j3}$$

   $$D_j=(1-\frac{\varepsilon^\mu_{j3}}{L_{e,j}})^{(\alpha-\frac{1}{\alpha})} \quad \text{if} \quad P^\mu\geq P^\mu_{th},$$

   $$D_j=1 \qquad\qquad \text{if} \quad P^\mu<P^\mu_{th},$$

   where P^μ_{th} is the damage threshold estimated as (Lemaitre, 2001)

   $$P^\mu_{th}=\varepsilon^\mu_u\left(\frac{\sigma_u\text{-}\sigma_f}{\sigma_{max}\text{-}\sigma_f}\right)$$ (4.46)

   ε^μ_u and σ_u are the ultimate static strain and stress, σ_f is the fatigue limit stress of FRP-concrete joint, and σ_{max} is the maximum stress when the maximum cycle load is applied to the joint.

5. Compute the equivalent nodal forces produced by the residual plastic strain and re-analyse the structure to compute the equivalent nodal displacement and other variables.
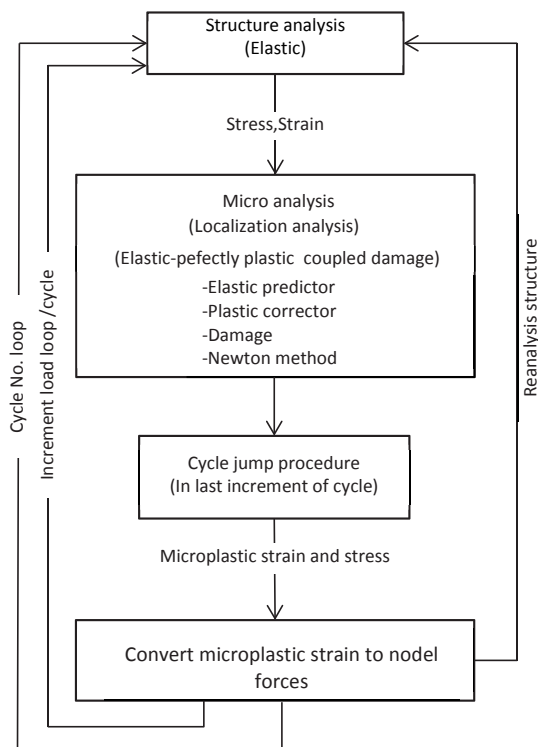
Figure 4.15. Numerical implementation.

4.6.4 The cycle jump concept

The increment-by-increment calculation for each cycle of the elastic-plastic model is computationally expensive (time consuming), and simulating fatigue behaviour for a large number of cycles might take several days depending on the available computational resources. Therefore, we implemented a simple cycle jump strategy in the FEM model. Because the long-term response of the structure can be determined without modelling the details of each cycle, the computation can "jump" across a large number of cycles. Several authors have considered similar ways of accelerating numerical simulations for cyclically loaded structures. To save computations for a model subjected to cyclic loadings, Kiewal et al. (2000) extrapolated the internal variables (displacements, stresses and strains) over a certain number of cycles. For each material point in the model, a spline function is obtained based on the evolution equations of the internal variables. The variables are then extrapolated using the obtained spline functions. Based on this method, Wang et al. (2012) utilized a linear shape function for extrapolation. Bogard et al. (2008) developed an accelerated scheme that incorporates a cycle jump algorithm. The internal variables are described as functions of time,

and expressed in Taylor series up to second order. The cycle jump method developed in this thesis depends on the nearly constant amount of residual stress or plastic strain present before the damage starts for each cycle at the integration point. The damage variable, strain, and stress at an integration point are computed for each cycle at maximum cycle load without the complete analysis of the structures during the cycle jump. Figure 4.16 shows the schematic of an evolving strain for a structure subjected to cyclic loading during the analysis when using the cycle jump method. Jump steps eliminate the need to simulate each individual cycle and significantly reduce the time required for analysis. The proposed method involves conducting detailed finite element analyses for a set of cycles to establish the residual micro-plastic strain or stress at all integration points of structure, implementing the cycle jump method using the procedure outlined below, and using the jumped variables as initial variables for additional finite element analysis calculations.
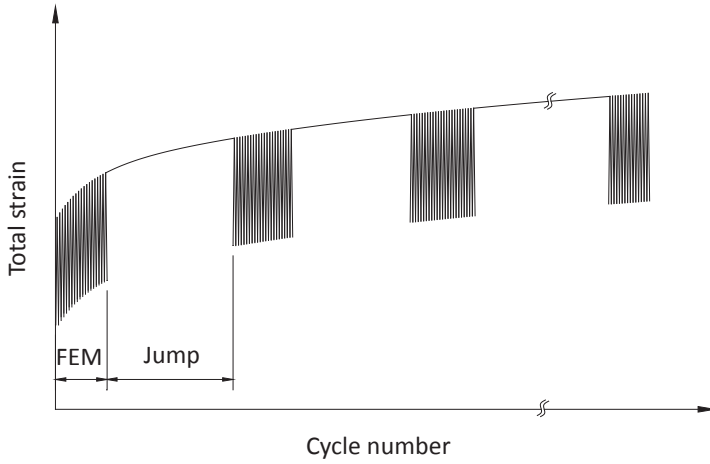
Figure 4.16. A schematic of the cycle jump method.

The cycle jump method is implemented in all directions as follows.

$$\varepsilon^{\mu}_{cycle+1}=\varepsilon^{\mu}_{cycle}+\Delta\varepsilon^{\mu p} \tag{4.47}$$

$$\Delta\varepsilon^{\mu p}=D_{cycle+1}.\Delta\varepsilon^{\mu p}_{G.P} \tag{4.48}$$

Where, $\Delta\varepsilon^{\mu p}_{G.P}$ is the maximum residual microplastic strain at an integration point.

$$\sigma^{\mu}_{cycle+1}=D_{cycle+1}.\sigma \tag{4.49}$$

$$D_{cycle}=1 \qquad\qquad if \qquad\qquad P^{\mu}<P_{th} \tag{4.50}$$

$$D_{cycle+1}=\left(1-\frac{\varepsilon^{\mu}_{cycle}}{L_e}\right)^{\left(\alpha-\frac{1}{\alpha}\right)} \qquad if \qquad P^{\mu}>P_{th} \tag{4.51}$$

4.6.5 3-D brick element

The quadratic 8-node brick element is adopted to represent the concrete and FRP in this analysis because elements of this sort offer superior performance to established alternatives. The local coordinate system is used to describe the displacement components of a point $p(\xi, \eta, \zeta)$ within the element. The origin of the local coordinates system is placed at the centre of the brick element; each of the local coordinate lines ranges from (-1) to (+1) and they are defined in terms of ξ, η and ζ. The isoparametric definition of the displacement components is:

$$\left.\begin{array}{l} u(\xi\eta,\zeta)=\sum_{i=1}^{8} N_i(\xi\eta,\zeta)u_i \\ v(\xi\eta,\zeta)=\sum_{i=1}^{8} N_i(\xi\eta,\zeta)v_i \\ w(\xi\eta,\zeta)=\sum_{i=1}^{8} N_i(\xi\eta,\zeta)w_i \end{array}\right\} \tag{4.52}$$

Where $N_i(\xi, \eta, \zeta)$ is the shape function at the i-th node and u_i, v_i and w_i are the corresponding nodal displacements. The shape functions of the quadratic 8- node brick element are:

$$N_i = \frac{1}{8}(1+\xi\xi_i)(1+\eta\eta_i)(1+\zeta\zeta_i) \tag{4.53}$$

Where ξ_i, η_i and ζ_i are the nodal coordinates. Within a three-dimensional finite element, the Cartesian components of strains are related to nodal displacements as:

$$\varepsilon_B^e = \begin{Bmatrix} \varepsilon_x \\ \varepsilon_y \\ \varepsilon_z \\ \gamma_{xy} \\ \gamma_{yz} \\ \gamma_{zx} \end{Bmatrix} = \begin{Bmatrix} \frac{\partial u}{\partial x} \\ \frac{\partial v}{\partial y} \\ \frac{\partial w}{\partial z} \\ \frac{\partial u}{\partial y}+\frac{\partial v}{\partial x} \\ \frac{\partial v}{\partial z}+\frac{\partial w}{\partial y} \\ \frac{\partial w}{\partial x}+\frac{\partial u}{\partial z} \end{Bmatrix} = \sum_{i=1}^{8} \begin{bmatrix} \frac{\partial N_i}{\partial x} & 0 & 0 \\ 0 & \frac{\partial N_i}{\partial y} & 0 \\ 0 & 0 & \frac{\partial N_i}{\partial z} \\ \frac{\partial N_i}{\partial y} & \frac{\partial N_i}{\partial x} & 0 \\ 0 & \frac{\partial N_i}{\partial z} & \frac{\partial N_i}{\partial y} \\ \frac{\partial N_i}{\partial x} & 0 & \frac{\partial N_i}{\partial z} \end{bmatrix} \begin{Bmatrix} u_i \\ v_i \\ w_i \end{Bmatrix} \tag{4.54}$$

The derivatives of the shape function can be obtained by the usual chain rule as:

$$\begin{bmatrix} \frac{\partial N_i}{\partial \xi} \\ \frac{\partial N_i}{\partial \eta} \\ \frac{\partial N_i}{\partial \zeta} \end{bmatrix} = \begin{bmatrix} \sum_{i=1}^{8}\frac{\partial N_i}{\partial \xi}x_i & \sum_{i=1}^{8}\frac{\partial N_i}{\partial \xi}y_i & \sum_{i=1}^{8}\frac{\partial N_i}{\partial \xi}z_i \\ \sum_{i=1}^{8}\frac{\partial N_i}{\partial \eta}x_i & \sum_{i=1}^{8}\frac{\partial N_i}{\partial \eta}y_i & \sum_{i=1}^{8}\frac{\partial N_i}{\partial \eta}z_i \\ \sum_{i=1}^{8}\frac{\partial N_i}{\partial \zeta}x_i & \sum_{i=1}^{8}\frac{\partial N_i}{\partial \zeta}y_i & \sum_{i=1}^{8}\frac{\partial N_i}{\partial \zeta}z_i \end{bmatrix} \begin{bmatrix} \frac{\partial N_i}{\partial x} \\ \frac{\partial N_i}{\partial y} \\ \frac{\partial N_i}{\partial z} \end{bmatrix} \tag{4.55}$$

4.6.6 3-D FEM interface model

The eight-node zero thickness interface element shown in Figure 4.17 is used to simulate the joint interface connecting the FRP laminate face with the concrete face. In the initial configuration, the two rectangular surfaces of the interface element are joined with no gaps. The surfaces separate when the adjacent solid elements deform.

Interface elements allow discontinuities in the displacement field and establish a direct relation between the tractions (t) and the relative displacements along the interface (Δu), which are given by

$$t=\{\tau_s \quad \tau_t \quad \sigma_n\} \tag{4.56}$$

$$\Delta u=\{\Delta u_s \quad \Delta u_t \quad \Delta u_n\} \tag{4.57}$$

Here, these quantities are conveniently defined using the generalized stress vector σ and generalized strain vector ε, so that the same notation is adopted for continuum and discontinuous elements. The local nodal displacements for the top and bottom faces of the element are defined as:

$$\left.\begin{array}{l} u_{top}=\{u_s^1\, u_t^1\, u_n^1 .... u_s^4\, u_t^4\, u_n^4\}^T \\ u_{bot}=\{u_s^5\, u_t^5\, u_n^5 .... u_s^8\, u_t^8\, u_n^8\}^T \end{array}\right\} \tag{4.58}$$

where s and t represent the tangential directions and n represents the normal direction. The displacement jump between two paired nodes of u_{top} and u_{bot} can be written as (Bfer, 1985):

$$\varepsilon_{local}=\begin{Bmatrix} \varepsilon_s \\ \varepsilon_t \\ \varepsilon_n \end{Bmatrix}=u_{top}\text{-}u_{bot} \tag{4.59}$$

The displacement jumps in the local directions (normal and tangential to the contact surface) can be obtained from the global displacement jumps:

$$\varepsilon_{local}=\theta^T\varepsilon_{global} \tag{4.60}$$

where

$$\varepsilon_{global}=\begin{Bmatrix} \varepsilon_x \\ \varepsilon_y \\ \varepsilon_z \end{Bmatrix} \quad \text{and} \quad \theta=[V_n, V_s, V_t].$$

V_n, V_s, and V_t are the local normal coordinate and tangential coordinate vectors, respectively The components of V_n, V_s, and V_t represent the direction cosines of the local coordinate system in the global coordinate system $(X_i, i = 1,2,3)$ and are obtained from

$$V_{\eta_i}=X_{i,\eta} \quad , \quad V_{\xi_i}=X_{i,\xi} \tag{4.61}$$

in the following way:

$$V_n=\frac{V_{\xi_i} X V_{\eta_i}}{|V_{\xi_i} X V_{\eta_i}|} \quad , \quad V_s=\frac{V_{\xi_i}}{|V_{\xi_i}|} \quad \text{and} \quad V_t=V_n X V_s \tag{4.62}$$
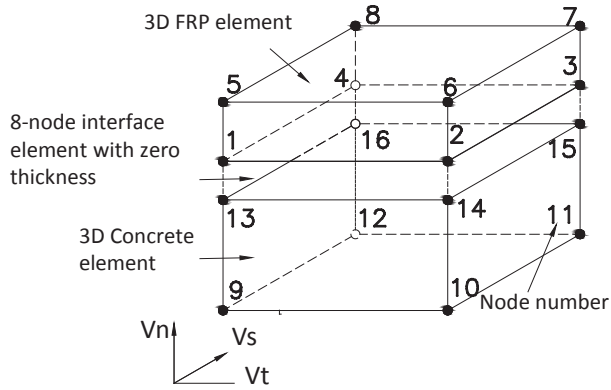
Figure 4.17. Eight-node interface element.

4.6.7 Model verification and parametric study

A double shear joint specimen under high-cycle fatigue without fracture (i.e. with no stiffness degradation) was analysed computationally using the developed bond slip model and the results obtained were compared to experimental data reported by Yun et al. (2008). Specifically, the modelled specimen corresponds to Yun's test specimen F-EB-A. In addition, a parametric study was conducted to determine how the model's parameters influence the specimen's fatigue behaviour. The material parameters used for the FRP-concrete joint are given in Table 4.3 and were determined from static testing of the joint performed by Yun et al. (2008). The dimensions, boundary conditions, and load conditions of the joint for the fatigue load case are shown in Figure 4.18. Because of the system's symmetry, only one fourth of the model was simulated. The fatigue load was distributed over an area of 25 mm × 200 mm, which is the size of the contact area between the FRP and concrete block when fully bonded.

Table 4.3. Properties of the simulated and experimental test specimen.

f_c (N/mm^2)*	E_f (GPa)**	K_n, K_s, K_t (N/mm²)	τ_f (N/mm²)	L_e (mm)	P_{th}	α
43.5	257	57.14	2.8	0.1	0.072	5.0

*Compressive concrete strength **Modulus of elasticity of FRP
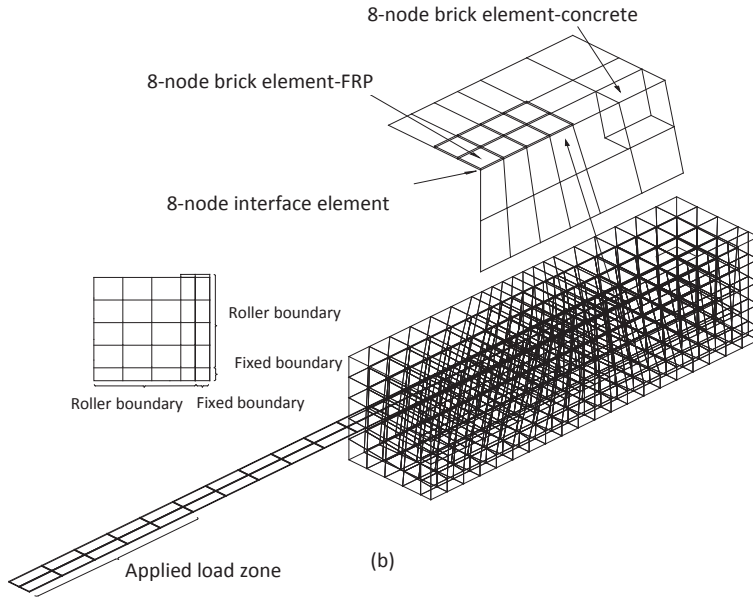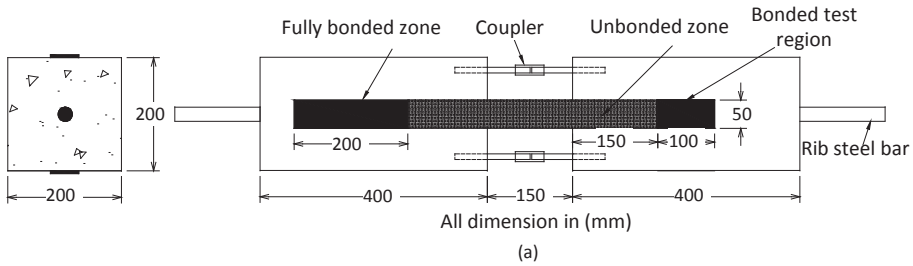
Figure 4.18. (a) Dimensions of the double shear joint specimen tested by Yun et al. (2008). (b) Finite element mesh, boundary conditions, and load conditions for one fourth of the specimen.

Figure 4.19 shows the output of the FEM calculations and the experimental results for the loaded-end slip at each cycle number for the minimum and maximum cyclic loads. The computed loaded-end slip generally agrees well with the experimental results. However, there is an 11% difference between the FEM and the experiment in the last cycle. This difference might have occurred because the damage of FRP plate was not accounted for in the model. Figure 4.20 shows the load-slip relationship computed with the FEM, and Figure 4.21 shows the slip computed at each cycle jump.
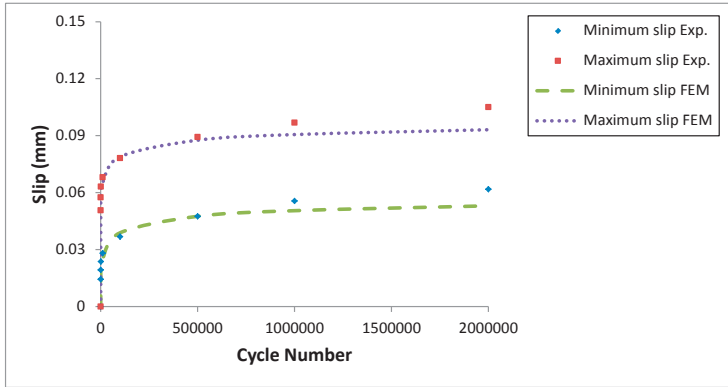
Figure 4.19. Comparison between the experimental and numerical results.
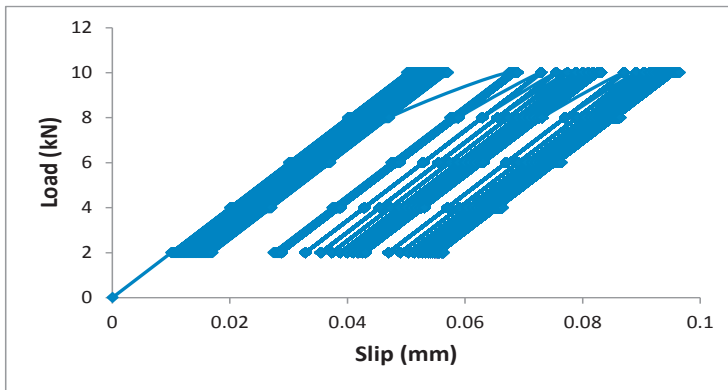
Figure 4.20. Load-slip relationship computed with the FEM.
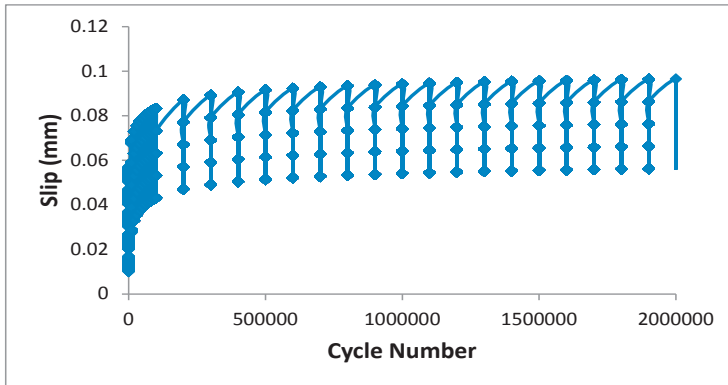
Figure 4.21. Computed slip at each cycle number.

After verifying the FEM model, we determined the sensitivity of the model at maximum cycle load to the following parameters: the damage exponent (α), damage threshold strain (P_{th}),

69

the length of the elastic zone (L_e), and the fatigue limit (τ_f). Each parameter was varied separately while the other parameters remained constant.

Figure 4.22 shows the loaded-end slip versus the number of cycles for different values of α. As can be seen, the slip damage under fatigue loading increases as the damage exponent decreases. The low values of α result in a low initial damage rate of residual stress. This causes an increase in plastic strain that produces an increase in slip damage during the initial stage. We can conclude from this that the lower values of α are more suitable for materials with limited ductility.
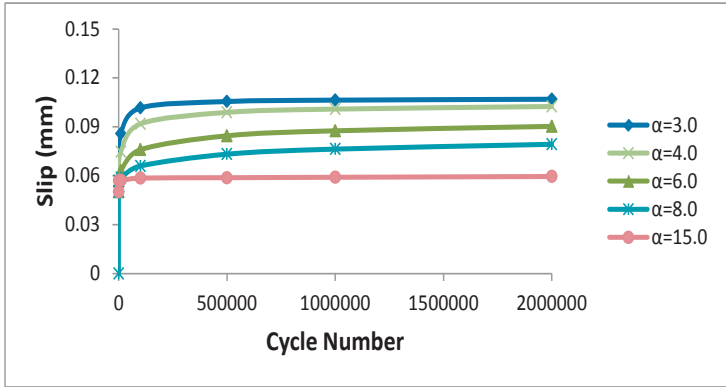
Figure 4.22. Influence of the α parameter on the fatigue behaviour of the joint.

Figure 4.23 shows the effect of L_e on the joint behaviour. It can be seen that the slip at the initial stage increases as L_e is increased. Increasing L_e delays the initiation of damage and reduces the damage rate. This increasing in slip is due to only the reduction in damage rate because the damage threshold and other parameters were fixed.
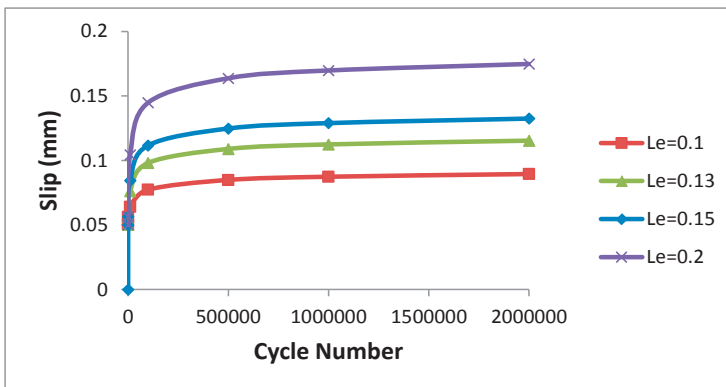
Figure 4.23. Influence of L_e on the fatigue behaviour of the joint.

Figure 4.24 shows the loaded-end slip versus the number of cycles with a constant applied load for different values of τ_f. When τ_f is higher than the maximum applied stress ($\tau_f =$

3 N/mm^2), no plastic strain or damage occurs. However, reducing τ_f to below nominal applied stress increases the plastic strain because of increased residual stress. The constant damage rate at very low τ_f it is due to the other parameters were held constant.
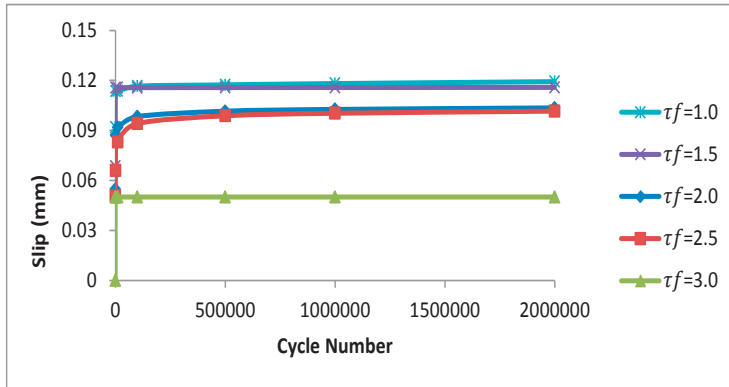
Figure 4.24. Influence of τ_f on the fatigue behaviour of the joint.

The effect of P_{th} on the fatigue behaviour is shown in Figure 4.25. Increasing P_{th} increases the period of microcrack nucleation and creates a large amount of plastic strain before the damage starts.
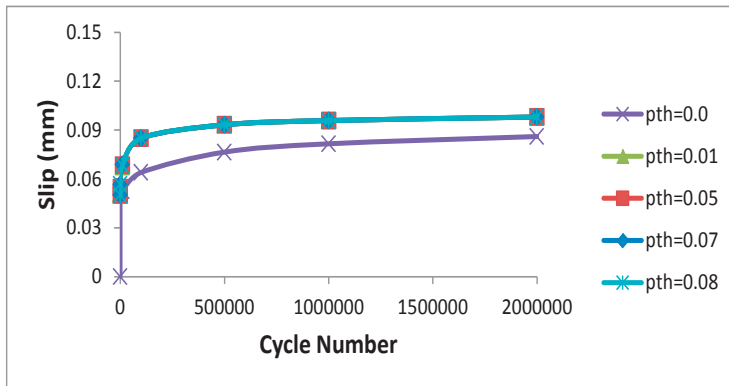
Figure 4.25. Influence of P_{th} on the fatigue behaviour of the joint.

Finally, the behaviour of the damage propagation with cyclic loading with respect to the longitudinal displacement along the bond length zone in the middle of the FRP plate is shown in Figure 4.26. We observed that the micro cracks started at the loaded end and propagated toward the free end as the number of fatigue cycles increased. The reduction in curvature of the displacement line, especially after 10,000 cycles, indicates an insignificant dissipation of energy due to the small plastic deformation (micro cracking) of the bond at the loaded end.
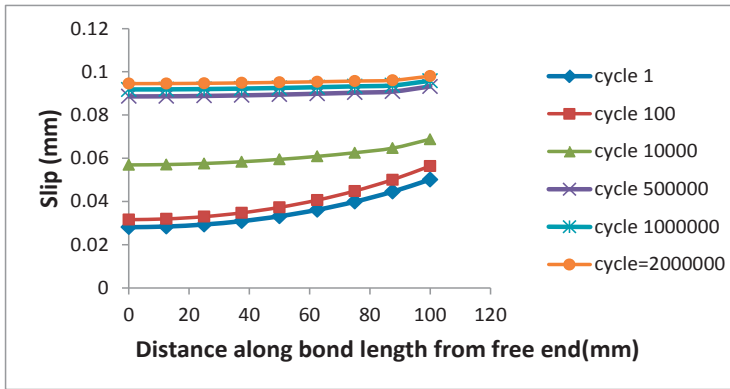
Figure 4.26. Slippage along the bond length at the maximum cycle load.

5 Discussion and Conclusions

5.1 Discussions

Reinforced concrete structures such as bridges need to be maintained, sometimes repaired and occasionally upgraded. The reason for the need varies; it may relate to deterioration due to steel corrosion or other environmental effects, or to a need for increased load carrying capacity due to an increasing load requirement or a changing traffic situation. Such upgrading must be performed safely, cost-effectively, and without creating problems of accessibility. Upgrading involves enhancing durability, increasing load carrying capacity, or a change in function. The measures might have to be taken in either the service limit state, the ultimate limit state or both. This thesis has focused on extending the fatigue life of RC structures. If it is not theoretically possible to upgrade a structure, there are not many physical methods that will allow its fatigue life to be increased. External pre-stressing can be used to lower stresses in the existing steel, or one can limit the permitted load. However, it may also be possible to apply EBR CFRP plates or NSM CFRP rods to prolong the fatigue life of a RC structure.

The main purpose of adding strengthening elements to RC structures is usually to reduce the stress applied to the tensile steel rebars. CFRP has become widely used for the repair and strengthening of reinforced concrete bridge members and is typically applied in the form of EBR plates or NSM bars. The life of a reinforced concrete structure exposed to fatigue loading is dependent on the stress range in its tensile steel bars, which may fail even if the maximum applied fatigue load is much lower than their yield stress. The primary aim of this thesis was to investigate the strengthening effects of EBR and NSM CFRP elements and their impact on the behaviour and fatigue life of reinforced concrete structural elements under fatigue load. In addition, analytical models have been developed that can predict the response of reinforced concrete under fatigue load.

The state of the art review (Paper I) showed that the behaviour and fatigue life of FRP-strengthened reinforced concrete structures exceeds that of non-strengthened structures when similar load levels are applied. These fatigue life improvements are due to strengthening arising from the relief of stress in tensile steel bars. It can be concluded that FRP strengthening is a promising method for relieving stress and increasing the fatigue life of structures. The review also showed that the effectiveness of strengthening materials at increasing the fatigue life of RC structures depends on the nature of the bond between the strengthening material and the concrete substrate. An adequately strong bond is required to efficiently distribute stress from the member to the strengthening element, reducing the stress within the steel reinforcement. Therefore beams strengthened using the epoxy-based NSM technique exhibited superior fatigue behaviour to those strengthened with EBR plates or sheets.

Furthermore, it has been shown through laboratory testing (paper II) that the fatigue life of strengthened beams will be less than that of unstrengthened beams if their tensile steel bars have the same stress level at loading. This is because the load applied to the strengthened beams will be much higher than those applied to the unstrengthened beams, causing high levels of local shear stress in the reinforcing steel at the locations of cracks, especially after

destroyed concrete interlock and crack growth due to cyclic loading of fractured interfaces. The locations of the steel bar's ruptures in the experimental tests strengthened this assumption: the ruptures occurred directly beneath the points at which the loads were applied, where the shear stresses were highest. In addition, the crack spacing in the strengthened beams was smaller than in unstrengthened ones, which caused the steel bars between adjacent cracks behave as a shear resistance element. With respect to the first steel bar rupture, the fatigue life of EBR plate-strengthened beams was greater than that for their NSM bar counterparts. This implies that the beams strengthened with NSM bars had higher local concentrated stresses than beams strengthened with EBR plates, probably because the EBR plates had larger contact areas on the lower faces of the beam and were thus more effective at restraining crack growth. The ductility of the NSM-strengthened beams at fatigue failure was greater than that of the EBR plate-strengthened beams, as demonstrated by their total deflection during the final fatigue cycle.

The fatigue life values of pre-cracked strengthened beams were greater than those of the strengthened beams without pre-cracking. This may indicate that pre-cracked beams are more like unstrengthened beams than initially uncracked strengthened beams. This behaviour was especially pronounced in the pre-cracked plate-strengthened beam, which is consistent with the suggestion that plate strengthening produces lower levels of concentrated stress than NSM bar strengthening. These results are interesting because they are the most likely to be reflective of the situation encountered in practical applications of CFRP strengthening, for example in bridges that have deteriorated due to increasing applied (traffic) loads.

The effect of strengthening on crack patterns, curvature, and the width and height of cracks was investigated using DIC (Digital Image Correlation) technique (Paper III). The major principal strain range distributions within the DIC measurement area were characterized using the DIC software and used to analyse the distribution of cracks across the surfaces of the tested beams at specific cycles during the fatigue tests. The major principal strain contours revealed the locations of surface cracks, showing that the presence of the CFRP plates and bars influenced the pattern of cracking. Strengthened beams exhibited a more localized crack distribution within their middle sections than were seen in the unstrengthened beam. The average crack spacing in beams strengthened with the EBR plate method was higher than in those strengthened with NSM bar method. This could be attributed to the larger contact area of the strengthening plates. DIC also proved to be useful for the calculating the vertical displacement within a region of interest of the tested beams. This in turn made it possible to determine the beams' flexural curvature by fitting a second degree polynomial to the vertical displacement along the length of the observation area. The curvature is equal to the second derivation of the fitted second degree polynomial function, which is equal to twice the coefficient of the polynomial's highest degree. The curvature profiles demonstrated that the strengthened beams had lower curvatures than the unstrengthened control, and that the greatest changes in curvature occurred during the first cycle. Thereafter, the curvature remained almost constant for the rest of the fatigue loading process. Crack widths were estimated from the distribution of the longitudinal displacement along the bottom edge of the beam at level of the reinforcing steel bars: jumps in the x-displacement were attributed to

crack openings, with the magnitude of the jump providing an estimate of the crack width. A crack bridging effect was observed in the strengthened specimens, where cracks bridged by strengthening materials were much narrower than those in unstrengthened beams. It was also observed that the crack width range in beams strengthened with EBR plates was lower than that in beams strengthened with NSM bars. This could again be attributed to the greater contact area of the plates compared to the bars.

The DIC data were also used to determine the heights of the newly formed cracks by colour post-processing of the DIC images. The cracks did not propagate through the beam at any point during the test and were shortest in the plate-strengthened beams.

An analytical model (Paper IV) was developed to predict the deflection and residual strain of strengthened reinforced concrete beams under fatigue loading. The model accounts for the fatigue properties of the concrete and CFRP strengthening material and was based on the fibre section technique. Its output correlated closely with the available experimental data. In addition, a number of fatigue life models for predicting the number of cycles until failure of FRP-strengthened RC beams were evaluated. For beams whose primary failure mode was reinforcing steel fracture, the equation of Helgason and Hanson (Zorn, 2006) or that included in the Model Code (2010) provided the best results.

Finally, a damage model of the FRP-concrete interface bond under high-cycle fatigue was developed (Paper V). This model combines an elastic meso-scale model with an elastic-plastic micro-scale model that is coupled with a damage model. The advantage of this two-scale model for high-cycle fatigue damage is that the plasticity and damage occur at the micro-scale, and the stiffness degradation of the material at the meso-scale does not need to be modelled as it does in other models to describe damage in the joint. The new model was implemented in an FE program and used to model a double shear joint specimen that had been studied under high-cycle fatigue in an earlier experimental investigation. The model can be used to perform calculations using a complete increment cyclical procedure or a faster cycle-jumping procedure. Its most important features are that its parameters are easily obtained from the results of static testing of FRP-concrete joints. The model efficiently computed the damage sustained by an FRP-concrete bond under high-cycle fatigue loading before the fracture stage is reached. The sensitivity of the model to different parameters was determined, and the results obtained demonstrated that it is useful for modelling different aspects of a joint's behaviour under high-cycle fatigue.

5.2 Conclusions

This thesis concludes by answering the research questions posed in the opening chapter and papers.

What is the most important factor that determines the impact of a strengthening material on the fatigue life of strengthened beams subject to fatigue loads?

The state of the art review indicated that the effectiveness of strengthening materials at increasing the fatigue life of reinforced concrete beams depended on the behaviour of the bond between the strengthening material and the concrete substrate. Effective strengthening

was achieved when the bond was robust enough to efficiently transfer stress from the member to the strengthening element and thereby reduce the stress on the steel reinforcement.

Are EBR plates better or worse than NSM bars for keeping the fatigue life of RC beams?

The results obtained in this work suggest that the fatigue life of strengthened beams should be calculated by summing the fatigue life of the steel reinforcement and the remaining fatigue life of the FRP-concrete bond after the fracture of the reinforcing steel. EBR plate-strengthened beams had greater fatigue life values prior to the first rupture of the reinforcing steel than did beams strengthened with NSM bars. However, for beams strengthened with CFRP having a low Young's modulus, the proportion of the total fatigue life remaining after the rupture of the first reinforcing steel bar was greater for NSM bar-strengthened beams than for EBR plate-strengthened equivalents. The opposite was true for beams strengthened with CFRP having a high modulus of elasticity. The fatigue lives of pre-cracked strengthened beams were greater than those of strengthened beams without pre-cracking. The comparison of the fatigue lives of strengthened and unstrengthened beams was influenced by the need to apply higher loads to the former in order to maintain the same level of axial stress in the reinforcing tension steel bars. This increased the local shear stress acting on the steel reinforcement of the strengthened beams and thus increased the localized concentrations of stresses at the surfaces of the reinforcing bars, thereby reducing their fatigue life.

How can the behaviour and fatigue life of EBR- and NSM-strengthened RC beams be estimated accurately?

A model that satisfies these criteria was developed using the fibre section technique. An analytical model is proposed for predicting the deflection and residual strain of strengthened reinforced concrete beams under fatigue loading, which accounts for the fatigue properties of concrete and CFRP strengthening material. The model's output correlated closely with the available experimental data.

A two scale damage model of the FRP-concrete interface bond under high-cycle fatigue was shown to accurately represent the bond between the concrete and the strengthening material. This model combines an elastic mesoscale model with an elastic-plastic damage-coupled microscale model.

Fatigue life models (S-N) are useful for predicting the number of cycles a strengthened reinforced concrete beam can endure before failure. For CFRP-strengthened beams whose primary failure mode is steel fracture, the fatigue life can be predicted conservatively using the equation of Helgason and Hanson (Zorn, 2006) or that presented developed in the Model Code (2010).

In addition to the research equations above, additional findings related to the research have been summarised in the following sections.

EBR plate-strengthening allowed the beams to tolerate applied fatigue loads after the rupture of the reinforcing steel bars but less effectively than NSM bar strengthening. The beams strengthened with NSM bars continued to support the fatigue loads even after ruptures of the

four reinforcing steel bars, whereas EBR plated beams were only able to tolerate rupture in one of the steel bars. In addition, the mid-span deflection for beams strengthened with EBR plates was lower than that seen for beams strengthened with NSM bars. Specifically, the mid-span deflections for beams strengthened with EBR plates having high and low Young's moduli were approximately 15 % and 7 % lower than those for the corresponding NSM bar-strengthened beams.

The Young's modulus of the CFRP strengthening material affected the deflection of the beams during the fatigue test. The maximum deflection of NSM bar-strengthened beams using CFRP material having a high modulus of elasticity increased by 25% relative to that observed during the first cycle; the corresponding value for the bar-strengthened beam prepared using low Young's modulus CFRP was 23 %. For EBR plate-strengthened beams, the corresponding values were 16 and 13 %, respectively.

NSM bar strengthening was more effective in pre-cracked beams than in those without pre-cracking: the relative increase in the deflection of the pre-cracked bar-strengthened beam after a given number of loading cycles was 9% lower than that for the equivalent beam without pre-cracking, however, EBR plate strengthening was more effective for pre-cracked beams than NSM bar strengthening.

EBR plate strengthened beams formed narrower, shorter, and more widely spaced cracks than those strengthened with NSM bars, and were also appreciably stiffer.

5.3 Future research

The research presented in this thesis covers some experimental and analytical issues related to the FRP flexural strengthening of RC beams under monotonic and fatigue loading. Areas where further experimental, FE modelling, and analytical work on FRP strengthening of RC beams might be fruitful are outlined in this section.

5.3.1 Experimental

-One of the difficulties in verifying the potential of the constitutive model for the 3D bond interface element developed in this study is the fact that very few experimental data for fatigue of FRP-concrete bond under high cyclic fatigue are available in the literature. Therefore, more FRP-concrete bond shear tests loaded under fatigue are needed to collect a more extensive data set.

- Digital image correlation (DIC) strain measurements provided very useful information on the concrete surface, which was exploited in Paper III. An advantage of DIC relative to conventional measurement techniques is that it provides reliable data on the distribution of strain. A DIC-based investigation into the full-field strain distribution on the surface of FRP elements and the surrounding concrete during fatigue loading could be very revealing.

- The stress range used in the experiments presented in this work exceeded the endurance limit of the reinforcing steel. Future studies should focus on lower stress ranges to provide a better understanding of the differences in the fatigue behaviour of the two strengthening methods considered in this study.

-More data are required on the behaviour of FRP-strengthened RC structures in the field under fatigue loading with environmental exposure.

5.3.2 FE analysis

A new two-scale (meso-scale to micro-scale) damage model of the fibre-reinforced polymer (FRP)-concrete bond under high-cycle fatigue has been developed. The model efficiently computes the damage sustained by the FRP-concrete bond under high-cycle fatigue loading until the fracture stage is reached. However, the two-scale damage model appears to be most appropriate for describing describe damage phenomena under high cycle fatigue. Two-scale damage models for concrete, steel rebar and FRP materials could be created. It would be worthwhile to conduct research aiming to create 3D finite element codes capable of predicting the behaviour of reinforced concrete beams strengthened with both EBR and NSM elements under fatigue loading.

5.3.3 Analytical work

-The regression based models (S-N) are derived from available experimental test results with a wide range of parameters, which limits their accuracy. Limiting the range of parameters varied in the experimental work may increase their accuracy.

- The analytical model based on the fibre section method assumes that the final failure of the beam occurs when the first reinforcing steel bar is ruptured. However, the experimental results presented herein demonstrate that strengthened beams can bridge the gaps formed by such ruptures. It may therefore be necessary to incorporate a bond slip model based on the mechanisms governing the formation of fractures between the concrete and strengthening material to describe the events that occur after the rupture of the reinforcing steel bars.

References

ACI 440.2R. (2008). *Guide for the Design and Construction of Externally Bonded FRP Systems for Strengthening Concrete Structures (ACI440.2R).* American Concrete Institute, Farmington Hills,USA.

ACI Committee. 318R-14 (2014). *Building code requirements for structural concrete (ACI 318-14) and commentary (ACI 318R-14).* American Concrete Institute, Farmington Hills,USA.

ACI Committee 215. (1997). *Considerations for Design of Concrete Structures Subjected to Fatigue Loading.* American Concrete Institute, ACI 215R-74 (Reapproved 1997) Farmington Hills,USA.

Adimi, M. R., Rahman, A. H., and Benmokrane, B. (2000). "New method for testing fiber-reinforced polymer rods under fatigue." *J.Composite Constr.,* 4(4), 206-213.

Aidoo, J., Harries, K. A., and Petrou, M. F. (2006). "Full-scale experimental investigation of repair of reinforced concrete interstate bridge using CFRP materials." *J.Bridge Eng.,* 11(3), 350-358.

Aidoo, J., Harries, K. A., and Petrou, M. F. (2004). "Fatigue behavior of carbon fiber reinforced polymer-strengthened reinforced concrete bridge girders." *J.Composite Constr.,* 8(6), 501-509.

Al-Hammoud, R., Soudki, K., and Topper, T. H. (2010). "Fatigue flexural behavior of corroded reinforced concrete beams repaired with CFRP sheets." *J.Composite Constr.,* 15(1), 42-51.

Al-Rousan, R., and Issa, M. (2011). "Fatigue performance of reinforced concrete beams strengthened with CFRP sheets." *Constr.Build.Mater.,* 25(8), 3520-3529.

Antrim, C.,John. (1965). *A study of the mechanism of fatigue in cement paste and plain concrete.* PhD diss., Purdue University.

Badawi, M. A. (2007). *Monotonic and fatigue flexural behaviour of RC beams strengthened with prestressed NSM CFRP rods.* PhD diss., University of Waterloo.

Badawi, M., and Soudki, K. (2009). "Flexural strengthening of RC beams with prestressed NSM CFRP rods–experimental and analytical investigation." *Constr.Build.Mater.,* 23(10), 3292-3300.

Barnes, R. A., and Mays, G. C. (1999). "Fatigue performance of concrete beams strengthened with CFRP plates." *J.Composite Constr.,* 3(2), 63-72.

Barsom, J. M., and Rolfe, S. T. (1999). *Fracture and fatigue control in structures: applications of fracture mechanics.* ASTM International, USA.

Bfer, G. (1985). "An isoparametric joint/interface element for finite element analysis." *Int J Numer Methods Eng,* 21(4), 585-600.

Bizindavyi, L., Neale, K., and Erki, M. (2003). "Experimental investigation of bonded fiber reinforced polymer-concrete joints under cyclic loading." *J.Composite Constr.,* 7(2), 127-134.

Bogard, F., Lestriez, P., and Guo, Y. (2008). "Numerical modeling of fatigue damage and fissure propagation under cyclic loadings." *Int J Damage Mech,* 17(2), 173-187.

Breña, S. F., Benouaich, M. A., Kreger, M. E., and Wood, S. L. (2005). "Fatigue tests of reinforced concrete beams strengthened using carbon fiber-reinforced polymer composites." *ACI Struct.J.,* 102(2), 305-313.

Carolin, A., Täljsten, B., and Hejll, A. (2005). "Concrete beams exposed to live loading during carbon fiber reinforced polymer strengthening." *J.Composite Constr.,* 9(2), 178-186.

Chaallal, O., Boussaha, F., and Bousselham, A. (2010). "Fatigue performance of RC beams strengthened in shear with CFRP fabrics." *J.Composite Constr.,* 14(4), 415-423.

Comité Euro-International du Beton. (2010). *CEB/FIB Model Code 2010.* Thomas Telford, London.

Concrete Society Technical Report 55. (2000). *Design guidance for strengthening concrete structures using fibre composite materials.* The Concrete Society, UK.

Curtis, P. (1989). "The fatigue behaviour of fibrous composite materials." *The Journal of Strain Analysis for Engineering Design,* 24(4), 235-244.

Dai, J., Saito, Y., Ueda, T., and Sato, Y. (2005). "Static and fatigue bond characteristics of interfaces between CFRP sheets and frost damage experienced concrete." *ACI Special Publication,* 230.

De Lorenzis, L., and Nanni, A. (2002). "Bond between near-surface mounted fiber-reinforced polymer rods and concrete in structural strengthening." *ACI Struct.J.,* 99(2), 123-132.

Derkowski, W. (2006). "Fatigue life of reinforced concrete beams under bending strengthened with composite materials." *Archives of Civil and Mechanical Engineering,* 6(4), 33-47.

Diab, H., Wu, Z., and Iwashita, K. (2007). "Experimental and numerical investigation of fatigue behavior of FRP-concrete interface." *Proceedings of the 8th International Symposium on Fiber-Reinforced Polymer Reinforcement for Concrete Structures,* Greece.

Diab, H., and Wu, Z. (2008). "Review of existing fatigue results of beams externally strengthened with FRP laminates." *Proceedings of the 4th International Conference on FRP Composites in Civil Engineering (CICE2008),* Switzerland.

Diab, H., Wu, Z., and Iwashita, K. (2009). "Theoretical solution for fatigue debonding growth and fatigue life prediction of FRP-concrete interfaces." *Adv.Struct.Eng.,* 12(6), 781-792.

Diab, Y. (1998). "Strengthening of RC beams by using sprayed concrete: experimental approach." *Eng.Struct.,* 20(7), 631-643.

Dong, Y., Ansari, F., and Karbhari, V. M. (2011). "Fatigue performance of reinforced concrete beams with externally bonded CFRP reinforcement." *Structure and Infrastructure Engineering,* 7(3), 229-241.

Ekenel, M., and Myers, J. J. (2009). "Fatigue performance of CFRP strengthened RC beams under environmental conditioning and sustained load." *J.Composite Constr.,* 13(2), 93-102.

El Refai, A. M. (2007). *Monotonic and fatigue flexural performance of RC beams strengthened with externally post-tensioned CFRP tendons*. PhD diss., University of Waterloo.

El-Tawil, S., Ogunc, C., Okeil, A., and Shahawy, M. (2001). "Static and fatigue analyses of RC beams strengthened with CFRP laminates." *J.Composite Constr.,* 5(4), 258-267.

Ferrier, E., Bigaud, D., Clement, J., and Hamelin, P. (2011). "Fatigue-loading effect on RC beams strengthened with externally bonded FRP." *Constr.Build.Mater.,* 25(2), 539-546.

Ferrier, E., Bigaud, D., Hamelin, P., Bizindavyi, L., and Neale, K. (2005). "Fatigue of CFRPs externally bonded to concrete." *Mater.Struct.,* 38(1), 39-46.

Gheorghiu, C., Labossière, P., and Proulx, J. (2007). "Response of CFRP-strengthened beams under fatigue with different load amplitudes." *Constr.Build.Mater.,* 21(4), 756-763.

Gheorghiu, C., Labossière, P., and Raiche, A. (2004). "Environmental fatigue and static behavior of RC beams strengthened with carbon-fiber-reinforced polymer." *J.Composite Constr.,* 8(3), 211-218.

Gorty, S. (1994). *Mechanical Properties of Composite Cables*, Master Thesis, South Dakota School of Mines and Technology, South Dakota.

Gunes, O., Karaca, E., and Gunes, B. (2006). "Design of FRP retrofitted flexural members against debonding failures." *Proceedings of the 8th US National Conference on Earthquake Engineering,USA* .

Gussenhoven, R., and Brena, S. (2005). "Fatigue behavior of reinforced concrete beams strengthened with different FRP laminate conFigurations." *ACI Special Publication,* 230.

Gylltoft, K. (1983). *Fracture Mechanics Models for Fatigue in Concrete Structures*, Luleå Institute of Technology, Division of Structural Engineering.

Harries, K. (2005). "Fatigue behaviour of bonded FRP used for flexural retrofit." *Proceedings of international symposium on bond behaviour of FRP in structures (BBFS 2005),* China.

Harries, K. A., and Aidoo, J. (2006). "Debonding-and fatigue-related strain limits for externally bonded FRP." *J.Composite Constr.,* 10(1), 87-90.

Harries, K. A., Reeve, B., and Zorn, A. (2007). "Experimental evaluation of factors affecting monotonic and fatigue behavior of fiber-reinforced polymer-to-concrete bond in reinforced concrete beams." *ACI Struct.J.,* 104(6), 667-674.

Hashin, Z. (1980). "Failure criteria for unidirectional fiber composites." *Journal of Applied Mechanics,* 47(2), 329-334.

Hassan, T. K., and Rizkalla, S. H. (2004). "Bond mechanism of near-surface-mounted fiber-reinforced polymer bars for flexural strengthening of concrete structures." *ACI Struct.J.,* 101(6), 830-839.

Heffernan, P., and Erki, M. (2004). "Fatigue behavior of reinforced concrete beams strengthened with carbon fiber reinforced plastic laminates." *J.Composite Constr.,* 8(2), 132-140.

Holmen, J. O. (1982). "Fatigue of concrete by constant and variable amplitude loading." *ACI Special Publication,* 75.

Huang, P., Zhou, H., Wang, H., and Guo, X. (2011). "Fatigue lives of RC beams strengthened with CFRP at different temperatures under cyclic bending loads." *Fatigue & Fracture of Engineering Materials & Structures,* 34(9), 708-716.

ISIS Canada. (2008). *FRP Rehabilitation of Reinforced Concrete Structures.* ISIS Canada Research Network, Canada.

ISO, E. "6892–1: 2009 (2009). *Metallic Materials-Tensile Testing-Part 1: Method of Test at Room Temperature,* Brussels: European committee for standardization (cen).

Johansson, U. (2004). "Fatigue tests and analysis of reinforced concrete bridge deck models." *Trita-BKN.Bulletin,* 76 1-197.

Jones, R. M. (1998). *Mechanics of composite materials.* Taylor&Francis, USA.

JSCE. (2001). *Recommendations for upgrading of concrete structures with use of continuous fiber sheets.* Japan Society of Civil Engineers, Japan.

Khan, A., Al-Gadhib, A., and Baluch, M. (2011). "Experimental and computational modeling of low cycle fatigue damage of CFRP strengthened reinforced concrete beams." *Int J Damage Mech,* 20(2), 211-243.

Kiewel, H., Aktaa, J., and Munz, D. (2000). "Application of an extrapolation method in thermocyclic failure analysis." *Comput.Methods Appl.Mech.Eng.,* 182(1), 55-71.

Kim, Y. J., and Heffernan, P. J. (2008). "Fatigue behavior of externally strengthened concrete beams with fiber-reinforced polymers: State of the art." *J.Composite Constr.,* 12(3), 246-256.

Ko, H., and Sato, Y. (2007). "Bond stress–slip relationship between FRP sheet and concrete under cyclic load." *J.Composite Constr.,* 11(4), 419-426.

Lee, M., and Barr, B. (2004). "An overview of the fatigue behaviour of plain and fibre reinforced concrete." *Cement and Concrete Composites,* 26(4), 299-305.

Lemaitre, J., Sermage, J., and Desmorat, R. (1999). "A two scale damage concept applied to fatigue." *Int.J.Fract.,* 97(1-4), 67-81.

Lemaitre, J. (2001). *Handbook of Materials Behavior Models, Three-Volume Set: Nonlinear Models and Properties.* Academic Press, USA.

Lemaitre, J., and Desmorat, R. (2005). *Engineering damage mechanics: ductile, creep, fatigue and brittle failures.* Springer, Netherlands.

Lin, R., Huang, P., Zhao, C., Guo, X., and Zheng, X. (2008). "Prediction of fatigue lives of RC beams strengthened with CFL under random loading." *Acta Mechanica Solida Sinica,* 21(4), 359-363.

Lloyd, J. P., Lott, J. L., and Kesler, C. E. (1968). "Fatigue of concrete." *University of Illinois, Urnana-Champkign.*

Loo, K. Y. M., Foster, S. J., and Smith, S. T. (2012). "FE modeling of CFRP-repaired RC beams subjected to fatigue loading." *J.Composite Constr.,* 16(5), 572-580.

Ma, Q. L., Lu, X. Z., Ye, L. P., and Zhang, K. (2007). "Study on fatigue behavior of RC beams strengthened with prestressed CFRP sheets." *Proceedings of the 8th International Symposium on Fiber-Reinforced Polymer Reinforcement for Concrete Structures (FRPRCS-8), Greece.*

Mahal, M., Blanksvärd, T., and Täljsten, B. (2013). "Examination at a Material and Structural Level of the Fatigue Life of Beams Strengthened with Mineral or Epoxy Bonded FRPs: The State of the Art." *Adv.Struct.Eng.,* 16(7), 1311-1328.

Mahal, M. (2015). *Experimental investigations of RC beams strengthened with FRP materials under monotonic and fatigue loads*. Luleå University of Technology, Sweden.

Masoud, S., Soudki, K., and Topper, T. (2001). "CFRP-strengthened and corroded RC beams under monotonic and fatigue loads." *J.Composite Constr.,* 5(4), 228-236.

Masoud, S., Soudki, K., and Topper, T. (2005). "Postrepair fatigue performance of FRP-repaired corroded RC beams: experimental and analytical investigation." *J.Composite Constr.,* 9(5), 441-449.

Mazzotti, C., and Savoia, M. (2009). "FRP-concrete bond behaviour under cyclic debonding force." *Adv.Struct.Eng.,* 12(6), 771-780.

M-Brace. (2002). *MBrace Composite Strengthening System-Engineering Design Guidelines.* 3rd Edition, Watson Bowman Acme Corp., USA.

Meier, U., Deuring, M., Meier, H., and Schwegler, G. (1992). "Strengthening of Structures with CFRP Laminates: Research and Applications in Switzerland." *Proceedings of the 1st International Conference on Advanced Composite Materials in Bridges and Structures,* Canadian Society of Civil Engineering, 228-236.

Minnaugh, P. L., and Harries, K. A. (2009). "Fatigue behavior of externally bonded steel fiber reinforced polymer (SFRP) for retrofit of reinforced concrete." *Mater.Struct.,* 42(2), 271-278.

Mogami, K., Hayashi, T., Ando, K., and Ogura, N. (1990). "Elastic-plastic fatigue-crack growth and tearing-instability behavior under cyclic loads." *Int.J.Pressure Vessels Piping,* 44(1), 85-97.

Newaz, G. M. (1985). "Influence of matrix material on flexural fatigue performance of unidirectional composites." *Composites Sci.Technol.,* 24(3), 199-214.

Nigro, E., Di Ludovico, M., and Bilotta, A. (2010). "Experimental investigation of FRP-concrete debonding under cyclic actions." *J.Mater.Civ.Eng.,* 23(4), 360-371.

NRC. (2004). *Guide for the Design and Construction of Externally Bonded FRP Systems for Strengthening Existing Structures*. National Research Council, Italy.

O'Neill, A., Harries, K. A., and Minnaugh, P. (2007). "Fatigue behavior of adhesive systems used for externally-bonded FRP applications." *Proceedings of the Third International Conference on Durability and Field Applications of Fiber Reinforced Polymer (FRP) Composites for Construction (CDCC 2007), Canada.*

Oudah, F., and El-Hacha, R. (2012). "Fatigue behavior of RC beams strengthened with prestressed NSM CFRP rods." *Composite Structures,* 94(4), 1333-1342.

Papakonstantinou, C. G., Balaguru, P. N., and Petrou, M. F. (2002). "Analysis of reinforced concrete beams strengthened with composites subjected to fatigue loading." *ACI Special Publication,* 206.

Papakonstantinou, C. G., Petrou, M. F., and Harries, K. A. (2001). "Fatigue behavior of RC beams strengthened with GFRP sheets." *J.Composite Constr.,* 5(4), 246-253.

Quattlebaum, J. B., Harries, K. A., and Petrou, M. F. (2005). "Comparison of three flexural retrofit systems under monotonic and fatigue loads." *J.Bridge Eng.,* 10(6), 731-740.

Ramakrishnan, V., and Jayaraman, N. (1993). "Mechanistically based fatigue-damage evolution model for brittle matrix fibre-reinforced composites." *J.Mater.Sci.,* 28(20), 5592-5602.

RILEM Recommendations, R. D. (1991). "TC89-FMT Fracture Mechanics of Concrete–Test Methods: Determination of Fracture Parameters of Plain Concrete using Three-Point Bending Test." *Mater.Struct.,* 23 457-460.

Romualdi, J. P. (1987). "Ferro-cement for infrastructure rehabilitation." *Concr.Int.,* 9(9), 24-28.

Rosenboom, O., and Rizkalla, S. (2006). "Behavior of prestressed concrete strengthened with various CFRP systems subjected to fatigue loading." *J.Composite Constr.,* 10(6), 492-502.

Salvia, M., Fiore, L., Fournier, P., and Vincent, L. (1997). "Flexural fatigue behaviour of UDGFRP experimental approach." *Int.J.Fatigue,* 19(3), 253-262.

Schütz, D., and Gerharz, J. (1977). "Fatigue strength of a fibre-reinforced material." *Composites,* 8(4), 245-250.

Sena-Cruz, J. M., Barros, J. A., Coelho, M. R., and Silva, L. F. (2012). "Efficiency of different techniques in flexural strengthening of RC beams under monotonic and fatigue loading." *Constr.Build.Mater.,* 29,175-182.

Senthilnath, P., Belarbi, A., and Myers, J. J. (2001). "Performance of CFRP strengthened reinforced concrete (RC) beams in the presence of delaminations and lap splices under fatigue loading." *Proceeding of the International Conference in Construction, Portuga.*

Shahawy, M., and Beitelman, T. E. (1999). "Static and fatigue performance of RC beams strengthened with CFRP laminates." *J.Struct.Eng.,* 125(6), 613-621.

SIS. (2009b). *SS-EN 12390-6:2009 Testing hardened concrete - Part 6: Tensile splitting strength of test specimens.* Swedish Standards Institute, Sweden.

SIS. (2009a). *SS-EN 12390-3:2009 Testing hardened concrete - Part 3: Compressive strength of test specimens.* Swedish Standards Institute, Sweden.

Skrzypek, J. J., and Ganczarski, A. (1999). *Modeling of material damage and failure of structures: Theory and applications.* Springer, Germany.

Täljsten, B., and Skanska Teknik, A. (2002). " CFRP-strengthening-concrete structures strengthened with near surface mounted CFRP laminates." *Department of Civil Engineering, Luleå University of Technology; Skanska Teknik AB.*

Täljsten, B. (2006). "The importance of bonding–a historic overview and future possibilities." *Adv.Struct.Eng.,* 9(6), 721-736.

Täljsten, B. (1997). "Defining anchor lengths of steel and CFRP plates bonded to concrete." *Int J Adhes Adhes,* 17(4), 319-327.

Täljsten, B. (1994). *Plate bonding strengthening of existing concrete structures with epoxy bonded plates of steel or fibre reinforced plastics.*PhD diss., Lulea University of Technology. Sweden.

Tan, K. H., and Saha, M. K. (2007). "Glass FRP bonded RC beams under cyclic loading." *International Journal of Concrete Structures and Materials,* 1(1), 45-55.

Techniques, G. O. M. (2005). *Aramis v5. 4 user manual.* Gom Mbh.

Toutanji, H., Zhao, L., Deng, Y., Zhang, Y., and Balaguru, P. (2006). "Cyclic behavior of RC beams strengthened with carbon fiber sheets bonded by inorganic matrix." *J.Mater.Civ.Eng.,* 18(1), 28-35.

Wahab, N. A. (2011). *Bond Behaviour of Beams Reinforced with Near Surface Mounted Carbon Fibre Reinforced Polymer Rods under Fatigue Loading.*PhD diss., University of Waterloo.

Wahab, N., Soudki, K. A., and Topper, T. (2012). "Experimental investigation of bond fatigue behavior of concrete beams strengthened with NSM prestressed CFRP rods." *J.Composite Constr.,* 16(6), 684-692.

Wang, P., Cui, L., Lyschik, M., Scholz, A., Berger, C., and Oechsner, M. (2012). "A local extrapolation based calculation reduction method for the application of constitutive material models for creep fatigue assessment." *Int.J.Fatigue,* 44, 253-259.

Wang, Y., Lee, M., and Chen, B. (2007). "Experimental study of FRP-strengthened RC bridge girders subjected to fatigue loading." *Composite Structures,* 81(4), 491-498.

Warner, R., and Hulsbos, C. (1966). "Probable fatigue life of prestressed concrete beams." *Pci j.,* 11(2), 16-39.

Xavier, J., Sousa, A. M., Morais, J. J., Filipe, V. M., and Vaz, M. (2012). "Measuring displacement fields by cross-correlation and a differential technique: experimental validation." *Optical Engineering,* 51(4), 043602-1-043602-12.

Yang, X., and Nanni, A. (2002). "Lap splice length and fatigue performance of fiber-reinforced polymer laminates." *ACI Mater.J.,* 99(4*), 386-392.*

Yao, G., Huang, P. Y., and Zhao, C. (2006). "Flexural fracture and fatigue behavior of RC beams strengthened with CFRP laminates under constant amplitude loading." *Key Eng Mat,* 306 ,1343-1348.

Yost, J. R., Gross, S. P., and Deitch, M. J. (2007). "Fatigue behavior of concrete beams strengthened in flexure with near surface mounted CFRP." *Proceedings of the 8th International Symposium on Fiber-Reinforced Polymer Reinforcement for Concrete Structures (FRPRCS-8), Greece.*

Yu, T., Li, C., Lei, J., and Zhang, H. (2011). "Fatigue of concrete beams strengthened with glass-fiber composite under flexure." *J.Composite Constr.,* 15(4), 557-564.

Yun, Y., Wu, Y., and Tang, W. C. (2008). "Performance of FRP bonding systems under fatigue loading." *Eng.Struct.,* 30(11), 3129-3140.

Zheng, S. S., Wang, B., Li, L., Zhang, L., and Hou, P. J. (2008). "Fatigue-Cumulative Damage Model of RC Crane Girders Strengthened with FRP Strips." *Key Eng Mat,* 385, 165-168.

Zorn, A. V. (2006). *Effect of Adhesive Stiffness and CFRP Geometry on the Behavior of Externally Bonded CFRP Retrofit Measures.* PhD diss., University of Pittsburgh.

Appendix A Deflection of fatigue tested beams
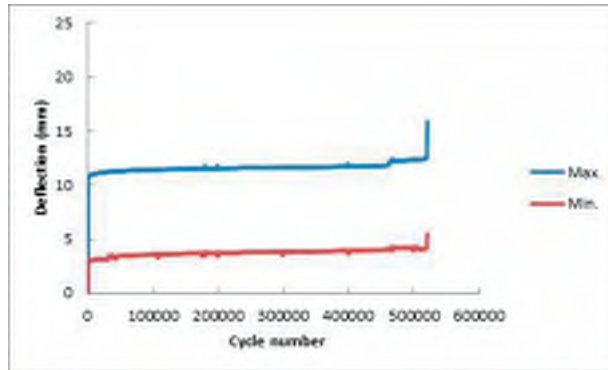
Figure A.1 Deflection - cycle number of Beam B1-EE1-F.
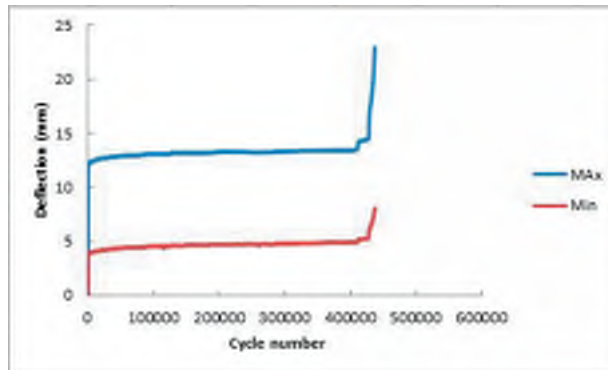
Figure A.2 Deflection - cycle number of Beam B3-NE1-F.
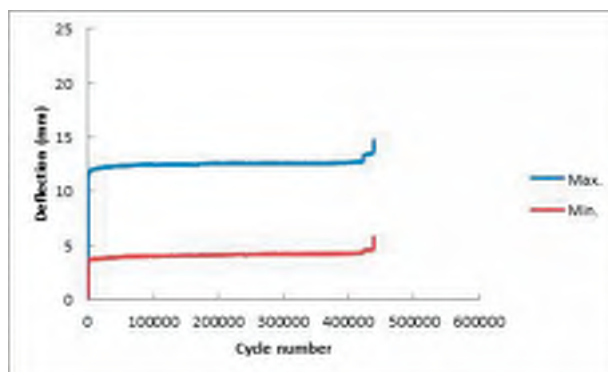
Figure A.3 Deflection - cycle number of Beam B6-EE2-F.
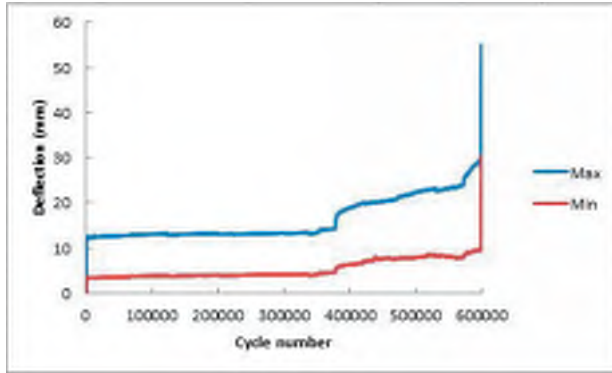
Figure A.4 Deflection - cycle number of Beam B8-NE2-F.
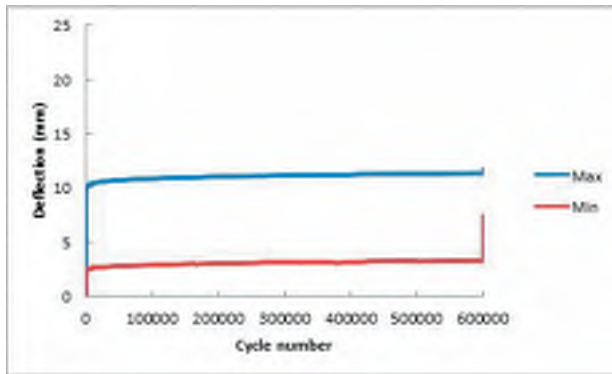
Figure A.5 Deflection - cycle number of Beam B9-EE1-F-C.
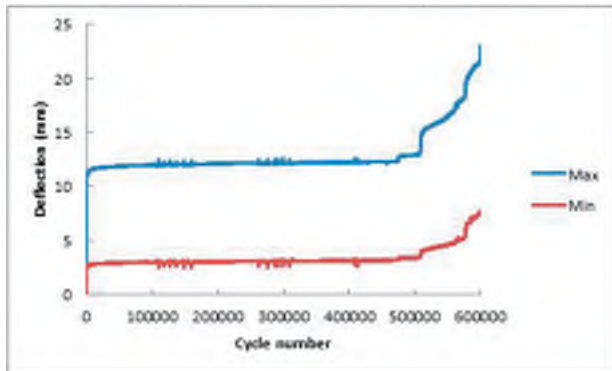
Figure A.6 Deflection - cycle number of Beam B10-NE1-F-C.
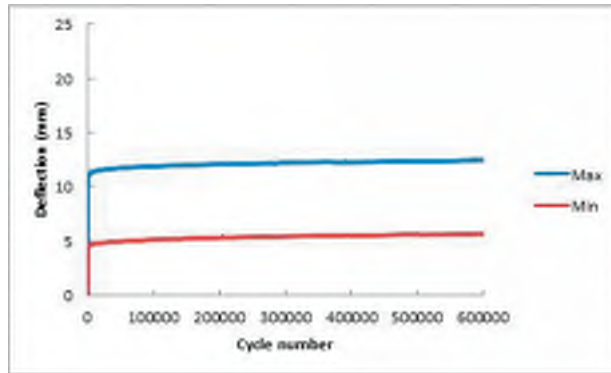
Figure A.7 Deflection - cycle number of Beam B13-0-F.

Appendix B Strain distribution

1. Strain distribution of fatigue tested beams
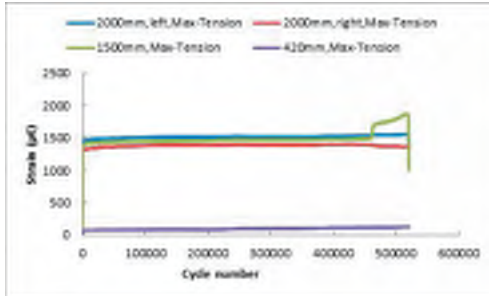
Max. tensile steel strain- cycle number.
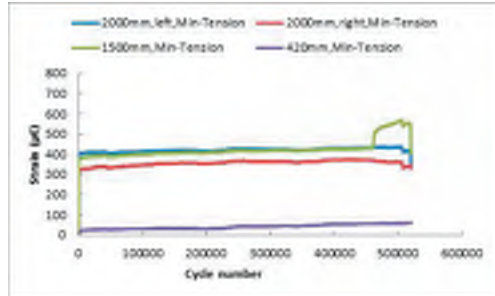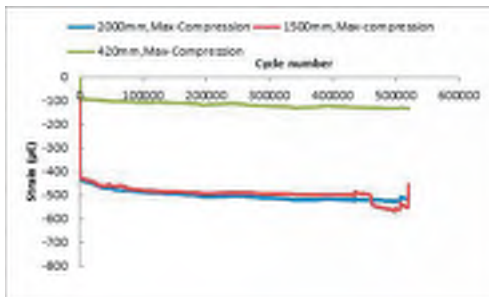
Min tensile steel strain- cycle number.

Max. compressive steel strain- cycle number.
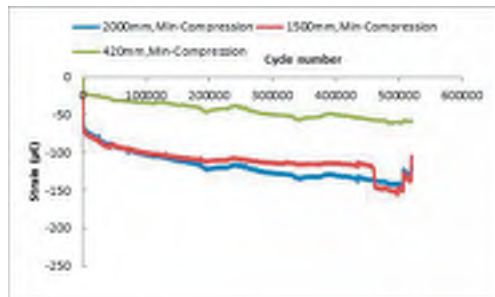
Min. compressive steel strain- cycle number.
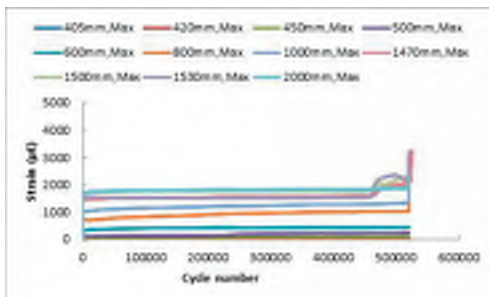
Max. Fibre strain- cycle number.
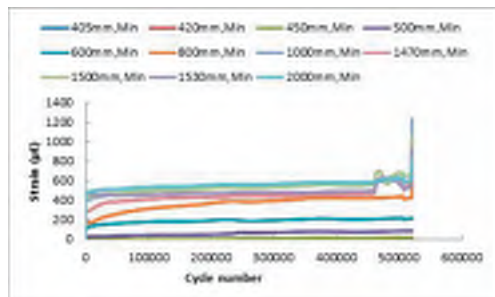
Min. Fibre strain- cycle number.

Figure B.1.1 Strain distribution of Beam B1-EE1-F.
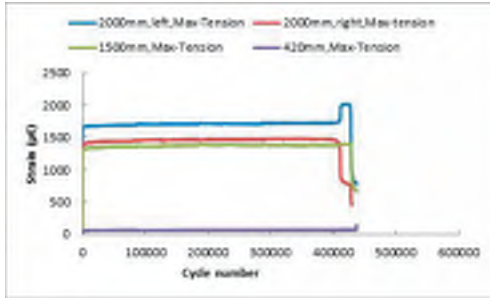
Max. tensile steel strain- cycle number.
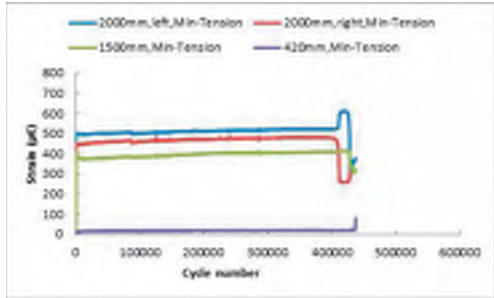
Min tensile steel strain- cycle number.

Max. compressive steel strain- cycle number.
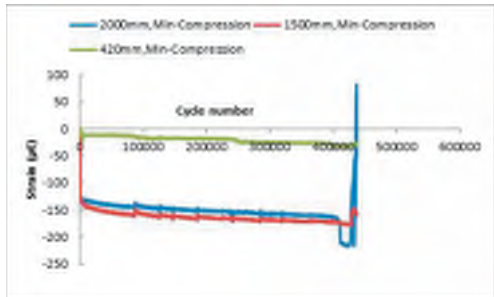
Min. compressive steel strain- cycle number.
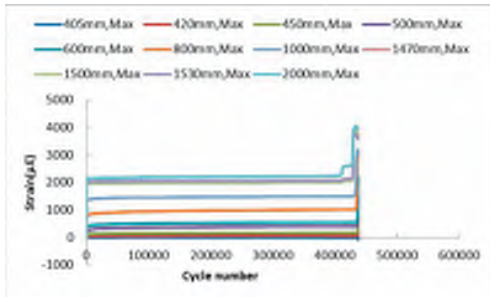
Max. Fibre strain- cycle number.
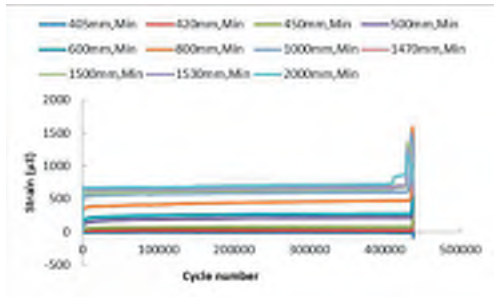
Min. Fibre strain- cycle number.

Figure B.1.2 Strain distribution of Beam B3-NE1-F.
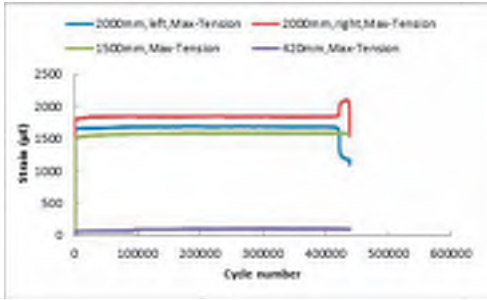
Max. tensile steel strain- cycle number.
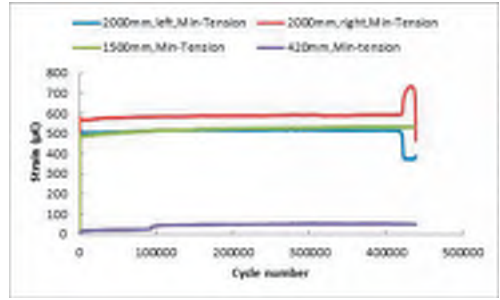
Min tensile steel strain- cycle number.

Max. compressive steel strain- cycle number.
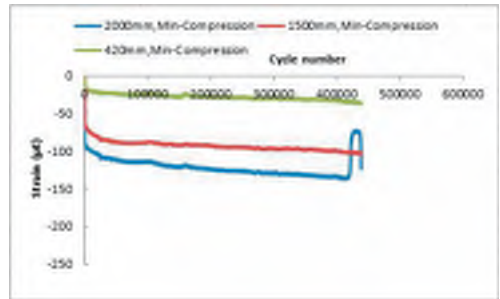
Min. compressive steel strain- cycle number.
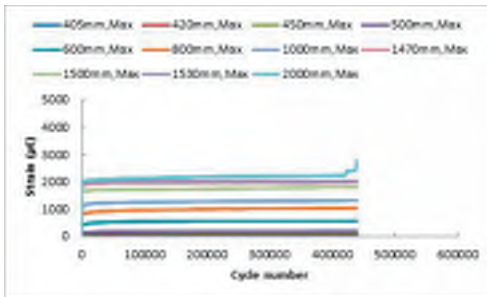
Max. Fibre strain- cycle number.
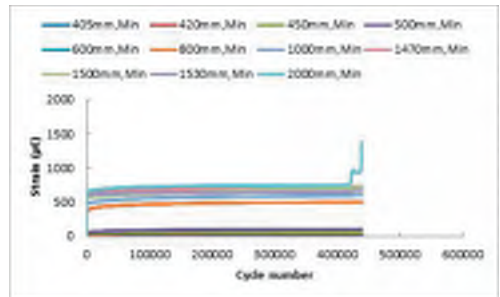
Min. Fibre strain- cycle number.

Figure B.1.3 Strain distribution of Beam B6-EE2-F.
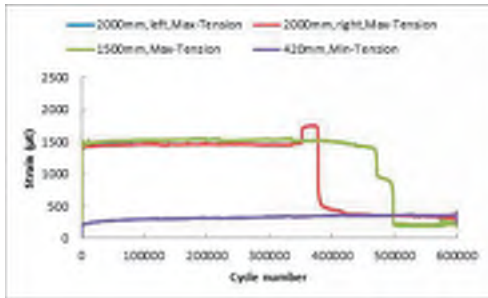
Max. tensile steel strain- cycle number.
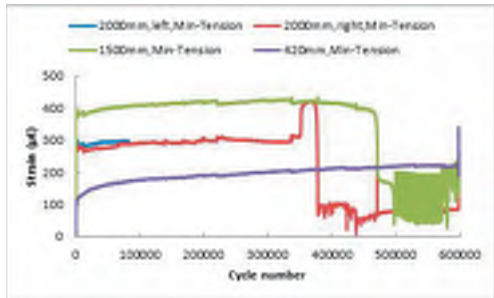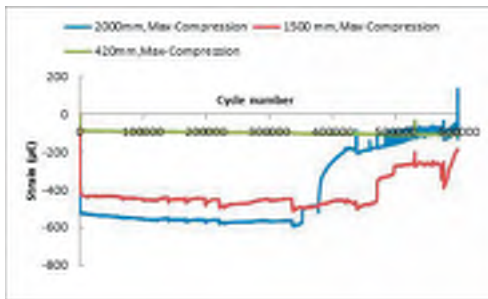
Min tensile steel strain- cycle number.

Max. compressive steel strain- cycle number.
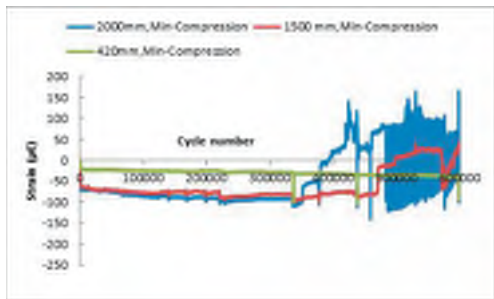
Min. compressive steel strain- cycle number.
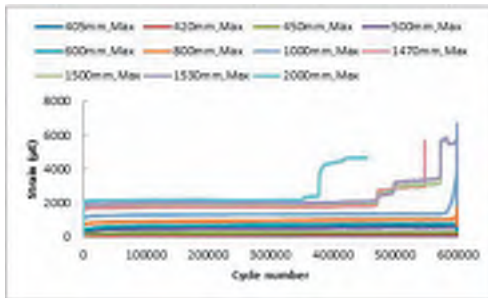
Max. Fibre strain- cycle number.
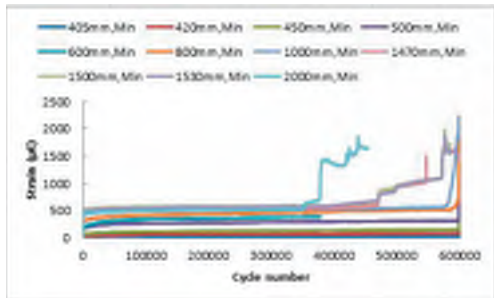
Min. Fibre strain- cycle number.

Figure B.1.4 Strain distribution of Beam B8-NE2-F.
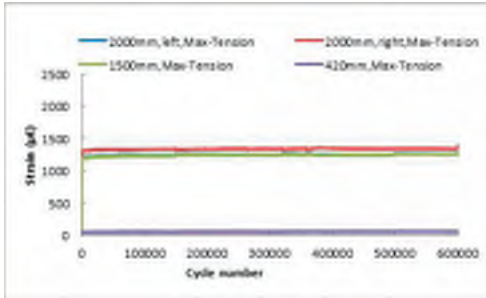
Max. tensile steel strain- cycle number.
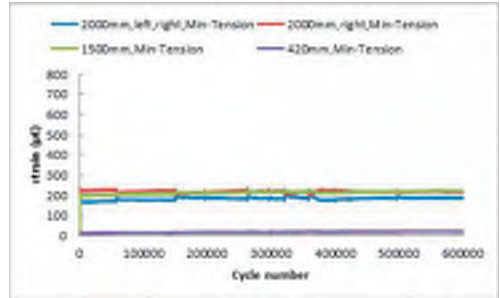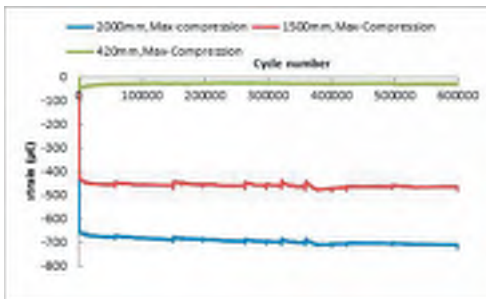
Min tensile steel strain- cycle number.

Max. compressive steel strain- cycle number.
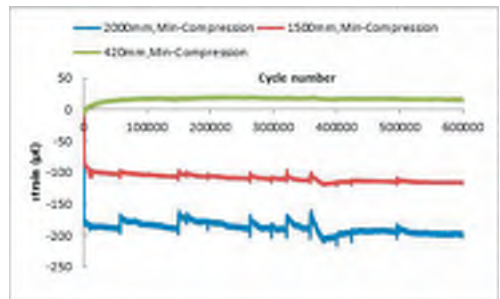
Min. compressive steel strain- cycle number.
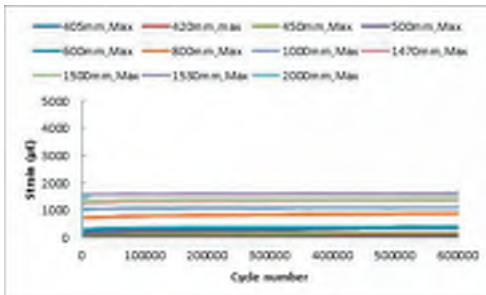
Max. Fibre strain- cycle number.
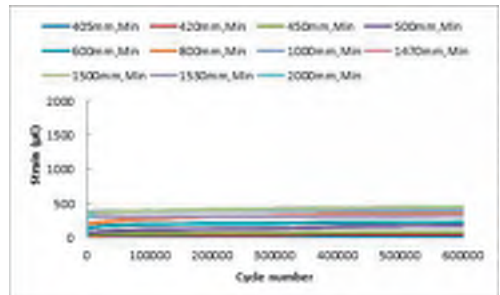
Min. Fibre strain- cycle number.

Figure B.1.5 Strain distribution of Beam B9-EE1-F-C.
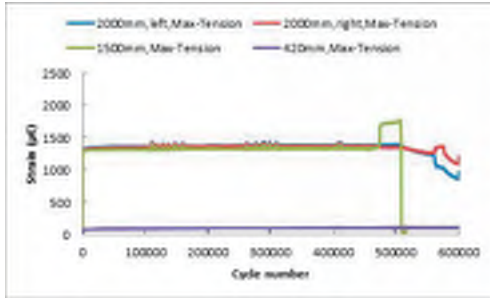
Max. tensile steel strain- cycle number.
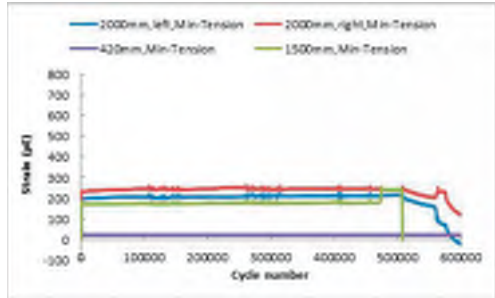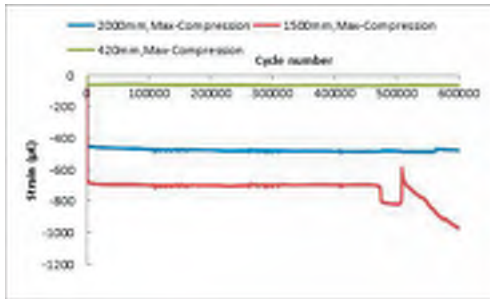
Min tensile steel strain- cycle number.

Max. compressive steel strain- cycle number.
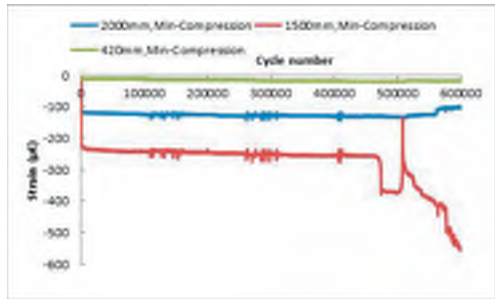
Min. compressive steel strain- cycle number.
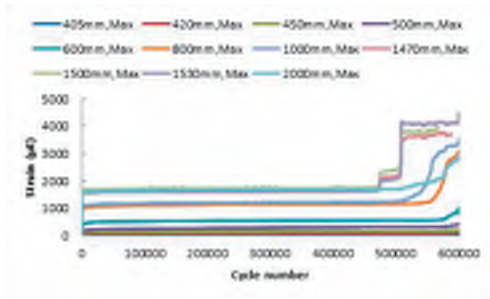
Max. Fibre strain- cycle number.
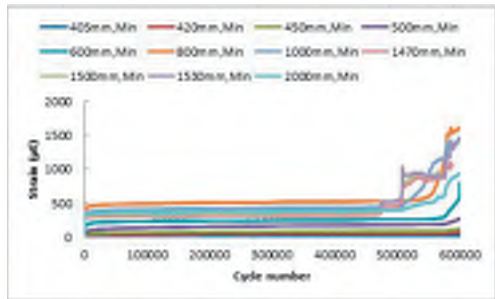
Min. Fibre strain- cycle number.

Figure B.1.6 Strain distribution of Beam B10-NE1-F-C.
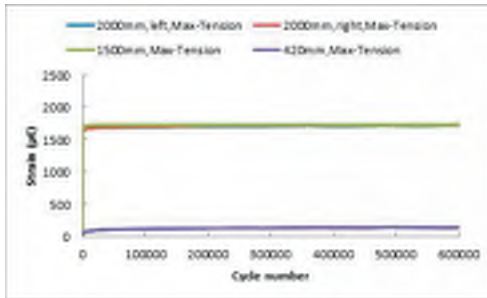
Max. tensile steel strain- cycle number.
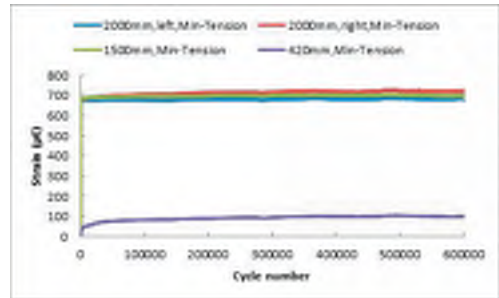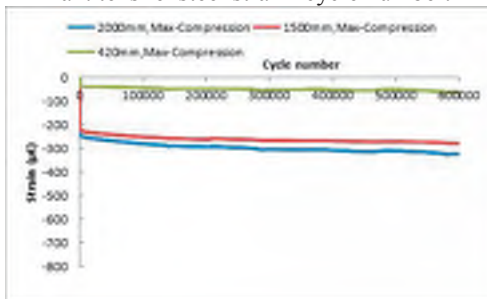
Min tensile steel strain- cycle number.

Max. compressive steel strain- cycle number.
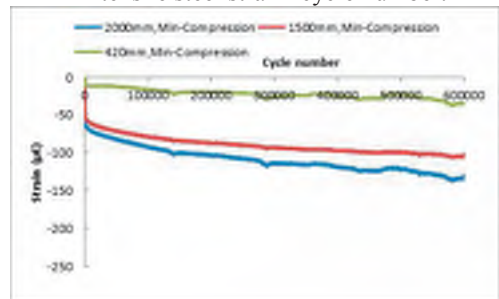
Min. compressive steel strain- cycle number.

Figure B.1.7 Strain distribution of Beam B13-0-F.

2. Strain distribution of statically tested beams

The variation of FRP strains and reinforcement strains with applied load are shown in this appendix. In general, the FRP strains of beam increased for strain gages that were closer to the midspan for a given applied load. This is because the FRP was fully bonded along the beam length and strains were proportional to the moment at that section. After cracks appeared at mid-span, the increase rate of strain at gages in the constant moment region were faster since the tension stress in concrete is released at the time of cracking.

In beams (B2-EE1-S and B5-EE2-S),after the peak load the sudden decreasing in strains at the constant moment regain can easily explained as the debonding failure of the beam from the mid span towards the cutoff point.In beam (B7-NE2-S), after the peak load the sudden faster decreasing in gauge strain under the applied load point than the remaining all gauges strain except the strain gauge at the mid span can explained as the debonding failure of the beam from the mid span towards the cutoff point.For beam (B4-NE1-S) , at the peak load, FRP gauge strains under the applied load point was only decreases and give no evidence of the propagation of NSM bar debonding.

The reinforcement strain gauges are named as the positions of gauge from the right support of the beam. Before cracking, the strains were very small and then gradually increased as loading progressed. The strain in the center of the beam increased more than the strain gauge in the shear span, in accordance with the variation of the bending moment in the beam.it was clear from all figures that the all beams have got yielding of steel bars.
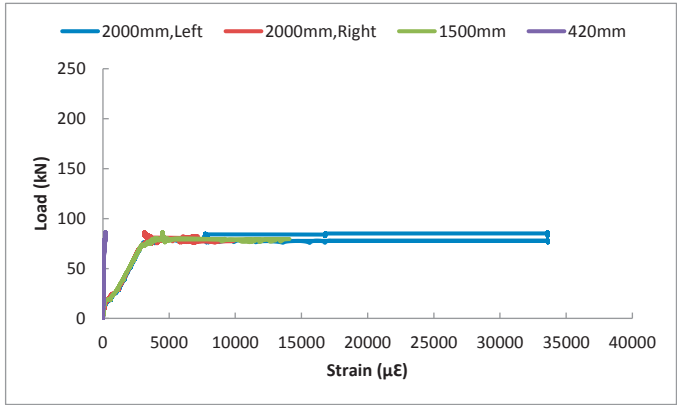
Figure B.2.1 Steel strain distribution of Beam B11-0-S.
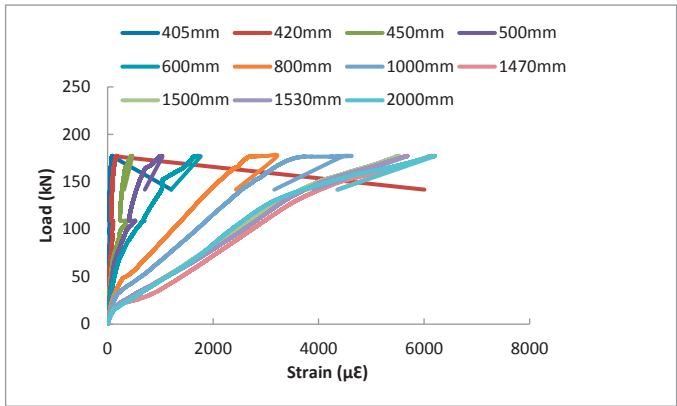
Figure B.2.2 Strain distribution of Beam B2-EE1-S: Fibre strain.
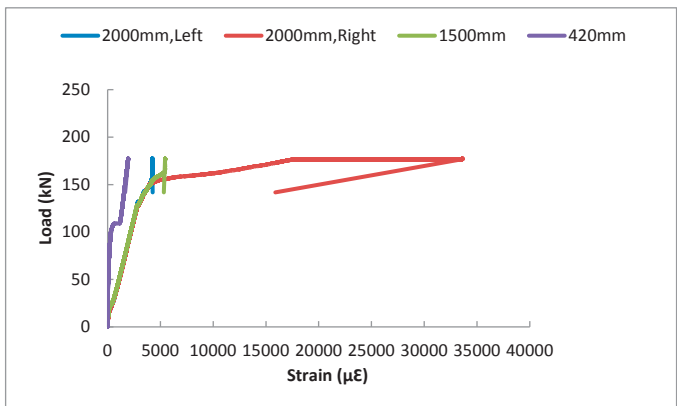
Figure B.2.3 Strain distribution of Beam B2-EE1-S: Steel strain.
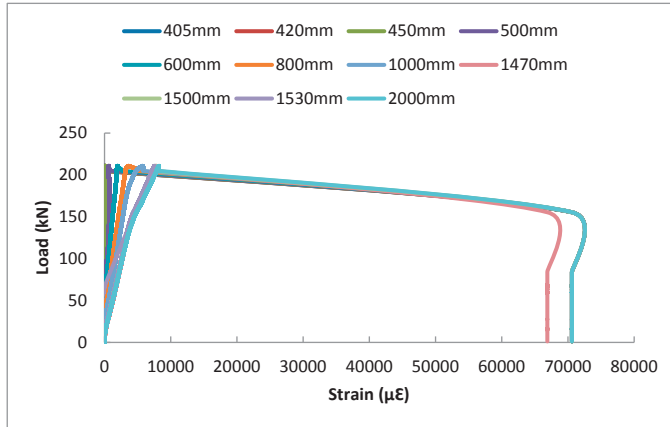
Figure B.2.4 Strain distribution of Beam B4-NE1-S: Fibre strain.
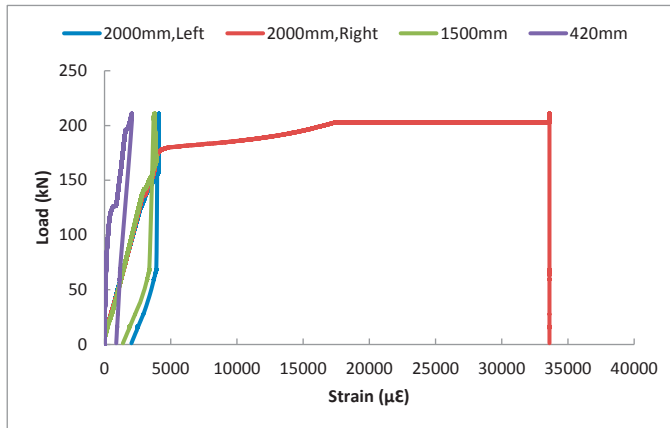
Figure B.2.5 Strain distribution of Beam B4-NE1-S: Steel strain.
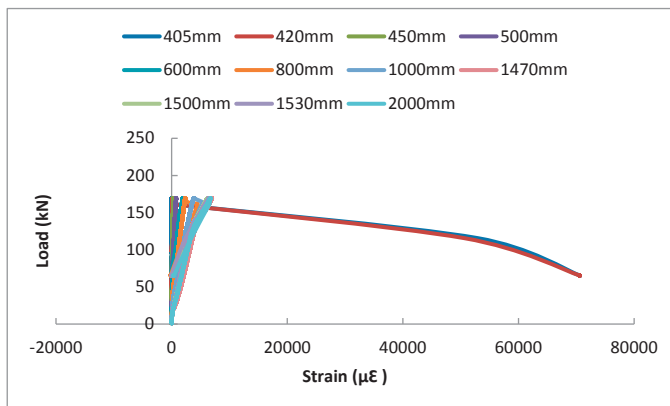
Figure B.2.6 Strain distribution of Beam B5-EE2-S: Fibre strain.
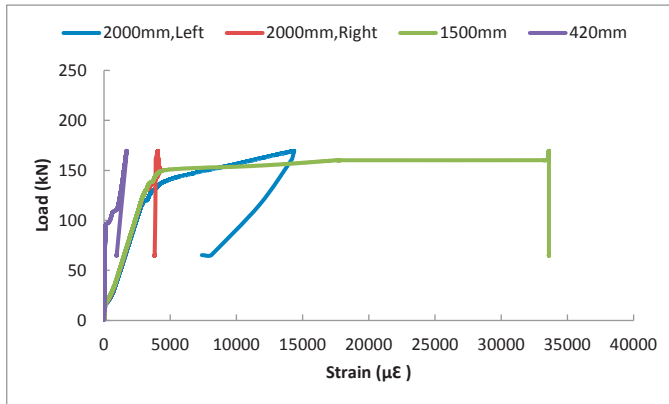
Figure B.2.7 Strain distribution of Beam B5-EE2-S: Steel strain.
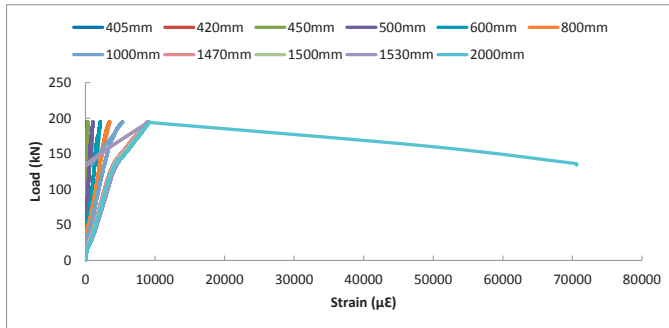
Figure B.2.8 Strain distribution of Beam B7-NE2-S: Fibre strain.
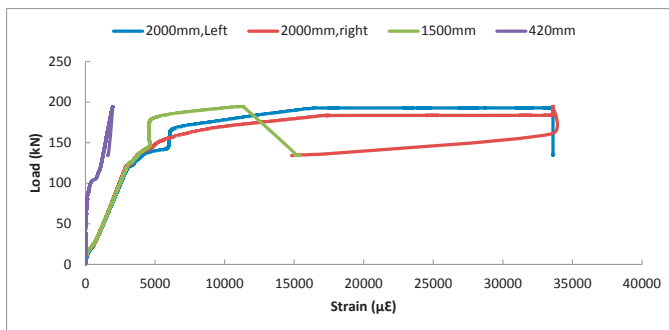
Figure B.2.9 Strain distribution of Beam B7-NE2-S: Steel strain.

Appendix C Slip curves
1. Slip of CFRP of statically tested beams
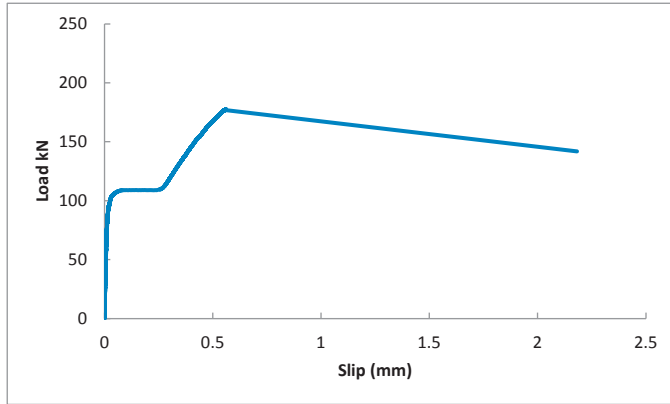
Figure C.1.1 Applied load-end slip Beam B2-EE1-S.
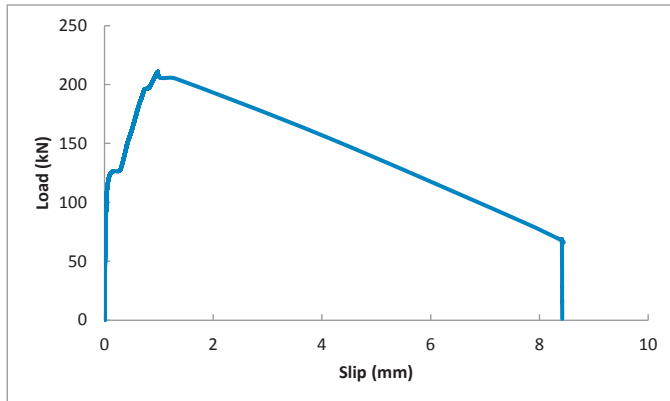
Figure C.1.2 Applied Load-end slip Beam B4-NE1-S.
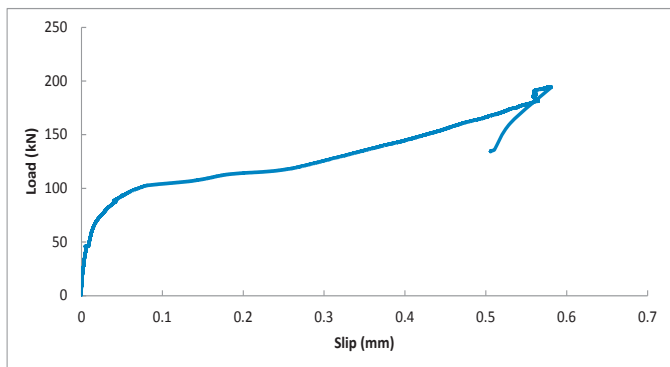
Figure C.1.3 Applied Load-end slip Beam B7-NE2-S.

2. Slip of CFRP of fatigue tested beams
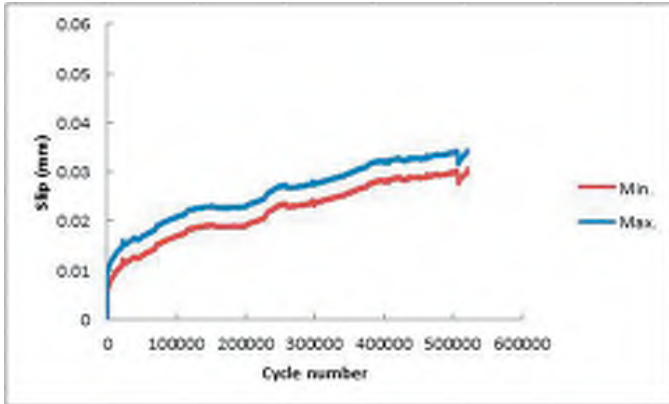
Figure C.2.1 Slip –cycle number Beam B1-EE1-F.
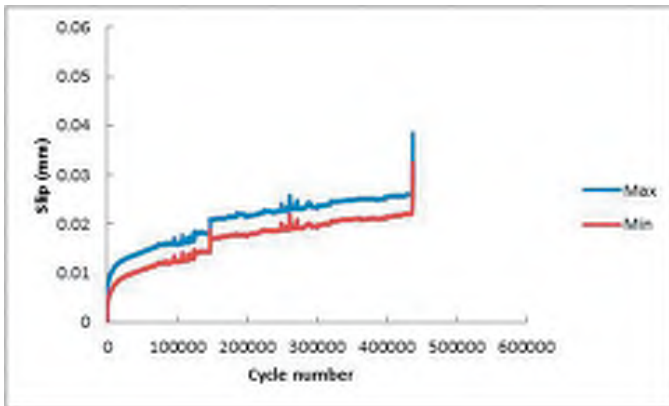
Figure C.2.2 Slip - cycle number Beam B3-NE1-F.
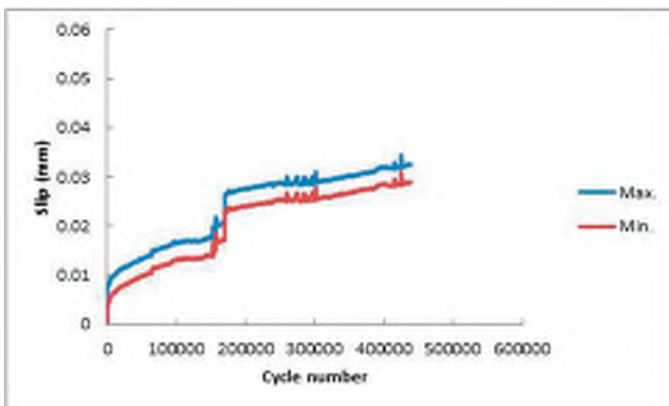
Figure C.2.3 Slip - cycle number Beam B6-EE2-F.
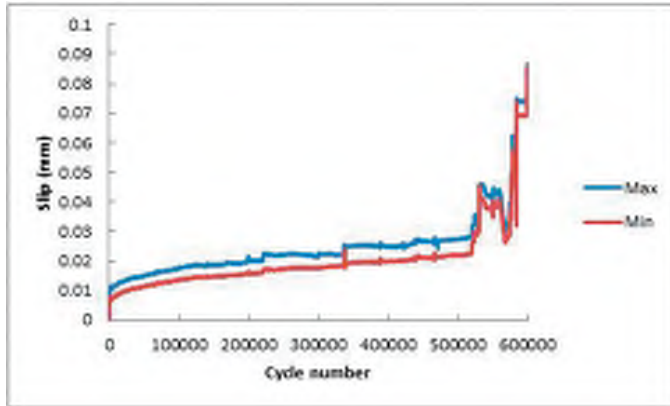
Figure C.2.4 Slip- cycle number Beam B8-NE2-F.
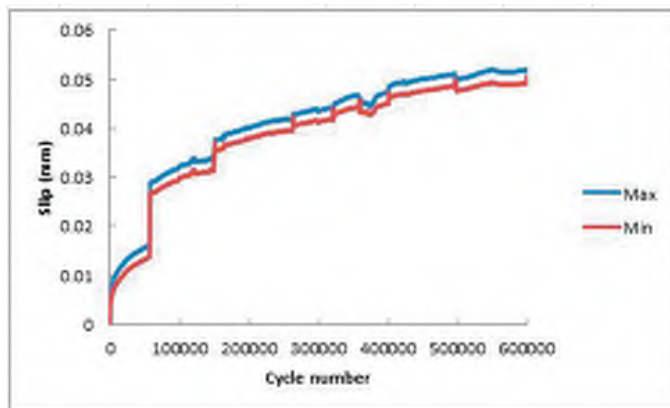
Figure C.2.5 Slip - cycle number Beam B9-EE1-F-C.
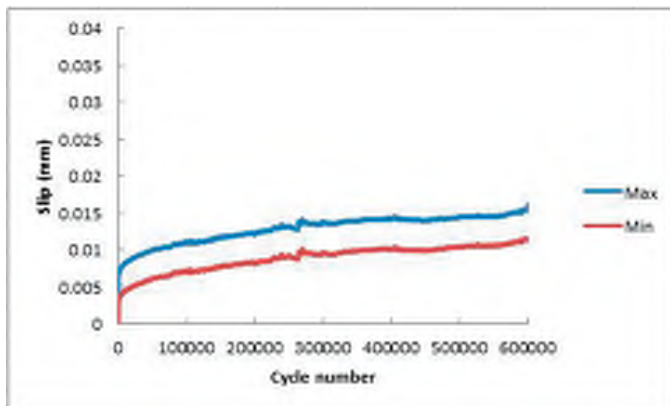
Figure C.2.6 Slip - cycle number Beam B10-NE1-F-C.

Appendix D Principle strain and crack pattern

1. Principle strain and crack pattern of statically tested beams

Figure D.1.1 Results of principle strain and crack pattern (Beam B4-NE1-S).
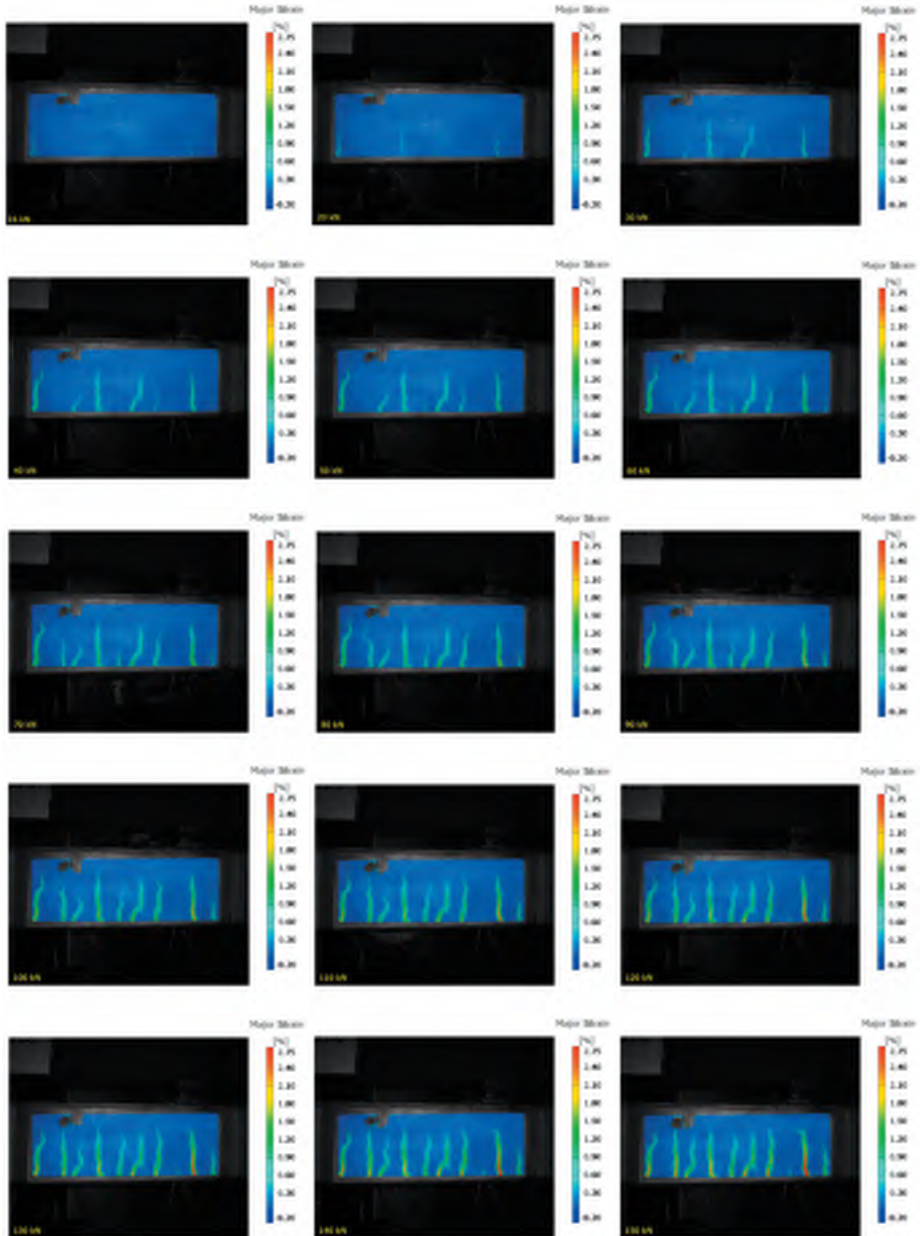
Continued
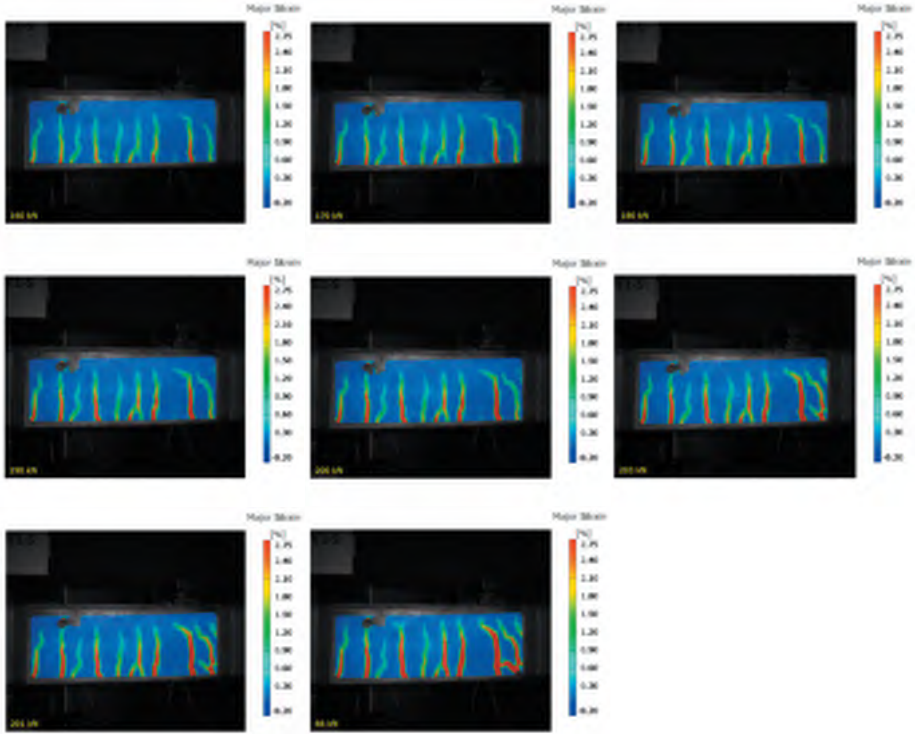
Figure D.1.2 Results of principle strain and crack pattern (Beam B7-NE2-S).
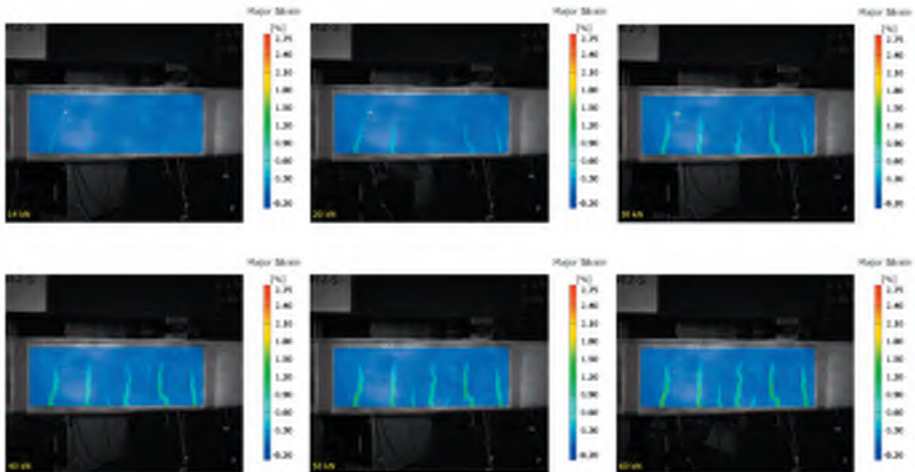
Continued
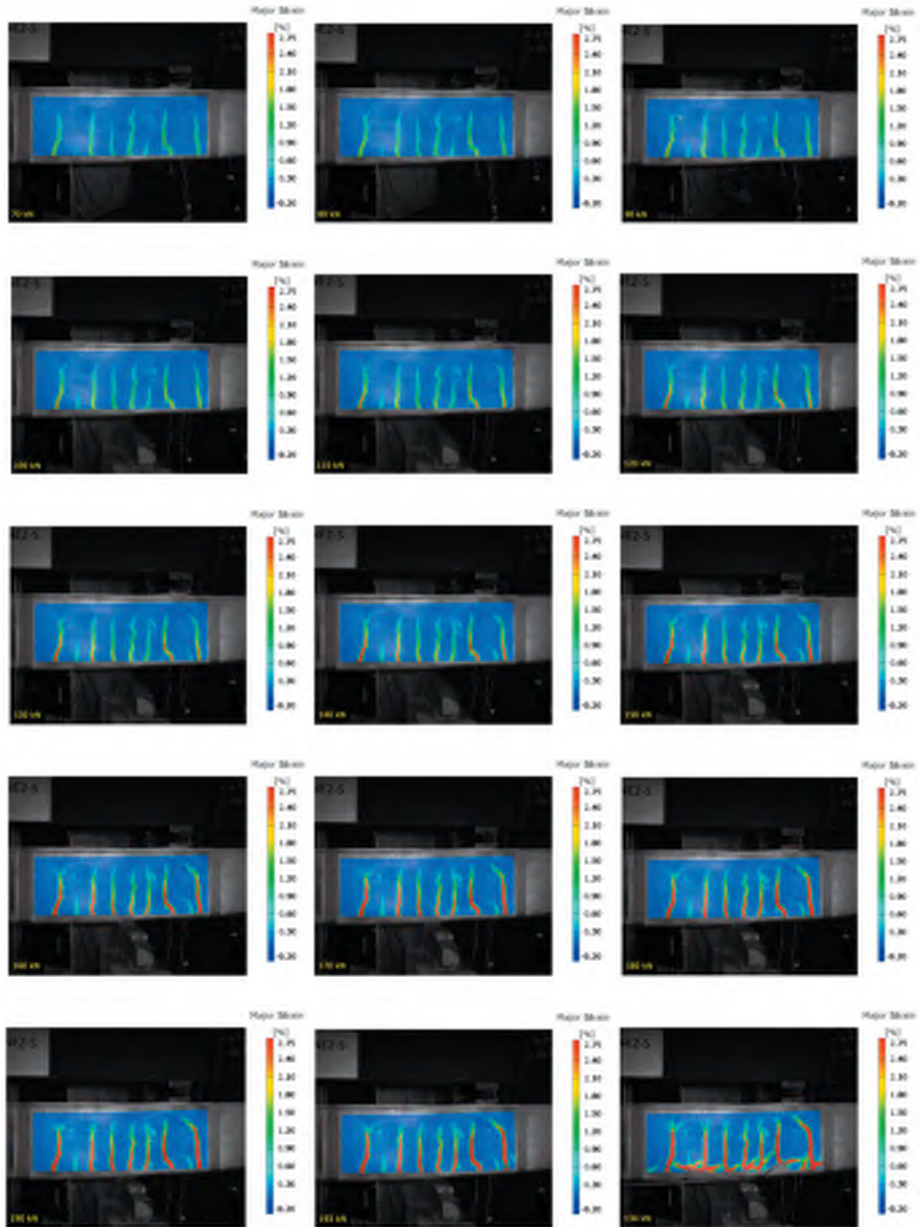
Figure D.1.3 Results of principle strain and crack pattern (Beam B5-EE2-S).
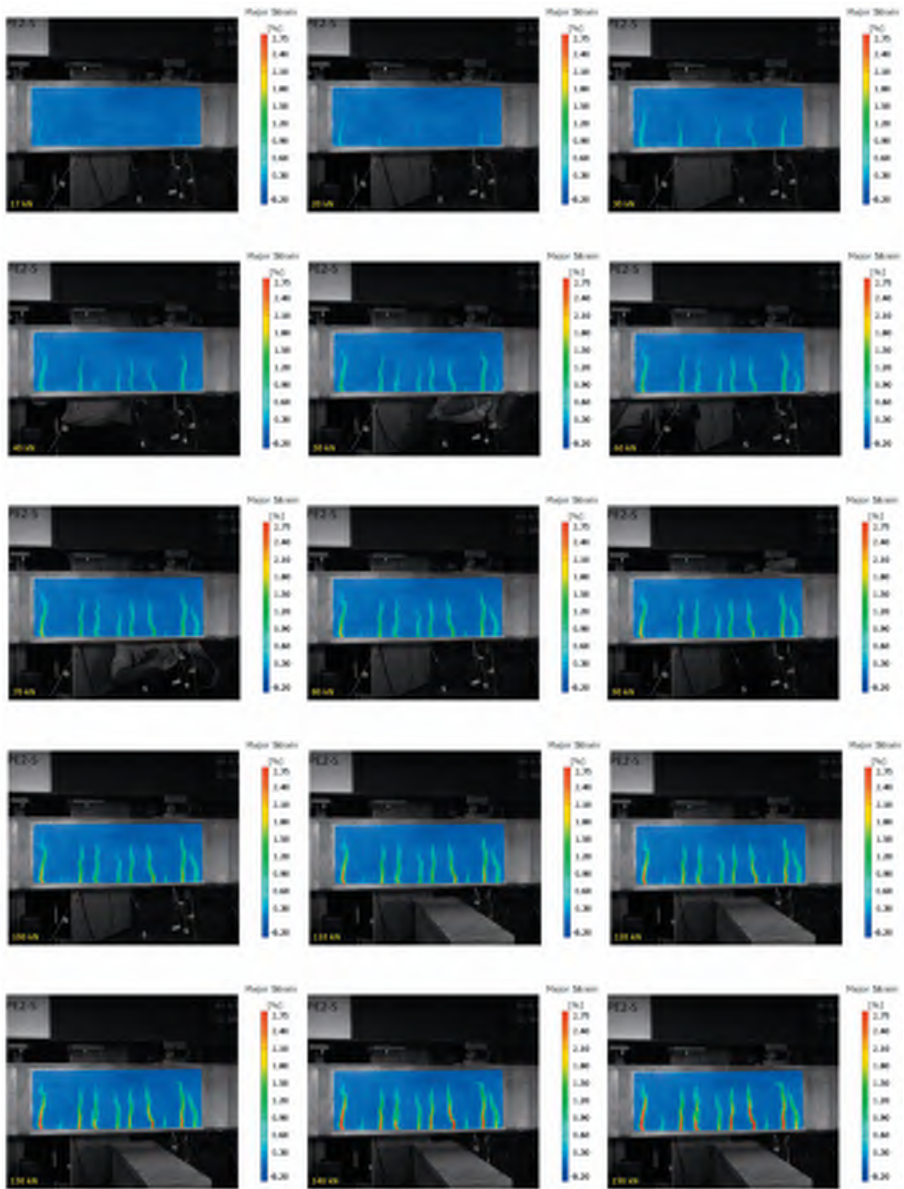
Continued
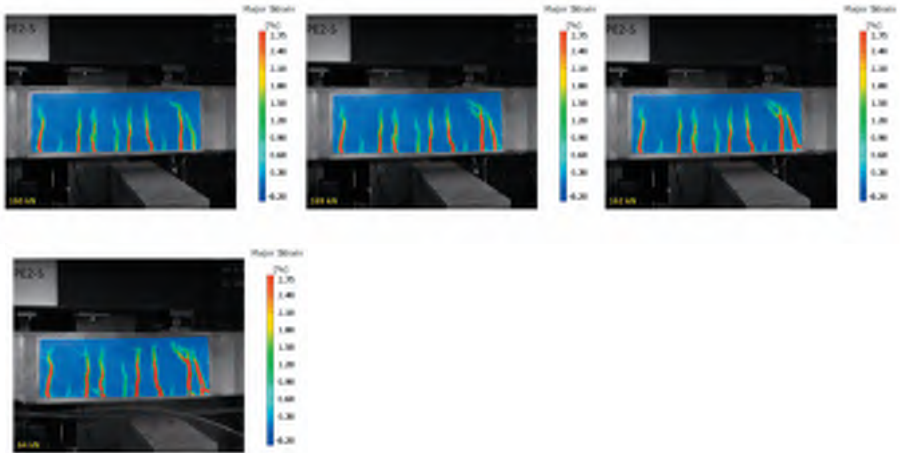
2. Principle strain and crack pattern of fatigue tested beams

Figure D.2.1 Results of principle strain and crack pattern (Beam B1-EE1-F).

Full 1st cycle
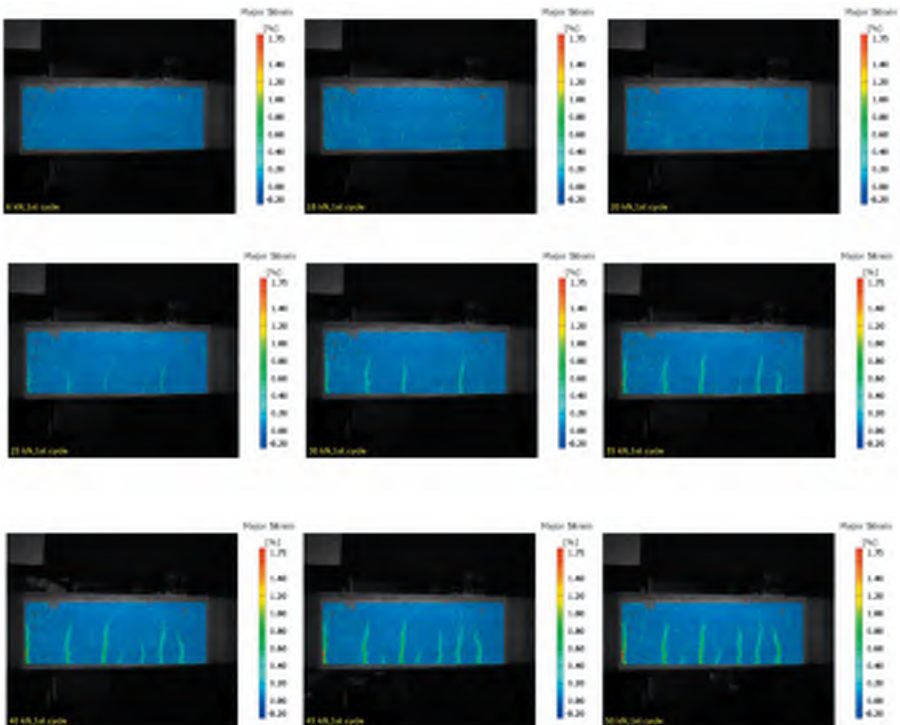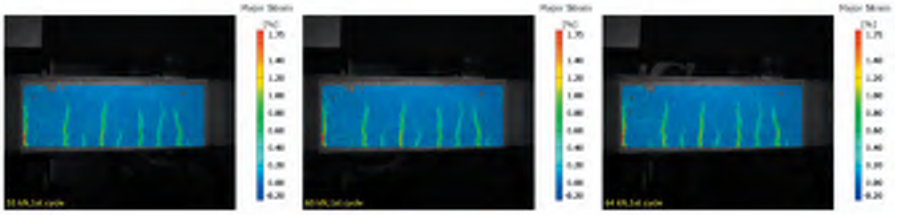
Continued
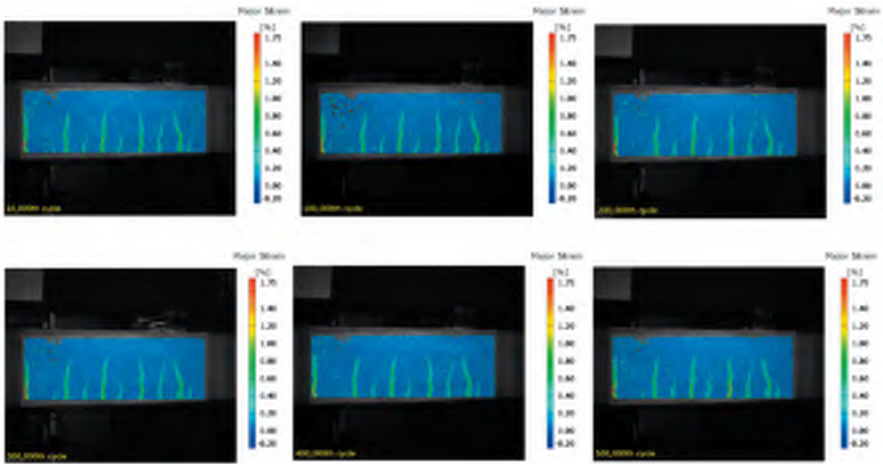
Specific cycles

Figure D.2.2 Results of principle strain and crack pattern (Beam B3-NE1-F)

Full 1st cycle
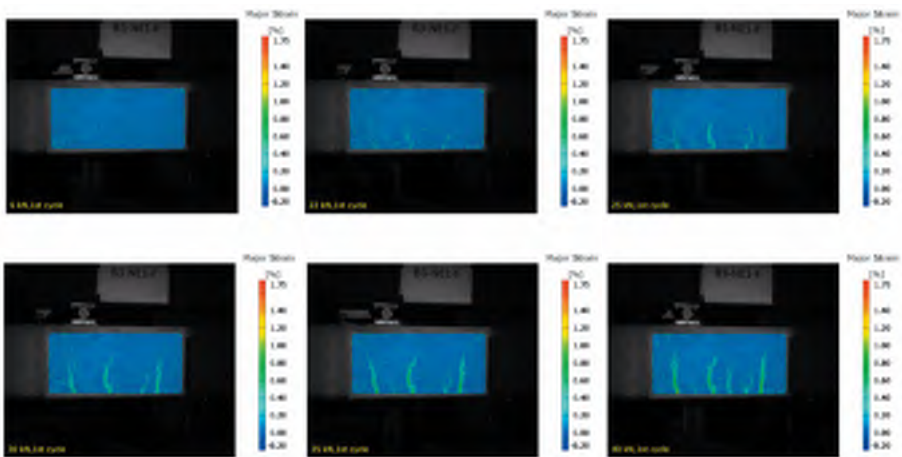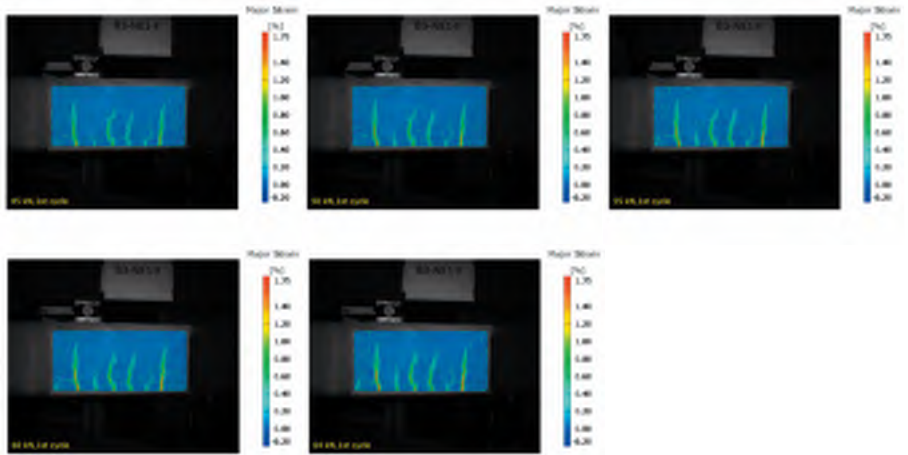
Continued
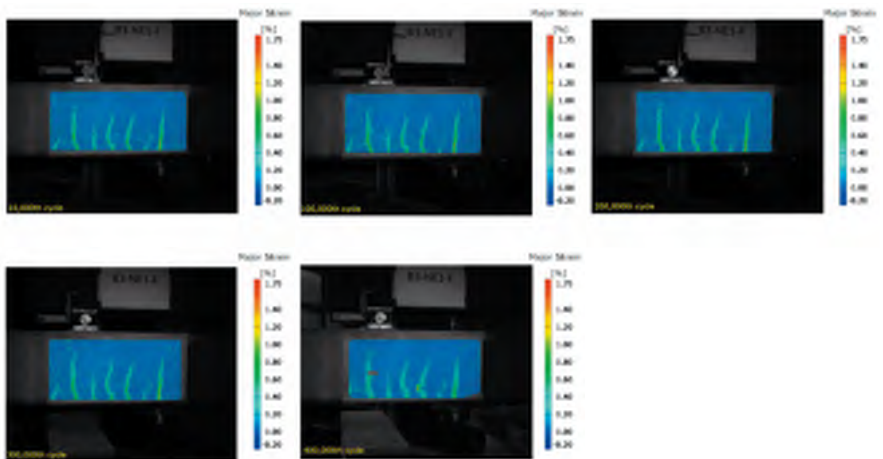
Specific cycles

Figure D.2.3 Results of principle strain and crack pattern (Beam B6-EE2-F).

Full 1st cycle
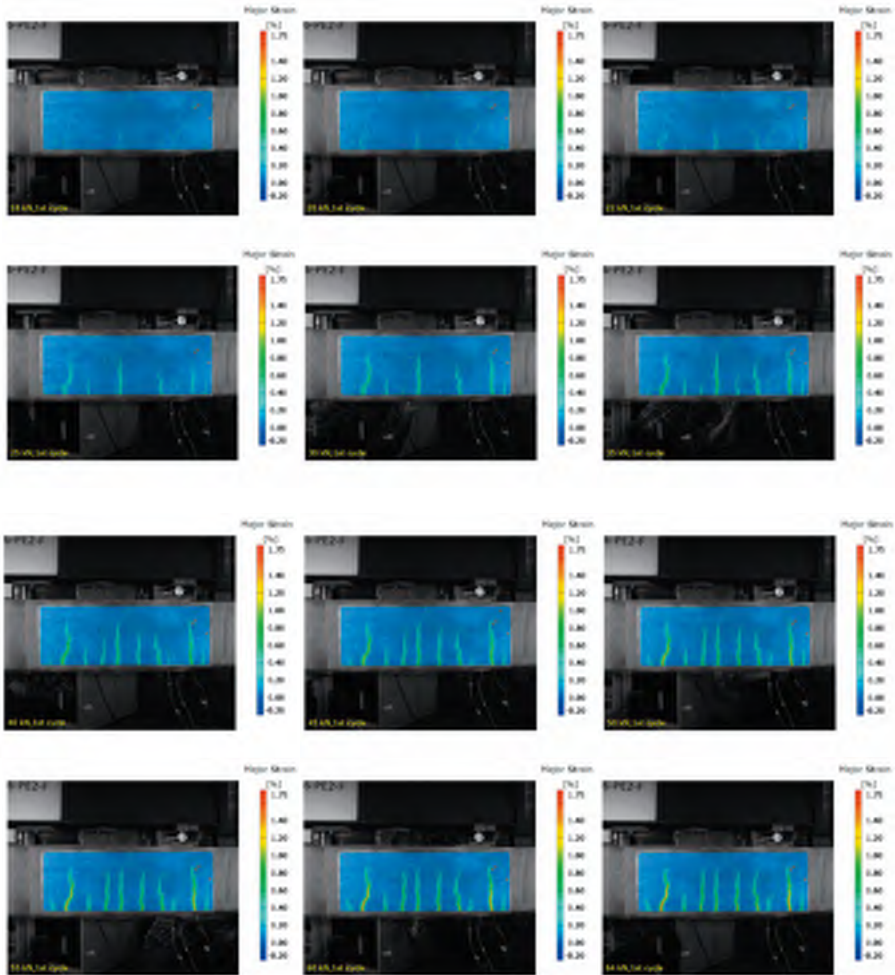
Specific cycles
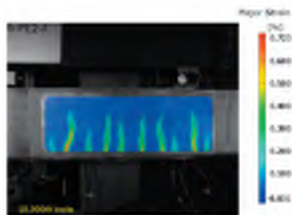
Figure D.2.4 Results of principle strain and crack pattern (Beam B8-NE2-F).

Full 1st cycle
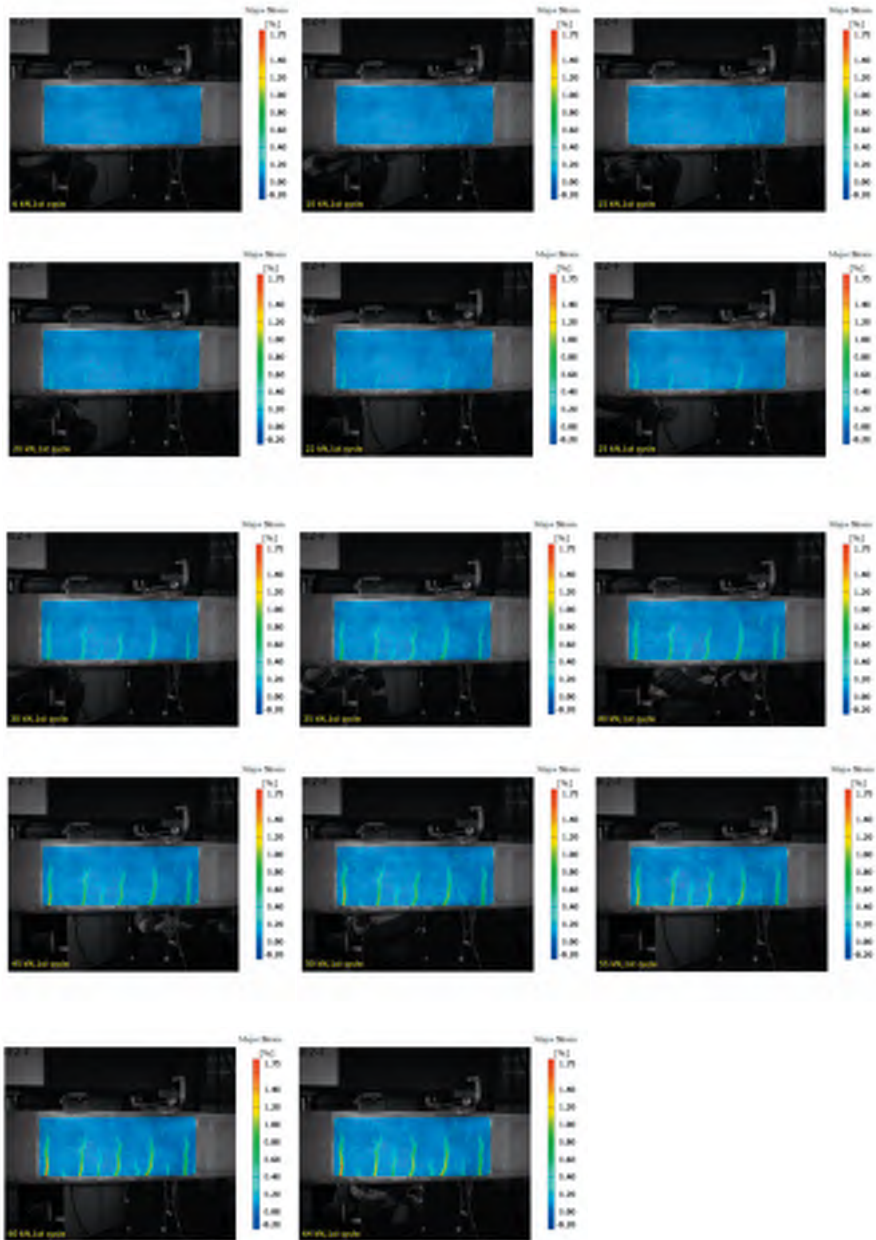
Continued   Specific cycles
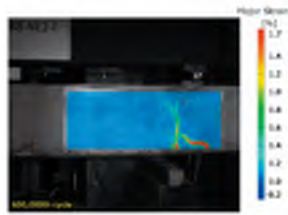
Figure D.2.5 Results of principle strain and crack pattern (Beam B9-EE1-F-C).

Full 1st cycle
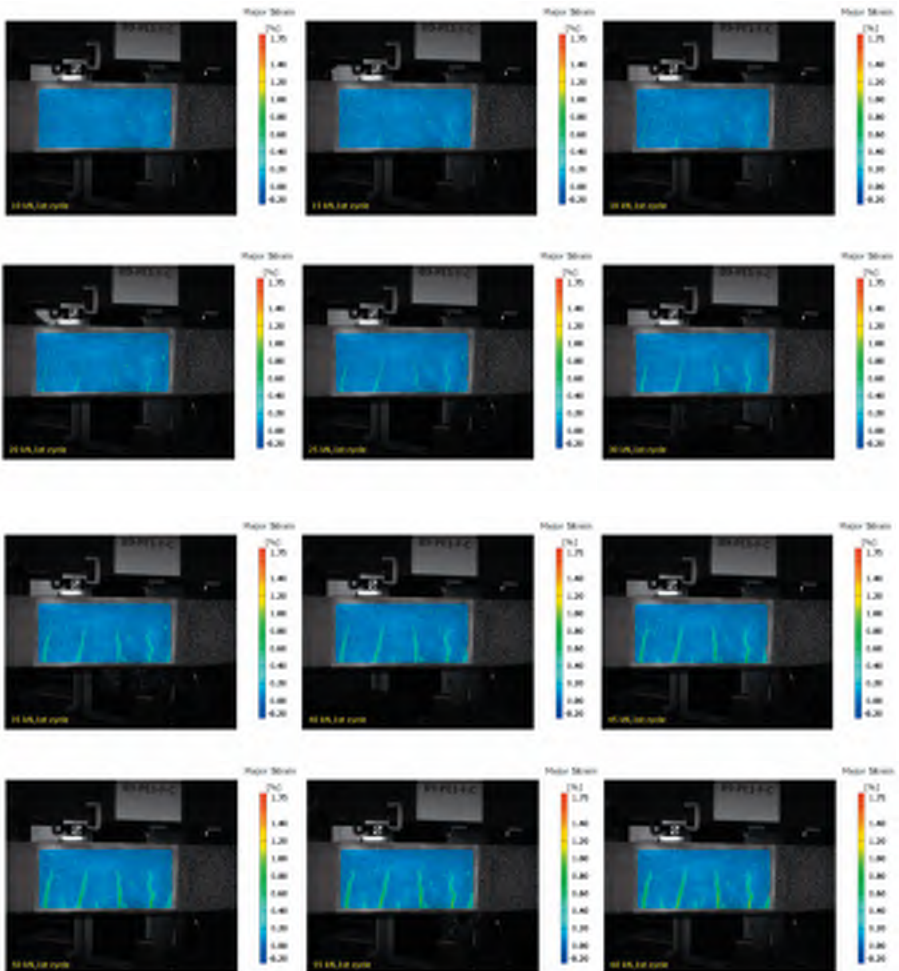
Continued
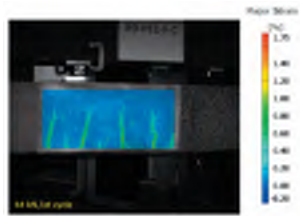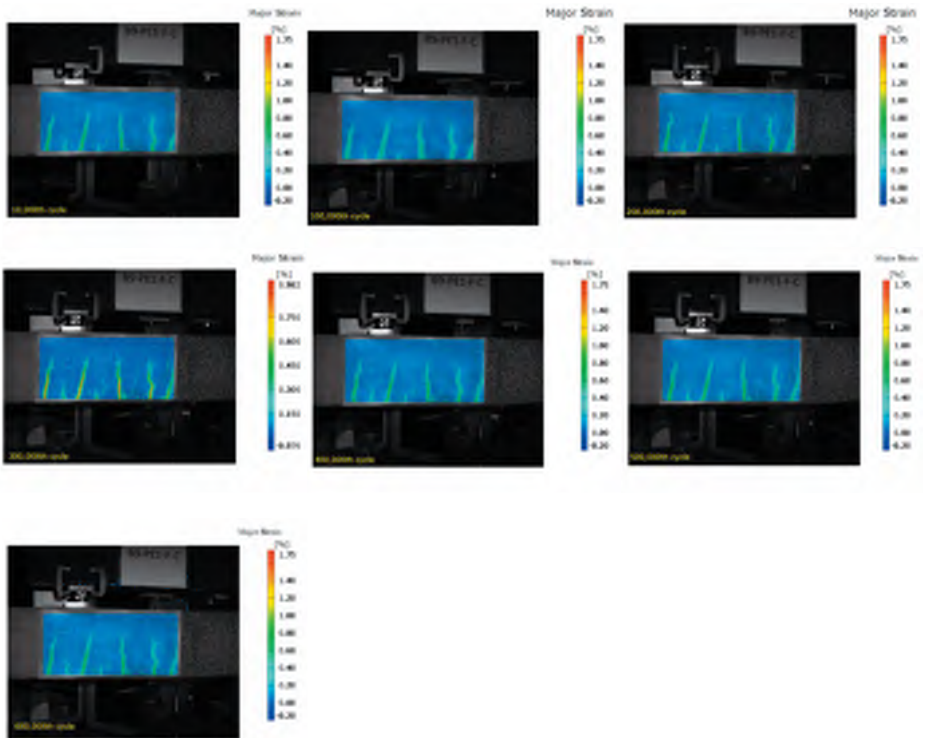
Specific cycles
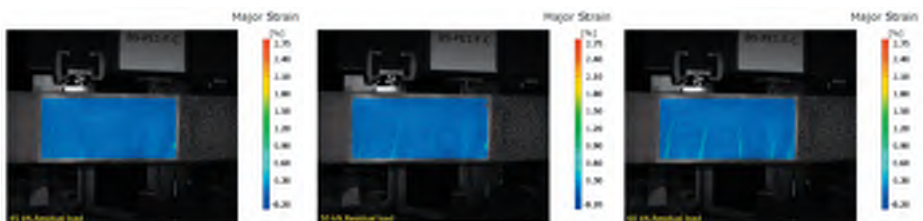
Residual load
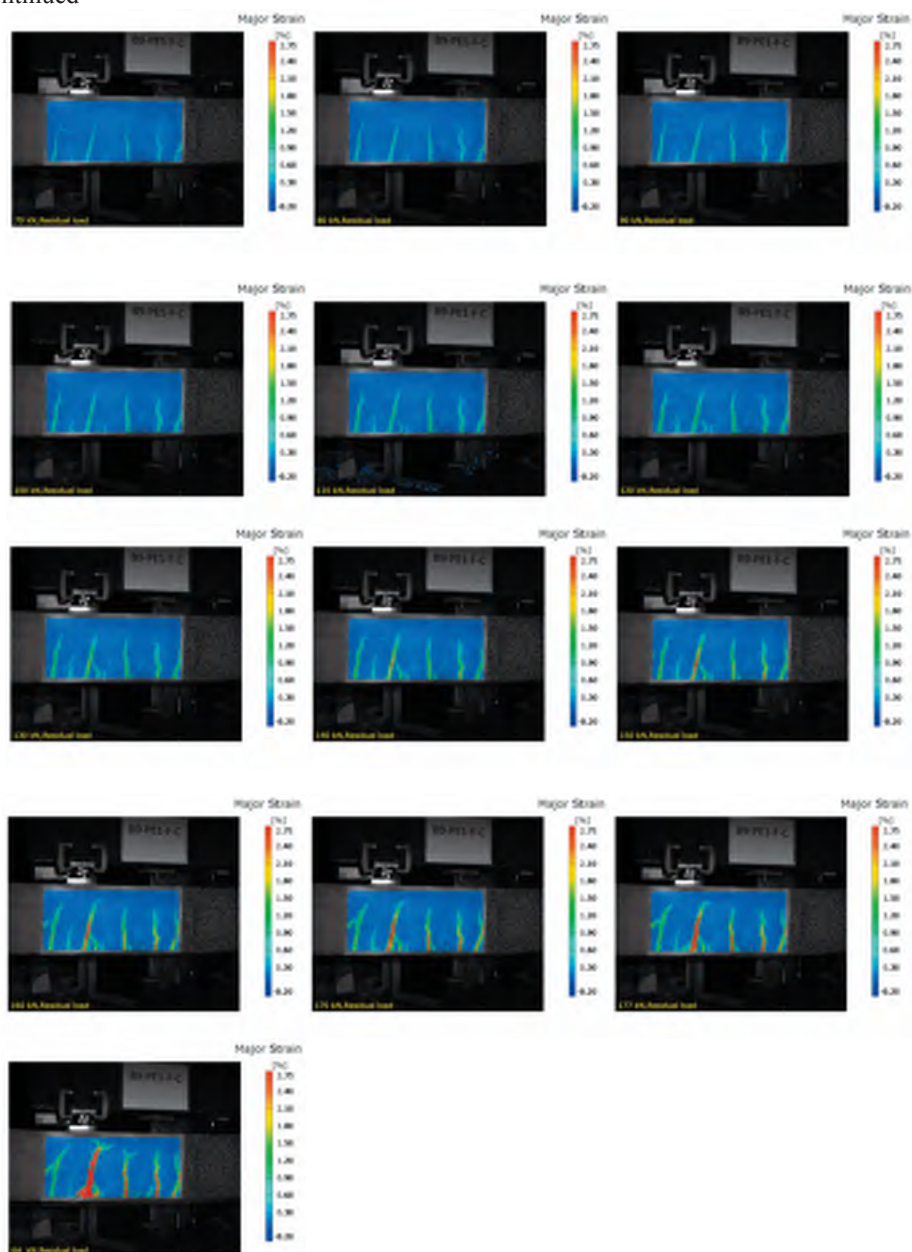
Continued

Figure D.2.6 Results of principle strain and crack pattern (B10-NE1-F-C).

Full 1st cycle
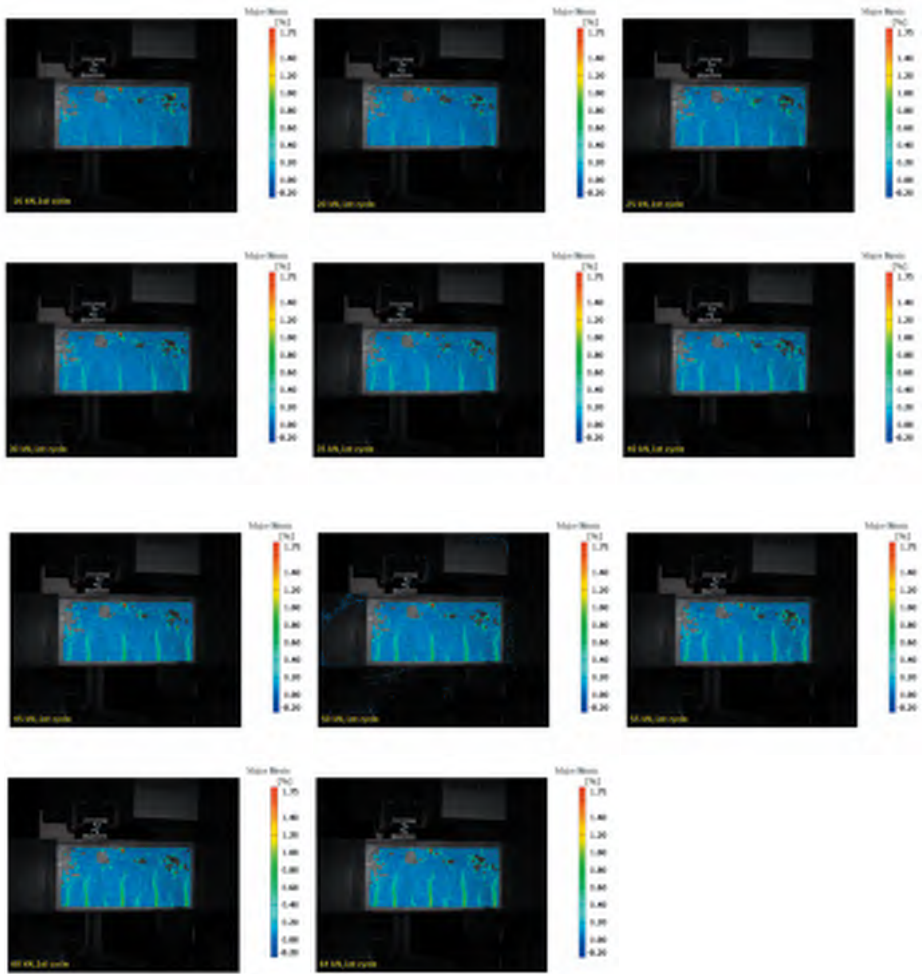
Specific cycles

Continued
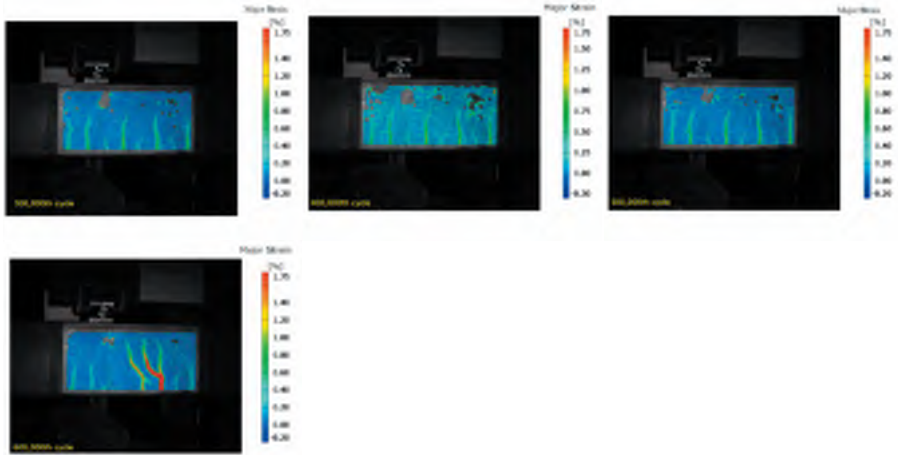
Residual load
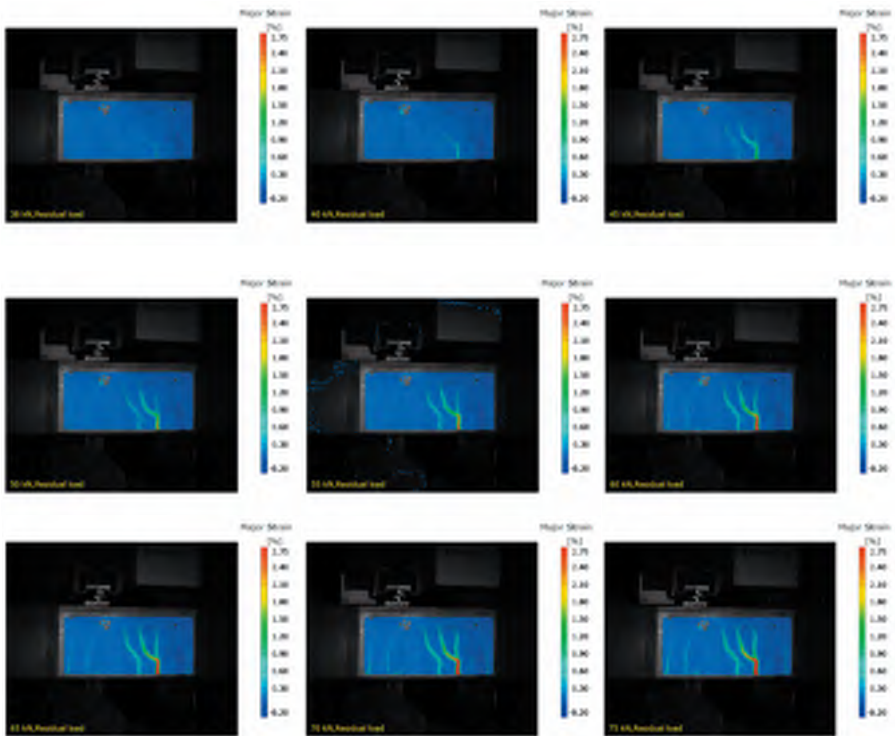
Continued
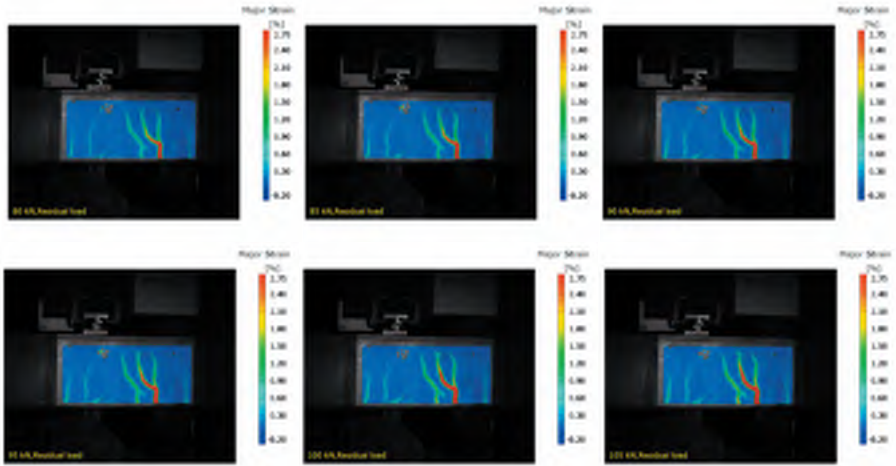
Figure D.2.7 Results of principle strain and crack pattern (Beam B13-0-F).

Full 1st cycle
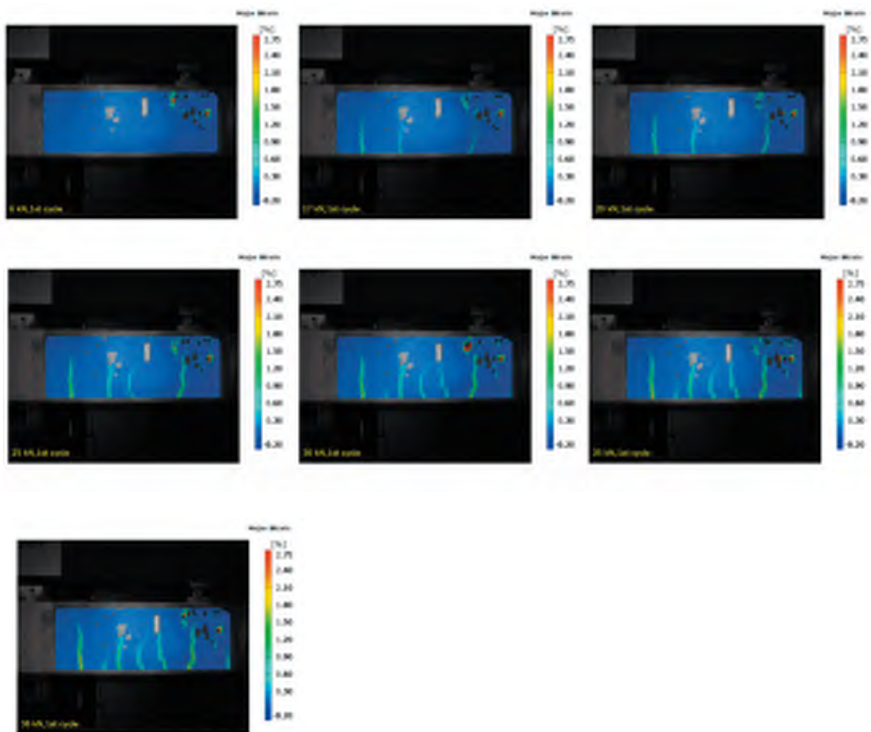
Continued   Specific cycles
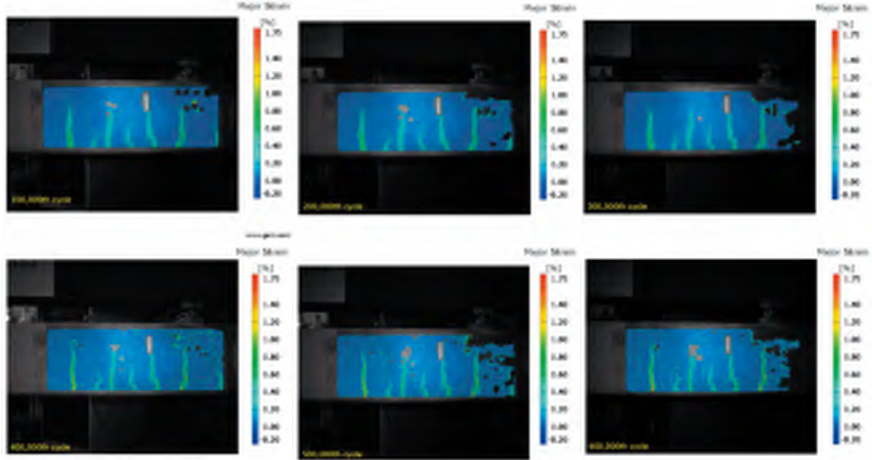
Residual load
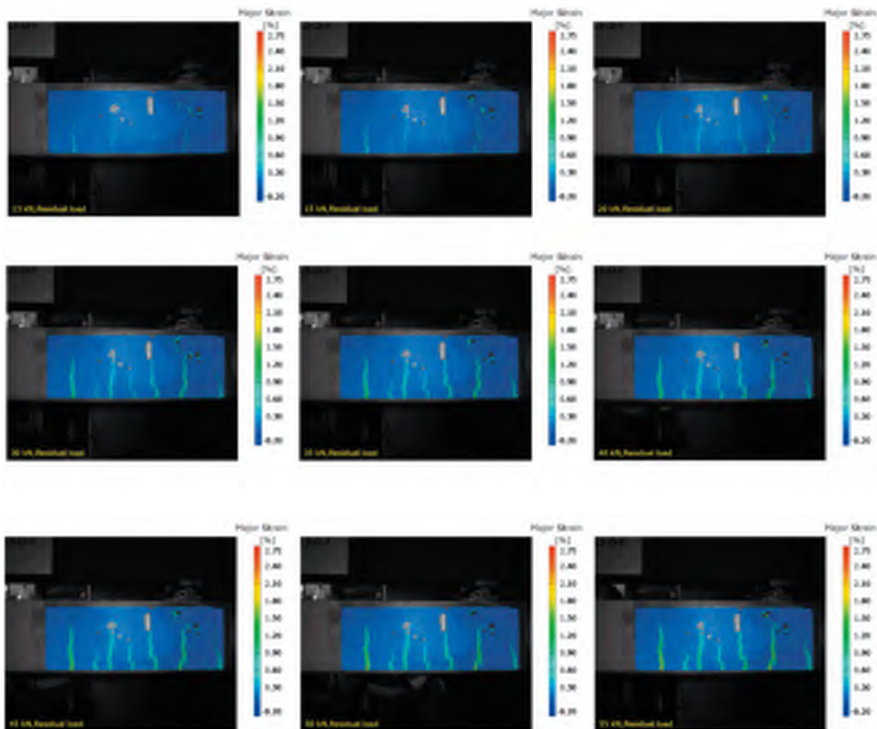
Continued
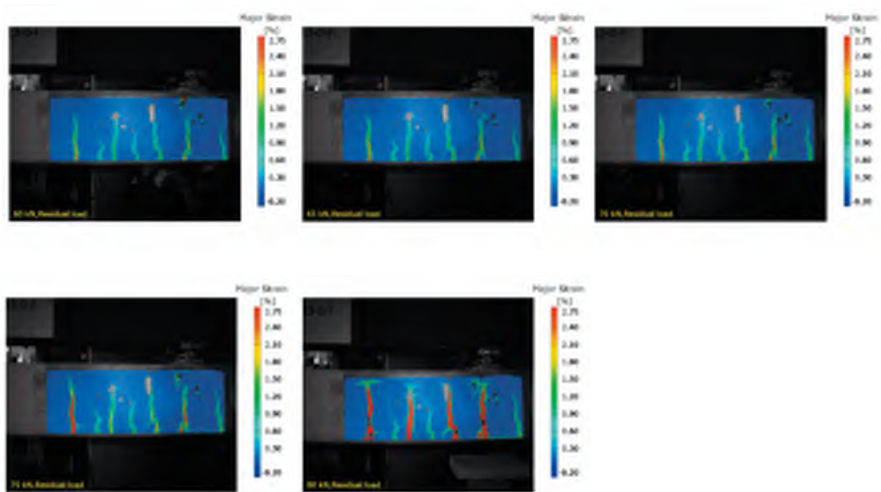
Appendix E Failure modes

1. Failure modes of statically tested beams

Figure E.1.1 Crushing of concrete (Beam B11-0-S).

Figure E.1.2 Failure mode (Beam B2-EE1-S).

Figure E.1.3 Debonding failure (Beam B2-EE1-S).

(a)   (b)

Figure E.1.4 Modes of failure of the tested beam: (a) Left side (b)-Right side (Beam B4-NE1-S)

126

Figure E.1.5 Shear cracks along the NSM groove (Beam B4-NE1-S).

| (a) | (b) |

Figure E.1.6 Modes of failure of the tested beam: (a) Left side (b) Right side (Beam B5-EE2-S)

Figure E.1.7 Debonding failure (Beam B5-EE2-S).

Figure E.1.8 Failure cracks pattern (Beam B7-NE2-S).

| (a) | (b) |

Figure E.1.9 Modes of failure of the tested beam (Beam B7-NE2-S): (a) Left side (b) Right side.

2. Failure modes of fatigue tested beams
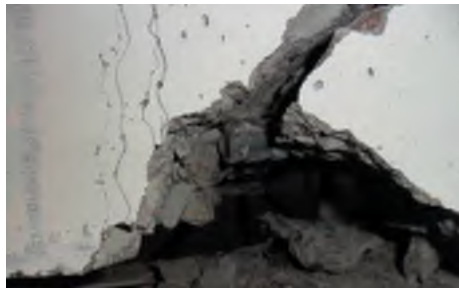
Figure E.2.1 steel bar ruptures (Beam B1-EE1-F).

Figure E.2.2 Crush of concrete beam (Beam B1-EE1-F).

Figure E.2.3 Debonding failure (Beam B1-EE1-F).

Figure E.2.4 Steel bar rupture (Beam B3-NE1-F).

$$(a) \qquad\qquad (b)$$

Figure E.2.5 Failure mode of beam (Beam B3-NE1-F): (a) Left side (b) Right side.

$$(a) \qquad\qquad (b)$$

Figure E.2.6 Failure mode of beam (Beam B6-EE2-F) : (a) Left side (b) Right side.

Figure E.2.7 Debonding failure (Beam B6-EE2-F).

(a)

(b)

Figure E.2.8 Failure mode (Beam B8-NE2-F) (a) Left side (b) Right side.

Figure E.2.9 Steel bar ruptures (Beam B8-NE2-F).

Figure E.2.10 Debonding of NSM bar (Beam B8-NE2-F).

(a)   (b)

Figure E.2.11 Failure modes of beam : (a) Left side (b) Right side (Beam B9-EE1-F-C).

Figure E.2.12 Debonding failure of beam (Beam B9-EE1-F-C).

Figure E.2.13 Failure mode of beam (Beam B10-NE1-F-C).

Figure E.2.14 Steel bar rupture (Beam B10-NE1-F-C).

Figure E.2.15 Failure mode of beam (Beam B13-0-F).

Appendix F Dissipation of the first cycle of beams

Area = 118.737 kN.mm

(a) B13-0-F

Area = 139.9967 kN.mm

(b) B1-EE1-F

Area = 162.6108N.mm

(c) B3-NE1-F

Area = 166.5058 kN.mm

(d) B6-EE2-F

Area = 147.5307 kN.mm

(e) B8-NE2-F

Area = 107.5246 kN.mm

(f) B9-EE1-F-C

Area = 103.3584 kN.mm
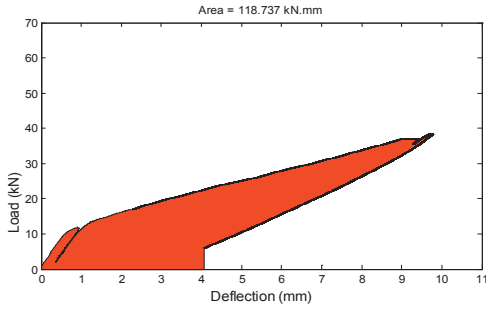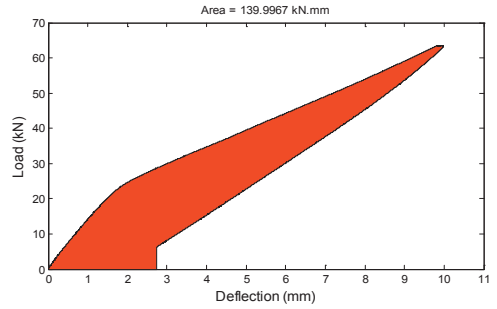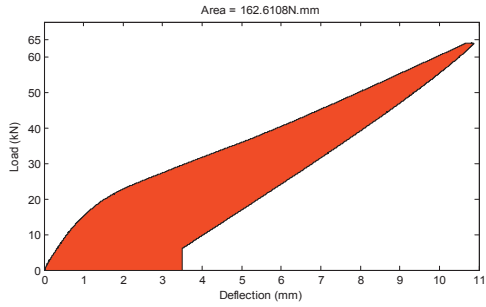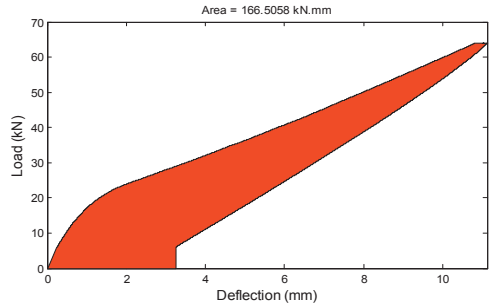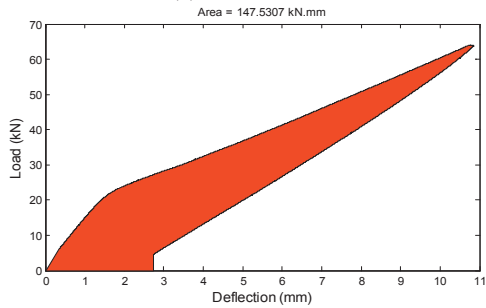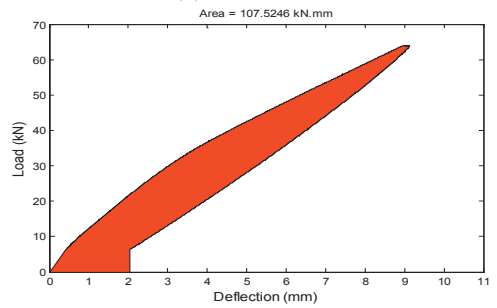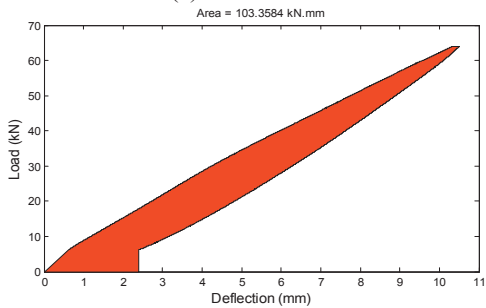
(g) B10-NE1-F-C

Appendix G Shear distribution of static tested beams
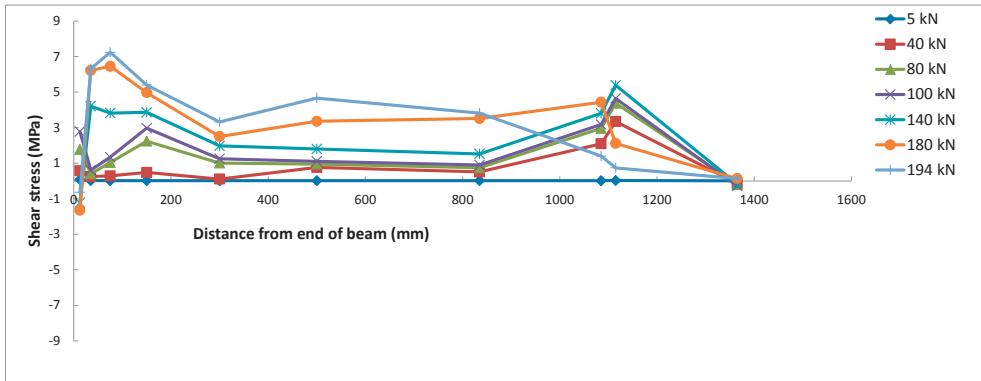
Figure G.1 Bond stress distributions B7-NE2-S.
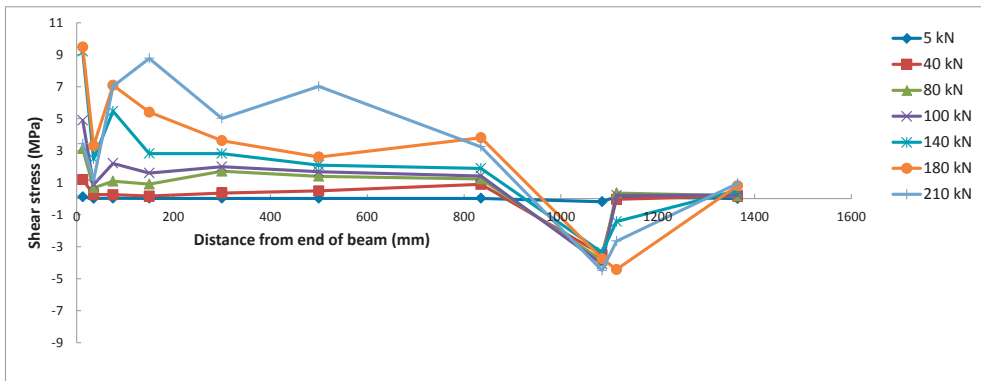
Figure G.2 Bond stress distributions B4-NE1-S.
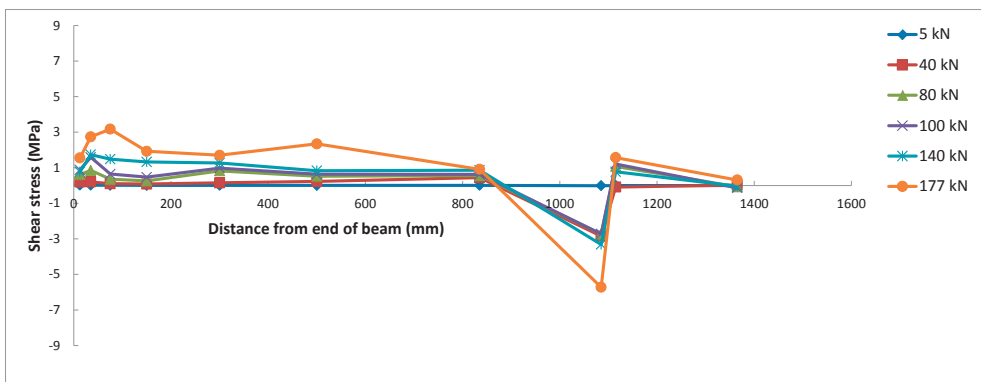
Figure G.3 Bond stress distributions B2-PE1-S.
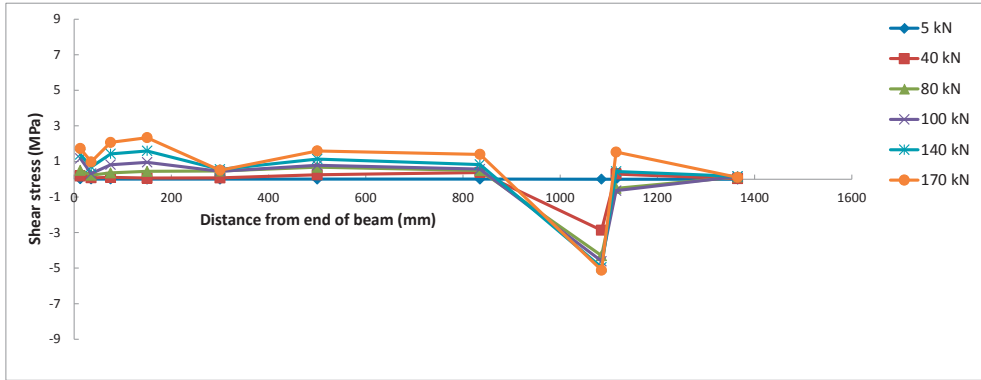
Figure G.4 Bond stress distributions B5-PE2-S.

Part II

Appended papers

PAPER I

"Examination at a Material and Structural Level of the Fatigue Life of Beams Strengthened with Mineral or Epoxy Bonded FRPs: The State of the Art"

BY
Mohammed Mahal, Thomas Blanksvärd and Björn Täljsten

Examination at a Material and Structural Level of the Fatigue Life of Beams Strengthened with Mineral or Epoxy Bonded FRPs: The State of the Art

M. Mahal, T. Blanksvärd* and B. Täljsten

Department of Civil, Environmental and Natural Resources Engineering, Luleå University of Technology, Luleå SE-971 87, Sweden

Abstract: This paper presents a state of the art review of different material combinations and applications of mineral-based and epoxy-based bonded Fiber Reinforced Polymers (FRP), used for the strengthening of concrete structures subjected to fatigue loading. In this review, models of the fatigue life at the material and structural level are presented. This study examines the mechanical behavior of the FRP-material, surface bonding behavior and concrete beams strengthened under fatigue loading with different types of FRP-systems. The parameters that are investigated are applied load value, time dependent effects, type of strengthened structures (shear, flexural or combined) and the configuration of sheets or plates. The building codes and researchers' recommendations are also discussed. As a result of this review, the reader will obtains an overview of suitable materials and methods for strengthening structures subjected to fatigue loading by referring to the estimated fatigue life of material and strengthening structures at various applied stress levels.

Key words: fatigue, reinforced concrete, bonding, fiber reinforced polymer, textile, mineral-based composites.

1. INTRODUCTION

With increased loads and traffic flows on highways and across bridges, it is not only the load carrying capacity that is of real concern but also the fatigue life of the structures. Fatigue can be defined as irreversible internal structural changes to a material when exposed to repeated loading. These changes occur due to initial microcracks that grow to macroscopic size and finally result in failure of the material. Two examples of systems for prolonging the fatigue life of concrete structures are: 1) mineral-based bonding system, where a fiber component is embedded into a mineral-based binder and then bonded to strengthen an existing concrete structure (Täljsten 2006) and 2) epoxy-based bonding systems, where an epoxy is used as an adhesive to bond a fiber component to an existing concrete structure. Previous literature reviews (Harries 2005; Diab and Wu 2008; Kim and Heffernan 2008) focused on the effectiveness of the epoxy-based method in enhancing the fatigue life of structures. The first section of this state-of-the-art paper describes the definition and behavior of both mineral-based and epoxy-based strengthening systems under fatigue loading, at the material, bonding surface and structural levels (see Figure 1). At the material level, the models and behavior of raw materials used in the strengthening of structures such as FRP reinforcement (textile, grids, dry fibers), matrices and bonding agents are also discussed. At the structural level, anchorage tests to concrete prisms and concrete beams strengthened with different strengthening configurations from various researchers are presented.

The second section of this paper includes the description of the behavior of common FRP-materials that have been used to strengthen concrete structures. In section three, the fatigue life models for these materials

*Corresponding author. Email address: thomas.blanksvard@ltu.se; Fax: 0920-491399; Tel: +46920-491642.
Associate Editor: J.G. Dai.
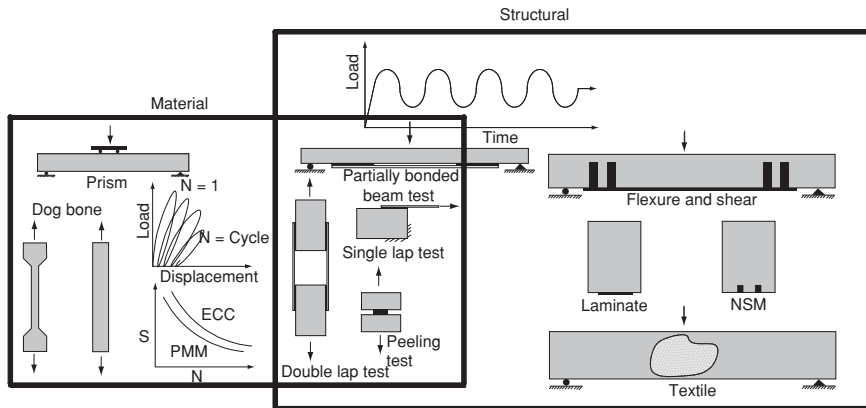
Figure 1. From the material to the structural level

either based on the regression analysis of the available data or taken from literature are presented. The fatigue life model is used mainly to predict the life of a material or structural component at specific fatigue stresses. The bond behavior and model of both the epoxy-based and the mineral-based methods are presented in section four. In section five, the description of fatigue behavior and models moves from the materials level to the structural level. Finally, the building codes and other researchers' recommendations related to strengthening structures are presented in section six.

This state-of-the-art review contributes to the selection of the most suitable materials and methods for strengthening concrete structures under fatigue loading and to identify the current research and building codes needs that are required in this field.

2. MATERIAL BEHAVIOR UNDER FATIGUE LOADING

2.1. Fiber Reinforced Polymer

Fiber Reinforced Polymer (FRP) is defined as a linear elastic composite material that consists of a fiber reinforced polymer matrix. The three common types of fibers used are aramid, glass and carbon, all of which have a higher ultimate strength than normal reinforcing steel. Polyesters and epoxies are often used as the matrix material because they have a higher strain to fracture than the fibers and because they bind to the fibers thus transferring the stresses between them. In addition, the matrix material protects the fibers from mechanical and environmental damage (Jones 1999). FRP has several different configurations including 1) rods that are used as internal reinforcement or for near-surface mounted reinforcement (NSM); 2) composite plates and sheets; 3)

FRP grid, which is typically a multidirectional prefabricated composite and 4) impregnated textiles, which provide a variety of textile structures that are used as reinforcement. 1) and 2) are often associated with epoxy-based bonding agents; 3) and 4) are often used together with mineral-based bonding agents. FRP normally has a better fatigue resistance than that of reinforcing steel, in particular when high modulus fibers such as carbon are used; but the fatigue strength of glass fiber composites is lower than steel with a low stress ratio (Badawi 2007). The fatigue failure mechanism of FRP composites is more complex than the failure of plain concrete or steel. Composite materials often show a much greater fatigue life than other homogenous materials (Papakonstantinou *et al.* 2001), where cracks, due to fatigue, format a weak point and continue to grow with each load cycle. Conversely, if the individual fibers within FRP composites develop a defect, this defect does not propagate across the other fibers; thus, the undamaged fibers reduce the number of cracks that grow. Once the FRP composite has been damaged, the damage propagates along the matrix between unidirectional fibers and does not pass through adjacent fibers (Kim and Heffernan 2008). A failure in an FRP composite is a combination of different degradation mechanisms such as matrix cracking, fiber breakage, fiber-matrix debonding and delamination (Adimi *et al.* 2000). When the surface fibers fail under a repeated load, the remaining fibers hold the redistributed load and this behavior repeats until total failure occurs. There are four stages that the FRP composites go through before failure due to fatigue (Ramakrishnan and Jayaraman 1993; Curtis 1989; Newaz 1985; Salvia *et al.* 1997). The first and second stages are matrix cracking combined with interfacial debonding.

The third stage is a delamination between the matrix and the fibers. The final stage is the failure of the remainder of the fibers due to tensile stress. An important behavior of FRP composites is their ineffectiveness under a compression load. The compression load leads to local layer instability and layer buckling that causes failure, perhaps even before resin and interfacial damage within the layers occurs. Because of that, the reversed axial fatigue, or tension-compression loading, is considered the worst type of loading for the FRP composite. For this reason, the most suitable use for FRP composites is to strengthen structures subjected to tension-tension fatigue load. Gorty (1994) showed that the modulus of elasticity of a CFRP rod did not change when the material was subjected to high cyclic loading. Badawi (2007) found that CFRP tendons exhibited good fatigue resistance in the tension-tension fatigue test. Demers (1998) investigated GFRP bars that were subjected to repeated cyclic loading with different stress ratio and frequency; it was found that GFRP bars can withstand a large amount of cyclic loading, exceeding 2 million cycles with maximum-ultimate stress ratio less than 0.5. Aramid fibers, under tension-tension fatigue loading, exhibit excellent behavior more than 2 million cycles in the range of 54 to 73 % of the ultimate tensile strength (Odagiri *et al.* 1997).

2.2. Textile Reinforced Matrix

A textile is anything that is made up of fibers, yarns or fabric. There are mainly two kinds of textile fibers: short chopped fibers and long continuous fibers. Textiles can take several forms such as plates, mats and woven or non-woven fabrics (Brand 2009). The most common form used for strengthening concrete structures is woven textile fiber, which consists of three components: longitudinal strands (warp), transverse strands (fill) and a pure matrix area of fine grain concrete or polymer modified mortar (Harris 2003). The main three types of yarns used in textile are AR (alkali resistant) glass, carbon and aramid. These fibers can be made into filaments or twisted yarns, with the filament yarns being the best for reinforcing since they have little in the way of elongation to their structure (Brameshuber 2006). When strengthening concrete, the textile used must have a stable open structure with a small displacement, a higher modulus of elasticity than the mortar matrix and good adhesion to the mortar (Brameshuber 2006). The density and separation distance of the yarns as well as the angle of wefts in textile reinforcement structures are placed according to the stress acting on the structure and the degree of bonding that is planned with the matrix. Textile Reinforced Matrixes (TRM) are inhomogeneous, anisotropic and their behavior is more complex than FRP composites under fatigue

loading. The main reason behind this is that the different types of fatigue damages that can occur are related to the microstructural damage within the impregnated strands and the macroscopic damage within the textile fabric composite, as described by Fuji *et al.* (1993), Takemuraand and Fujii (1994), Hansen (1999), Harris (2003), Cuypers (2001) and Zhu *et al.* (2011). Microcracking in the matrix, fiber-matrix interface debonding and fiber fracture are considered to be part of the microstructural damage mechanism. The macroscopic damage mechanisms are understood to be transverse cracking of the fill, shear failure in the warp, cracking of the pure matrix area, delamination between longitudinal and transverse strands, delamination between adjacent layers and finally tensile failure of the strands. All of these possible damages are shown in Figure 2. Depending on how the above two mechanisms of damage play out, the fatigue damage process can be divided into the following stages. The first stage is the characteristic damage state, where the microstructural damages and transverse cracks in the fill are formed and continue until the cracks have stabilized; the second stage of damage is as hear failure in the warp, with cracking in the pure matrix areas and the start of the delamination and propagation between the fill and the warp and between the layers. In the final stage, all the damage types develop rapidly and, because of the complex nature of woven fabric composites, although damage development is potentially slower, the fibers finally fracture and there is a complete failure. Fujii *et al.* (1993) showed that specimens, consisting of polyester resin forming the matrix and a plain weave glass cloth as reinforcement, under fatigue loading experience a rapid modulus decay at the beginning of the fracture process and then have a gradual modulus decay in the middle stages. Van Paepegem and Degrieck (2001) investigated the fatigue behavior of plain woven glass/epoxy composites and found a gradual stiffness degradation with fatigue. Zhu *et al.* (2011) tested cement-based composites reinforced with three types of fabric [carbon, ARglass and polyethylene (PE)] under high-rate loading conditions. The tests showed that the highest load carrying capacity was achieved by the carbon composite followed by the
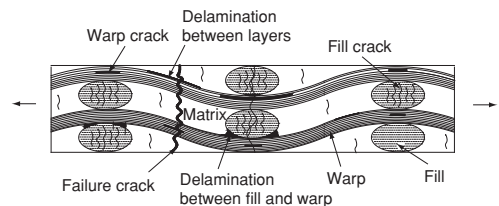
Figure 2. Schematic illustration of various types of fatigue damage in TRM

AR glass composite and lastly, the PE composite. Cuypers (2001) evaluated cyclic stiffness and residual strain of a textile-reinforced matrix consisting of inorganic phosphate cement with E-glass fiber. The results showed that there was a clear loss of stiffness and accumulation of residual strain with extra deflection during the first stage of repeated loading.

2.3. Polymer Modified Mortar

Polymer Modified Mortar (PMM) can be defined as a mortar where the admixture modifies or improves the properties of the mortar, proper ties such as strength, bond strength, adhesion, damage-absorbing deformation nor resistance to environmental effects (Ohama 1998). The polymer modified mortar plays a major part when used as the matrix with grid or textile fibers to strengthen structures (Blanksvärd *et al.* 2009). Different types of polymer modified mortars are available, such as latex-redispersible polymer powder, liquid resin, water-soluble polymer and monomer (Ohama1995). When any of these types are used, it is most important that both the hydrated cement and polymer thoroughly mix to produce a monolithic matrix. Under fatigue loading, the way in which PMM fails can be split into three phases (Suthiwarapirak *et al.* 2002). First, after the initial few applications of the cyclic load, numerous microcracks on the tension surface start that lead to significantly increased damage. Second, microcracks gradually start without forming a macroscopic crack; no visible crack is observed at this stage. It is difficult to see when the first stage of damage moves to the second stage. The microcracks in stage two lead to an almost steady state in the progression of the damage. Finally, large localized cracks appear that rapidly grow until failure occurs. The second stage resists the effects of fatigue loading longer than the first stage. Suthiwarapirak *et al.* (2002) found from their study that the PMM exhibited very brittle behavior under fatigue loading.

2.4. Engineered Cementitious Composite

Engineered Cementitious Composite (ECC) is one of a number of high performance fiber-reinforced cementitious composites (HPFRCC), optimizes the quantity and the properties of the fibers in it and exhibits strain-hardening behavior after yielding (Chun and Matsumoto 2011; Chun and Ohga 2012). The optimization can be achieved through designing the micromechanical interactions between fibers in the cementitious matrix and the interfacial bond between the fibers and the cementitious matrix. ECC is part of a family of materials with adjustable ductility and tensile strength to best match the structures they are used in (Li 2003). Both polyvinyl alcohol fibers (PVA) and the high modulus polyethylene

fibers (PE) are used in ECC (Li 2008). In general, ECC exhibits high ductility under fatigue loading and its general behavior shows three phases similar to the previous material (Suthiwarapirak *et al.* 2002; Xu and Liu 2011). However, its behavior under fatigue loading is different from the previously mentioned materials. The first stage starts with a few visible cracks appearing after the first cyclic loading followed by a rapid increase in damage. As the fatigue loading increases, new cracks start that join with existing cracks, leading to a gradual increase in damage and energy dissipation of the fatigue loading. The second stage sees the amount of damage stabilize before the last stage where one crack expands leading to failure of the material.

3. MODELS OF THE FATIGUELIFE OF MATERIALS

The most common way of modeling the effect of applied stress on the fatigue life of a material is the stress-life (*S-N*) approach, also known as Wöhler curves, where *S* is the stress range. These empirical curves give a graphical representation of the fatigue performance under a certain load. Fatigue life models do not take into account the actual degradation mechanisms though, such as matrix cracks, fiber ruptures, delamination and damage progress, but use *S-N* curve diagrams to infer some sort of fatigue failure criteria. In this paper, fatigue models for fiber, textile, polymer modified mortar and epoxy resin are presented. The mathematical symbols used in the models have not been changed from those used in the literature to avoid any confusion. An extensive summary of the fatigue life model and behavior of plain concrete and steel bars can be found in ACI 215-74 (ACI 1997).

3.1. Fiber Reinforced Polymer

A review of the research to date shows that, by considering different factors that affect the fatigue life of FRP composites under fatigue loading, different models for fatigue life result. Some of these models include:

- Stress ratio: several researchers, such as Elkadi and Ellyin (1994), Hwang and Su (2006), Reis *et al.* (2009), Toutanji *et al.* (2006) and Kawai and Suda (2004), have tested the effect of stress ratio (ratio of the minimum stress to the maximum stress) on the fatigue strength of FRP composites. In general, test data showed an increase in fatigue life with increased stress ratios, where the stress amplitude decrease as the stress ratio increased, which cause an increase in the fatigue life. Toutanji *et al.* (2006) defined the relationship between the applied cyclic stress level (*S*), the number of cycles to

failure (N) and the stress ratio (R) for carbon fiber sheet as follows:

$$S = \frac{\sigma_{\max}}{f_{fu}} = 1 - \alpha(1-R)\log(N) \qquad (1)$$

where $\sigma_{\max}$ is the maximum applied stress, f_{fu} is the ultimate strength and α is a constant determined experimentally.

- Stress frequency: the fatigue life increases as the stress frequency increases (Hwang and Su 2006). The reason of this behavior, that the maximum strain for the same maximum applied stress is reduced with increased frequency. Where, the time of the strain to reach the maximum strain at lower frequency is decreased due to viscoelastic behaviors of polymer matrix composite. Epaarachchi and Clausen (2003) proposed a model of the relationship between stress ratio, stress frequency, the number of cycles to failure and applied maximum stress:

$$\sigma_u - \sigma_{\max} = \alpha \sigma_u^{1-\gamma} \sigma_{\max}^{\gamma} (1-R)^y \frac{1}{f^{\beta}} (N^{\beta} - 1) \qquad (2)$$

where γ and β are material constants and f is frequency (Hz), $\sigma_{\max}$ is the maximum applied stress, σ_u is the ultimate static stress and R is the stress ratio.

- Temperature: polymer matrix composites of viscoelastic materials and their mechanical properties are significantly influenced by temperature. Kawai and Taniguchi (2006) and Jen *et al.* (2008) found the fatigue life deceased with increased temperature. Increasing the temperature change the matrix composite status due to caused reductions in both modulus of elasticity and ultimate strength of matrix, thereby weaken the bond performance of FRPs. Mivehchi and Varvani-Farahani (2010) proposed a model that showed the relationship between *S-N* and temperature as follows:

$$\sigma_{\max} = A(T_0) \left[1 - \frac{\left(\frac{A(0)}{A(T_0)} - 1\right)}{\ln\left(1 - \frac{T_0}{T_m}\right)} \ln\left(\frac{\left(1 - \frac{T}{T_m}\right)}{\left(1 - \frac{T_o}{T_m}\right)}\right) \right] (N_f(T))^{m(To)\left[\frac{\ln\left(1 - \frac{T}{T_m}\right)}{\ln\left(1 - \frac{T_o}{T_m}\right)}\right]} \qquad (3)$$

where $\sigma_{\max}$ is the maximum applied stress, $A(T)$ and $m(T)$ are the curve characteristics, T_o is room temperature and T_m is the polymer melting temperature of the composites. T, T_o, and T_m are all in Kelvin.

- Matrix type: the matrix type of FRP has a significant effect on the fatigue life of FRP composites. Where the matrix type affect the ability of composite to resist crack and fiber-matrix debonding Newaz (1985) carried out fatigue tests on two types of composite fiber consisting of the same E-glass fiber with different matrix materials: epoxy matrix [Dow Epoxy Resin (DER) 331] and vinyl ester matrix (Derakane411 – 45) Using this data, the fatigue life models, respectively, are as follows:

$$\frac{S_{\max}}{S_{ult}} = 0.7557 - 0.10626 \, \mathrm{Log} \, N \qquad (4)$$

$$\frac{S_{\max}}{S_{ult}} = 0.68 - 0.106 \, \mathrm{Log} \, N \qquad (5)$$

Papakonstantinou and Balaguru (2007) also showed the effect that the type of matrix has on the fatigue behavior by comparing the results of their tests on carbon fiber with a geopolymer resin matrix (Eqn 6 below) to the results of tests collected by Demers (1998) on anepoxy matrix (Eqn 7 below). Geopolymer resin was prepared by mixing an aqueous solution containing silica and potassium oxide with silica powder. The *S-N* models were:

$$\frac{S_{\max}}{S_{ult}} = 1.1055 - 0.046903 \, \mathrm{Log} \, N \qquad (6)$$

$$\frac{S_{\max}}{S_{ult}} = 0.8227 - 0.0519 \, Log \, N \qquad (7)$$

where $S_{\max}$ and S_{ult} are the maximum applied fatigue stress and ultimate static stress respectively.

- Fiber Type: Wu *et al.* (2010) evaluated the effect of fiber type on the fatigue behavior of FRP composite sheets. Experiments were conducted on various types of FRP [carbon(CFRP), E-glass (GFRP) and basalt (BFRP) fibers] and hybrid FRP sheets [carbon/E-glass (C1G1)] with the same epoxy matrix. The results showed that the carbon and polyparaphenylene FRP sheets exhibited, which

they have higher tensile modulus of elasticity, superior fatigue resistance, whereas the E-glass and basalt FRP sheets showed similar fatigue behavior. In addition, it was found that the hybrid FRP sheet (C1G1) had slightly improved fatigue behavior, where the fatigue behavior of hybrid FRP depended mainly on the interaction surface of different fibers .The *S-N* relationship for four types was modeled as follows:

$$\frac{P_{\max}}{P_{\mathrm{av}}} = A - \alpha \, \mathrm{Log} \, N \qquad (8)$$

where $P_{\max}$ and P_{av} are the maximum applied load and the average of the monotonic load-carrying capacity, respectively. A and α are constants as shown in Table 1.

- Fiber load angle: Hashin and Rotem (1973) and Awerbuch and Hahn (1981) carried out an investigation to evaluate the effect of loading on the fatigue strength of FRP composites using GFRP and CFRP respectively. In these investigations, different loading angles were used. The results indicated that the fatigue life was strongly dependent upon the fiber load angle, where the wider angle gives a lower fatigue life. Based on their data, the fatigue life model for CFRP and GFRP is as follows:

$$S_{\max} = A - \alpha \, \mathrm{Log} \, N \qquad (9)$$

where $S_{\max}$ is the maximum applied stress (MPa). A and α are constants as shown in Table 2 and Table 3.

Table 1. Fatigue constants for the *S-N* model of fiber types and material constants

Fiber type	A	α	Tensile modulus (GPa)	Tensile strength (MPa)	Ultimate strain (%)
CFRP	1.001	0.020	230	3400	1.48
GFRP	1.004	0.062	73	1500	2.05
C1G1	1.015	0.069	152	2242	1.48
BFRP	0.997	0.071	91	2100	2.31

Table 2. Fatigue constants for the *S-N* model for CFRP load angle

Fiber angle (Degree)	A	α
10^0	427.9	40.1
20^0	191.4	13.2
45^0	89.5	7.3
60^0	57.1	1.4

Table 3. Fatigue constants for the *S-N* model for GFRP load angle

Fiber angle (Degree)	A	α
10^0	151.4	9.7
20^0	95.9	9.1
30^0	73.4	7.3
60^0	29.8	1.1

3.2. Textile Reinforced Matrix

Several investigations of the fatigue life of textile fiber, impregnated with epoxy or polyester to act as a matrix, have been carried out (Harris 2003; Curtis and Moore 1987; Van Paepegem and Degrieck 2001). Textile fiber is considered to be part of the FRP family. To date, a model of textile fiber impregnated with cement mortar has not been developed. Cuypers (2001) presented the results from tests of a textile reinforced matrix, consisting of inorganic phosphate cement with E-glass fiber, under fatigue loading, as shown in Figure 3. A horizontal arrow extending from a data point in the plot indicates the specimen had not failed at the indicated number of fatigue cycles. The S-N relationship was modeled as follows:

$$S_{\max} = 37.029 - 3.231 \, \mathrm{Log} \, N \qquad (10)$$

where $S_{\max}$ is the maximum applied stress of the fatigue load.

3.3. Polymer Modified Mortar

The fatigue life models for two types of polymer modified mortar were described by Suthiwarapirak *et al.* (2002). They used a low ratio of fibers (less than 0.5%) which did not improve the tensile properties of the mortar. The first type, which consisted of cement, fine aggregate, lightweight aggregate and a low ratio of acrylic polymer fibers, was modeled as follows:

$$\frac{S_{\max}}{S_{\mathrm{ult}}} = 1.001 - 0.067 \, \mathrm{Log} \, N \qquad (11)$$
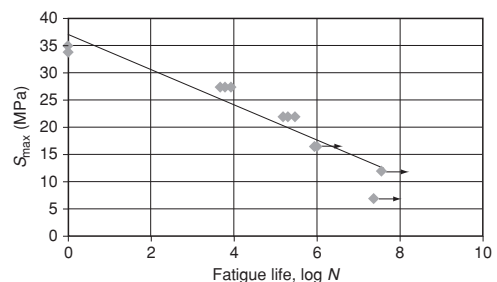
Figure 3. *S-N* curve for the textile reinforced matrix

The second type of polymer modified mortar consisted of cement, fine aggregate, SBR polymer and also a small amount of polyvinyl alcohol fibers; it was modeled as follows:

$$\frac{S_{max}}{S_{ult}} = 0.928 - 0.0808 \, Log \, N \qquad (12)$$

where S_{max} and S_{ult} represent the maximum applied fatigue stress and average ultimate static stress respectively. From the models we can see that the type one have higher fatigue life than the second type due to presence light weight aggregates which make it behave more ductile under fatigue load.

3.4. Engineering Cementitious Material

The models of the *S-N* relationships for two types of ECCs containing polyvinyl alcohol (PVA) and polyethylene (PE) fibers were proposed by Suthiwarapirak *et al.* (2004); the models describe a bilinear fatigue stress-life line as follows:

• ECC with polyvinyl alcohol

$$\frac{S_{max}}{S_{ult}} = 1.00 - 0.0226 \, Log \, N \quad 1 \le N \le 1 \times 10^4 \quad (13)$$

$$\frac{S_{max}}{S_{ult}} = 1.595 - 0.1750 \, Log \, N \quad 1 \times 10^4 \le N < 2 \times 10^6 \quad (14)$$

• ECC with polyethylene

$$\frac{S_{max}}{S_{ult}} = 1.00 - 0.032 \, Log \, N \quad 1 \le N < 3 \times 10^2 \quad (15)$$

$$\frac{S_{max}}{S_{ult}} = 1.157 - 0.0903 \, Log \, N \quad 3 \times 10^2 \le N < 2 \times 10^6 \quad (16)$$

where S_{max} and S_{ult} represent the maximum applied fatigue stress and average ultimate static stress respectively. The reason behind that the ECC with polyvinyl alcohol have higher fatigue life than ECC with polyethylene is the behavior of fibre in post cracking stage.

3.5. Epoxy Resin

The literature study identified different types of fatigue test in epoxy resin: cyclic bending fatigue (Nagasawa *et al.*1995), uniaxial cyclic fatigue (Tao and Xia 2007) and shear cyclic fatigue (Tao and Xia 2008). Tao and Xia (2007) proposed that the relationship between stress
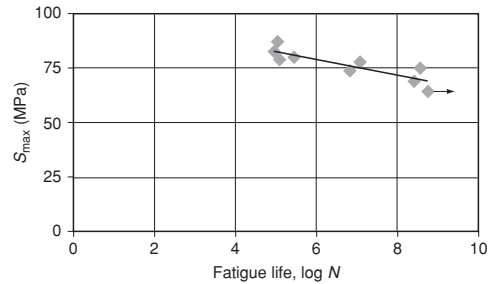
Figure 4. *S-N* curve for epoxy resin material

amplitude and fatigue life using a uniaxial cyclic fatigue test for epoxy resin with a modulus of elasticity 2900 MPa was as follows:

$$S_{max} = 192.6 \, N^{-0.362} + 35 \qquad (17)$$

The model proposed from the cyclic bending fatigue test data with tensile strength (82.1 MPa), presented by Nagasawa *et al.* (1995), as shown in Figure 4 is as follows:

$$S_{max} = 100.54 - 3.6228 \, Log \, N \qquad (18)$$

where S_{max} is the maximum applied fatigue stress .We can see that the epoxy resin have very high fatigue stress which make it more suitable as bonding material for different strengthening purposes under different load values.

4. BOND

The most significant effect on the behavior of a strengthened structure is the bond between that structure and the strengthening material. The bond determines the failure behavior of the structure: a strong bond can lead to the brittle failure of the structure whereas a weak bond can lead to ductile failure. The bond performance is determined by the strength of the adhesives used and the tensile strength of concrete. The bonding can be classified as an epoxy-based method, which uses epoxy resin as a binder and a mineral-based method, which uses fine grade mineral as a binder.

4.1. Epoxy Bonded System

The properties of epoxy resin are mainly dependent on the hardener used, the choice of which depends on the properties required for the specific application (Täljsten 2006). The mechanical behavior of epoxy material is analogous to brittle material under cyclic loading and passes through three stages (Nagasawa *et al.* 1995; Tao

and Xia 2007). The first stage sees the start of microcracking, which continues through the whole of the low stress amplitude fatigue life cycle, causing no damage to the material itself until a fracture is imminent. Throughout this stage, there is a linear relationship between stress and strain. The strength of bonded joints not only depends on the cohesive strength of the adhesive (Neil *et al*. 2007) but also on the degree of adhesion to the bonding surface (Täljsten 2006) and the type of FRP being used (Ko and Sato 2007). For these reasons, the fatigue life of epoxy material is not representative of the fatigue life of the whole epoxy bond system even if the failure is only in the epoxy layer. The different test methods used to evaluate the bond behavior of externally-bonded FRP composite sheets and plates under fatigue loading include the single shear (single lap joint) test (Bizindavyi *et al*. 2003; Mazzotti and Savoia 2009), the double lap joint test (Ferrier *et al*. 2005), the pull-out specimen method for measuring peeling stresses (Khan *et al*. 2011) and the partially bonded beam test (Gheorghiu *et al*. 2004) as shown schematically in Figure 1. The single lap joint test gives inaccurate results because it creates undesirable flexural loading. From experiments conducted (Dai *et al*. 2005; Bizindavyi *et al*. 2003; Yun *et al*. 2008; Nigro *et al*. 2011; Diab *et al*. 2007; Ko and Sato 2007), it can be seen that the local slip of FRP-concrete joints increases gradually with cyclic loading. The general behavior is similar to monotonic load behavior except for the rate of change of debonding propagation. The rate of change of slip slope increased with increasing stress amplitude (Dai *et al*. 2005; Bizindavyi *et al*. 2003; Yun *et al*. 2008).There are different types of failure caused by debonding: debonding between the epoxy resin and the epoxy primer, debonding into the coarse aggregate (split of

concrete cover) and debonding between the plies for joints with more than one plies (Bizindavyi *et al*. 2003). Ferrier *et al*. (2005) showed that the lap joint that used the epoxy with a higher glass transition temperature behaved the best under fatigue loading. In their tests, Ferrier *et al*. (2005) used three types of epoxy with different glass transition temperatures: type A (46 °C), type B (55 °C) and type C (80°C). Dai *et al*. (2005) and Bizindavyi *et al*. (2003) showed that an increase in bond length under cyclic fatigue loading led to an increase in fatigue life unlike under static loading, where an increase of length beyond the effective length made no difference. Nigro *et al*. (2011) found that under cyclic loading with 70% of the maximum debonding static load, the fatigue loading was negligible even when the bond length was less than the effective bond length by 50% for carbon sheet and plates. Diab *et al*. (2007) showed that the fatigue endurance limit (2 million cycles) is reached when the stress level is below 30% of the maximum debonding static load.

CFRP and GFRP are well-known types of fiber used for strengthening concrete structures. In order to produce fatigue life models for bonding FRP-concrete joints only showing the effect of fiber type, data have been collected from existing literature as shown in Table 4 and Figure 5 [carbon fibers (marked with filled shapes) and glass fibers (marked with unfilled shapes)]. The fatigue life models of CFRP and GFRP can be estimated from this data and can be predicted from the following equations respectively:

$$S_{max} = 1.4926 - 0.1428 \text{ Log } N \qquad (19)$$

$$S_{max} = 1.9321 - 0.212 \text{ Log } N \qquad (20)$$

where S_{max} is the maximum applied average bond stress.

Table 4. Summary of available material data and test setup

| Reference | Lap type test | Compressive concrete strength (MPa) | FRP | |
			Modulus of elasticity (GPa)	Tensile strength (MPa)
Diab et al. (2009)	Double	32	240	3500
Bizindavyi *et al*.				
(2003) - CFRP	Single	42.5	75.7	1014
GFRP	Single		29.2	472
Ferrier *et al*.				
(2005) Type A	Double	NA	70	340
Type B	Single and double		75	885
Type C	Double		88	1000
Diab *et al*. (2007)	Double	32	240	3500

NA = not available
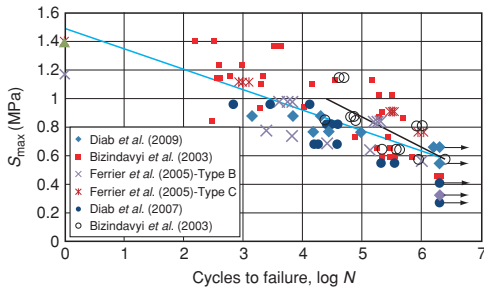
Figure 5. *S-N curve for bonds of CFRP and GFRP to concrete*

Figure 7. *S-N curve of alkali-resistant glass reinforced matrix*

It can be seen in Figure 5 that the CFRP results show improved *S-N* behavior when compared to GFRP. This improvement is represented by a reduction in the slope of the *S-N* curve. The shallow slope means that a small reduction in stress gives a greater increase in fatigue life.

4.2. Mineral Bonded System
There are two types of strengthening systems using mineral-based bonding agents: the ECC overlay system and the mortar impregnated with textile fibers or grid fibers system. There have been few studies investigating bonding using the mineral-based method under fatigue loading. Zhang and Li (2002) investigated the effect of surface bonding on the fatigue performance of the ECC overlay system using a flexural test. The result showed that the layer–based interface characteristics, rough or smooth, do not influence the fatigue life. The *S-N* model of the results as shown in Figure 6 is as follows:

$$S_{max} = 12.251 - 0.6202 \log N \qquad (21)$$

where S_{max} is the maximum flexural stress applied.

In the second system, the bonding failure can theoretically be classified as either being a micro or macro level failure. Besides the debonding between the

yarns and mortar, the debonding between the outer and inner filaments of the yarns, which form the main components of textile fabrics (Brameshuber 2006), can be considered to be a micro level debonding failure. There are different types of macro level bonding failure: debonding between composites of the textile and the matrix with the concrete substrate, delamination of the matrix at the textile layer, delamination between the layers of textile if more than one layer is used in the matrix, delamination in the concrete substrate and finally fiber-pullout in the mortar matrix layer (Brameshuber 2006).

At the micro level, Kang and Brameshuber (2006) investigated the bond behavior under a cyclic load at three different stress levels. The textile reinforcement was made of alkali-resistant glass embedded in a fine-grained concrete matrix, which consisted of two symmetric parts separated by a very thin baffle. Further details about the test and materials data can be found in Kang and Brameshuber (2006). The results showed that the stress levels produced by the cyclic load were indicative of the rate of damage accumulation and the failure of the specimens. The *S-N* relationships from these tests are shown in the Figure 7; the model is:

$$S_{max} = 172.98 - 27.431 \log N \qquad (22)$$

where S_{max} is the maximum applied stress of the fatigue load.

To date, to the author's knowledge, there has been no study that investigates the behavior of macro level bonding under fatigue loading.

5. STRENTHENED BEAM BEHAVIOR UNDER FATIGUE LOADING
5.1. Epoxy Bonded System
Several studies have been carried out on the effects of fatigue on structures strengthened with FRP bonded using the epoxy-based method. These studies investigated fatigue using different material types (e.g. fibers), different applied load values, time

Figure 6. *S-N curve for bonds using the ECC overlay system*

dependent effects (e.g. temperature, relative humidity, freeze and thaw), different types of strengthened structures (shear, flexural or combined) and different configurations of sheet or plate. In order to evaluate the fatigue performance of beams strengthened with externally bonded FRP laminate, this section presents the test results of beams subjected to fatigue loading under different conditions, drawn from the literature. Among them, Yu *et al.* (2011) carried out fatigue testing of RC beams strengthened with GFRP sheet and this study showed that GFRP sheets reduce the stress in reinforcing steel and increase the fatigue life of a strengthened beam under fatigue loading. IN addition, the fatigue failure of strengthened beams with GFRP are similar to the beams strengthened with CFRP. The fatigue behavior of flexurally strengthened concrete beams with near surface mounted (NSM) CFRP was investigated by Yost *et al.* (2007). The results appeared to show that the bond action between NSM CFRP and the concrete was not affected by fatigue loading. The response of CFRP-strengthened beams under fatigue loading with different load amplitudes were studied by Gheorghiu *et al.* (2007). The results showed that the higher fatigue amplitude significantly increased the cracking strain of the CFRP-concrete joint. The fatigue performance of RC beams shear strengthened with CFRP fabrics was investigated by Chaallal *et al.* (2010), who discovered that the fatigue life of two layers of CFRP was lower than that of one layer, where the greater rigidity of FRP (two layer) changed the stress distribution in concrete causing crush of concrete rather than yielding of steel stirrups. Ekenel and Myers (2009) exposed test beams to severe environments and defects caused by delamination in order to study the durability of RC beams strengthened with CFRP. By using cycles of continuous freeze and thaw, prolonged exposure to extreme temperatures, continuous relative humidity cycles and ultraviolet light, they showed that fatigue loads combined with harsh environmental conditions significantly affected the flexural stiffness of the beams as a result of environmental effect on bond strength of the adhesive. Gussenhoven and Breña (2005) discovered that wider laminates are more effective than narrower laminates atincreasing the fatigue life of strengthened beams, due to that the wider laminates reduce shear lag effects and are also able to restrain crack opening more than narrower laminates. Al-Rousan and Issa (2011) studied the effect of using different CFRP sheet configurations, different numbers of CFRP layers, a differing CFRP contact area with the concrete, a variety of frequencies and number of fatigue cycles, varying stress ranges and severe salt-water exposure on flexural beams strengthened with CFRP.

The results showed that the stress ranges have a noticeable effect on fatigue life. Furthermore, the frequency of the fatigue loading did not significantly affect the strengthened beam in the range of 1 – 4 Hz. This conclusion help to accelerate the fatigue test by increase the frequency within this limit, whilst the fatigue life increased with increasing numbers of CFRP layers and greater contact area due to more release of the stresses in the tension steel bar. Barnes and Mays (1999) carried out experimental work to study the effects of different types of load on fatigue behavior. When they applied the same stress range in the rebar for both the strengthened and the unstrengthened beams, they found that the fatigue life of the strengthened beams was higher than that of the unstrengthened beams. Conversely, they found that when applying an equal percentage of the ultimate static load capacity to each beam, the fatigue life of the plated beam was shorter than that of the unplated beam. The reason for this is that, the ultimate load for strengthened beam was much higher than from unplated beam and thereby the same percentage of ultimate load gave a high stress range in tension steel bars of plated beam. Masoud *et al.* (2001) showed that the fatigue life of a corroded beam improved using transverse CFRP wrapping and flexural sheet causing reduction of stress level in the corroded tension steel bars. Khan *et al.* (2011) found from their study that shear end anchorages enhanced the fatigue performance of flexurally strengthened RC beams. The arguments for this behavior is that the end anchorage reduce the high interfacial shear and peeling stresses at the point of plate cut-off, which cause debonding of CFRP laminate. Huang *et al.* (2011) studied the effect of temperature on the fatigue behavior of strengthened beams. The results showed that the fatigue life decreased with increased temperature, where the failure modes of strengthened beams changed from steel yielding to interface debonding of laminate. Senthilnath *et al.* (2001) showed that when the delamination exceeded the worst case delamination as recommended by ACI, there was minimal effect on the fatigue performance of the CFRP strengthened RC beams. Minnaugh and Harries (2009) discussed the fatigue behavior of RC beams strengthened with steel fiber reinforced polymer (SFRP) and CFRP and suggested that SFRP largely improved the fatigue behavior of RC beams and superior compared with CFRP, where no evidence of debonding for the (relatively high) stress ranges. Derkowski (2006) tested beams under fatigue loading with two flexural strengthening systems on the bottom of the beam, with the system consisting of one or two CFRP strips. The results showed that the fatigue life of beams strengthened with two strips was greater than

when using one strip because two strip have more efficient to restrain cracks opening. Wang *et al.* (2007) discovered that an FRP strengthened T-beam exhibited excellent behavior under fatigue loading when using hybrid FRP, consisting of CFRP plates for flexure and a GFRP U-strip for shear. Harries *et al.* (2007) studied the effect of adhesive stiffness; the results showed that the generated stress in tensile steel under fatigue loading was greater with more flexible adhesive due to reduce ability of the adhesive to transfer stress to the strengthening material.

From most of the studies (Harries *et al.* 2007; Toutanji *et al.* 2006; Barnes and Mays 1999; Shahawy and Beitelman 1999; Papakonstantinou *et al.* 2001; Aidoo *et al.* 2004; Masoud *et al.* 2001; Dong *et al.* 2011), the general behavior of beams strengthened with FRP is that there is an initial change in stiffness and increase of deflection due to a redistribution of the cracks in the beams. This is then followed by unchanging stiffness with increasing deflection due to the cyclic creep, the time evolution of the plastic strain under cyclic load, of the concrete as explained by Papakonstantinou *et al.* (2001). Finally, there is a sudden increase of deflection just before the failure. The behavior of strengthened beams under fatigue loading depends mainly on the maximum stress generated in the main tension reinforcement, the bond strength between the FRP and the concrete as well as the configuration of the FRP. If the bonding strength between the concrete and the FRP is sufficient, the initial failure will be due to steel rupture, followed by rupture of the FRP or debonding from the concrete substrate or delamination of the concrete cover caused by flexural-shear cracking. FRP debonding rarely occurs because both the tensile strength and the shear strength of epoxy adhesive are twice as great as those of the concrete cover (Derkowski 2006). If the bonding of the FRP with the concrete substrate is defective, either because of sub-standard workmanship or design problems with the anchorage, any failure due to the debonding of the FRP will, for most cases, cause a steel rebar rupture; the fatigue life will obviously be impaired. Figure 8 shows the *S-N* data for sheet, laminate FRP strengthened beams and NSM strengthened beams from the literature (Barnes and Mays 1999; Breña *et al.* 2005; Dong *et al.* 2011; Heffernan and Eriki 2004; Papakonstantinou *et al.* 2001; Yu *et al.* 2011; Quattlebaum *et al.* 2005; Badawi 2007 and Abdel Wahab 2011). This figure only includes data for rectangular beams to avoid any effects due to beam shape on the *S-N* model. The stress range (S_r) reported is the stress range in the internal reinforcing tension steel at the first cycle. Regression curves for CFRP, GFRP and NSM strengthened beams are also shown in Figure 8 and are
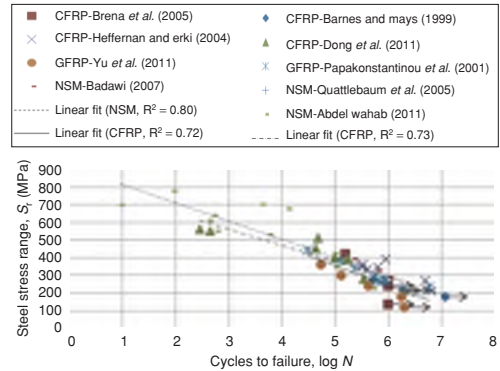
Figure 8. *S-N* curves for FRP laminates, sheets and NSM

modeled with the following equations respectively:

$$S_r = 834.31 - 91.329 \log N \qquad (23)$$

$$S_r = 913.19 - 111.52 \log N \qquad (24)$$

$$S_r = 917.81 - 103.64 \log N \qquad (25)$$

where S_r is the steel stress range in steel.

It can be seen in Figure 8 that the near surface mounted applications have an improved fatigue performance over both the CFRP and the GFRP laminate For a given steel stress range, the NSM strengthened beams appear to have the longest fatigue life with GFRP having the shortest. The strength of FRP and bond of the FRP bar to the concrete plays a major role in the improved fatigue behavior. The bond is responsible for transferring the forces between FRP bar and the surrounding concrete, so that the section acts as one unite with NSM.

5.2. Mineral-Based Method

Mineral-based method is used to avoid some of epoxy adhesive drawbacks like working environment, minimum application temperature, often above 10 ºC, and epoxy creating diffusion-closed surfaces which may imply moisture and freeze/thaw problems for concrete structures (Blanksvärd *et al.* 2009). Very little research had been conducted on beams strengthened with mineral material as an adhesive under fatigue loading. Papanicolau *et al.* (2006) experimentally compared the fatigue behavior of beams strengthened with one layer of textile reinforcement with a cementitious binder to beams strengthened with one layer of textile reinforcement with a resin-based matrix. Although the cementitious bonding proved less effective than the resin

bonding, if given sufficient shear resistance under fatigue loading, the effectiveness of the cementitious bonding increased with increased numbers of textile layers. The main feature of fatigue behavior of beams strengthened with a textile cementitious matrix compared with an epoxy-based system was the increase in the beam ductility under fatigue loading due to clearly visible cracks in the cementitious mortar matrix. The results of the research by Leung *et al.* (2007) showed that the ECC layer significantly improved the fatigue life of the plain concrete beam, handling large deflection without failure because the ECC controls the growth of fatigue cracks. An inorganic matrix consisting of an aluminosilicate powder blended with a water-based activator was used by Toutanji *et al.* (2006) as a matrix to bond unidirectional carbon fiber fabric to reinforced concrete beams, which were subjected to fatigue loading. The result showed that the fatigue life increased and the behavior of failure was analogous to epoxy-based methods using for strengthening. Steel-reinforced inorganic polymer tapes consisting of steel fiber tapes with a modulus of elasticity of 210 MPa and an inorganic matrix, Geopolymer, were used as flexural strengthening for beams by Katakalos and Papakonstantinou (2009). The results showed that the fatigue life increased and failure was determined by the main steel tension reinforcement and the steel-reinforced inorganic polymer system. The fatigue life model for beams strengthened with steel-reinforced inorganic polymer system was proposed to be:

$$S_r = 624 - 67 \, \text{Log} \, N \qquad (26)$$

where S_r is the stress range in steel.

6. BUILDING CODES AND RESEARCHERS RECOMMENDATIONS

Presently, there are no recommendations in the building codes for strengthening structures under fatigue loading using mineral-based methods. Extracted from the different building codes and research literature, the following recommendations deal with epoxy-based methods:

(1) The ACI 440.2R-08 (2008) recommendation to prevent fatigue and creep failure for GFRP, AFRP and CFRP material is to have a total stress to FRP ultimate strength ratio below of 0.2, 0.3 and 0.55 respectively. Diab and Wu (2008), Breña *et al.* (2005) and Harries and Aidoo (2006) considered this recommendation to be inadequate and impossible to achieve. The author's consider this recommendation to be good in order to ensure that the FRP itself does not fail under fatigue load.

(2) The JSCE recommendations (JSCE 2001) recommended a reduction factor of $\mu = 0.7$ on the interfacial fracture energy relating to the bonding of fiber reinforced polymer sheets to concrete under fatigue loading. Harries and Aidoo (2006) considered this reduction factor too small when compared to the recommended reduction factor for a monotonic load to prevent debonding. In the author's opinion, this recommendation is suitable for high cyclic fatigue, where the load is less than the yield static load of beam.

(3) The Italian design guide CNR-DT200 (NRC 2004) recommended a long-term conversion factor, $\eta = 0.5$, multiplied by a property of FRP composites to prevent possible fatigue failure. However, this does not take into account the stress range of the fatigue loading and the properties of the concrete.

(4) ISIS Canada design manual (ISIS Canada 2008) only recommended a reduction factor to account for the effect of creep on FRP composites without fatigue load.

(5) The model code 2010 (draft) indicated different values of stress range for different types of FRP bar which can be used as reinforcement bars in concrete. These values are unsuitable for NSM application due to a difference in bonding systems.

Kim and Heffernan (2008), as well as Barnes and Mays (1999), recommended, good recommendation, that the conventional method of using unstrengthened reinforced concrete to prevent fatigue failure can be used for FRP-strengthened structures. Ferrier *et al.* (2011) did not take into account the stress range in steel and limited the shear stress between the concrete and CFRP to 0.8 MPa to prevent fatigue failure over 1×10^6 cycles. Yao *et al.* (2006) proposed, to prevent fatigue failure of CFRP, that the ultimate fatigue strength of a carbon fiber laminate strengthened reinforced concrete beam is 0.58 times of its ultimate static loading. Breñ~ a *et al.* (2005) indicated that the maximum composite stress in CFRP laminates is 15 to 25% of the ultimate strength lower than the ACI 440.2R-08 (2008) recommendation. Senthilnath *et al.* (2001) performed fatigue tests on beams with different sizes of delamination and got important results that the maximum delamination area of 16000 mm², as recommended by ACI 440.2R-08 (2008), has little effect on the fatigue behavior of strengthened flexural beams. They also considered the lap length of 50 mm to be insufficient for CFRP sheets under fatigue loading as currently recommended for the MBrace composite strengthening system (2002) under a static load. Yang

Table 5. Summary of available material data and test setup

Reference	Tested beam numbers	Beam dimensions (mm)	Load configuration	Compressive concrete strength (MPa)	Steel yield stress (MPa)	FRP Modulus of elasticity (GPa)	FRP Tensile strength (MPa)
arnes and Mays (1999)	3	$125 \times 230 \times 2300$	Four-point bending	50	NA	135	1226
Dong *et al.* (2011)	10	$152.4 \times 304.8 \times 2896$	Four-point bending	38.2	414	731	960
Brena *et al.* (2005)	3	$203 \times 356 \times 2692$	Four-point bending	40	434	227.7	3800
Heffernan and Erki (2004)	6	$150 \times 300 \times 2850$	Four-point bending	37	511	233	NA
	3	$300 \times 574 \times 4800$		32.9	479	325	NA
Papakonstantinou *et al.* (2001)	8	$152.4 \times 152.4 \times 1220$	Third-point bending	39.3	427	72.4	1730
Yu *et al.* (2011)	5	$150 \times 250 \times 2300$	Four-point bending	20	335	30.2	643
Quattlebaum *et al.* (2005)	2	$152 \times 254 \times 4572$	Third-point bending	29.5	446	154.2	2785
Badawi (2007)	4	$152 \times 254 \times 3300$	Four-point bending	40	440	136	1970
Abdel Wahab (2011)	7	$150 \times 250 \times 2000$	Four-point bending	60	510	136	1970
	4					130	2166

and Nanni (2002) recommended a lap splice length of 101.6 mm, if the maximum applied stress does not exceed 40% of the ultimate static strength. Diab *et al.* (2007) recommended that the FRP fatigue stress for FRP-strengthened beams should not exceed 30% of the static bond capacity of the FRP-concrete interface. Gunes *et al.* (2006) recommended that a minimum bond anchorage be provided on the end regions of the FRP flexural reinforcement, at a distance equal to the beam depth to ensure improved cyclic load performance. From the above recommendations, we can find complete criteria to design strengthening of beams under fatigue load include important parts, such as bond, FRP and steel.

7. CONCLUSION
This paper has provided an inclusive review of available studies of the fatigue behavior of materials used in external strengthening of concrete structures with FRP; it has also considered beam strengthening using epoxy-based methods or mineral-based methods. The damage to the FRP-concrete interface under fatigue loading was discussed. The existing building codes and recommendations from other researchers, related to the fatigue behavior of FRP-strengthened structures, were also reviewed. From this state of the art review, it is interesting to note that the effectiveness of strengthening material on the fatigue life of beams depended on the bond behavior between the strengthening material and the concrete substrate. Where, enough bond strength between strengthening system and substrate helps to distribute the stress in the member and reduce the stress level generated in the steel reinforcement. Various environmental conditions affected the behavior of FRPs at the material and structural level by affecting the durability of the strengthening material. The mineral-based

strengthening method appeared more ductile than the epoxy-based strengthening method under fatigue loading. The epoxy-based FRP NSM technique demonstrated superior fatigue life compared to using plate or sheet bonded strengthening. Most composite materials under fatigue loading went through three different stages: an initial matrix cracking stage, a steady state damage stage and finally a failure stage where the fibers broke. The duration of each stage depended on the matrix and the types of fibers. However, this is different for TRM, where the matrix cracking occurs at the second stage of damage after initial transverse cracks in the fill have appeared. Testing double lap joint under fatigue loading produced more accurate results compared with single lap joint testing, where there was undesirable flexural loading. As ECC exhibits excellent behavior under fatigue loading, it is assumed that ECC, when combined with grid stows of fibers, would be able to be more effective at enhancing the fatigue life of strengthened structures. This study also showed that bonded CFRP joints have better *S-N* behavior than GFRP. Further research should be carried out into the influence of bonding, both between the base concrete and binder along with the transition zone and between binder and fiber composites under fatigue loading. More studies on the effect of FRP laminate thickness and modulus of elasticity on the fatigue behavior of strengthening beam are needed. Further research should also be carried out into the fatigue life of beams strengthened using mineral–based and epoxy-based FRP NSM techniques under different environmental conditions, in order to produce fatigue life models and to find the best conditions in which to use mineral-based strengthening and NSM techniques under fatigue loading. Lap joint tests are needed to construct the

fatigue life model of bonding using the mineral-based system at a macro level. Furthermore, fatigue testing is needed to optimize the properties of the mortar, which is used as the binder and matrix in mineral-based strengthening systems. Further studies are needed to find the recommendations to prevent fatigue failure of mineral-based method (maximum stress or strain to FRP ultimate ratio, FRP material properties and properties of bond to the concrete substrate) for both flexural and shear strengthening. Studying the effect of mechanical fasteners of FRP grid in fatigue behavior of mineral-based method are needed together with the suitable lap length of FRP used with mineral materials. More studies are also needed to find fatigue models of textile fiber and FRP grid impregnated with polymer-modified mortar. In addition, comparison studies of different strengthening material (FRP laminates, FRP grid or textile fiber with polymer modified material, ECC) under fatigue load are also needed. The effect of number of layers for FRP grid with mineral based bonding material on the behavior of strengthening beam under fatigue load are also needed.

REFERENCES

Abdel Wahab, N. (2011). *Bond Behaviour of Beams Reinforced with Near Surface Mounted Carbon Fibre Reinforced Polymer Rods under Fatigue Loading*, PhD Thesis, University of Waterloo, Waterloo, Canada.

ACI 215R-74 (1997). *Considerations for Design of Concrete Structures Subjected to Fatigue Loading (ACI 215R-74)*, American Concrete Institute, Farmington Hills, Michigan, USA.

ACI440.2R (2008). *Guide for the Design and Construction of Externally Bonded FRP Systems for Strengthening Concrete Structures (ACI440.2R)*, American Concrete Institute, Farmington Hills, Michigan, USA.

Adimi, M.R., Rahman, A.H. and Benmokrane, B. (2000). "New method for testing fiber-reinforced polymer rods under fatigue", *Journal of Composites for Construction,* ASCE, Vol. 4, No. 4, pp. 206–213.

Aidoo, J., Harries, K. and Petrou, M. (2004). "Fatigue behavior of carbon fiber reinforced polymer strengthened reinforced concrete bridge girders", *Journal of Composites for Construction*, ASCE, Vol. 8, No. 6, pp. 501–509.

Al-Rousan, R. and Issa, M. (2011). "Fatigue performance of reinforced concrete beams strengthened with CFRP sheets", *Construction and Building Materials*, Vol. 25, No. 8, pp. 3520–3529.

Awerbuch, J. and Hahn, H. (1981). "Off-axis fatigue of graphite/epoxy composite", *Fatigue of Fibrous Composite Materials,* ASTM STP 723, American Society for Testing and Materials, Philadelphia, USA, pp. 243–273.

Badawi, M. (2007). *Monotonic and Fatigue Flexural Behavior of RC Beams Strengthened with Prestressed NSM CFRP Rods,* PhD Thesis, University of Waterloo, Canada.

Barnes, R. and Mays, G. (1999). "Fatigue performance of concrete beams strengthened with CFRP plates", *Journal of Composites for Construction*, ASCE, Vol. 3, No. 2, pp. 63–72.

Bizindavyi, L., Neale, K. and Erki, M. (2003). "Experimental investigation of bonded fiber reinforced polymer-concrete joints under cyclic loading", *Journal of Composites for Construction*, ASCE, Vol. 7, No. 2, pp. 127–134.

Blanksvärd, T., Täljsten, B. and Carolin, A. (2009). "Shear strengthening of concrete structures with the use of mineral-based composites (MBC)", *Journal of Composites for Construction*, ASCE, Vol. 13, No. 1, pp. 25–34.

Brameshuber, W. (2006). *State-of-the-Art Report of RILEM Technical Committee 201-TRC: Textile Reinforced Concrete*, RILEM Publications S.A.R.L., Bagneux, France.

Brand, A.M. (2009). *Cement-Based Composites. Materials, Mechanical Properties and Performance*, 2nd Edition, Taylor & Francis, London, UK.

Breña, S., Kreger, M. and Wood, S. (2005). "Fatigue tests of reinforced concrete beams strengthened using carbon fiber reinforced polymer composites", *ACI Structural Journal,* Vol. 102, No. 2, pp. 305–313.

Chaallal, O., Boussaha, F. and Bousselham, A. (2010). "Fatigue performance of RC beams strengthened in shear with CFRP fabrics", *Journal of Composites for Construction*, ASCE, Vol. 14, No. 4, pp. 415–423.

Chun, P. and Matsumoto, T. (2011). "Optimal design of DFRCC subjected to fatigue loading", *Advanced Materials Research,* Vol. 250–253, pp. 430–433.

Chun, P. and Ohga, M. (2012). "Effect of fiber diameter on fatigue strength of fiber reinforced concrete and its design", *Applied Mechanics and Materials*, Vol. 138–139, pp. 810–815.

Curtis, P. (1989). "The fatigue behaviour of fibrous composite materials", *Journal of Strain Analysis*, Vol. 24, No. 4, pp. 235–244.

Curtis, P. and Moore, B. (1987). "A comparison of the fatigue performance of woven and non-woven CFRP laminates in reversed axial loading", *International Journal of Fatigue*, Vol. 9, No. 2, pp. 67–78.

Cuypers, H. (2001). *Analysis and Design of Sandwich Panels with Brittle Matrix Composite Faces for Building Applications*, PhD Thesis, Vrije Universiteit Brussel, Brussels, Belgium.

Dai, J.G., Sato, Y., Ueda, T. and Sato, Y. (2005). "Static and fatigue bond characteristics of interfaces between CFRP sheets and frost damage experienced concrete", *Proceedings of Fourth International Symposium on Fiber Reinforced Polymer Reinforcement for Reinforced Concrete Structures (FRPRCS-4),* Kansas City, USA, pp. 1515–1530.

Demers, C. (1998). "Fatigue strength degradation of E-glass FRP composites and carbon FRP composites", *Construction and Building Materials*, Vol. 12, No. 5, pp. 311–318.

Derkowski, W. (2006). "Fatigue life of reinforced concrete beams under bending strengthened with composite materials", *Archives of Civil and Mechanical Engineering*, Vol. 6, No. 4, pp. 33–47.

Diab, H., Wu, Z. and Iwashita, K. (2007). "Experimental and numerical investigation of fatigue behavior of FRP-concrete interface", *Proceedings of the 8th International Symposium on Fiber-Reinforced Polymer Reinforcement for Concrete Structures* (FRPRCS-8), Patras, Greece.

Diab, H. and Wu, Z.S. (2008). "Review of existing fatigue results of beams externally strengthened with FRP laminates", *Proceedings of the 4th International Conference on FRP Composites in Civil Engineering (CICE2008)*, Zurich, Switzerland.

Dong, Y., Ansari, F. and Karbhari , V. (2011). "Fatigue performance of reinforced concrete beams with externally bonded CFRP reinforcement", *Journal of Structure and Infrastructure Engineering*, Vol. 7, No. 3, pp. 229–241.

Ekenel, M. and Myers, J. (2009). "Fatigue performance of CFRP strengthened RC beams under environmental conditioning and sustained load", *Journal of Composites for Construction*, ASCE, Vol. 13, No. 2, pp. 93–102.

El Kadi, H. and Ellyin, F. (1994). "Effect of stress ratio on the fatigue of unidirectional Glass fibre/epoxy composite laminae", *Composites*, Vol. 25, No. 10, pp. 917–924.

Epaarachchi, J. and Clausen, P. (2003). "An Empirical model for fatigue behavior prediction of glass fiber-reinforced plastic composites for various stress ratios and test frequencies", *Composites: Part A*, Vol. 34, No. 4, pp. 313–326.

Ferrier, E., Bigaud, D., Clément, J. and Hamelin, P. (2011). "Fatigue-loading effect on RC beams strengthened with externally bonded FRP", *Construction and Building Materials*, Vol. 25, No. 2, pp. 539–546.

Ferrier, E., Bigaud, D., Hamelin, P., Bizindavyi, L. and Neale, K. (2005). "Fatigue of CFRPs externally bonded to concrete", *Materials and Structures*, Vol. 38, No. 1, pp. 39–46.

Fujii, T., Amijima, S. and Okubo, K. (1993). "Microscopic fatigue processes in a plain-weave glass-fibre composite", *Composites Science and Technology*, Vol. 49, No. 4, pp. 327–333.

Gheorghiu, C., Labossiere, P. and Proulx, J. (2007). "Response of CFRP-strengthened beams under fatigue with different load amplitudes", *Construction and Building Materials*, Vol. 21, pp. 756–763.

Gheorghiu, C., Labossiere, P. and Raihe, A. (2004). "Environmental fatigue and static behavior of RC beams strengthened with carbon fiber-reinforced polymer", *Journal of Composites for Construction*, ASCE, Vol. 8, No. 3, pp. 211–218.

Gorty, S.S. (1994). *Mechanical Properties of Composite Cables*, Master Thesis, South Dakota School of Mines and Technology, South Dakota.

Gunes, O., Karaca, E. and Gunes, B. (2006). "Design of FRP retrofitted flexural members against debonding failures", *Proceedings of the 8th U.S. National Conference on Earthquake Engineering*, San Francisco, California, USA.

Gussenhoven, R. and Breña, S.F. (2005). "Fatigue behaviour of reinforced concrete beams strengthened with different FRP laminate configurations", *Proceedings of the Seventh Fiber Reinforced Polymers for Reinforced Concrete Structures (FRPRCS7) Conference*, New Orleans, USA.

Hansen, U. (1999). "Damage development in woven fabric composites during tension–tension fatigue", *Journal of Composite Materials*, Vol. 33, No. 7, pp. 614–639.

Harries, K.A., Reeve, B. and Zorn, A. (2007). "Experimental evaluation of factors affecting monotonic and fatigue behavior of fiber-reinforced polymer-to-concrete bond in reinforced concrete beams", *ACI Structural Journal*, Vol. 104, No. 6, pp. 667–674.

Harries, K. and Aidoo, J. (2006). "Debonding- and fatigue-related strain limits for externally bonded FRP", *Journal of Composites for Construction*, ASCE, Vol. 10, No. 1, pp. 87–90.

Harris, B. (2003). *Fatigue in Composites*, Woodhead Publishing Ltd, Cambridge, UK.

Harris, K. (2005). "Fatigue behaviour of bonded FRP used for flexural retrofit", *Proceedings of International Symposium on Bond Behaviour of FRP in Structures (BBFS 2005)*, International Institute for FRP in Construction, Hong Kong, China, pp. 547–552.

Hashin, Z. and Rotem, A. (1973). "A fatigue failure criterion for fiber reinforced materials", *Journal of Composite Materials*, Vol. 7, No. 4, pp. 448–464.

Huang, P., Zhou, H., Wang, H. and Guo, X. (2011). "Fatigue lives of RC beams strengthened with CFRP at different temperatures under cyclic bending loads", *Fatigue & Fracture of Engineering Materials & Structures*, Vol. 34, No. 9, pp. 708–716.

Hwang, S.F. and Su, Y.D. (2006). "Effects of stress frequency and stress ratio on the fatigue of glass/epoxy composite materials", *Key Engineering Materials*, Vol. 326–328, pp. 1031–1034.

ISIS Canada (2008). *FRP Rehabilitation of Reinforced Concrete Structures*, ISIS Canada Research Network, Canada.

JSCE (2001). *Recommendations for Upgrading of Concrete Structures with Use of Continuous Fiber Sheets*, Japanese Society of Civil Engineering, Tokyo, Japan.

Jen, M., Tseng, Y., Kung, H. and Huang, J. (2008). "Fatigue response of APC-2 composite laminates at elevated temperatures", *Composites: Part B*, Vol. 39, No. 7, pp. 1142–1146.

Jones, R. (1999). *Mechanics of Composite Materials*, 2nd Edition, Taylor & Francis, PA, USA.

Kang, B.G. and Brameshuber, W. (2006). "Bond behaviour of textile reinforcement made of AR-glass under cyclic loading", *Proceedings of the 1st International RILEM Symposium, RILEM Proceedings PRO 50*, RILEM Publications S.A.R.L., Bagneux, France, pp. 111–119.

Katakalos, K. and Papakonstantinou, C. (2009). "Fatigue of reinforced concrete beams strengthened with steel-reinforced inorganic polymers", *Journal of Composites for Constructions*, ASCE, Vol. 13, No. 2, pp. 103–112.

Kawai, M. and Suda, H. (2004). "Effects of non-negative mean stress on the off-axis fatigue behavior of unidirectional carbon/epoxy composites at room temperature", *Journal of Composite Materials*, Vol. 38, No. 10, pp. 833–854.

Kawai, M. and Taniguchi, T. (2006). "Off-axis fatigue behaviour of plain weave carbon/epoxy fabric laminates at room and high temperatures and its mechanical modeling", *Composites: Part A*, Vol. 37, No. 2, pp. 243–256.

Khan, A., Al-Gadhib, A. and Baluch, M. (2011). "Experimental and computational modeling of low cycle fatigue damage of CFRP strengthened reinforced concrete beams", *International Journal of Damage Mechanics*, Vol. 20, No. 2, pp. 211–243.

Kim, Y. and Heffernan, P. (2008). "Fatigue behavior of externally strengthened concrete beams with fiber reinforced polymers: state of the art", *Journal of Composites for Construction,* ASCE, Vol. 12, No. 3, pp. 246–256.

Ko, H. and Sato, Y. (2007). "Bond stress–slip relationship between FRP sheet and concrete under cyclic load", *Journal of Composites for Construction*, ASCE, Vol. 11, No. 4, pp. 419–426.

Leung, C., Cheung, Y. and Zhang, J. (2007). "Fatigue enhancement of concrete beam with ECC layer", *Journal of Cement and Concrete Research,* Vol. 37, No. 5, pp. 743–750.

Li, V.C. (2003). "On engineered cementitious composites (ECC)—a review of the material and its applications", *Journal of Advanced Concrete Technology*, Vol. 1, No. 3, pp. 215–230

Li, V.C. (2008). "Chapter 24: Engineered cementitious composites (ECC)–material, structural, and durability performance", *Concrete Construction Engineering Handbook*, CRC Press, USA.

Masoud, S., Soudki, K. and Topper, T. (2001). "CFRP-strengthened and corroded RC beams under monotonic and fatigue loads", *Journal of Composites for Construction*, ASCE, Vol. 5, No. 4, pp. 228–236.

Mazzotti, C. and Savoia, M. (2009). "FRP-concrete bond behaviour under cyclic debonding force", *Advances in Structural Engineering*, Vol. 12, No. 6, pp. 771–780.

M-Brace (2002). *MBrace Composite Strengthening System-Engineering Design Guidelines*, 3rd Edition, Watson Bowman Acme Corp., New York, USA.

Minnaugh, P. and Harries, K. (2009). "Fatigue behavior of externally bonded steel fiber reinforced polymer (SFRP) for retrofit of reinforced concrete", *Materials and Structures*, Vol. 42, No. 2, pp. 271–278.

Mivehchi, H. and Varvani-Farahani, A. (2010). "The effect of temperature on fatigue strength and cumulative fatigue damage of FRP composites", *Procedia Engineering*, Vol. 2, No. 1, pp. 2011–2020.

Nagasawa, M., Kinuhata, H., Koizuka, H., Miyamoto, K., Tanaka, T., Kishimoto, H. and Koike, T. (1995). "Mechanical fatigue of epoxy resin", *Journal of Materials Science*, Vol. 30, No. 5, pp. 1266–1272.

NRC (2004). *Guide for the Design and Construction of Externally Bonded FRP Systems for Strengthening Existing Structures*, National Research Council, Rome, Italy.

Newaz, G. (1985). "Influence of matrix material on flexural fatigue behavior of unidirectional composites", *Composites Science and Technology,* Vol. 24, No. 3, pp. 199–214.

Nigro, E., Di Ludovico, M. and Bilotta, A. (2011). "Experimental investigation on FRP – concrete debonding under cyclic actions", *Journal of Materials in Civil Engineering*, ASCE, Vol. 23, No. 4, pp. 360–371.

O'Neill, A., Harries, K.A. and Minnaugh, P. (2007). "Fatigue behavior of adhesive systems used for externally-bonded FRP applications", *Proceedings of the Third International Conference on Durability and Field Applications of Fiber Reinforced Polymer (FRP) Composites for Construction (CDCC 2007),* Quebec City, Canada, pp. 41–48.

Odagiri, T., Matsumoto, K. and Nakai, H. (1997). "Fatigue and relaxation characteristics of continuous aramid fiber reinforced plastic rods", *Third International Symposium on Non-Metallic (FRP) Reinforcement for Concrete Structures (FRPRCS-3)*, Tokyo, Japan, pp. 227–234.

Ohama, Y. (1995). *Handbook of Polymer-Modified Concrete and Mortars, Properties and Process Technology*, Noyes Publications, Park Ridge, New Jersey, USA.

Ohama, Y. (1998). "Polymer-based admixtures", *Cement and Concrete Composites*, Vol. 20, No. 2–3, pp. 189–212.

Papakonstantinou, C. and Balaguru, P. (2007). "Fatigue behavior of high temperature inorganic matrix composites", *Journal of Materials in Civil Engineering*, ASCE, Vol. 19, No. 4, pp. 321–328.

Papakonstantinou, C.G., Petrou, M.F. and Harries, K.A. (2001). "Fatigue of reinforced concrete beams strengthened with GFRP sheets", *Journal of Composites for Construction,* ASCE, Vol. 5, No. 4, pp. 246–253.

Papanicolau, C., Triantafillou, T., Bournas, D. and Lontou, P. (2006). "TRM as strengthening and seismic retrofitting material of concrete structures", *Textile Reinforced Concrete. Proceedings of the 1st International RILEM Symposium, RILEM Proceedings PRO 50,* RILEM Publications S.A.R.L., Bagneux, France, pp. 331–340.

Quattlebaum, J., Harries, K.A. and Petrou, M.F. (2005). "Comparison of three CFRP flexural retrofit systems under monotonic and fatigue loads", *Journal of Bridge Engineering,* ASCE, Vol. 10, No. 6, pp. 731–740.

Ramakrishnan, V. and Jayaraman, N. (1993). "Mechanistically based fatigue-damage evolution model for brittle matrix fibre-reinforced composites", *Journal of Material Science,* Vol. 28, No. 20, pp. 5592–5602.

Reis, P., Ferreira, J., Costa, J. and Richardson, M. (2009). "Fatigue life evaluation for carbon/epoxy laminate composites under constant and variable block loading", *Composites Science and Technology,* Vol. 69, No. 2, pp. 154–160.

Salvia, M., Fiore, L. and Fournier, P. (1997). "Flexural fatigue behaviour of UDGFRP experimental approach", *International Journal of Fatigue*, Vol. 19, No. 3, pp. 253–262.

Senthilnath, P., Belarbi, A. and Myers, J. (2001). "Performance of CFRP strengthened reinforced concrete (RC) beams in the presence of delaminations and lap splices under fatigue loading", *Proceeding of the International Conference in Construction,* Porto, Portugal, pp. 323–328.

Shahawy, M. and Beitelman, T.E. (1999). "Static and fatigue performance of RC beams strengthened with CFRP laminates", *Journal of Structural Engineering*, ASCE, Vol. 125, No. 6, pp. 613–621.

Suthiwarapirak, P., Matsumoto, T. and Kanda, T. (2004). "Multiple cracking and fiber bridging characteristics of engineered cementitious composites under fatigue flexure", *Journal of Materials in Civil Engineering*, ASCE, Vol. 16, No. 5, pp. 433–443.

Suthiwarapirak, P., Matsumoto, T. and Kanda, T. (2002). "Flexural fatigue failure characteristics of an engineered cementitious composite and polymer cement mortar", *Journal of Materials, Concrete Structures and Pavements,* Vol. 718, No. 57, pp. 121–134.

Takemura, K. and Fujii, T. (1994). "Fatigue damage and fracture of carbon fabric/epoxy composites under tension–tension loading", *JSME International Journal, Series A*, Vol. 37, No. 4, pp. 472–480.

Täljsten, B. (2006). "The Important of bonding - a historic overview and future possibilities", *Advances in Structural Engineering,* Vol. 9, No. 6, pp. 721–736.

Tao, G. and Xia, Z. (2007). "An experimental study of uniaxial fatigue behavior of an epoxy resin by a new non-contact real-time strain measurement and control system", *Polymer Engineering and Science*, Vol. 47, No. 6, pp. 780–788.

Tao, G. and Xia, Z. (2008). "Fatigue behavior of an epoxy polymer subjected to cyclic shear loading", *Materials Science and Engineering: A* , Vol. 486, No. 1–2, pp. 38–44.

Toutanji, H., Zhao, L., Deng, Y., Zhang, Y. and Balaguru, P. (2006). "Cyclic behavior of RC beams strengthened with carbon fiber sheets bonded by inorganic matrix", *Journal of Materials in Civil Engineering*, ASCE, Vol. 18, No. 1, pp. 28–35.

Van Paepegem, W. and Degrieck, J. (2001). "Fatigue degradation modelling of plain woven glass/epoxy composites", *Composites: Part A*, Vol. 32, No. 10, pp. 1433–1441.

Wang ,Y., Lee, M. and Chen, B. (2007). "Experimental study of FRP-strengthened RC bridge girders subjected to fatigue loading", *Composite Structures*, Vol. 81, No. 4, pp. 491–498.

Wu, Z., Wang, X., Iwashita, K., Sasaki, T. and Hamaguchi, Y. (2010). "Tensile fatigue behavior of FRP and hybrid FRP sheets", *Composites: Part B*, Vol. 41, No. 5, pp. 396–402.

Xu, S. and Liu, W. (2011). "Experimental study on flexural fatigue property of ultra-high toughness cementitious composites", *Advanced Materials Research*, Vol. 150–151, pp. 1369–1378.

Yang, X. and Nanni, A. (2002). "Lap splice length and fatigue performance of fiber-reinforced polymer laminates", *ACI Materials Journal*, Vol. 99, No. 4, pp. 386–392.

Yao, G., Huang, P. and Zhao, C. (2006). "Flexural fracture and fatigue behavior of RC beams strengthened with CFRP laminates under constant amplitude loading", *Key Engineering Materials*, Vol. 306–308, pp. 1343–1348.

Yost, J.R., Gross, S.P. and Deitch, M.J. (2007). "Fatigue behavior of concrete beams strengthened in flexure with near surface mounted CFRP", *Proceedings of the 8th International Symposium on Fiber-Reinforced Polymer Reinforcement for Concrete Structures (FRPRCS-8)*, Patras, Greece.

Yu, T., Li, C., Lei, J. and Zhang, H. (2011). "Fatigue of concrete beams strengthened with glass-fiber composite under flexure", *Journal of Composites for Construction*, ASCE, Vol. 15, No. 4, pp. 557–564.

Yun, Y., Wu, Y. and Tang, W. (2008). "Performance of FRP bonding systems under fatigue loading", *Engineering Structures*, Vol. 30, No. 11, pp. 3129– 3140.

Zhang, J. and Li, V.C. (2002). "Monotonic and fatigue performance in bending of fiber reinforced engineered cementitious composite in overlay system", *Cement and Concrete Research*, Vol. 32, No. 3, pp. 415–423.

Zhu, D., Peled, A. and Mobasher, B. (2011). "Dynamic tensile testing of fabric-cement composites", *Construction and Building Materials*, Vol. 25, No. 1, pp. 385–395.

PAPER II

"Experimental performance of RC beams strengthened with FRP
materials under monotonic and fatigue loads"

BY
Mohammed Mahal, Björn Täljsten and Thomas Blanksvärd

Experimental performance of RC beams strengthened with FRP materials under monotonic and fatigue loads

M. Mahal[1], B. Täljsten[2], T. Blanksvärd[3]

[1]Ph.D. Student, Division of Structural Engineering, Luleå Univ. of Technology, SE-971 87 Luleå, Sweden (corresponding author). E-mail: mohammed.salih@ltu.se

[2]Professor, Division of Structural Engineering, Luleå Univ. of Technology, SE-971 87 Luleå, Sweden .E-mail: Bjorn.Taljsten@ltu.se

[3]Assistant Professor, Division of Structural Engineering, Luleå Univ. of Technology, SE-971 87 Luleå, Sweden. E-mail: thomas.blanksvard@ltu.se

Abstract

Carbon fiber-reinforced polymers (CFRPs) are increasingly being used to repair and strengthen reinforced concrete (RC) structural members. CFRP strengthening may be applied by bonding polymeric plates to the exterior of the member's tension surface or by placing CFRP bars inside the concrete member cover to provide near-surface mounted reinforcement. It is not clear which of these approaches is most effective at resisting fatigue loads. To compare their efficacy, four-point bending tests with reinforced concrete beams were conducted under monotonic and fatigue loading using both strengthened and unstrengthened RC beams having steel reinforcements with identical stress levels. The influence of the strengthening material's properties and prior cracking of the member are investigated and discussed by analyzing failure mechanisms, load-deflection curves, and strain measurements for steel bars and CFRP materials observed during loading experiments. The results obtained indicate that the efficiency of strengthening is primarily determined by the relief of local stress in the member's reinforcing steel bars before they rupture, and the fatigue life of the reinforcing steel after its initial fracturing. The latter of these quantities is related to the strengthened member's ability to absorb the energy released at the moment the reinforcing bar fractures.
Author keywords: Fiber-reinforced polymer; Reinforced concrete; Beam; Fatigue test.

Introduction

The use of carbon fiber reinforced polymer (CFRP) materials to strengthen reinforced concrete (RC) members in highway bridges is becoming increasingly common around the world because CFRP exhibits excellent corrosion resistance and tolerance of environmental agents while also offering a high stiffness to weight ratio together with easy transportation and handling, limited thermal expansion, and good fatigue performance. The most common techniques for strengthening concrete members in bridges involve the insertion of strengthening CFRP rods into grooves carved into the concrete of the soffit girder or the application of bonded sheets or plates to the member's soffit surface. The former approach is referred to as near-surface mounted (NSM) reinforcement. These techniques are discussed in detail by Täljsten (2002).

Several recent studies have investigated the effect of FRP plates on the fatigue strength of reinforced concrete beams (Aidoo et al. 2004; Aidoo et al. 2006; Barnes and Mays 1999; Brena et al. 2005; Gussenhoven and Brena 2005; Harries et al. 2007; Heffernan and Erki 2004; Masoud et al. 2001; Meier et al. 1992; Papakonstantinou et al. 2001; Toutanji et al. 2006) and some have examined the effect of strengthening with NSM bars (Aidoo et al. 2006; Badawi and Soudki 2009; Oudah and El-Hacha 2012; Quattlebaum et al. 2005; Rosenboom and Rizkalla 2006; Wahab et al. 2012; Yost et al. 2007) . In addition, the authors of this paper have presented an extensive investigation into the behavior of CFRP-strengthened RC beams in which the behavior of the strengthening material and the strengthened reinforced concrete members was examined under fatigue loading (Mahal et al. 2013).

Despite these works, there have only been a few comparative studies examining beams strengthened with NSM bars and plates under fatigue loading. Aidoo et al. (2006)studied the performance of full-scale interstate bridge girders strengthened with CFRP materials under fatigue loading. Three strengthening methods were investigated: the bonding of CFRP strips to the soffit surface, strengthening with NSM CFRP strips, and strengthening with hybrid strips using powder actuated fasteners. Under monotonic loads, all three methods increased the girders' load-carrying capacity. However, it was not clear whether plate or NSM strengthening offered the best performance under fatigue loading because a certain degree of relative slippage or debonding occurred with the CFRP strips.

A similar study was conducted by Quattlebaum et al. (2005) using small-scale specimens strengthened with CFRP in three different ways. Their results contradicted the findings of Meier et al. (1992) and suggested that

CFRP strips were unable to bridge cracks resulting from failure of the primary reinforcing steel. Consequently, they found that NSM CFRP strips performed better than either CFRP strips or powder actuated fasteners.

Sena-Cruz et al. (2012) conducted a similar comparison to those reported by Quattlebaum et al. (2005) and Aidoo et al. (2006), testing reinforced concrete beams strengthened in the same three ways under monotonic and fatigue loads. The greatest decrease in stiffness due to fatigue loading occurred in beams strengthened with NSM strips.

In keeping with earlier studies, it was not clear whether NSM bars or surface-mounted plates offered better overall strengthening performance, and many aspects of CFRP strengthening remain unclear. To shed further light on these issues, this manuscript describes a study on the response of the CFRP plate and NSM bar strengthening methods under monotonic and fatigue loading in reinforced concrete beams constructed with steel reinforcements having identical steel stress levels. The influence of the properties of the strengthening CFRP material is also investigated, along with that of pre-existing cracks in the beams. The results obtained provide new insights into the behavior of FRP-strengthened RC beams under fatigue loading conditions, and illustrate some important advantages and disadvantages of the plate and NSM bar approaches.

Specimen Details

The beams used in this study were 4,000 mm long with rectangular cross sections of 200x300 mm as shown in Fig. 1. The size of the beams were selected to complete the series of tests of the previous full-scale tests with the same size (Carolin et al. 2005; Nordin and Täljsten 2006).Their longitudinal steel reinforcements in tension and compression were two rods with nominal diameters of Ø16 mm. The shear reinforcement, which was designed to ensure flexural failure in the strengthened beams, consisted of Ø 10 mm stirrups at a spacing of 75 mm. Three beam types were tested – beams strengthened with NSM bars, beams strengthened with traditional laminate plate bonding, and beams without FRP strengthening. The plate- and NSM-bar strengthened beams were further subdivided into two classes depending on the Young's modulus of the CFRP used, which was either 150 GPa or 200 GPa. The length of the strengthening laminates and rods (3,200 mm) was chosen to match the beams' critical anchorage length (Täljsten 1997).

Plate strengthening was performed with two strips of 1.4 mm thick CFRP material, one with a width of 100 mm and another with a width of 43 mm. For beams strengthened with 200 GPa CFRP, the strengthening materials used were StoFRP Plate IM 100C and StoFRP Plate IM 60C, respectively. For beams strengthened with 150 GPa CFRP, the materials used were StoFRP Plate 100E and StoFRP Plate 50E, respectively. In both cases, the 43 mm wide strengthening strips were prepared by cutting narrow strips supplied by the CFRP manufacturer. The laminate strips were bonded to the surface of the beam soffit using StoPox SK41 epoxy after surface grinding to expose the gravel and primer application; the thickness of the adhesive epoxy layer after plate bonding was 2 mm. After the strengthening plates had been applied, two layers of CFRP sheeting were wrapped around one end of the plate-strengthened beam to form a 300 mm wide U-jacket (with the fiber direction being perpendicular to the longitudinal axis of the beam) in order to ensure that any debonding of the strengthening plates would occur at the other end of the beam's span. The jacket was formed using the wet lay-up technique and bonded to the beam using StoPox LH epoxy.

NSM strengthening for beams strengthened using 200 GPa CFRP was performed using two 10x10mm quadratic rods (StoFRP BAR IM 10C), each having a modulus of elasticity of 200 GPa. The rods were fitted to the beam by cutting two parallel grooves along the beam's length using a concrete saw with two parallel saw blades. After chipping away the cut concrete, two grooves with widths of 15 mm and depths of 17 mm were obtained, with smooth sides and rough lower surfaces. The surfaces of the grooves were coated with primer and epoxy (StoPox SK41) before placing the NSM bars into the groove. The thickness of the adhesive layer surrounding the bonded NSM bars was 2.5 mm on the three bonded sides. NSM-strengthened beams using 150 GPa CFRP were prepared in the same way but with StoFRP BAR E 10C rods.

The prepared beams were assigned labels of the form W-X-Y-Z, where the initial W term is a meaningless identifier, the X term provides information on the beam's strengthening, the Y term provides information on the type of load to which the beam was subjected, and the Z term provides information on whether the beam was pre-cracked prior to testing. The W term is always the letter "B" followed by a one- or two-digit number. The X term is "0" for control beams without CFRP strengthening, "N" for NSM-strengthened beams, or "P" for plate-strengthened beams; in the case of strengthened beams, the letter is followed by "E1" or "E2" to indicate whether strengthening was done using CFRP with a Young's modulus of 200GPa or 150GPa, respectively. The Y term is "F" for beams subjected to fatigue loading or "S" for beams subjected to a static load. Finally, the Z term is only used for pre-cracked beams, in which case it takes a value of "C". The label B10-NE1-F-C thus refers to a pre-cracked beam strengthened with NSM bars having a 200GPa modulus of elasticity and subjected to fatigue loading, while the beam labeled B13-0-S was unstrengthened and subjected to static loading.

FRP Gauge	1	2	3	4	5	6	7	8	9	10	11
Location, X(mm)	405	420	450	500	600	800	1000	1470	1500	1530	2000
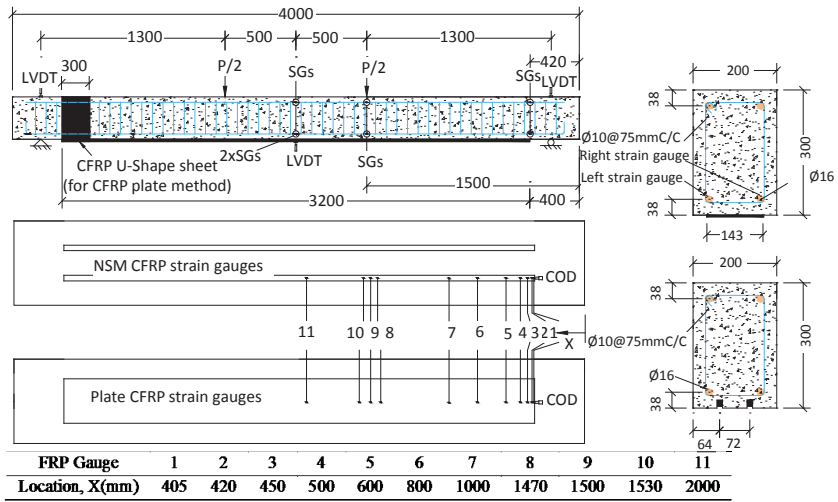
Fig. 1. Beam setup

Material properties

The compressive and tensile strengths of the concrete used can be seen in Table 1. These strengths were measured three times for each beam type by testing companion cubes while the fatigue tests were being conducted. The concrete quality was tested using 150 mm cubes. The mechanical properties of the beams' reinforcing steel bars were determined using experimental tensile tests; the mean yielding strength and modulus of elasticity of the longitudinal steel reinforcement were 578 MPa and 208 GPa, respectively, with a yield strain of 0.003626, which was used as reference for strains generated during fatigue test. The mean yielding strength and modulus of elasticity for the stirrups were 533 MPa and 202 GPa, respectively. The key properties of all materials used in the construction of the test beams are listed in Table 2; the properties of the composites and the adhesive were supplied by the manufacturer and not verified.

Table 1. Beams prepared and tested in this work.

Specimen	Type of load	Concrete compressive strength (MPa)	Concrete Tensile strength (MPa)	Young's modulus of CFRP (GPa)
B13-0-F	Fatigue	71	4.2	-
B10-NE1-F-C	Fatigue	73	4.3	200
B9 -EE1-F-C	Fatigue	72	3.9	200
B8-NE2-F	Fatigue	75	4.5	150
B7-NE2-S	Static			
B3-NE1-F	Fatigue	71	4.7	200
B4-NE1-S	Static			
B1-EE1-F	Fatigue	71	4.2	200
B2-EE1-S	Static			
B5-EE2-S	Static	72	3.9	150
B6-EE2-F	Fatigue			
B11-0-S	Static	64	4.0	-

Table 2. Properties of the carbon fiber reinforced polymer and adhesive used in this work.

Material	compressive strength (MPa)	Tensile strength (MPa)	Young's modulus (GPa)	Ultimate strain (‰)
Composite[a]				
StoFRP E	-	1800	150	12
StoFRP IM	-	2900	200	14
Adhesive[a]				
StoPox LH	100	90	3.500	-
StoPox SK 41	82	19	7.872	-

[a] Supplier's data

Instrumentation

The beams were fitted with strain gauges on their internal steel bars (KFG-5-120-C1-11 L3M3R) and on the FRP composites (KFRP-5-120-C1-11 L3M3R). In addition to the strain gauges (SG), the midpoint deflection and support settlement were recorded using linear voltage differential transducers (LVDTs) and crack opening displacement (COD) gauges were placed at one end of the NSM bar or CFRP plate of each beam to measure the slippage of the FRP element relative to the base of the concrete member. For the NSM bar-strengthened beams, only one of the two strengthening bars was instrumented in this way. The setup of the instruments is shown in Fig. 1.The ARAMIS optical strain measuring system (GOM-Gesellschaft für Optische Messtechnik GmbH) was used in the tests of beams B1-EE1-F and B3-NE1-F to monitoring crack evolution during fatigue loading, necessitating the painting of a stochastic or systematic pattern on the specimen's surface. A suitable pattern was created using the stencil-spray technique as shown in Fig. 2. The measuring system consists of two high-resolution cameras connected to a computer running the ARAMIS image recognition software, which was used to match images of the painted recorded by the two cameras over the course of a loading experiment. Reference images are acquired at the start of the load cycle, and subsequently recorded image is compared to these references to detect displacements and deformations of the painted pattern in 3D space. By characterizing the deformation of the beam in this way, it is possible to calculate the strain using established theories of solid mechanics.

Fig. 2. Point pattern used for photometric strain measurement

Test setup and Procedure

The 12 reinforced concrete beams were tested in a four-point bending configuration with a simply supported span of 3600 mm as shown in Fig. 1. One beam of each type (i.e. unstrengthened control, 150 GPa plate-strengthened, 150 GPa NSM bar-strengthened, 200 GPa plate-strengthened, and 200 GPa NSM bar-strengthened) was tested under monotonically increasing loads until failure in order to acquire reference data.

The remaining seven specimens were tested in fatigue. The objective of these tests was to explore the effects of the different strengthening methods (NSM bar-strengthening and plate-strengthening), the Young's modulus of the strengthening material, and the effect of pre-existing cracks on beam behavior under fatigue loading. The seven beams tested in this way were an unstrengthened beam, a E2 plate-strengthened beam, a E2 NSM bar-strengthened beam, a E1 plate-strengthened beam, a E1 NSM bar-strengthened beam, a pre-cracked E1 plate-strengthened beam, and a pre-cracked E1 NSM bar-strengthened beam.

The minimum load applied to both strengthened and unstrengthened beams was 6 kN. This value was chosen to avoid impact loads during cycling, which cause the beams to shift on their supports. The stress range of the reinforcing steel was 258 MPa in both the strengthened and unstrengthened beams. This value was selected to achieve a design fatigue life of 600,000 cycles based on the Tilly and Moss model (Barnes and Mays 1999). Based on the stress range of the reinforcing steel and the minimum applied load, the calculated maximum applied load was 38.7 kN for unstrengthened control beam and 64 kN for strengthened beams. In the fatigue tests, all the specimens were loaded at a rate of 1.7 Hz. This frequency is comparable to that of vehicle loads on bridge decks (Masoud et al. 2005). The fatigue tests were performed under load control while monotonic loading was performed under displacement control. During the first load cycle in each test, the load was applied

monotonically in order to monitor cyclic load damage and the pattern of cracking on the entire surface of beams. In subsequent load cycles, a sine wave load was applied. The tests were terminated after a predetermined number of fatigue life cycles (600,000).

For photometric strain measurement, the servo/hydraulic load frame was controlled by the ARAMIS software package so that the recorded images could be linked to the corresponding maximum and minimum load levels. Consequently, the strains determined from these measurements correspond to the range of strains induced under the maximum and minimum loads applied during the studied cycles.

Monotonic beam behavior

Fig. 3 shows the midspan deflection of the beams during the monotonic loading tests as a function of the applied load. The initial stiffness of the strengthened specimens (which is indicated by the slope of their load-deflection curves) was quite similar to that of the unstrengthened control beam before cracking because the strengthening element has relatively little influence on the second moment of inertia in the uncracked section. This was demonstrated by the similarity of the slopes of the different beams' load-deflection curves at low loads. The post-cracking stiffness of the strengthened beams was greater than that of the unstrengthened beams. This was attributed to the restraint of crack opening and growth due to the external strengthening elements, which increased the strengthened beams' stiffness. The increase in stiffness and ultimate strength are largely dependent on the properties of the FRP material and the method of beam strengthening. The results for the B4-NE1-S and B7-NE2-S beams indicate that increasing the Young's modulus of the NSM strengthening bars increased the capacity of the strengthened beam. The same was observed for the plate-strengthened beams B2-EE1-S and B5-EE2-S, whose capacities were 177kN and 173 kN, respectively.

Beams strengthened with CFRP elements having the same Young's modulus had almost identical stiffness values at sub-maximal loads, regardless of their method of strengthening. The strengthened beams were less ductile than the unstrengthened control and exhibited different cracking patterns, with fewer and narrower cracks that were more evenly distributed along the beam. The crack spacing in the plate-strengthened beams was greater than that in their NSM bar-strengthened counterparts. This may be because the contact surface between the strengthening element and the beam's soffit is larger in the plate-strengthened beams. Conversely, the NSM bar-strengthened beams had greater capacities than their plate-strengthened counterparts because better bond between the bars and the concrete. Failure of all strengthened beams was initiated by intermediate crack interfacial debonding at the mid span which then progressed towards the supports until the remaining anchorage length was insufficient to resist the force acting on the CFRP, at which point a sudden debonding failure occurred.
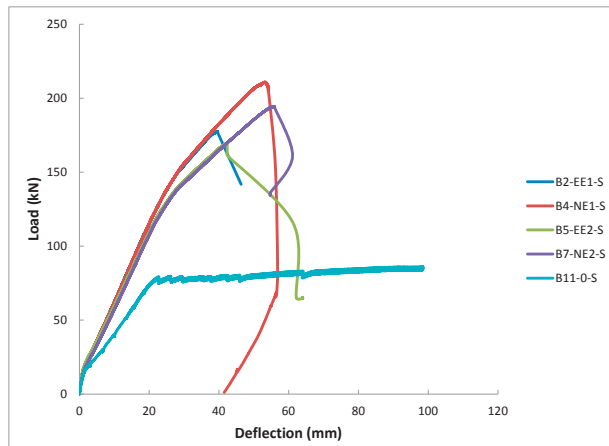
Fig. 3. Applied load versus midspan deflection for the five beam types under monotonic loading

Failure modes during fatigue tests

Table 3 summarizes the results of the beams tests. Specifically, it lists the failure mode observed for each beam, the number of load cycles prior to failure, the number of cycles prior to the rupturing of the reinforcing steel bars, and the load required to induce failure under monotonic loading for those specimens that did not fail under cyclic loading.

The cracking pattern for the beams tested in fatigue depended on whether the beam was a control beam, strengthened beam, or cracked and strengthened beam. Beams strengthened with CFRP plates and NSM bars exhibited similar failure modes under fatigue loading.

Generally, the rate of crack growth and the development of new cracks were both rapid during the first loading cycle but did not change appreciably in subsequent cycles until the tensile reinforcing steel bars ruptured. Studies on the evolution of the beams' crack patterns during fatigue loading indicated that cracks occurred over almost the entire span of the unstrengthened beams but were more strongly localized to the central regions of the strengthened beams. The cracks in the unstrengthened beams were also more widely spaced than those in the strengthened beams. In pre-cracked strengthened beams, the presence of CFRP plates or bars reduced the width of existing vertical cracks. In addition, new flexural cracks formed between the existing cracks but these new cracks did not extend far beyond the height of the bottom reinforcement layers.

It was generally easy to detect the occurrence of ruptures in the beams' reinforcing steel rods because the fractured bars were usually visible to the naked eye. Moreover, the fatigue fracture of the reinforcing steel was associated with a sudden increase in the recorded strain of the beam (Fig. 9), although the CFRP elements continued to support the applied load in strengthened beams. There was no physical sign of debonding of any of the strengthened beams for all cases where steel reinforcement rupture occurred.

For all of the CFRP-strengthened beams in which steel rupture was observed, the stress in the second reinforcing bar increased sharply after the first was ruptured, causing the second to rupture shortly after the first.

The failure of beams by debonding was initiated when pieces of concrete in the vicinity of the ruptures in the reinforcing steel bars started to separate from the beam. Debonding then propagated towards the near end of the beam. However, in contrast to previous reports, delamination failures did not occur immediately after the rupture of the reinforcing steel bars as in for example (Aidoo et al. 2004; Barnes and Mays 1999; Heffernan and Erki 2004; Papakonstantinou et al. 2001).

Of the 7 beams subjected to fatigue loading in this work, 4 failed by debonding of the CFRP reinforcement after fatigue fracture of one or more of the tensile steel reinforcing bars, which is the typical mode of fatigue failure for under-reinforced concrete beams. Interestingly, the reinforcing steel bars of the unstrengthened control beam B13-0-F did not rupture during the fatigue loading tests. Images of typical failures in plate- and NSM bar-strengthened RC beams are shown in Fig. 4.

Table 3. Monotonic and Fatigue loading testing results

Beam	Load range (kN)	1st cycle dissipation energy (area 1st cycle/max. load)	Total No. cycles	Total deflection during last cycle	No. cycles at steel rupture	Percentage of fatigue life remaining after first rupture	Fatigue Failure mode	Ultimate static load (kN)	Static Failure mode
B3-NE1-F	6-64	2.5	437,222	22.9	408,094	6.6	ID*	-	-
B8-NE2-F	6-64	2.3	599,107	54.9	348,245 373,460 463,394 491,492	41.8	ID	-	-
B1-EE1-F	6-64	2.2	520,733	15.9	456,213	12.4	ID	-	-
B6-EE2-F	6-64	2.6	438,593	14.7	416,866	4.9	ID	-	-
B9-EE1-F-C	6-64	1.7	600000	11.7	-	-	-	177	ID*
B10-NE1-F-C	6-64	1.6	600000	23	470305 503841	21.6	-	115	ID
B13-0-F	6-38.7	3.1	600000	12.45	-	-	-	82.7	SY*+CC*
B7-NE2-S	Static	-	-	-	-	-	-	194.4	SY+ID
B4-NE1-S	Static	-	-	-	-	-	-	210.9	SY+ID
B2-EE1-S	Static	-	-	-	-	-	-	177.4	SY+ID
B5-EE2-S	Static	-	-	-	-	-	-	169.5	SY+ID
B11-0-S	Static	-	-	-	-	-	-	86.1	SY+CC

*ID=intermediate debonding, CC=concrete crushing, SY=steel yielding

(a)NSM strengthened beam (B8-NE2-F)

(b) Plate strengthened beam (B1-EE1-F)

Fig. 4. Fatigue fractures of the beams' reinforcing steel bars

Deflection

All of the beams tested in fatigue that failed before reaching the limit of 600,000 cycles, exhibited the same deflection behavior. The deflections for all of the tested beams under the maximum and minimum loads are shown as functions of the number of load cycles in Fig. 5. Notable deflection is accumulated rapidly within the early cycles. This was attributed to initial micro damage in the steel, bond and concrete, all of which sustain damage rapidly during the first few load cycles. The deflection then increased very slowly until the reinforcing steel bars ruptured, at which point it increased sharply and suddenly. The deflections then increased steadily, indicating that the CFRP element compensates for the steel rupture and helps to maintain a relatively steady deformation profile. This behavior was observed more than once in some cases, reflecting the ruptures of the reinforcing bars. Finally, the deflection increased rapidly around the point when the beam failed.

The maximum deflection curves for beams B3-NE1-F and B8-NE2-F showed that after 325,000 cycles, their deflections had increased by 25% and 23% relative to the first cycle, respectively. The corresponding values for beams B1-EE1-F and B6-EE2-F were 16% and 13%, respectively. In addition, after 325,000 cycles, the mid-span deflection for the beam strengthened with a CFRP plate having a high modulus of elasticity (200 GPa) was approximately 15% lower than that for the corresponding NSM bar-strengthened beam. In contrast, the mid-span deflection for the beam strengthened with a CFRP plate having a low modulus of elasticity (150 GPa) was only 7% lower than that for the corresponding NSM bar-strengthened beam. These results indicate that the Young's modulus of the CFRP element and the strengthening method used both affected the deflection of the RC beam during fatigue loading. The effect of prior cracking in strengthened RC beams under cyclic load can be demonstrated by comparing the results for beams B9-EE1-F-C and B10-NE1-F-C. After 325,000 cycles, the deflection of the pre-cracked plate-strengthened beam B9-EE1-F-C was 22% greater than that observed in the first cycle; the corresponding increase for its initially uncracked counterpart beam B1-EE1-F was only 16%. Conversely, the deflection of the pre-cracked NSM bar-strengthened beam B10-NE1-F-C increased by only 16% between the first and 325,000th cycle; the corresponding value for its uncracked counterpart beam B3-NE1-F was 25%. The NSM bar approach was thus more effective than the bonded plate approach for strengthening pre-cracked RC beams.

The maximum deflection of the control beam B13-0-F increased by 26% between the first and 325,000th cycles. This value is very similar to that seen for beams strengthened with NSM bars, which indicates that the NSM bars

do not improve the deformation behavior of strengthened beams relative to that of unstrengthened beams whose reinforcing steel has the same stress value.
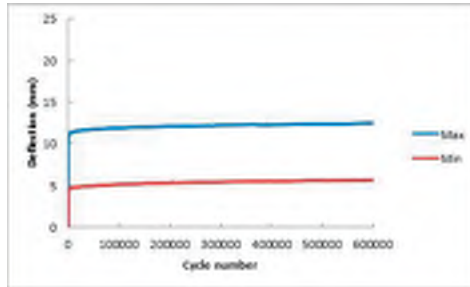
(a) B13-0-F
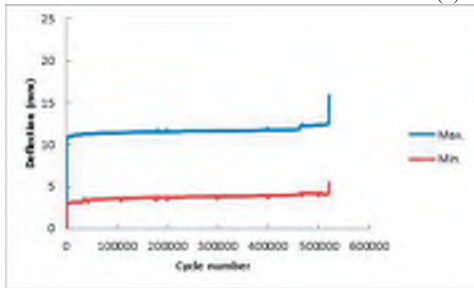
(b) B1-EE1-F
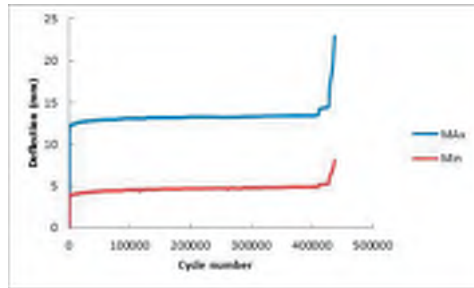
(c) B3-NE1-F
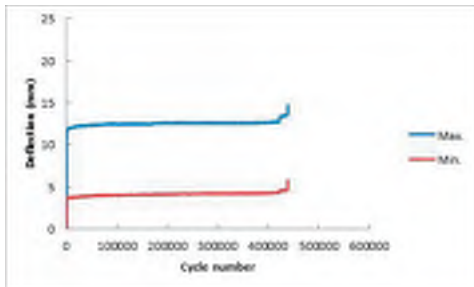
(d) B6-EE2-F
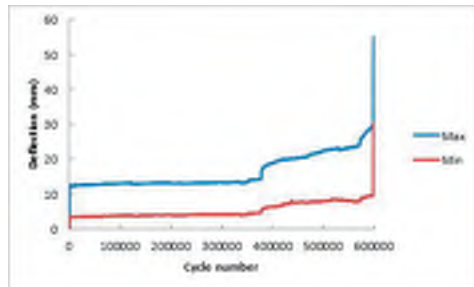
(e) B8-NE2-F
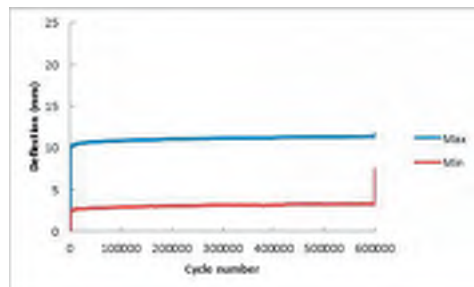
(f) B9-EE1-F-C
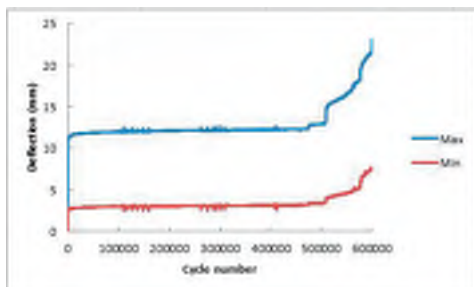
(g) B10-NE1-F-C

Fig. 5. Midspan deflection versus number of load cycles

Fig. 6 shows the load–deflection response for typical beam during the fatigue test. For all cycles between the second and those in which the reinforcing steel ruptures, all of the beams have very similar hysteresis curves. The area enclosed by the hysteresis curves and the axes of the graph is reflective of the energy released during the load cycle. Because the area enclosed by the first hysteresis loop is much greater than that for subsequent

loops until the cycle in which the reinforcing steel ruptures, it is clear that much more energy is dissipated during the first cycle than in any other. Due to the effect of crack initiation, the ascending branch of the first cycle loop contains two different slopes, the first of which is much steeper than the second. This change in slope was less pronounced in the pre-cracked beams because they had already been cracked before being strengthened.

Table 3 shows the rate of first cycle energy dissipation for different beams, which was calculated as the ratio of the area under the first cycle curve to the maximum load applied in the first cycle. The unstrengthened control beam (B13-0-F) exhibited a much higher rate of energy dissipation than the strengthened beams because the strengthening material in the latter limited the extent of crack growth. The rates of energy dissipation in the pre-cracked beams were significantly lower than in the others, suggesting that the presence of pre-existing cracks largely prevents the dissipation of much energy during the first cycle.

Regardless of the initial stiffness; all the beams have almost the same rate of stiffness degradation up to steel rupture. After steel rupture, the rate of stiffness degradation was very high in beams strengthened with NSM. This could be attributed to the ability of beams strengthened with NSM bars to maintain more fatigue loads after steel ruptures. In general, the beams showed a gradual reduction in stiffness after steel bar rupture, which made the failures of beams as a ductile failure as shown in Fig. 6 by increasing the deflection.
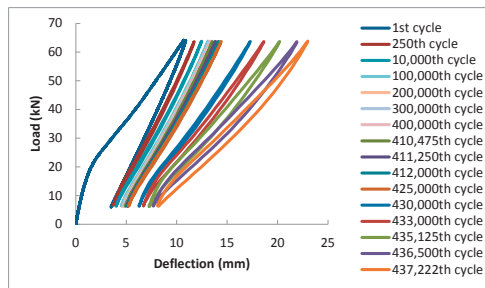
Fig. 6. Load-deflection curves under fatigue loading of B3-NE1-F

Slippage

Fig. 7 and Fig.8 show typical end slip curves for plate- and NSM bar-strengthened beams, and plots of the slip values as functions of the number of cycles (at both the maximum and minimum loads). The slip-cycle number plots show that the slippage increased significantly between the first cycle and the 20,000th, after which it increased much more slowly. The load-slip plots show that the bonding materials maintained their stiffness until failure. Although the stiffness did not change, the permanent deformations and slippage seem to increase with the number of cycles. This can be attributed mainly to the micro-damage in the bond-zone, which creates a permanent micro-plastic strain (slip). The areas under the curves for the first cycle are significantly larger than the areas under the other curves. This behavior could be explained; that the most degradation of the bond at the micro level occurred during first load cycle. It should be noted that the end slip was not affected by the local effects induced by the rupture of the steel bars.
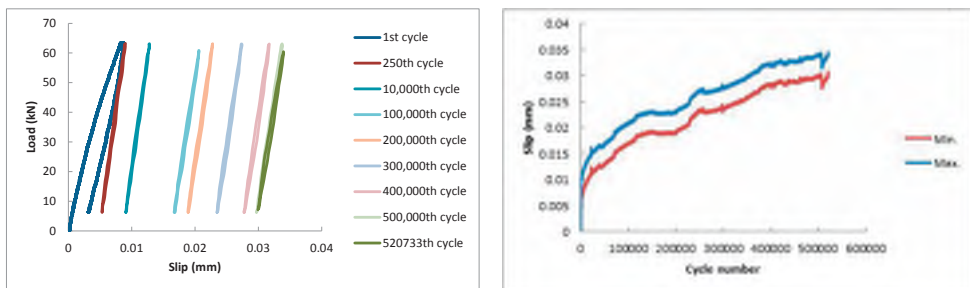
(a) Load-End slip   (b) End slip-Number of load cycles
Fig. 7. Typical slip behaviors under fatigue loading for plate-strengthened beam B1-EE1-F

(a) Load-end Slip.	(b) End slip - cycle number.
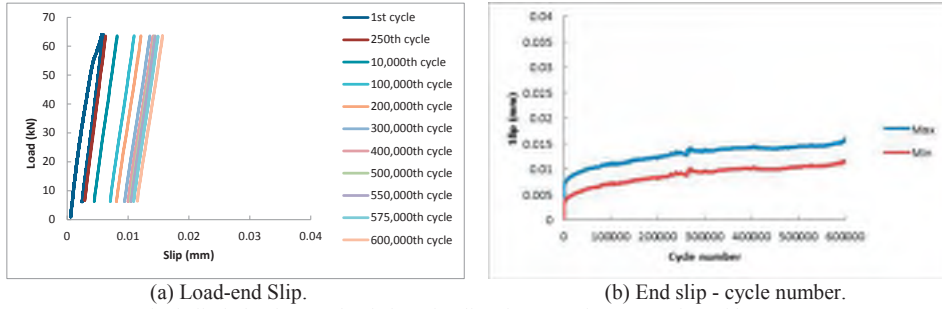
Fig. 8. Typical slip behaviors under fatigue loading for NSM bar-strengthened beam B10-NE1-F-C

Strain

Table 4 and Table 5 show the maximum strains in the longitudinal reinforcing steel and CFRP material under the maximum applied loads for the first and 325,000[th] cycles. The following observations can be drawn from this table. The highest strains in the longitudinal tension steel bars at the first cycle of the strengthened beams ranged from 1233 µε in the B9-EE1-F-C beam to 1778 µε in the B6-EE2-F beam; the latter value is around 49% of the steel's yield strain. In the compressed steel, the strains ranged between 483.3 µε in the B6-EE2-F beam and 638.1 µε in the B10-NE1-F-C beam. The maximum strain in the longitudinal tension steel of the unstrengthened beam was 1635 µε, which is about 45% of the yield strain of the reinforcing steel bars under static load; the unstrengthened beam's maximum compression strain was 243.8 µε. In general, the compressive strains in the strengthened beam were around twice as high as in the unstrengthened beam and the highest compressive strains generally occurred in the pre-cracked beams.

The highest maximum applied strains in the CFRP material varied between 1445 µε for B10-NE1-F-C and 2006 µε for B3-NE1-F. In general, the highest strains occurred in beams strengthened with NSM bars and the lowest in the pre-cracked beams. For each beam, the strain in the CFRP was greater than that in the reinforcing steel. This is expected because the CFRP is farther from the neutral axis of the beam.

Fig. 9 shows the typical strains in the tension reinforcement along half the beam's length at maximum load. The highest recorded strains in the longitudinal tension steel bars was 2020.89 $\mu\varepsilon$ in beam B3-NE1-F, which is about 56 % of the bar's measured yield strain under static load. Similar behaviors were observed for all the beams. For example, in beam B8-NE2-F (which exhibits complex behavior), the steel strains increased during the early load cycles and then stabilized until steel rupture. This was attributed to high levels of micro plastic strain during the first few cycles, a hypothesis that was consistent with the deflection response of the beams under fatigue loading as previously described. The left strain gauge at the beam's mid span was lost after 82,328 load cycles. However, the initiation of reinforcing steel fracture after 331,562 load cycles was detected because it caused a modest increase in the strain measured by the right hand strain gauge at the beam's mid span. The strain measured by this gauge increased rapidly between load cycles 348,245 and 352,547. This was due to a fatigue failure process in the tensile bar on the left hand side of the beam near the mid span caused by transmission stress to the second bar; the corresponding position of the fractured bar is shown in Fig. 4a (in the rightmost image). The bond length, from the measuring point to the bar fracture, was longer for the measuring point under the applied load than the measuring point in mid span. This may be why the effect was not pronounced on the strain gauge under the applied load. After complete steel bar rupture, the strain measured by the right hand gauge at the midspan of the beam increased slowly between load cycles 352,547 and 373,460. This indicates steady cracks development at the location of the steel rupture. During this process, the NSM bars compensate for the steel rupture and help to maintain relatively steady strains. After 373,460 load cycles, the strain recorded by the right strain gauge at the mid span decreased significantly due to the rupture of the right hand steel bar, at approximately the same point at which the first steel bar was ruptured. This behavior was accompanied by a decrease in strain rate in the strain gauge under the applied load, where the steel bar bond was affected by second steel rupture. Between load cycles 463,394 and 471,813, the strain recorded by the strain gauge fell due to a third rupture in the left steel bar near the right applied load point. The strain in strain gauge under the applied load decreased again in the 491,492[nd] load cycle, when a fourth rupture occurred in the right hand side steel bar in the same section of the beam. None of these ruptures affected the steel strain near the support due to the length of the steel bar's bond.

(a) B6-EE2-F   (b) B8-NE2-F
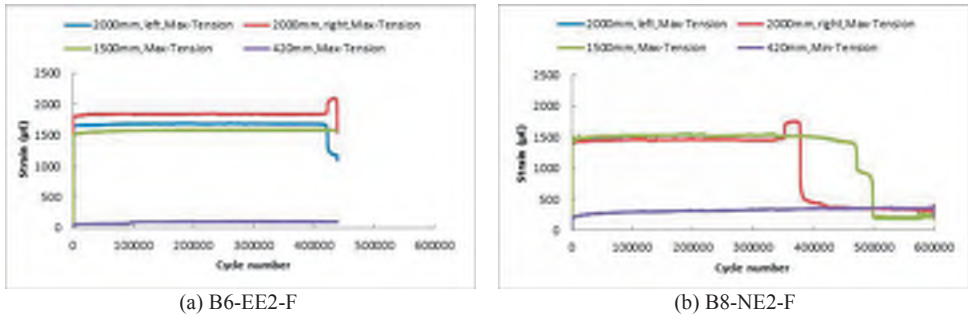
Fig. 9. Maximum tensile steel strains as functions of the number of load cycles

Fig. 10 shows the typical strains measured at maximum loads in the strain gauges that were attached to the strengthening plates at small intervals running from the beam's midspan to one of its far ends. The gauges were placed on the centerline of the NSM bars or strengthening plates as appropriate. In most cases, the measured strain increased with distance from the beam's supports. This is because the strains were proportional to the moment at the position where the gauge was mounted. In addition, the strains measured by individual gauges increased with the number of cycles. Similar behaviors were observed for all the beams.

In general, as shown by the results for beam B8-NE2-F, when the reinforcing steel ruptured, the cracks in the beam rapidly grew wider, leading to rapid increases in the strain measured by strain gauges mounted in the vicinity of the rupture. The immediate effects of the rupture were localized and it did not greatly affect the strains measured by distant strain gauges as shown in Fig. 10. After this rapid increase, the measured strain remained relatively steady over many cycles because the cracks grew steadily around the location of the rupture. As mentioned before, the NSM bars compensated for the rupture of the reinforcing steel, helping to maintain a steady level of strain. The strains measured in the CFRP elements of the strengthened beams were higher than those observed in the tensile steel bars during the fatigue test (see Figs. 9 and 10), indicating the superior bonding of the beams. Conversely, where the strain in the CFRP elements is lower than that in the steel, there is incomplete stress transfer between the CFRP and concrete substrate. By comparing the increase in the strain in the CFRP and the longitudinal tensile steel for all beams during load cycles 1-325,000 from Table 4 and Table 5, revealing that the strain in the constant moment region increased less than it did elsewhere. In addition, the rate of increase in the strain in the longitudinal tensile steel at the midspan was greater than that in the CFRP elements of beams strengthened with NSM. Conversely, in plate-strengthened beams, the rate of increase in the strain of the CFRP elements was greater than that in the reinforcing steel of the beams. The rate of strain increase in plate-strengthened beams using CFRP material with a low Young's modulus was generally lower than that in the beam strengthened with a high Young's modulus CFRP material. However, this trend was not observed for the NSM bar-strengthened beams. Finally, after 325,000 load cycles, the tensile strains measured in the pre-cracked beams were substantially lower than in their initially uncracked counterparts.

(a) B1-EE1-F   (b) B8-NE2-F
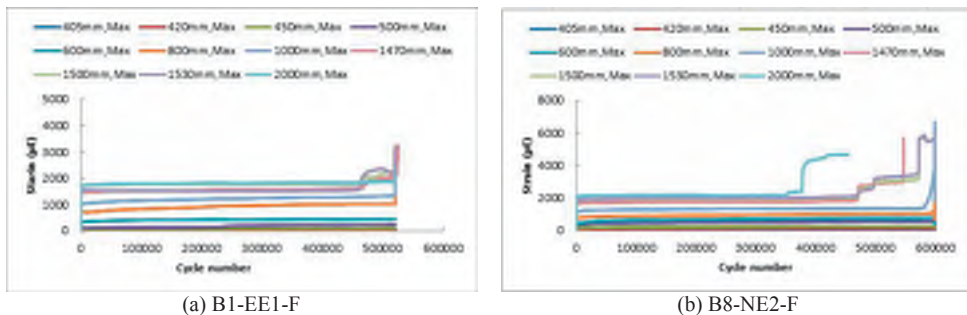
Fig. 10. Maximum CFRP strain measurements versus number of load cycles

11

Table 4. Maximum steel strains during specific cycles

Specimen	Gauge location (mm)	1	325,000	1	325,000
B3-NE1-F	2000(left)	1586	1723.848	-548.7	-618.074
	2000(right)	1280	1477.67		
	1500	1252	1380.69	-504.9	-586.83
	420	57.79	68.32	-60.13	-78.15
B8-NE2-F	2000(left)	1320	1465.86	-504.7	-565.28
	2000(right)	1374	1450.18		
	1500	1296	1542.14	-411.4	-448.85
	420	149.1	340.46	-81.26	-94.97
B1-EE1-F	2000(left)	1337	1522.39	-425.1	-515.69
	2000(right)	1228	1391.81		
	1500	1278	1470.89	-409.4	-494.86
	420	65.36	104.03	-85.29	-125.35
B6-EE2-F	2000(left)	1646	1682.68	-483.3	-532.47
	2000(right)	1778	1838.24		
	1500	1421	1580.99	-399	-420.58
	420	51.39	101.32	-70.27	-83.51
B9-EE1-F-C	2000(left)	1154	1263.82	-624.9	-691.93
	2000(right)	1233	1332.82		
	1500	1121	1252.15	-393.9	-451.36
	420	48.07	56.62	-54.32	-28.45
B10-NE1-F-C	2000(left)	1246	1377.06	-428.7	-483.44
	2000(right)	1218	1363.05		
	1500	1242	1329.10	-638.1	-699.71
	420	58.87	96.42	-59.45	-67.69
B13-0-F	2000(left)	1622.568	1715.73	-243.83	-307.48
	2000(right)	1566.006	1726.61		
	1500	1635.108	1730.46	-222.2	-269.73
	420	36.01	133.42	-37.17	-53.89

Table 5. Maximum CFRP strains during specific cycles

Gauge location (mm)	405	420	450	500	600	800	1000	1470	1500	1530	2000
B3-NE1-F 1st Cycle	3.98	33.56	72.75	128.9	269.4	574.5	1195	1856	1838	1877	2006
325,000th cycles	1.851	60.168	168.82	401.27	548.19	1007.63	1491.26	2033.80	2004.29	2068.73	2232.72
B8-NE2-F 1st Cycle	8.78	50.13	99.88	235.5	244	573.5	959	1521	1667	1653	2002
325,000th cycles	20.76	115.42	226.57	506.94	709.25	969.26	1331.76	1764.25	1937.20	2015.52	2171.60
B1-EE1-F 1st Cycle	14.21	31.82	51.04	88.96	161.3	654.1	856.7	1486	1502	1440	1580
325,000th cycles	22.34	48.83	81.69	209.52	426.78	975.27	1248.83	1564.69	1774.87	1517.40	1817.34
B6-EE2-F 1st Cycle	20.82	49.89	70.42	102.6	226.7	656.7	1025	1570	1622	1823	1911
325,000th cycles	36.93	94.58	125.57	188.96	562.38	1016.97	1293.95	1975.49	1776.00	2012.74	2206.03
B9-EE1-F-C 1st Cycle	25.01	48.33	71.44	111.6	169.2	603.8	856.8	1140	1235	1492	1268
325,000th cycles	34.85	88.31	129.68	273.19	365.29	833.83	1078.30	1343.52	1382.95	1589.03	1554.63
B10-NE1-F-C 1st Cycle	14.75	46.94	70.74	118.1	263.1	724.7	961.1	1486	1540	1445	1432
325,000th cycles	26.001	89.97	144.76	285.48	544.91	1139.37	1208.62	1605.82	1730.46	1616.95	1671.39

The distributions of the maximum CFRP bond stresses over the half length of the beam at different cycles were determined from the measured maximum strains and are plotted in Fig. 11. The average shear stress in NSM-strengthened bars between points i and i+1, $\tau_{i,i+1}$ was determined from the strains at these two points using the expression shown below (Carolin et al. 2005):

$$\tau_{i,i+1} = \frac{\varepsilon_{i+1} - \varepsilon_i}{x_{i+1} - x_i} \frac{Et}{3} \qquad (1)$$

The corresponding values for plate-strengthened beams were obtained using the expression of Nigro et al. (2010):

$$\tau_{i.i+1} = \frac{\varepsilon_{i+1} - \varepsilon_i}{x_{i+1} - x_i} Et \tag{2}$$

Here, the strains at points x_i and x_{i+1} are ε_i and ε_{i+1}, E is the Young's modulus of the CFRP element, and t is its thickness.

The shear bond stresses are around zero within the constant moment region and constant but non-zero throughout the shear span, in accordance with the variation in the shear force acting on the beam. The calculated bond stresses values oscillate around these average levels due to the presence of cracks and the consequent non-uniform transfer of stresses between concrete and FRP. High shear bond stresses are seen in the cutoff region. Notable increased in shear stresses in cutoff region and applied load location was occurred during the 10,000 cycles. Then, the shear stresses were almost steady until beams failed. The shear stresses in beams strengthened with NSM bars (B8-NE2-F) at final cycle are increased sharply under the applied load, near location of steel bar rupture, and slightly at cutoff region. These increases indicating intermediate cracks induced debonding failure mode in that beam. For beam strengthened with external plate (B6-EE2-F), decreases and increases in shear bond stresses are identified under the applied load point and cutoff region, respectively. These data clearly reflect the progression of debonding from intermediate crack to the cutoff point.

(a) B6-PE2-F   (b) B8-NE2-F
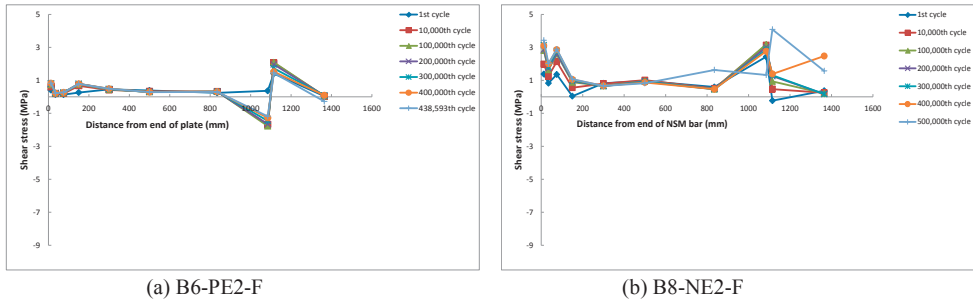
Fig. 11. Bond stress distributions

Fig. 13 shows the principal strain range (i.e. the difference between the strains measured under the maximum and minimum loads applied during a single cycle) distributions determined by photometric strain monitoring of 750x300 mm areas on the beams' surfaces during selected fatigue testing cycles of beams B1-PE1-F and B3-NE1-F. The monitored areas of these beams were painted with a stochastic or regular pattern by spraying as shown in Fig. 12. Note that the photometric strain data clearly reveals crack formation before the cracks become visible to the naked eye. The plots in Fig. 13 clearly display the evolution of cracking patterns in the beams and demonstrate the advantages of digital image processing as a tool for identifying crack geometries and the strain field distribution. The cracks' lengths and widths appear to remain fairly steady over the first 500,000 load cycles prior to the rupture of the reinforcing steel. Unfortunately, no DIC data were recorded when the beams failed because this occurred outside the planned measurement period.

(a)   (b)

Fig.12. Location of the photometric measurement regions in beams (a) B1-PE1-F and (b) B3-NE1-F

13

(a) B1-EE1-F

(b) B3-NE1-F
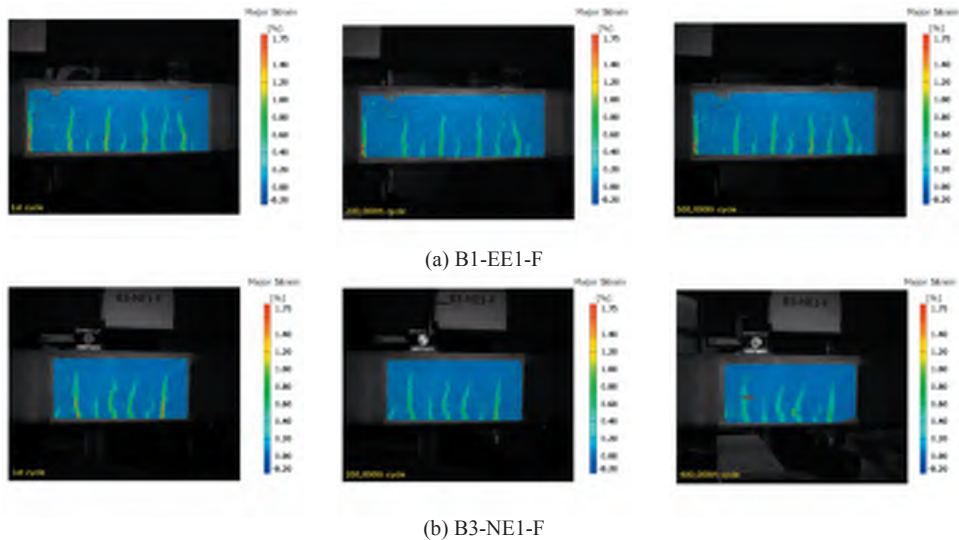
Fig. 13. Changes in principal strain range and cracking patterns in (a) plate-strengthened and (b) NSM bar-strengthened beams during fatigue loading, as determined by optical measurement.

Fatigue life

Fatigue life data for the control and strengthened beams beam are presented in Table 3, along with information on the number of steel bar ruptures observed for each beam type during fatigue loading. The fatigue life of an unstrengthened beam is the number of cycles prior to the rupture of the reinforcing steel, which is assumed to equal the life until crack initiation in the steel rebar plus the life during crack growth. In contrast, Toutanji et al. (2006) suggest that the fatigue life of FRP-strengthened beams is equal to the sum of the fatigue life of the reinforcing steel and the fatigue life of the strengthening FRP element after the steel fractures. This assumption will only hold if the fatigue life of the FRP-concrete bond exceeds that of the strengthening material, which was generally not the case in previous studies. Here, the fatigue life of the strengthened beam is defined as the sum of the fatigue life of the steel and the remaining fatigue life of the FRP–concrete bond after the steel's fracture.

Even though the axial stresses of the tensile steel bars in the control beam (B13-0-F) and the strengthened beams were almost identical, no fracturing of the reinforcing steel of the control beam occurred during the fatigue test. To explain this result, it is necessary to consider the fatigue behavior of the steel bars. The report of the ACI Committee 215 (1997) suggests that when a steel bar is subjected to fatigue testing in air, its fatigue is caused by microscopic defects that are formed at stress concentrations on the bar's surface. The locations of these concentrations are normally determined by the local geometry of the bar (Heffernan et al. 2004). Consequently, a fracture occurs at the locations of defects in the steel bar where the stress concentration is highest rather than at the point of maximum tensile stress. The cracks formed in this way gradually propagate until fracture occurs suddenly, when the remaining cross section of the rebar is too small to support the applied load.

In contrast, if a steel bar in an unstrengthened reinforced concrete beam has flexural cracks, the maximum stress concentrations will occur at the locations of the cracks. If the bar has a defect at such a point, its fatigue life will be similar to that of a bar tested in air; otherwise its fatigue life will be increased despite a slight increase in the local shear stress acting on the bar at the faces of the crack. In reinforced concrete beams strengthened with CFRP, the strengthening reinforcement on the beam's lower surface helps the steel bar to resist the applied tensile stress, and bridging effects reduce the increase in crack width, thereby reducing the stress concentration (localized stress) on the steel bar's surface even in cases where the bar has a default at the location of the crack. The bar's fatigue life will thus be greater than it would be in an unstrengthened beam under the same load. In this work, the tensile steel bars in the strengthened and unstrengthened beams had the same levels of stress, so the loads applied to the strengthened beams were greater than those for the unstrengthened beam. This greater load caused a greater local shear stress in the steel bar at cracked positions, especially after the destruction of the concrete interlock at crack faces and crack growth due to cyclic loading. The positioning of the ruptures in the steel bars observed during the fatigue tests was consistent with this model because they occurred at positions of high shear stress. In addition, the crack spacing in strengthened beams was smaller than in unstrengthened beams, allowing the steel bar sections between adjacent cracks to function more effectively as shear resistance

14

elements. Consequently, the fatigue life values of strengthened beams will be lower than those for unstrengthened beams containing tensile reinforcing steel of the same stress level.

The fatigue life prior to the first reinforcing bar rupture in plate-strengthened beams was greater than in those with NSM bar strengthening. This indicates that the NSM bar-strengthened beams have more pronounced localized stress concentrations than those strengthened with plates because the contact surface between the plates and the beams is greater than that between the bars and the beams, making plates more effective at limiting crack development.

The ductility of fatigued NSM bar-strengthened beams was superior to that of plate-strengthened beams, as demonstrated by the total deflection values for each beam type observed during the final load cycle of the fatigue tests (see Table 3).

The percentage of each beam's total fatigue life remaining after the first steel rupture (see Table 3) was higher in the NSM bar-strengthened beam having CFRP strengthening with a low Young's modulus than in the corresponding plate-strengthened beam even though the same mass of CFRP material was used in both cases. Conversely, for beams strengthened with CFRP having a high Young's modulus, the percentage of total fatigue life remaining after the first steel rupture was greater in the plate-strengthened beam than in that strengthened with NSM bars.

The fatigue life values for the pre-cracked strengthened beams B10-NE1-F-C and B9-PE1-F-C were greater than those for all of the strengthened beams without pre-cracking. These results may indicate that pre-cracked beams behave more like unstrengthened beams than initially uncracked strengthened beams. This behavior was especially pronounced in the pre-cracked plate-strengthened beam, which is consistent with the suggestion that plate strengthening produces lower levels of concentrated stress than NSM bar strengthening. These results are interesting because they are the most likely to be reflective of the situation encountered in practical applications of CFRP strengthening.

To identify a model capable of reliably estimating the fatigue life of strengthened beams, the experimentally determined fatigue life values reported in this work were compared to the predictions of various previously reported models for steel stressed at 258 MPa (see Table 6). The model whose results are in best agreement with the measured fatigue life values obtained in this work is that of Helgason and Hanson.

Table 6. Fatigue life values predicted for different beam types using various model equations.

	Fatigue life model	Estimated fatigue life
RC beam ,Tilly and Moss (Barnes and Mays 1999)	$S_r{}^9 * N = 3.09 * 10^{27}$	600,000
RC beam, CEB/FIB (2010)	$S_r{}^5 * N = 4.0841 * 10^{17}$	353,986
Helgason and Hanson model for steel under direct tension in air (Zorn 2006)	$\log(N) = 6.969 - 0.00555S$	342,336

Conclusions

The behavior of reinforced concrete beams strengthened with CFRP plates and NSM bars under monotonic and fatigue loading by four-point bending has been investigated. Strengthening materials with two different Young's modulus values were examined, and the effect of pre-existing cracks in the beams before the application of the strengthening material was investigated. The results obtained indicate that:

1-The first cracking load of the unstrengthened beam was equal to that of beams strengthened with NSM bars and plates. This indicates that neither strengthening methods was able to delay crack formation under monotonic loads.

2-The increase in the ultimate strength of strengthened beams relative to an otherwise identical unstrengthened beam is largely dependent on the properties of the FRP material and the method of strengthening. The ultimate load of beams strengthened with NSM bars increased by 144% and 125% when the Young's modulus of the CFRP strengthening element was 200 and 150 GPa, respectively. In specimens strengthened with plates, ultimate load increases of 106% and 96% were achieved using CFRP materials with Young's moduli of 200 and 150 GPa, respectively.

3-The stiffness of the strengthened beams under monotonic load was independent of the strengthening method used provided that the Young's modulus of the strengthening material was kept constant.

4-Under monotonic loading, the unstrengthened beam was more ductile than any strengthened specimen. In addition, the NSM bar-strengthened beams were more ductile than their plate-strengthened counterparts. Specimens strengthened with CFRP having a low modulus of elasticity were more ductile than those strengthened with CFRP having a higher modulus of elasticity.

5-Plate strengthening allowed the beams to tolerate the applied fatigue loads after the rupture of the reinforcing steel bars, but less effectively than NSM bar strengthening. The beams strengthened with NSM bars continued to support the fatigue loads even after four ruptures of the reinforcing steel bar whereas plate-reinforced beams were only able to tolerate one rupture.

6- The crack patterns formed during the first load cycle did not change until the rupture of the first reinforcing steel bar and neither did the rate of crack growth.

7- The dominant failure mode in all beams that failed during fatigue loading involved intermediate debonding at the position where the steel bars ruptured. In general, the stiffness of the beams declined gradually after the first rupture, so their failure was ductile.

8- The Young's modulus of the CFRP strengthening material affected the deflection of the beams during the fatigue test. The maximum deflection of NSM bar-strengthened beams made using CFRP material having a high modulus of elasticity increased by 25% relative to that observed during the first cycle; the corresponding value for the bar-strengthened beam prepared using low Young's modulus CFRP was only 23 %. For plate-strengthened beams, the corresponding values were 16 and 13 %, respectively.

9- The mid-span deflection for beams strengthened with CFRP plates was lower than that seen for beams strengthened with NSM bars. Specifically, the mid-span deflections for beams strengthened with CFRP plates having high and low Young's moduli were approximately 15 % and 7 % lower than those for the corresponding NSM bar-strengthened beams.

10- The relative increase in the maximum deflection of the control beam over the course of the fatigue loading process (26%) was very similar to that seen for beams strengthened with NSM bars.

11- NSM bar strengthening was more effective in pre-cracked beams for improving behavior than in those without pre-cracking: the relative increase in the deflection of the pre-cracked bar-strengthened beam after a given number of loading cycles was 9% lower than that for the equivalent beam without pre-cracking.

12- Plate strengthening was more effective for improving fatigue life than NSM bar strengthening in the case of pre-cracked beams.

13- The rates of energy dissipation in strengthened pre-crack beams were significantly lower than in beams without pre-cracking. In addition, all strengthened beams without pre-cracking exhibited similar rates of energy dissipation regardless of their method of strengthening.

14-After the first load cycle, all of the tested beams exhibited only micro-scale damage until the rupture of the first steel bar.

15-The measured load-end slip values for plate- and NSM bar-strengthened beams showed that the joint bond maintained its stiffness until the beams failed.

16-The rate of strain increase in the longitudinal tensile steel bar at the mid span of the beams was higher than the strain measured in the CFRP elements of NSM bar-strengthened beams. Conversely, in plate-strengthened beams, the rate of strain increase in the CFRP elements was greater than that in the reinforcing steel. Additionally, the rate of strain increase in plate-strengthened beams featuring CFRP with a low Young's modulus was lower than in beams having CFRP strengthening with a high modulus of elasticity. Finally, during the fatigue tests, the pre-cracked beams exhibited lower levels of tensile strain in both their reinforcing steel and CFRP elements than were observed in the corresponding beams without pre-cracking.

17- The results presented herein suggest that the fatigue life of strengthened beams should be calculated by summing the fatigue life of the steel reinforcement and the remaining fatigue life of the FRP-concrete bond after the fracture of the reinforcing steel. Plate-strengthened beams had greater fatigue life values prior to the first rupture of the reinforcing steel than did beams strengthened with NSM bars. However, for beams strengthened

with CFRP having a low Young's modulus, the proportion of the total fatigue life remaining after the rupture of the first reinforcing steel bar was greater for the NSM bar-strengthened beam than for its plate-strengthened counterpart. The opposite was true for beams strengthened with CFRP having a high modulus of elasticity. The fatigue lives of pre-cracked strengthened beams were greater than those of strengthened beams without pre-cracking.

18- The results presented herein also suggest that the best model for estimating the fatigue life of CFRP-strengthened beams is the Helgason and Hanson model for steel bars in air.

19- The comparison of the fatigue lives of strengthened and unstrengthened beams was influenced by the need to apply higher loads to the former in order to maintain the same level of axial stress in the reinforcing tension steel bars. This increased the shear stress acting on the steel reinforcement of the strengthened beams and thus increased the localized concentrations of stresses at the surfaces of the reinforcing bars, thereby reducing their fatigue life.

Acknowledgments

References

ACI Committee 215. (1997). "Considerations for design of concrete structures subjected to fatigue loading." Proc., American Concrete Institute,ACI 215R-74, ACI, Farmington Hills.

Aidoo, J., Harries, K. A., Petrou, M. F. (2006). "Full-Scale Experimental Investigation of Repair of Reinforced Concrete Interstate Bridge using CFRP Materials." J. Bridge Eng., 11(3), 350-358.

Aidoo, J., Harries, K. A., Petrou, M. F. (2004). "Fatigue Behavior of Carbon Fiber Reinforced Polymer-Strengthened Reinforced Concrete Bridge Girders." J. Composite Constr., 8(6), 501-509.

Badawi, M., and Soudki, K. (2009). "Flexural Strengthening of RC Beams with Prestressed NSM CFRP Rods–experimental and Analytical Investigation." Constr. Build. Mater., 23(10), 3292-3300.

Barnes, R. A., and Mays, G. C. (1999). "Fatigue Performance of Concrete Beams Strengthened with CFRP Plates." J. Composite Constr., 3(2), 63-72.

Brena, S. F., Benouaich, M. A., Kreger, M. E., Wood, S. L. (2005). "Fatigue Tests of Reinforced Concrete Beams Strengthened using Carbon Fiber-Reinforced Polymer Composites." ACI Struct. J., 102(2).

Carolin, A., Täljsten, B., Hejll, A. (2005). "Concrete Beams Exposed to Live Loading during Carbon Fiber Reinforced Polymer Strengthening." J. Composite Constr., 9(2), 178-186.

Comité Euro-International du Beton. (2010). CEB/FIB Model Code 2010, Thomas Telford, London.

Gussenhoven, R., and Brena, S. (2005). "Fatigue Behavior of Reinforced Concrete Beams Strengthened with Different FRP Laminate conFigurations." ACI Special Publication, 230.

Harries, K. A., Reeve, B., Zorn, A. (2007). "Experimental Evaluation of Factors Affecting Monotonic and Fatigue Behavior of Fiber-Reinforced Polymer-to-Concrete Bond in Reinforced Concrete Beams." ACI Struct. J., 104(6).

Heffernan, P. J., Erki, M., DuQuesnay, D. L. (2004). "Stress Redistribution in Cyclically Loaded Reinforced Concrete Beams." ACI Struct. J., 101(2).

Heffernan, P., and Erki, M. (2004). "Fatigue Behavior of Reinforced Concrete Beams Strengthened with Carbon Fiber Reinforced Plastic Laminates." J. Composite Constr., 8(2), 132-140.

Mahal, M., Blanksvärd, T., Täljsten, B. (2013). "Examination at a Material and Structural Level of the Fatigue Life of Beams Strengthened with Mineral Or Epoxy Bonded FRPs: The State of the Art." Adv. Struct. Eng., 16(7), 1311-1328.

Masoud, S., Soudki, K., Topper, T. (2005). "Postrepair Fatigue Performance of FRP-Repaired Corroded RC Beams: Experimental and Analytical Investigation." J. Composite Constr., 9(5), 441-449.

Masoud, S., Soudki, K., Topper, T. (2001). "CFRP-Strengthened and Corroded RC Beams Under Monotonic and Fatigue Loads." J. Composite Constr., 5(4), 228-236.

Meier, U., Deuring, M., Meier, H., Schwegler, G. (1992). "Strengthening of structures with CFRP laminates: Research and applications in switzerland." Proc., Proceedings of the 1st International Conference on Advanced Composite Materials in Bridges and Structures, Canadian Society of Civil Engineering, Sherbrooke, 228-236.

Nigro, E., Di Ludovico, M., Bilotta, A. (2010). "Experimental Investigation of FRP-Concrete Debonding Under Cyclic Actions." J. Mater. Civ. Eng., 23(4), 360-371.

Nordin, H., and Täljsten, B. (2006). "Concrete Beams Strengthened with Prestressed Near Surface Mounted CFRP." J. Composite Constr., 10(1), 60-68.

Oudah, F., and El-Hacha, R. (2012). "Fatigue Behavior of RC Beams Strengthened with Prestressed NSM CFRP Rods." Composite Structures, 94(4), 1333-1342.

Papakonstantinou, C. G., Petrou, M. F., Harries, K. A. (2001). "Fatigue Behavior of RC Beams Strengthened with GFRP Sheets." J. Composite Constr., 5(4), 246-253.

Quattlebaum, J. B., Harries, K. A., Petrou, M. F. (2005). "Comparison of Three Flexural Retrofit Systems Under Monotonic and Fatigue Loads." J. Bridge Eng., 10(6), 731-740.

Rosenboom, O., and Rizkalla, S. (2006). "Behavior of Prestressed Concrete Strengthened with various CFRP Systems Subjected to Fatigue Loading." J. Composite Constr., 10(6), 492-502.

Sena-Cruz, J. M., Barros, J. A., Coelho, M. R., Silva, L. F. (2012). "Efficiency of Different Techniques in Flexural Strengthening of RC Beams Under Monotonic and Fatigue Loading." Constr. Build. Mater., 29, 175-182.

Täljsten, B. (1997). "Strengthening of Beams by Plate Bonding." J. Mater. Civ. Eng., 9(4), 206-212.

Toutanji, H., Zhao, L., Deng, Y., Zhang, Y., Balaguru, P. (2006). "Cyclic Behavior of RC Beams Strengthened with Carbon Fiber Sheets Bonded by Inorganic Matrix." J. Mater. Civ. Eng., 18(1), 28-35.

Wahab, N., Soudki, K. A., Topper, T. (2012). "Experimental Investigation of Bond Fatigue Behavior of Concrete Beams Strengthened with NSM Prestressed CFRP Rods." J. Composite Constr., 16(6), 684-692.

Yost, J. R., Gross, S. P., Deitch, M. J. (2007). "Fatigue behavior of concrete beams strengthened in flexure with near surface mounted CFRP." Proc., Proceedings of the 8th International Symposium on Fiber-Reinforced Polymer Reinforcement for Concrete Structures (FRPRCS-8), .

Zorn, A. V. (2006). Effect of Adhesive Stiffness and CFRP Geometry on the Behavior of Externally Bonded CFRP Retrofit Measures Subject to Fatigue Loads, .

PAPER III

"Using digital image correlation to evaluate fatigue behaviour of strengthened reinforced concrete beams"

BY

Mohammed Mahal, Thomas Blanksvärd ,Björn Täljsten and Gabriel Sas

Using digital image correlation to evaluate fatigue behavior of strengthened reinforced concrete beams

Mohammed Mahal[a, b,*], Thomas Blanksvärd[a], Björn Täljsten[a, c], Gabriel Sas[a]

[a]Department of Civil, Environmental and Natural resources engineering, Luleå University of Technology, SE-971 87 Luleå, Sweden.

[b]Department of Civil Engineering, Mosul University, Mosul, Iraq

[c]Sto Scandinavia AB, Sweden

[*]Corresponding author: E-mail address: mohammed.salih@ltu.se (Mohammed Mahal)

Abstract

The fatigue behavior of reinforced concrete beams strengthened with externally bonded carbon fiber reinforced polymer (EBR) plates and near-surface mounted (NSM) bars has been investigated using a digital image correlation (DIC) technique. Displacement fields obtained from digital images recorded during specific load cycles in fatigue tests are analyzed to provide information on crack width, beam deflection and curvature, and major principal strains to enable crack detection. The results obtained in this way were compared to data gathered using conventional sensors, revealing that the DIC technique provided very accurate and detailed information, which is not possible to obtain using conventional techniques. The experimental results for plate-strengthened, bar-strengthened and unstrengthened beams are discussed.

Keywords: Digital image correlation, Reinforced concrete beam, Fatigue, Crack detection

1. Introduction

In recent years, the use of Fiber Reinforced Polymer (FRP) elements to strengthen reinforced concrete members has become a widely accepted method for stabilizing existing deteriorating or deficient structures. Two types of FRP element are used, both of which are bonded to the concrete surface with epoxy: plates or sheets that are externally bonded to the member's tension surface – externally bonded reinforcement (EBR), or solid square rods that are positioned inside the member at a near-surface mounted (NSM) location.

Several studies on reinforced concrete beams strengthened with CFRP under fatigue loads have been reported [1-8]. The most common fatigue failure modes observed in these works involved the rupture of the tensile reinforcing steel followed by FRP debonding. Most of these studies did not consider the effect of crack distribution on the fatigue behavior of strengthened beams nor did they seek to determine which strengthening techniques are most effective at limiting crack spacing and width so as to prevent or reduce the corrosion of the steel reinforcement bars during the expected fatigue life of reinforced concrete members. In addition, there have been few investigations into the mechanical responses of cracks bridged by a bonded composite laminate under fatigue load.

Digital Image Correlation (DIC) is very accurate method for studying the cracking of concrete. It can be used to monitor concrete members of various sizes under a wide range of loading conditions, and has a number of important advantages over conventional sensor-based methods. In particular, it permits measurement over the entire visible surface of the studied member rather than only at a limited number of discrete points, is capable of detecting early cracks, and does not require tests to be paused so that new cracks can be marked and measured as they form; the latter quality is particularly useful in dynamic tests.

Destrebecq et al. [9] used DIC to detect and measure the widths of cracks in reinforced concrete beams, and to measure the beams' midspan deflection profiles. The deflection profiles were then used to calculate the evolution of the beams' curvature over five load cycles. DIC has also been used to examine the bonding between CFRP

elements and concrete in single lab tests [10, 11], reinforced concrete specimens strengthened with composite plates [12], crack behavior in a RC beam [13], and for crack detection in a concrete beam [14] ,full-scale of prestressed concrete structures [15]. However, to the author's knowledge, DIC has not previously been used to study reinforced concrete members strengthened with CFRP under fatigue loads.

The DIC approach involves painting the area to be studied with a stochastic pattern and then imaging the painted surface with a digital camera of known resolution to monitor the pattern's deformation over time. The captured digital images are divided into grids of square pixels known as facets. The greyscale values of each pixel in a facet are recorded, enabling its deformation and displacement to be tracked over time in order to determine the full field displacement of the imaged area.

This work presents fatigue test results for unstrengthened reinforced concrete beams and beams strengthened with either EBR plates or NSM bars. The main objectives of the experimental work were to analyze the displacement fields determined by DIC to determine the evolution of the beams' deflection and flexural curvature during fatigue loading, to investigate crack initiation and propagation during fatigue loading, and to compare the results obtained for the different types of beams. The DIC software used for these purposes was the ARAMIS v6.3.0 (GOM GmbH, Braunschweig, Germany) non-contact optical strain measurement system. The results obtained confirm that DIC is an accurate method for measuring full field displacement and locating cracks, and provides a very easy way of measuring displacement at multiple points on a beam's surface.

2. Specimen Details and Material Properties

The beams used in this study were 4,000 mm long with rectangular cross sections of 200x300 mm as shown in Fig. 1. Their longitudinal steel reinforcements in tension and compression were two rods with nominal diameters of 16 mm. The shear reinforcement, which was designed to ensure flexural failure in the strengthened beams, consisted of 10 mm stirrups at a spacing of 75 mm. Three beam types were tested - one strengthened with NSM bars, one with traditional EBR plate, and one without FRP strengthening. The unstrengthened beams were used as controls in the fatigue load tests. The same mass of FRP material was used in each of the strengthened beams so as to compare systems with similar specifications. The length of the strengthening laminates and rods (3,200 mm) was chosen to match the beams' critical anchorage length [16].

Plate strengthening was performed with two strips of 1.4 mm thick CFRP, one with a width of 100 mm (StoFRP Plate IM 100C) and another with a width of 43 mm that was cut from a strip of material with a width of 60 mm (StoFRP Plate IM 60C). The laminate strips were bonded to the surface of the beam soffit using StoPox SK41 epoxy after surface grinding to expose the gravel and primer application; the thickness of the adhesive epoxy layer after plate bonding was 2 mm. After the strengthening plates had been applied, two layers of CFRP sheeting were wrapped around the plate-strengthened beam to form a 300 mm wide U-jacket with the fiber direction being perpendicular to the longitudinal axis of the beam. The jacket was formed using the wet lay-up technique and placed towards one of the beam's far ends, well away from the midspan. It was bonded to the beam using StoPox LH epoxy.

NSM strengthening was performed using two 10x10mm quadratic rods (StoFRP BAR IM 10C), Fig. 1, each having a modulus of elasticity of 200 GPa. The rods were fitted to the beam by cutting two parallel grooves along the beam's length using a concrete saw with two parallel saw blades. After chipping away the cut concrete, two grooves with widths of 15 mm and depths of 17 mm were obtained, with smooth sides and rough lower surfaces. The surfaces of the grooves were coated with primer and epoxy (StoPox SK41) before placing the NSM bars into the groove. The thickness of the adhesive layer surrounding the bonded NSM bars was 2.5 mm on the three bonded sides.

The compressive and tensile strengths of the concrete used can be seen in Table 1. For each beam, three tests were made for both the compressive and tensile strength of the concrete at time of test companion beam. The concrete quality is tested on 150 mm cubes. The mechanical properties of the beams' reinforcing steel bars were determined using experimental tensile tests; the mean yielding strength and modulus of elasticity of the

longitudinal steel reinforcement were 578 MPa and 208 GPa, respectively. The corresponding values for the stirrups were 533 MPa and 202 GPa, respectively. The key properties of all materials used in the construction of the test beams are listed in Table 2. The properties of the composites and the adhesive were supplied by the manufacturer and not verified. The plate-strengthened, NSM bar-strengthened, and unstrengthened beams are henceforth referred to as B1-PE1-F, B3-NE1-F, and B13-0-F, respectively.
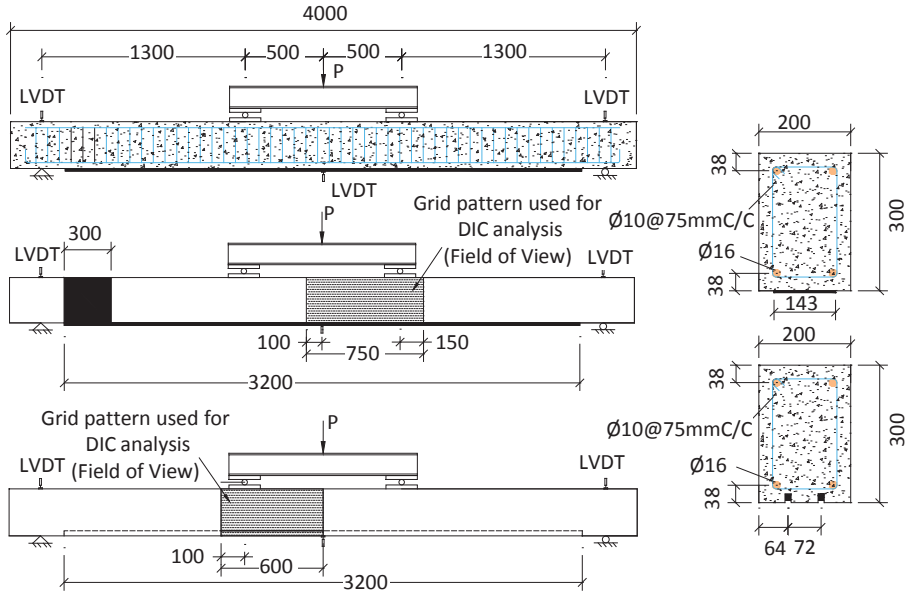
Fig. 1. Beam details and setup. All dimensions are in millimeters.

Table 1 Concrete properties.

Specimen	Concrete compressive strength (MPa)	Concrete Tensile strength (MPa)
B13-0-F	71	4.2
B3-NE1-F	71	4.7
B1-PE1-F	71	4.7

Table 2 Properties of CFRP composite systems and resin.

Material	compressive strength (MPa)	Tensile strength (MPa)	Young's modulus (GPa)	Ultimate strain (‰)
Composite[a]				
StoFRP Composite IM	-	2900	200	14
Adhesive[a]				
StoPox LH	100	90	3.500	-
StoPox SK 41	82	19	7.872	-

[a] Supplier's data

3. Digital Image Correlation

Digital image correlation (DIC) is an optical and noncontact measurement technique that is used to visualize displacements on the surface of an object of interest. This displacement is then used to calculate the object's surface strain. DIC involves comparing a series of images taken in sequence over a period of time by a digital camera with specific resolution. The distributions of grey scale values in successive images are compared, and their differences are used to characterize the deformation of the surface. For the process to be most effective, the area of interest should be painted with a random speckle pattern prior to the start of the process [17].

Three dimensional (3D) DIC requires two sets of images of the object taken from separate camera angles at the same time. The system must be calibrated to define the 3D space in which the event or process to be studied will occur. The results of this calibration process are then used to correlate the images from the two cameras to enable the determination of the studied material's deflection and strain [18]. An advantage of DIC is that it can be used to monitor large surface areas and can detect unexpected phenomena occurring on the surface such as crack formation, which might be difficult or impossible to identify and measure using traditional techniques.

The fundamental principle of DIC is based on the fact that the distribution of grey scale values in the image of the undeformed state can be related to that in the deformed state [19]. For this purpose, the initial grey level distribution in the reference image for any pixel area is represented by a function $g(x, y)$. This function becomes $g(x_t, y_t)$ in the deformed image. The relationship between the grey scale values for this pixel area in the initial and deformed states is given by the following expression [19]:

$$g(x, y) = g(x_t, y_t)$$

The pixels in the reference image are then transformed into the destination image as follows:

$$x_t = a_1 + a_2 x + a_3 y + a_4 xy$$

$$y_t = a_5 + a_6 x + a_7 y + a_8 xy$$

The values a_1 and a_5 describe the translation of the pixel's center; the others describe its rotation and deformation.

The investigations presented herein were conducted using the ARAMIS optical strain measuring system. This measuring system consists of two high-resolution metrology CCD cameras, enabling the 3-dimensional localization of each point on the sample surface. The cameras have resolutions of 2024 ×2024 pixels with 1 inch CCDs, and shutter times that can be varied between 0.1 ms and 2 s. They were connected to a computer running the ARAMIS image recognition software package, which matched the images from the two cameras. The recorded images consist of grouped pixels known as facets. The initial digital image is divided into a grid of square facets with a defined size and step size. The facet size is the dimension of the square, and the step size is the distance between the centers of two adjacent facets. Each facet contains multiple pixels, each with their own greyscale value, so the evolution of the facets' shape and size can be monitored over the course of the experiment.

To determine the surface displacement of the target object, each facet is tracked from one image to the next, creating a series of data points that are mapped to create the displacement field. For 3D displacement mapping, two views (left and right) are required for each time step. The corresponding facets from the left and right images are identified in each image in the series. The specimen's deformation is then mapped by monitoring the changes in each facet's orientation and shape.

To facilitate 3D DIC, a 750×300 mm region of each concrete beam was painted with a carrier speckle pattern, which the ARAMIS system uses to identify facets and follow their displacement. To create the pattern, the area was coated with a thin basal layer of white paint and the stencil-spray technique was then used to create a black-on-white grid pattern containing speckles of around 2 mm and sharp contrast, as shown in Figs. 1 and 2. The facet size was set at 17 pixels and the step size at 15 pixels for all tested beams.

The three-dimensional DIC setup was calibrated for a 700 mm × 560 mm field of view using standard calibration panels according to the procedure outlined in the User's Manual for the ARAMIS system [20, 21]. This process yielded a set of calibration data including camera angles , values for the distance between the object and each camera and calibration deviation. After calibration, the measurement field of view was set to 750×300 mm for all beams other than B3-NE1-F, for which a 600×300 mm field of view was used. A calibration deviation limit of ±0.021 pixels was applied in all of the tests.

In brief, the ARAMIS system works by recording sequential images of the specimen as its load is increased during a monotonic load or while it is under cycle load during fatigue testing. Each recorded image defines a separate stage in the loading process; the number of stages depends on the type of test being conducted and the specimen's behavior. The first image in all tests is referred to as stage 0 and was used as a reference image of the undeformed specimen for displacement calculations. The stage 0 image for the first load was acquired with no load on the specimen; for all subsequent load cycles, the stage 0 image was acquired with the specimen under the minimum load for that cycle. The region of interest in each of the initial images of each specimen was defined manually within the ARAMIS system.

Fig. 2. Point pattern used for DIC measurement.

4. Test setup and Procedure

In the fatigue load tests, the three reinforced concrete beams were tested in a four-point bending configuration with a simply supported span of 3600 mm as shown in Fig. 1. The midpoint deflection and support settlement were registered using linear voltage differential transducers (LVDTs). The instruments used in the tests are shown in Fig. 1. The minimum applied load, 6 kN, was selected to avoid impact loads during cycling, which cause shifting of the beams on the supports. The same reinforcing steel stress range (258 MPa) was used for all three beams. This value was selected to match the design fatigue life of 600,000 cycles suggested by the model of Tilly and Moss [22]. Based on this stress range and minimum applied load, the calculated maximum applied loads were 38 kN for the unstrengthened control beam and 64 kN for the two strengthened beams. In the fatigue tests, all the specimens were loaded at a rate of 1.7 Hz. This frequency is in the same range as the frequencies of vehicle loads on bridge decks [23]. The fatigue tests were performed under load control. In the first cycle, the load was monotonically applied in order to monitor the cyclic load damage and cracking pattern. Thereafter, a sine wave load was applied. The tests were terminated after 600,000 fatigue life cycles.

For photometric strain measurement, the servo/hydraulic load frame was controlled by the ARAMIS package, which made it possible to link each recorded image with the corresponding load level in the first full cycle, or the corresponding maximum and minimum load levels in subsequent cycles. Consequently, the strains and displacements determined for cycles other than the first represent the ranges of strains and displacements between maximum and minimum loads.

During the fatigue test, the ARAMIS system was used to record images over the course of the first full cycle as the load was increased from zero (when the reference image was acquired). The specimen was then held in place without being moved to ensure that the measured deformations could be compared between cycles. Additional images were recorded during the 100,000th, 200,000th, 300,000th, 400,000th, 500,000th and 600,000th load

cycles. Two images were acquired for each of these cycles, one at the minimum load (which was used as the reference image for that cycle) and one at the maximum load.

5. Experimental results

5.1 Deflection

The beam's deflection is its vertical displacement at mid-span. The vertical displacement at any point on the beam's surface is readily obtained from the displacement field for any given load level or cycle during the fatigue test. The vertical displacements obtained by DIC at a point close to the bottom of the specimen beam at the mid-span (indicated by square symbols) are plotted alongside the values measured using an LVDT (indicated by solid lines) in Fig. 3, as functions of the vertical load applied during the ascending and descending arms of the first cycle. The DIC and LVDT values are quite similar, with no pronounced discrepancies in any case. Fig. 4 compares the displacement ranges observed by DIC at a point close to the bottom center of the beam to the stroke range in each cycle. Again, the two measurements are in good agreement, although there is a small discrepancy because the stroke was not measured at exactly the same height as the spot chosen for determination of the vertical displacement by DIC.

These results indicate that the DIC technique used in this study is suitable for measuring the deformations of full scale reinforced concrete members under fatigue loading and gives confidence in the following results.

(a)

(b)

(c)
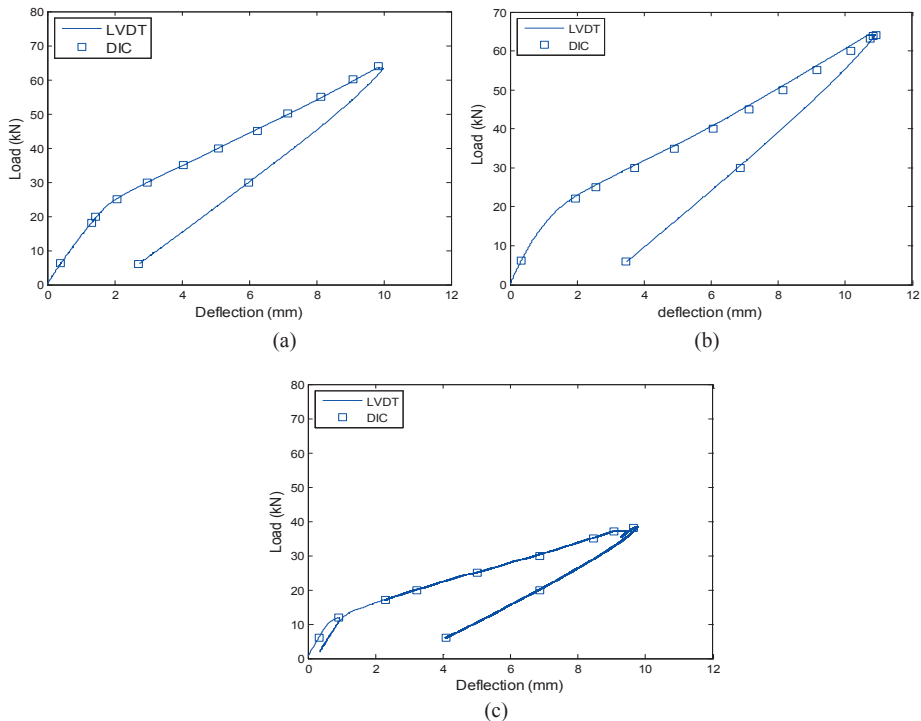
Fig. 3. Load versus midspan deflection during the first cycle for the studied beams: (a) B1-PE1-F; (b) B3-NE1-F; (c) B13-0-F
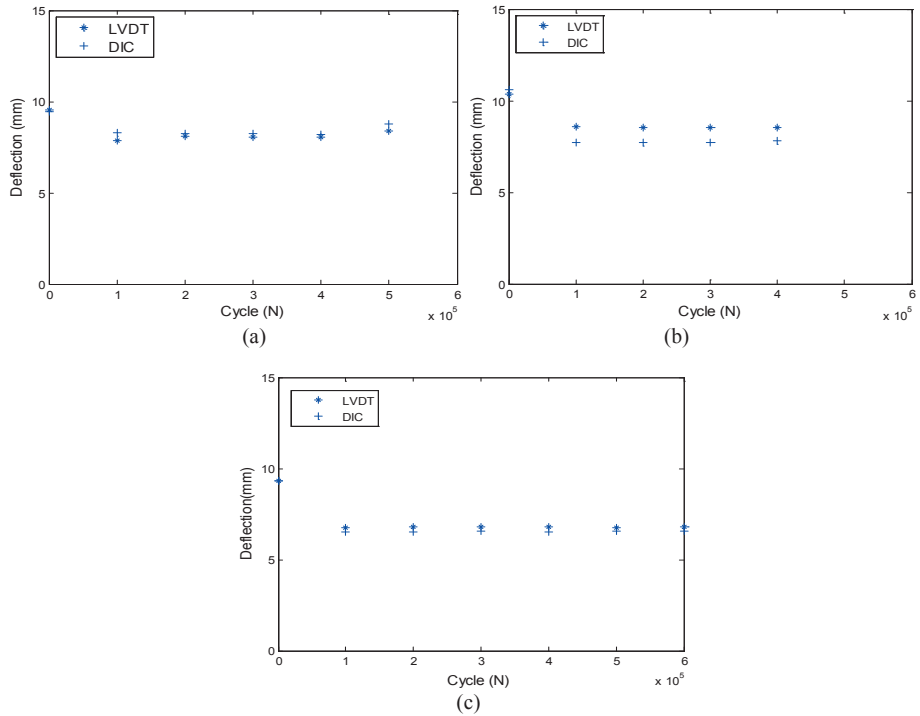
Fig. 4. Midspan deflection range versus the number of load cycles for the beams: (a) B1-PE1-F; (b) B3-NE1-F; (c) B13-0-F

The slope of the load-deflection curve plotted in Fig. 5 shows that before the beam's start cracking, the initial stiffness of the strengthened beams is equal to that of the unstrengthened control beam, indicating that the strengthening materials have little effect under such conditions. However, their influence is readily apparent when comparing the post-cracking stiffness of the strengthened and unstrengthened beams. The plate-strengthened beam was appreciably stiffer than the NSM-bar strengthened beam. Fig. 6 shows that the deflection (stroke) ranges for all beams during the first cycle were greater than those during subsequent cycles because relatively large amounts of energy were dissipated by crack initiation during the first cycle but not during later cycles. The reinforcing steel bars in the EBR plate-strengthened beam ruptured after 456,213 cycles while those in the NSM bar-strengthened beam ruptured after 408,094 cycles. Before the rupture of the reinforcing bars, the deflection ranges were almost constant. After rupture, the CFRP reinforcement continued to resist the applied fatigue load and the deflection range increased gradually until the strengthening failed after 520,733 cycles for the beam strengthened with EBR plate B1-PE1-F and 437,222 cycles for the NSM bar-strengthened beam B3-NE1-F. The unstrengthened beam B13-0SF exhibited a near-constant deflection range until the test was terminated because the specified number of test cycles had been completed.
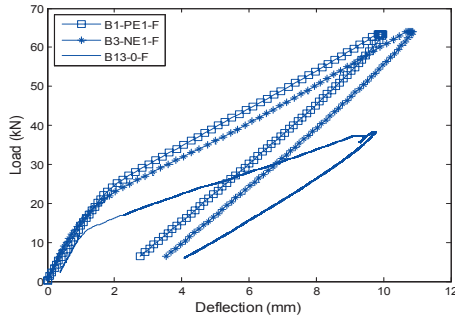
Fig. 5. Load-deflection relationships for the three studied beams during the first cycle.
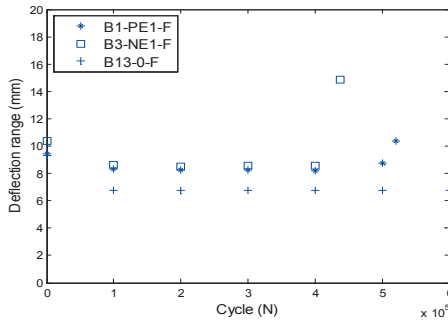
Fig. 6. Midspan deflection range versus the number of load cycles for different beams

5.2 Curvature

DIC is useful for the calculating the vertical displacement in a given region of a specimen as can see in Fig. 7. This capability was used to derive each beam's flexural curvature under different loads during the first cycle by fitting the vertical displacements measured at different positions along the beam's length at constant depth of beam using a second degree polynomial as shown in Fig. 8. The curvature is equal to the second derivative of the fitted second degree polynomial. Fig. 9 shows the evolution of the beam's curvature with increasing load during the first cycle. The curvatures for the strengthened beams are smaller than those for the unstrengthened beam at equal loads. All three beams' curvatures were approximately linear until the maximum load was achieved, and the planar sections remained planar throughout.
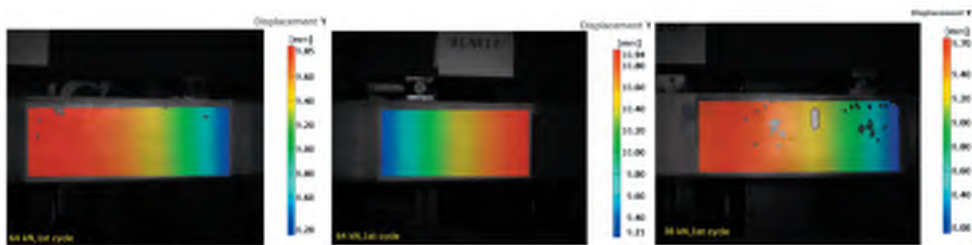
(a)   (b)   (c)

Fig. 7. Displacement field in y direction: (a) B1-PE1-F;(b) B3-NE1-F;(c) B13-0-F

8

(a)

(b)

(c)
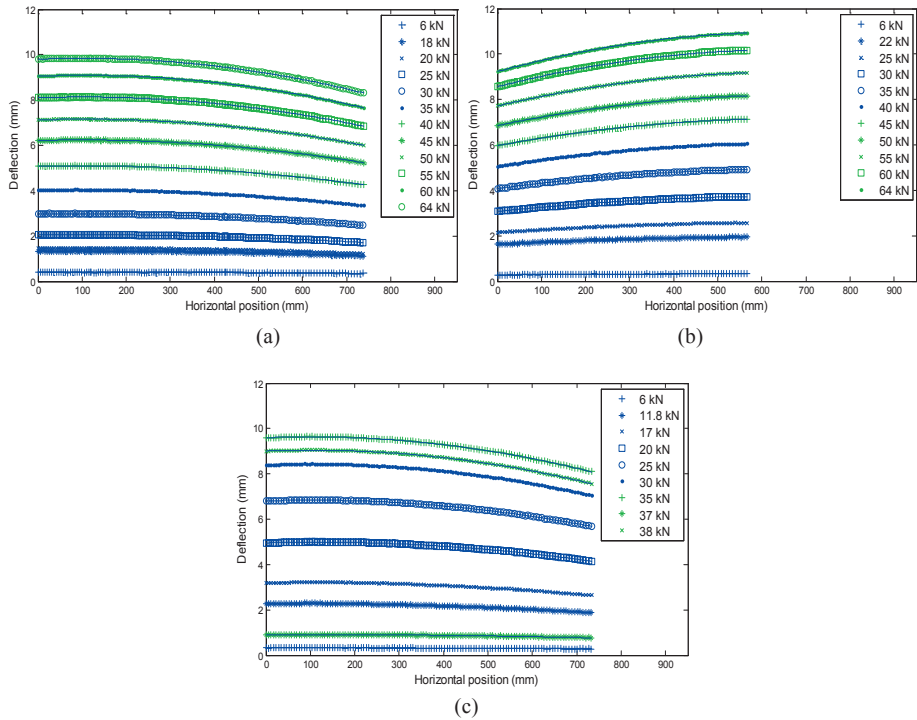
Fig. 8. Vertical displacements measured by DIC (symbols) under different loads as a function of horizontal distance during the first load cycle. Solid lines represent second degree polynomial fits to the DIC data. (a) B1-PE1-F; (b) B3-NE1-F; (c) B13-0-F
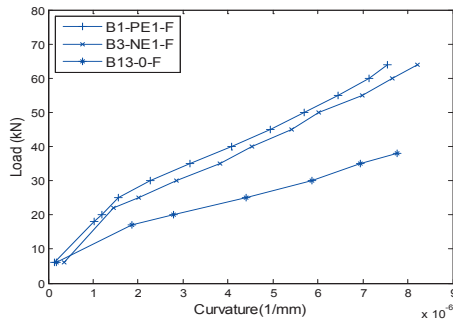
Fig. 9. Load-curvature relationships for the three beams during the first cycle

DIC was also used to measure the range of deflections observed for each beam over the course of a load cycle (i.e. the difference between the deflections under the minimum and maximum loads) at multiple points along the beam's length. As before, polynomial curves were fitted to these measured datapoints, yielding the plots shown in Fig. 10. Fig. 11 shows curvature range for each beam as a function of the number of load cycles. The greatest change in the curvature range occurs during the first cycle, after which the range remains almost steady. After 437,222 cycles, the curvature of the NSM bar-strengthened beam (B3-NE1-F) increases due to steel bar rupture and also that happened for the EBR Plate strengthened.

(a)

(b)

(c)
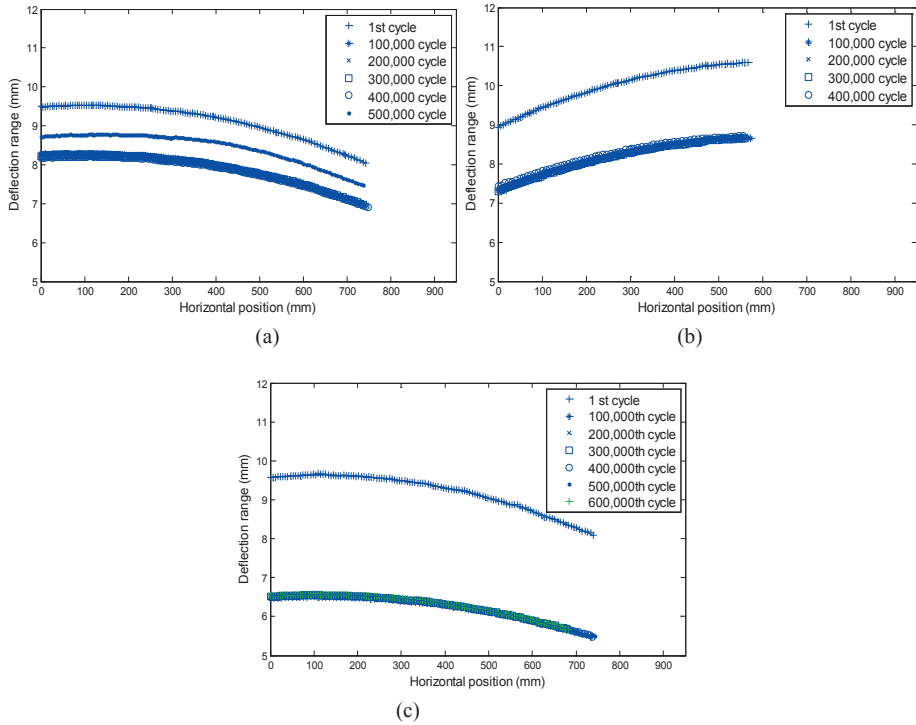
Fig. 10. Vertical displacement ranges measured by DIC at different horizontal positions along each beam's length (symbols). Solid lines represent curves fitted to the DIC data. (a) B1-PE1-F; (b) B3-NE1-F; (c) B13-0-F
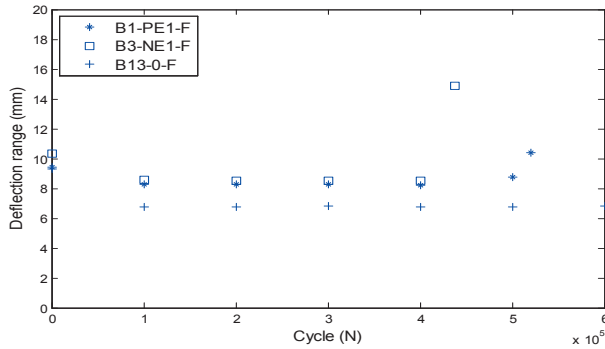
Fig. 11. Curvature ranges for the three beams as functions of the number of load cycles

5.3 Crack measurement

This section describes the use of digital image correlation technique to investigate the beams' cracking patterns and the expansion of cracks during the fatigue tests.

5.3.1 Crack patterns

The major principal strain range distributions over the measurement area during different cycles of the tests were analyzed in order to assess the distribution of cracks over the beams' surfaces. Cracks can be located by studying

the major principal strain contours of the studied surface. The DIC data plotted in Fig. 12 show that the presence of a CFRP laminate influenced the pattern of crack formation: compared to the unstrengthened control, the strengthened beams show a more localized crack distribution within the middle portion of the beams. The average crack spacing in the EBR plate-strengthened beam was greater than that in the NSM bar-strengthened beam. This may be due to the greater contact area between the plate and the concrete compared to that achieved with NSM bars.

(a)
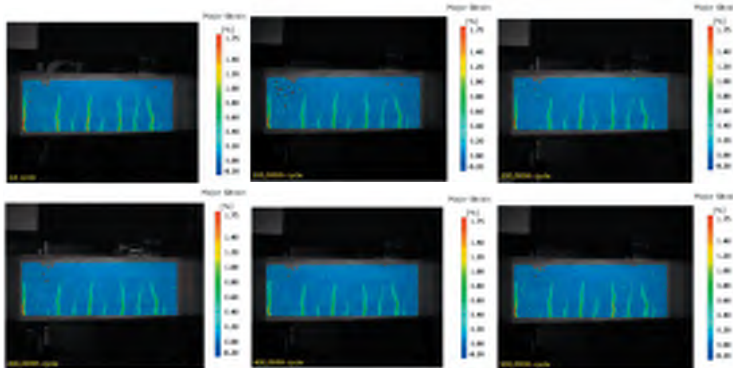
(b)
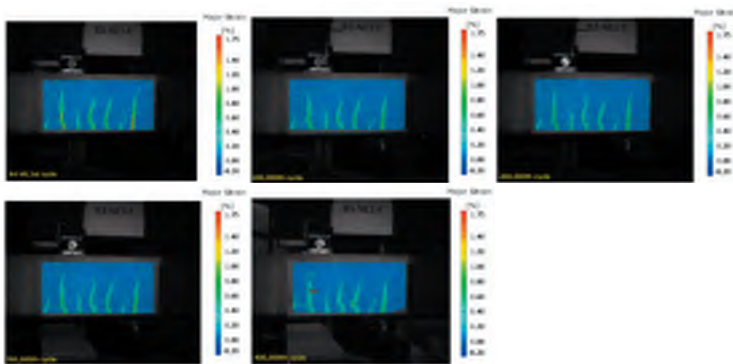
(c)
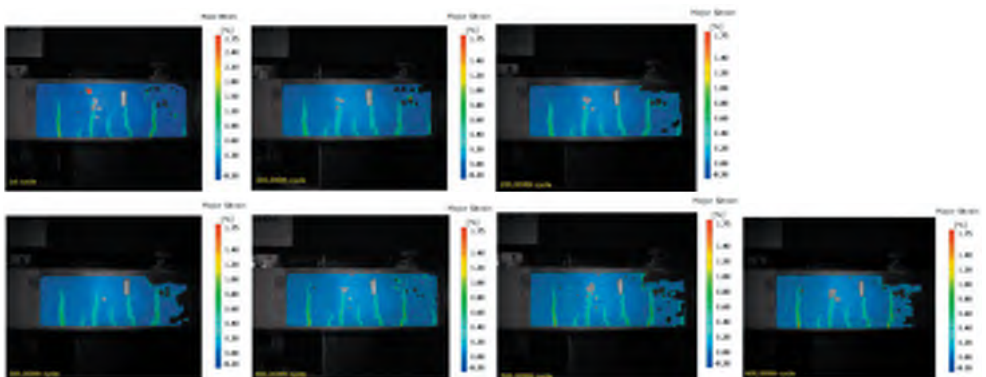
Fig. 12. Evolution of cracks observed by DIC during beam testing: (a) B1-PE1-F; (b) B3-NE1-F; (c) B13-0-F

5.3.2 Crack width

The crack width can be estimated by measuring the distribution of longitudinal displacements along the bottom edge of the beam, at the level of the reinforcing steel bars. The longitudinal component of the displacement field can be measured by creating a section line near the steel bar level. Sudden jumps in this component are due to crack openings, and the magnitude of the jump provides an estimate of the crack's width. Fig. 13 shows the distribution of the longitudinal component of the displacement field for each beam at the level of the reinforcing steel bars as measured by DIC under different loads during the first loading cycle. As the load increases, the crack may expand and give rise to displacement discontinuities. Also, it can be seen from Fig. 13 that the maximum values of longitudinal component of the displacement field were at the right side of figures, which is the right side of image analysis. This due to effect of roller support of the beam at the right side. Fig. 14 shows the evolution of mean crack width as a function of the applied load. Larger crack openings are associated with larger crack spacings, and vice-versa. This result is consistent with standard assumptions about the behavior of reinforced concrete.

A crack bridging effect is observed in strengthened specimens (B1-PE1-f) and (B3-NE1-F): the width ranges for cracks bridged by strengthening materials are much lower than those seen in unstrengthened beams (B13-0-F). It can be seen from Fig. 14 that the crack width range in plate-strengthened beams was lower than that is beams strengthened with NSM bars. This again was attributed to the larger contact surface between beam and strengthening element in the former case.

(a)

(b)

(c)
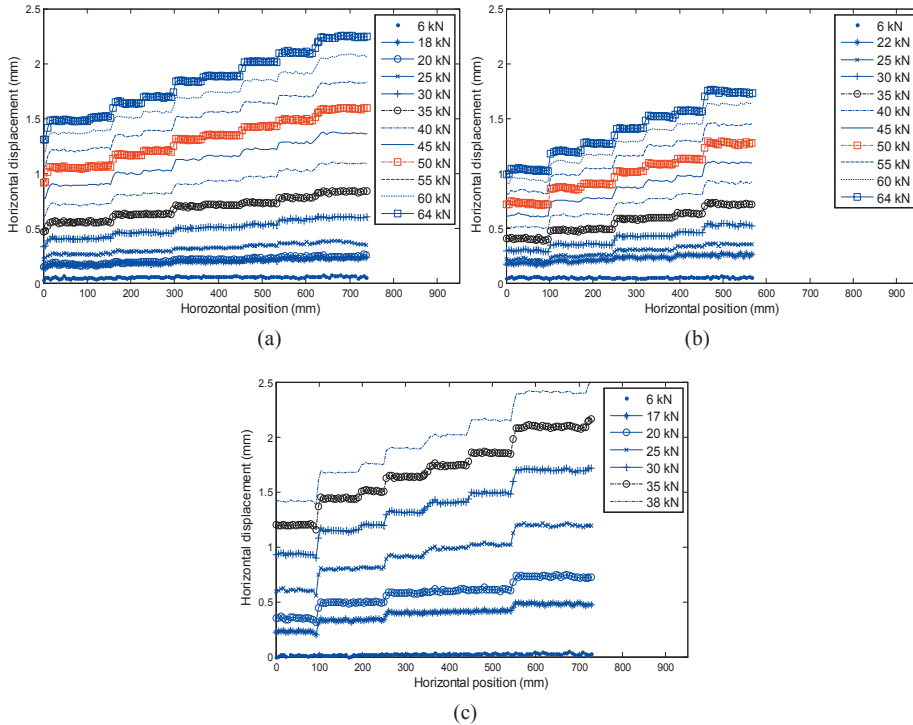
Fig. 13. Horizontal displacements measured by DIC under different loads during the first loading cycle, plotted as a function of horizontal position along the beam's length: (a) B1-PE1-F; (b) B3-NE1-F; (c) B13-0-F
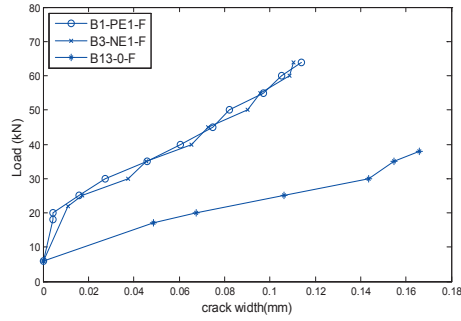
Fig. 14. Loads plotted against mean crack widths during the first load cycle for each beam type

Because the DIC method relies on comparisons between images of the beam under maximum and minimum load during the fatigue tests, it was only possible to measure the longitudinal displacement range along the bottom edge of the beam at the level of the reinforcing steel bars, as shown in Fig.15 and Fig. 16. As expected the displacement ranges in the first cycle were greater than in subsequent cycles because most of the cracks formed during the first cycle.

Fig. 17 plots the mean crack width range for each beam type as a function of the number of load cycles. The crack width ranges for all beams during the first cycle were higher than during subsequent cycles because all of the observed cracks were initiated during the first cycle, so the difference between the crack widths at the maximum and minimum loads was very close to the total width of the crack under the maximum load, or equal to the total width for cracks that did not form under the minimum load of 6 kN. In the later cycles, the cracks had non-zero widths in the initial state (i.e. when the beam was under the minimum load), so the measured range of crack widths was lower. The crack width range of the EBR plate-strengthened beam remained constant during subsequent cycles until its reinforcing steel bars ruptured after 456,213 cycles, after which the crack width range increased gradually. Unfortunately, no DIC data were recorded when the beam failed (on cycle 520,733) because this occurred outside the planned measurement period. The mean crack width range in the NSM bar-strengthened beam also remained roughly constant until DIC recording was halted after 400,000 cycles. The reinforcing steel bars subsequently ruptured on the 408,094[th] cycle and failure occurred on the 437,222[th] cycle. The mean crack width range for the unstrengthened beam remained almost constant throughout the test until it was terminated after 600,000 cycles.

(a)   (b)
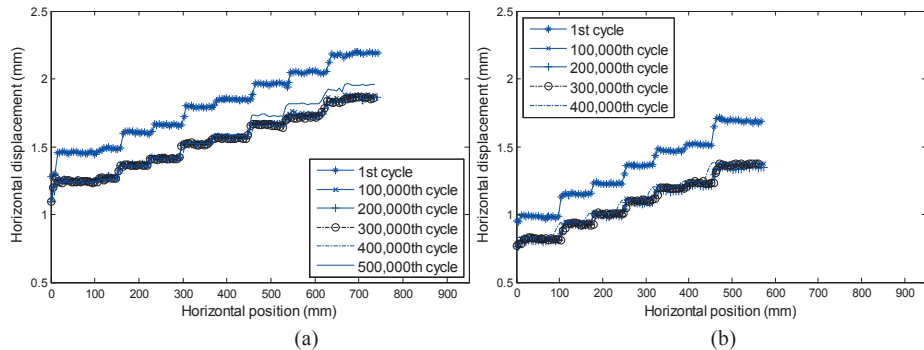
Fig. 15. Horizontal displacement range measured by DIC versus horizontal distance along the beam: (a) B1-PE1-F; (b) B3-NE1-F

13
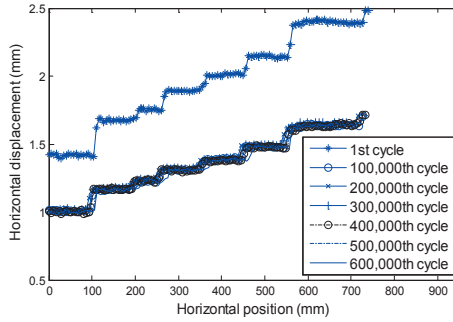
Fig. 16. Horizontal displacement range measured by DIC versus horizontal distance along the beam B13-0-F
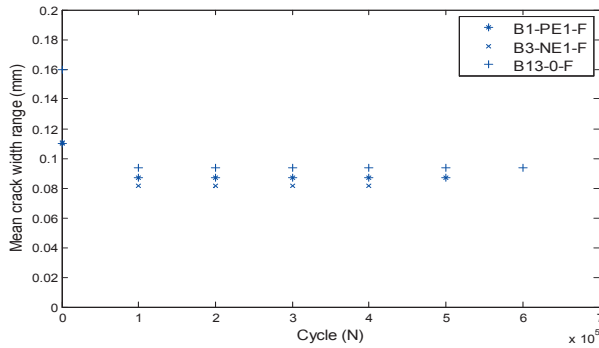
Fig. 17. Crack width range as a function of the load cycle number for each beam

5.3.3 Crack height

The crack height as a function of the cycle number was also estimated from the displacement fields and is presented in Fig. 19. The method used to determine crack height was based on color post-processing of the DIC images as shown in Fig. 18. Fig. 19 indicates that the cracks did not propagate during the test in any of the beams. For comparative purposes, mean crack heights were computed for all of the recorded images and plotted against the cycle number as shown in Fig. 20. The shallowest cracks occurred in the EBR plate-strengthened beam. Even though the reinforcing steel bars of this beam ruptured after 456,213 cycles, the crack height remained constant during the fatigue test after the first cycle.
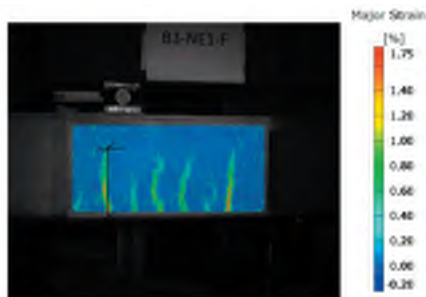
Fig. 18. Evolution of crack height
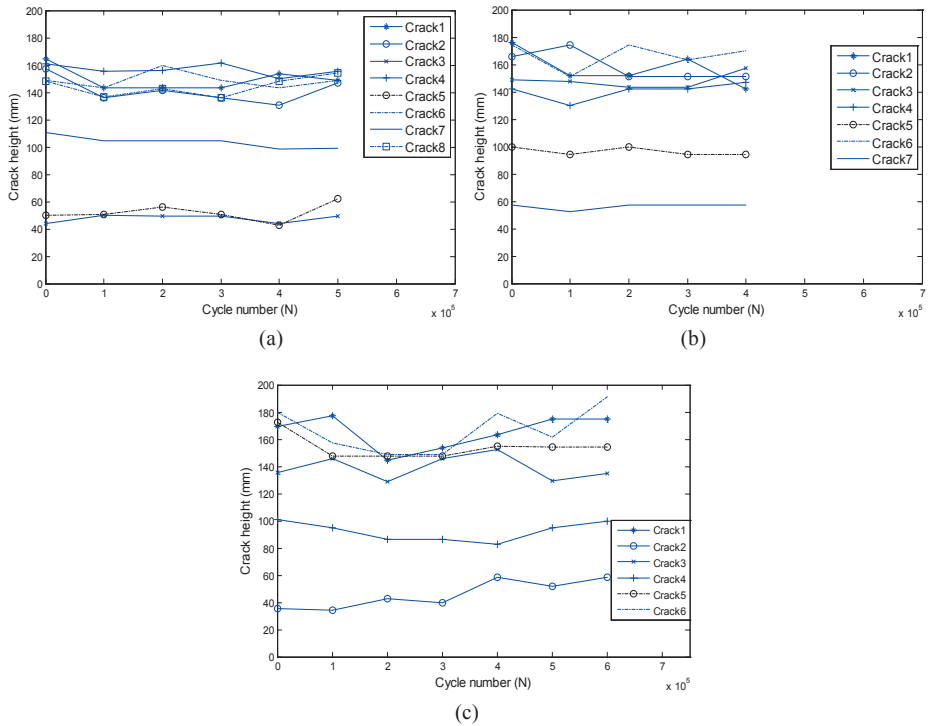
Fig. 19. Crack height as a function of the load cycle number for each beam: (a) B1-PE1-F; (b) B3-NE1-F; (c) B13-0-F
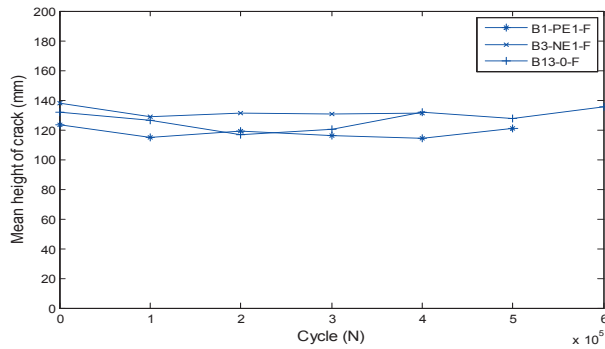
Fig. 20. Mean crack height as a function of the load cycle number for each beam.

6. Conclusions

Fatigue tests on unstrengthened and CFRP-strengthened reinforced concrete beams have shown that:

- The digital image correlation (DIC) technique enables straightforward crack detection and can be used to measure the actual mechanical behavior of a full scale reinforced concrete beam under monotonic and fatigue load.

- The advantage of DIC is that it can measure crack opening and displacement at every point within the studied area of the beam's surface along the beam simultaneously. This is not possible when using conventional experimental sensors because it is impossible to predict in advance exactly how the cracks will be distributed.

- Displacement fields derived from the DIC data provided accurate data on the deflection and curvature of the strengthened and unstrengthened beams. Mid-span deflections measured using DIC were in good agreement with values measured by LVDT sensors under monotonic loading during the first load cycle and during fatigue testing.

-The use of CFRP strengthening materials increased the stiffness of strengthened beams relative to their unstrengthened counterparts because the CFRP systems bridged cracks when they formed.

- EBR plate-strengthened beams were appreciably stiffer than NSM bar-strengthened beams, having lower crack widths and heights, and greater crack spacings.

- The curvatures of the all beams were approximately linear up to maximum load and the planar sections remained planar throughout the tests.

- The greatest change in the curvature range occurs during the first cycle because most of cracks growth and development of new cracks were both rapid during the first loading cycle but did not change appreciably in subsequent cycles until the tensile reinforcing steel bars ruptured.

- Because there was no discernible change in crack width or height before the steel bars of the strengthened beams ruptured, it is assumed that strengthened beams will generally fail due to fatigue of the reinforcing bars.

References

[1] Meier U, Deuring M, Meier H, Schwegler G. Strengthening of Structures with CFRP Laminates: Research and Applications in Switzerland 1992:228-36.
[2] Heffernan P, Erki M. Fatigue behavior of reinforced concrete beams strengthened with carbon fiber reinforced plastic laminates. J Composite Constr 2004;8:132-40.
[3] Masoud S, Soudki K, Topper T. CFRP-strengthened and corroded RC beams under monotonic and fatigue loads. J Composite Constr 2001;5:228-36.
[4] Papakonstantinou CG, Petrou MF, Harries KA. Fatigue behavior of RC beams strengthened with GFRP sheets. J Composite Constr 2001;5:246-53.
[5] Aidoo J, Harries KA, Petrou MF. Full-scale experimental investigation of repair of reinforced concrete interstate bridge using CFRP materials. J Bridge Eng 2006;11:350-8.
[6] Wahab N, Soudki KA, Topper T. Experimental investigation of bond fatigue behavior of concrete beams strengthened with NSM prestressed CFRP rods. J Composite Constr 2012;16:684-92.
[7] Al-Rousan R, Issa M. Fatigue performance of reinforced concrete beams strengthened with CFRP sheets. Constr Build Mater 2011;25:3520-9.
[8] Dong J, Wang Q, Guan Z. Structural behaviour of RC beams externally strengthened with FRP sheets under fatigue and monotonic loading. Eng Struct 2012;41:24-33.
[9] Destrebecq J, Toussaint E, Ferrier E. Analysis of cracks and deformations in a full scale reinforced concrete beam using a digital image correlation technique. Exp Mech 2011;51:879-90.
[10] Corr D, Accardi M, Graham-Brady L, Shah S. Digital image correlation analysis of interfacial debonding properties and fracture behavior in concrete. Eng Fract Mech 2007;74:109-21.
[11] Carloni C, Subramaniam KV, Savoia M, Mazzotti C. Experimental determination of FRP–concrete cohesive interface properties under fatigue loading. Composite Structures 2012;94:1288-96.

[12] Muller M, Toussaint E, Destrebecq J, Grédiac M. Experimental and numerical study of reinforced concrete specimens strengthened with composite plates. Composites Part A: Applied Science and Manufacturing 2004;35:885-93.

[13] Küntz M, Jolin M, Bastien J, Perez F, Hild F. Digital image correlation analysis of crack behavior in a reinforced concrete beam during a load test. Canadian Journal of Civil Engineering 2006;33:1418-25.

[14] Lecompte D, Vantomme J, Sol H. Crack detection in a concrete beam using two different camera techniques. Structural Health Monitoring 2006;5:59-68.

[15] Gencturk B, Hossain K, Kapadia A, Labib E, Mo Y. Use of digital image correlation technique in full-scale testing of prestressed concrete structures. Measurement 2014;47:505-15.

[16] Täljsten B. Strengthening of beams by plate bonding. J Mater Civ Eng 1997;9:206-12.

[17] Gencturk B, Hossain K, Kapadia A, Labib E, Mo Y. Use of digital image correlation technique in full-scale testing of prestressed concrete structures. Measurement 2014;47:505-15.

[18] Pickerd V. . Optimisation and Validation of the ARAMIS Digital Image Correlation System for Use in Large-scale High-strain-rate Events 2013.

[19] Shah S, Kishen JC. Fracture properties of concrete–concrete interfaces using digital image correlation. Exp Mech 2011;51:303-13.

[20] ARAMIS. user manual–Software – v6.0.2-6, 2009.

[21] Xavier J, de Jesus A, Morais J, Pinto J. Stereovision measurements on evaluating the modulus of elasticity of wood by compression tests parallel to the grain. Constr Build Mater 2012;26:207-15.

[22] Barnes RA, Mays GC. Fatigue performance of concrete beams strengthened with CFRP plates. J Composite Constr 1999;3:63-72.

[23] Masoud S, Soudki K, Topper T. Postrepair fatigue performance of FRP-repaired corroded RC beams: experimental and analytical investigation. J Composite Constr 2005;9:441-9.

PAPER IV

"Fatigue analysis of reinforced concrete beams strengthened in flexure using CFRP"

BY
Mohammed Mahal, Björn Täljsten and Thomas Blanksvärd

Fatigue analysis of RC beams strengthened in flexure using CFRP

M. Mahal[a, b,*], B. Täljsten[a, c], T. Blanksvärd[a]

[a]Department of Civil, Environmental and Natural resources engineering, Luleå University of Technology, Luleå, Sweden

[b]Department of Civil Engineering, Mosul University, Mosul, Iraq

[c]Sto Scandinavia AB, Sweden

*corresponding author (Mohammed S. Mahal):
    Email: mohammed.salih@ltu.se ; mohammed.mahal@uomosul.edu.iq
    Tel: 0046 720027539
    Fax: 0920-49 13 99

Abstract

The increasing use of Fiber Reinforced Polymers (FRP) to repair, strengthen or upgrade reinforced concrete (RC) structural elements means that there is a need to develop analytical methods for analyzing the behavior of strengthened members under fatigue loading. This paper describes an analytical model for simulating the fatigue behavior of RC beams strengthened with Carbon Fiber Reinforced Polymer (CFRP). Fatigue calculations are performed using a lamellar model that considers the fatigue behavior of the RC and CFRP strengthening materials during loading. The model's output is compared to experimental data for four CFRP-strengthened beams, showing that the new model accurately predicted the deflection and strain of each one. In addition, various models for predicting the fatigue life of CFRP-strengthened RC beams were tested and a model capable of providing conservative fatigue life estimates was identified.

Keywords: Analysis, fatigue, reinforced concrete, strengthening, fiber reinforced polymer

1. Introduction

In recent decades, fiber-reinforced polymer composites have been used successfully to strengthen diverse concrete structural elements. This is partly because of the desirable material properties of the reinforcing fibers: they exhibit high stiffness and strength, are lightweight, do not corrode, are easily installed, and can be obtained in almost any size or length that may be required. The design and analysis of durable concrete structures requires the consideration of all possible deterioration mechanisms, including both time- and cycle-dependent effects. Fatigue loading is one of these effects and can have significant effects on overall structural performance.

The fatigue behavior of RC beams strengthened with CFRP has received relatively little attention compared to their behavior under static loading conditions. Recent publications have described the behavior of RC beams strengthened with FRP materials under fatigue loading [1-4]. In the last of these reports, it was concluded that strengthened beams tolerated fatigue loading significantly better than unstrengthened controls over the same load ranges. It was also noted that the mechanical properties of the beams' components were modified by fatigue loading, which caused a permanent increase in strain and reduced stiffness.

The failure of CFRP-strengthened RC members in flexure appears to be governed by the fatigue rupture of the internal reinforcement. Even under high initial compressive stresses that might be expected to fatigue the concrete, reinforced members fail systematically due to the

1

brittle fatigue fracture of the tensile steel reinforcing bars [5]. This is due to concrete's high capacity for stress redistribution [6]. It is therefore recommended [2] that the stress ranges of the rebars used in strengthened members should not exceed those permitted for unstrengthened RC members.

Theoretical models based on a variety of approaches have been developed to predict the effects of fatigue on strengthened RC beams. Most of the models presented in the literature are based on S-N curves and the static stress state [7-9]. This approach focuses on the number of cycles to failure without considering the redistribution process or the evolution of strain, and thus cannot adequately describe the influence of fatigue on the response of the RC.

Alternative theoretical models are based on damage theory, in which it is assumed that the rate of damage accumulation is independent of the level of applied stress. However, this cannot be true because the material response is greatly influenced by the magnitude of the applied load. Additionally, the assumption of linear damage in this theory ignores the effects of loading sequence. Predictions generated using this model diverged significantly from experimental results [10-12].

Finally, models based on the lamellar technique account for the fatigue of strengthened reinforced concrete beams by dividing the member's cross section into a series of discrete lamellae or segments, each of which is described separately using a uniaxial fatigue stress model. This approach produces accurate predictions, is easy to understand, and has facilitated analyses of the development of stresses and strains during the fatigue life of various structures and predictions of their ultimate failure modes based on their capacity for stress redistribution [13,14].

This work describes a sectional lamellar model for the analysis of CFRP-strengthened reinforced concrete beams under fatigue loading. The model is based on the uniaxial fatigue properties of the concrete and CFRP material under fatigue loading as well as the known stress and strain responses of concrete, CFRP and steel under static loading. The analytical results are compared to experimental data generated by the authors. The model is simple and accurately describes the overall response of strengthened reinforced concrete beams as well as the development of stresses and strains during fatigue loading.

2.Fatigue models

The behavior of RC structures subjected to fatigue loading is very complex. The mechanical and deformation properties of RC beam components change significantly as the time spend under fatigue loading increases, generating residual strains. Multiple analytical models have been developed to predict the residual strain of reinforced concrete beams during fatigue loading [13-15]. This section briefly describes the analytical model used to estimate the fatigue properties of strengthened RC beam components used in this work.

2.1. Fatigue of concrete

Cyclic loading of concrete causes an increase in its strain as the number of cycles increases, i.e. it creates residual strains that resemble creep. The residual strain of concrete in the compression zone under cyclic loading was found to contribute significantly to increases in the deflection of loaded beams [16]. The effects of cyclic residual strain are accounted for using an effective cycle-dependent secant modulus of the elasticity of concrete, $E_{e,N}$ [17]:

$$E_{e,N} = \frac{\sigma_{max}}{\varepsilon_{c_{N,max}}} \tag{1}$$

Where N is the number of cycles, σ_{max} is the average stress in the concrete at the maximum load level and $\varepsilon_{N,max}$ is the total maximum strain at any time. Holmen [18] proposed that the total maximum strain at any time after a given number of cycles is the sum of two components: the elastic strain, ε_{ce}, and the evolution of the concrete compressive strain (ε_{c_N}) with the number of loading cycles (N) ,knowing the cyclic creep strain:

$$\varepsilon_{c_{N,max}} = \varepsilon_{ce} + \varepsilon_{c_N} \tag{2}$$

The evolution of the concrete compressive strain ε_{c_N} with the number of loading cycles (N) is defined as a function of the mean stress (σ_c^m), stress range (σ_c^r) ,number of cycles (N), loading cycle frequency (f) and nominal compressive strength of concrete (f_c') ,as described in Eq. (3) [19]:

$$\varepsilon_{c_N} = 8.417 \times 10^{-6} \cdot \left(\frac{\sigma_c^m}{f_c}\right) \cdot \left[\left(\frac{N}{f}\right)^{\frac{1}{3}} + 3.87 \cdot \left(\frac{\sigma_c^r}{f_c}\right) \cdot \left(\frac{N}{9.75}\right)^{\frac{1}{3}}\right] \tag{3}$$

Where the mean stress and the stress range are calculated from the maximum (σ_{max})and minimum (σ_{min}) compressive stress applied to the concrete:

$$\sigma_c^m = (\sigma_{max} + \sigma_{min})/2 \tag{4}$$

$$\sigma_c^r = (\sigma_{max} - \sigma_{min}) \tag{5}$$

Knowing the total maximum strain, the cycle-dependent secant modulus of elasticity for concrete in compression ($E_{e,N}$) after N fatigue cycles can be computed using Eq.(1). Concrete under tension is assumed to have no significant tensile strength during cyclic fatigue calculations.

2.2. Fatigue of steel

For most civil engineering applications involving reinforced concrete subject to high cyclic fatigue, only the fatigue of the reinforcing steel in the elastic range is taken into account. The elastic fatigue mechanism is responsible for the fracture of the reinforcing steel because the maximum stress during the fatigue life is below the yield point [20]. Fatigue failure of reinforcing steel is caused by microcracking initiated at a stress concentration on the bar surface. The crack gradually propagates as the stress continues to cycle. Sudden fracture occurs when a crack reaches a critical length at which its propagation becomes unstable. The experimental results of Barsom and Rolfe [21] suggest that the modulus of elasticity of the steel remains unchanged until just before the point at which it fails due to high cycle fatigue. It is therefore reasonable to assume that no degradation in residual capacity (strength and stiffness) occurs when reinforcing steel is subjected to service fatigue loading conditions.

2.3. Fatigue of CFRP and epoxy

The fatigue performance of FRP composite materials depends on the composition of the matrix and, to some extent, on the type of fiber used [22]. Ferrier et al. [19] found that the decrease in ultimate strength can be neglected in the case of carbon/epoxy composites and those cyclic loading causes the stiffness of FRP laminates to degrade according to the following expression:

$$E_{f_N} = m - nlog(N) \tag{6}$$

Where E_{f_N} is the Young's modulus at cycle (N), m is the initial Young's modulus, and n is a constant with a value of 1100. The epoxy between the CFRP laminates and the concrete is

assumed to be stiff and not influenced by fatigue loading. This is a reasonable assumption for beams in which failure is initiated in high moment zones, where shear stresses in the epoxy are low [13]. In keeping with this assumption, negligible slippage or debonding between the concrete and CFRP plate was observed before the rupture of the steel bars in the experimental studies presented herein.

3. Material Models

The material model used to analyze the behavior of concrete in compression under fatigue loading is that of Warner [23], which accounts for the effect of the concrete's modulus of elasticity in the stress-strain relationship:

$$f = \gamma E + (3 - 2\gamma)E^2 + (\gamma - 2)E^3 \tag{7}$$

Where

$$f = f_c/\acute{f}_c$$

$$E = \varepsilon_c/\varepsilon_{cu}$$

$$\gamma = E_{e,N} \cdot \varepsilon_{cu}/\acute{f}_c$$

Here, f is the normalized concrete stress, E the normalized strain, γ a dimensionless quantity defining the shape of the concrete's stress-strain relationship, $E_{e,N}$ the modulus of elasticity of concrete in the nth load cycle, $\acute{f}_c$ the compressive strength of concrete, f_c the stress in concrete, ε_c the strain in the concrete, and ε_{cu} is the ultimate concrete strain. The concrete's strength is taken to be $0.85\,\acute{f}_c$; the factor of 0.85 is included to account for the difference between concrete in a test cube and concrete in a reinforced structure, which stem from differences in geometry, steel reinforcement, load type, rate of loading, and variations in concrete compaction. The reinforcing steel is assumed to exhibit linear elastic-perfect plastic behavior; their loading and unloading moduli are both assumed to be equal to its initial elastic modulus. The CFRP material is assumed to exhibit linear brittle failure with the same modulus of elasticity (E_{f_N}) during both unloading and reloading.

4. Predicting the Fatigue of CFRP-Strengthened Reinforced Beams

The fatigue analyses presented in this paper are based on the lamellar technique in which the cross section of the beam is divided into a series of discrete lamellae or segments (see Fig. 1).The fatigue responses of the beams are predicted by calculating the moment-curvature response for the beam under an axial load at equilibrium during each load cycle. The moment-curvature response is obtained by incrementally increasing the beam's curvature and solving for the corresponding value of the applied load. For a given curvature, the moment–curvature response of the cross-section (i.e. the slope of the strain distribution profile) during each load cycle can be obtained by using an iterative process in which the position of the neutral axis for a given strain distribution is adjusted so as to maintain the horizontal force equilibrium within the cross-section of the beam. Assuming that the planar sections remain planar after bending, the location of the neutral axis and the strains in each individual segment are functions of the strain in the topmost segment, $\varepsilon_{top,N}$, and the curvature, φ. The stresses in each segment are calculated from the corresponding strains using the constitutive relationships mentioned earlier. The modulus of elasticity of the concrete and CFRP plate segments are updated in

each fatigue cycle. The concrete, CFRP plate, and reinforcing steel within each segment will experience different stresses because each material has a different modulus.

The resultant axial force and the bending moment are obtained by summing the results for all of the segments in the cross-section according to the following equations

$$\sum_{i=1}^{m} \sigma_i A_i + Tol = F = 0 \tag{8}$$

$$\sum_{i=1}^{m} \sigma_i A_i y_i + Tol = M \tag{9}$$

where F is the axial load; M the major bending moment along the beam; σ_i the longitudinal stress at the centroid of fiber i; A_i the area of fiber i; y_i the distance between the centroid of fiber i and the top of the section; m the total number of segments in the cross-section, and Tol is the maximum tolerable deviation between the calculated force and moment and the externally applied axial load and moment at equilibrium.
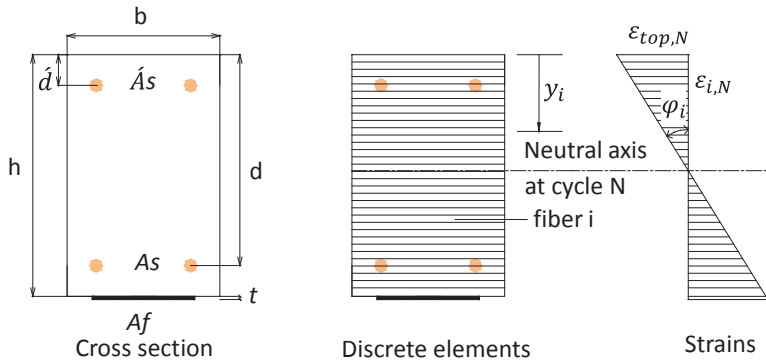
Fig. 1. The cross-sectional discretization of a reinforced concrete member strengthened with a CFRP plate.

The moment-curvature calculations for a given load cycle are halted once the number of curvature increments is high enough to resist the maximum applied load.
 Once the moment curvature relationship of the cross section has been determined at the end of a load cycle, the load-deflection response of the beam is calculated using a well-known expression from beam bending theory and the flexural stiffness (EI) obtained from the slope of the moment-curvature curve (Fig. 2)

$$(EI)_N = \frac{\Delta M}{\Delta \varphi} \tag{10}$$

Where $(EI)_N$ is the flexural beam stiffness after N cycles while ΔM and $\Delta \varphi$ are the moment and curvature differences between two load stages during cycle, respectively.
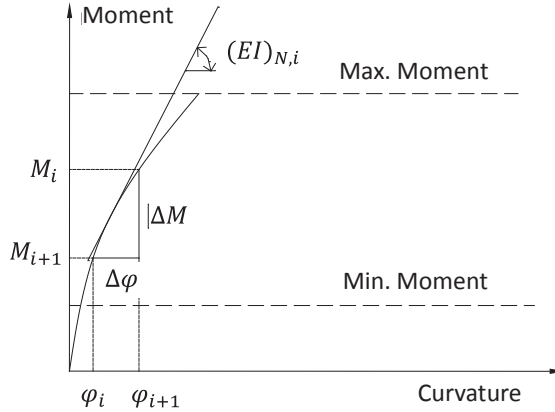
Fig. 2. Calculation of flexural stiffness from the moment-curvature relationship

The main assumptions and limitations of the proposed model are:
1-The strain in each fiber is assumed to be constant over the thickness of a single layer.
2- Negligible contribution of the tensile strength from concrete.
3- Perfect bonding is assumed between concrete and other materials (steel reinforcement and CFRP laminates).
4- The final failure of the structure is governed by the rupture of the first steel reinforcement.
5- Planar sections are assumed to remain planar after bending.
6- The concrete stress-strain behavior implemented in this model represents the behavior of conventional concrete.

5. Fatigue life

A fatigue prediction model should accurately describe the fatigue response of a strengthened beam and also predict the number of cycles to failure. Existing fatigue behavior models are discussed in the previous sections. Since the fatigue life of a CFRP composite is generally greater than that of the reinforcing steel [24], the fatigue life of reinforced concrete beams (whether strengthened or un-strengthened) can be estimated easily using existing steel fatigue life prediction models if the structural members are designed to be under-reinforced [25,26]. Since no delamination occurred before the fatigue fracture of the steel reinforcement, the fatigue life of strengthened beams depends on steel bar rupture. This is assumed to be equal to the life of crack initiation in the steel rebar plus the life during crack growth. In order to produce fatigue life models for strengthened reinforced concrete beams, S-N data for sheets, laminate FRP strengthened beams and NSM-strengthened beams were collected from the literature as shown in Fig. 3 [1-4,8,14,27-34] The figure only includes data for beams that failed by steel bar rupture due to fatigue loading. The stress range (S_r) reported is that experienced by the internal reinforcing tension steel during the first cycle. Fig. 3 shows a regression curve for strengthened beams obtained using the following equation:

$$S_r = 1038.5 - 132.2 \, Log \, N_f \tag{11}$$

where S_r is the stress range of the steel.
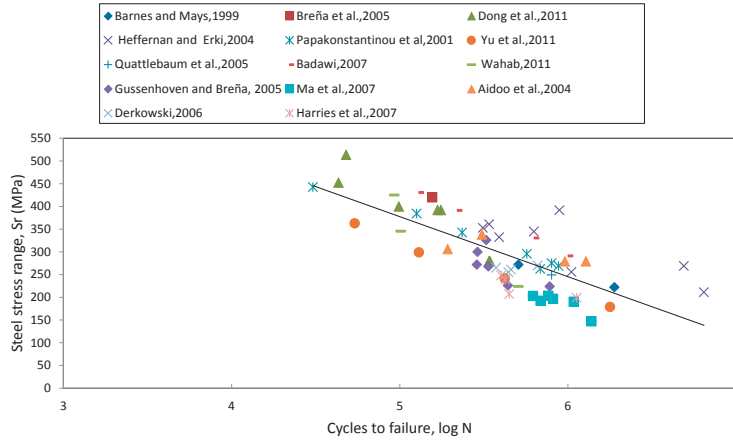
Fig. 3. S-N curve for strengthened reinforced concrete beam

Three established models for estimating the fatigue life of strengthened beams were considered, as shown in Table 1. All three describe the relationship between the reinforcing steel's stress range (S_r) and the number of cycles to failure (N_f) .

Table 1. Fatigue life models.

	Fatigue life model
RC beam ,Tilly and Moss [2]	$S_r{}^9 * N_f = 3.09 * 10^{27}$
RC beam, Model Code [35]	$S_r{}^5 * N_f = 4.0841 * 10^{17}$
Steel under direct tension in air [36,37]	$\log(N_f) = 6.969 - 0.00555 S_r$

6. Model verification

To evaluate the validity of the fatigue model developed in this study, experimental tests were conducted using four CFRP-strengthened RC beams, two strengthened with NSM (Near Surface Mounted) bars and two with traditional plate bonding. One beam of each type was prepared using CFRP with a modulus of elasticity of 200 GPa and the other using CFRP with a modulus of elasticity of 150 GPa. The beams, whose structure is shown in Fig. 4, were 300 mm deep, 200 mm wide and had a span length of 3600mm (with a total beam length of 4000mm). Four steel rebars (Ø = 16 mm) were used as steel reinforcement (two in the tension and two in the compression region) and stirrups (Ø = 10 mm) were installed at a spacing of 75 mm along the beam's span. The average compressive and tensile strengths of the concrete were 71.0 MPa and 4.7 MPa, respectively. The mechanical properties of the steel bars were evaluated in experimental tensile tests. The mean yield strength and modulus of elasticity of the longitudinal steel reinforcement were 578 MPa and 208 GPa, respectively, while those for the stirrups were 533 MPa and 202 GPa, respectively. All of the CFRP strengthening materials were obtained from Sto Scandinavia. The laminates used to strengthen the plate-bonded beams were StoFRP Plate IM (B1-PE1-F; modulus of elasticity = 200 GPa) and StoFRP Plate E (B6-PE2-F; modulus of elasticity = 150 GPa) units, both of which had widths of 143 mm and thicknesses of 1.4 mm. The CFRP bars used to strengthen the NSM bar-strengthened beams were StoFRP BAR IM 10C (B3-NE1-F; modulus of elasticity = 200 GPa)

and StoFRP BAR E 10C (B8-NE2-F; modulus of elasticity = 150 GPa) units. The cross sectional areas of both bar types were 10x10 mm. In the fatigue tests, the specimens were subjected to loads of 6 - 64 kN at a frequency of 1.7 Hz using a four-point loading system.
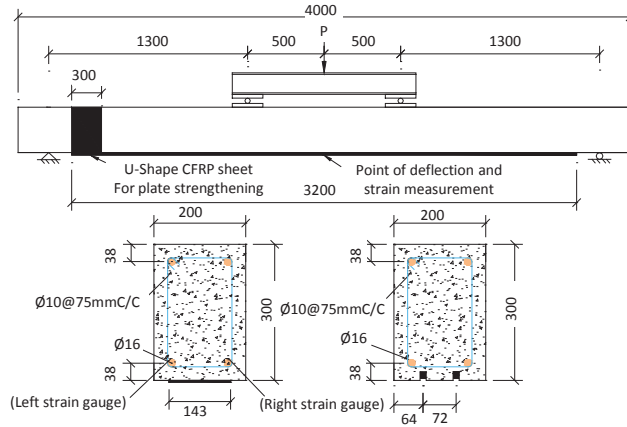
Fig. 4. The dimensions of the beam and the four-point loading system used in the experimental studies (top) and cross sections of the plate- and NSM-strengthened reinforced concrete beams (bottom)

Fig. 5 and Fig.6 show the deflection of the beam as a function of the number of load cycles for all of the tested specimens and compares these experimental results to the predictions of the new fatigue model. The model's output agrees quite well with the experimental data for all of the beams until the rupture of the first steel rebar. However, the deflections predicted for the beams strengthened with NSM bars seem to be slightly lower than those observed experimentally. This could be because the model assumes that the strengthening CFRP is present as a thin layer covering the underside of the beam rather than in near-surface mounted bars, making the real beams less stiff than would be expected according to the model's assumptions. In addition, the model assumes a perfect bond between the concrete and the carbon fiber reinforcement, which may also contribute to the discrepancy.
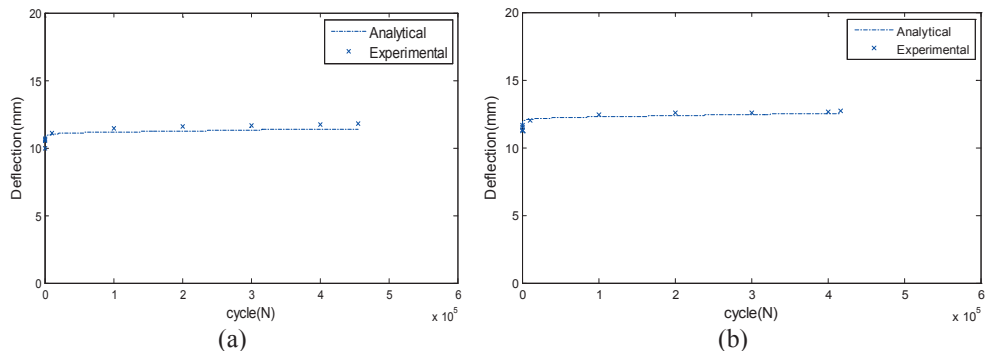
Fig. 5. Mid-span deflection as a function of cycle number: (a) Beam B1-PE1-F; (b) Beam B6-PE2-F
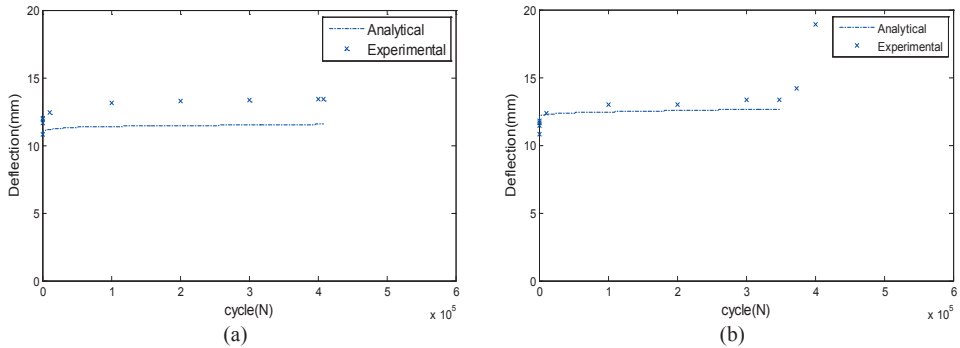
Fig. 6. Mid-span deflection as a function of cycle number: (a) Beam B3-NE1-F; (b) Beam B8-NE2-F

Fig. 7 and Fig. 8 compare the experimental and predicted tensile strains of the internal steel and CFRP. Both strain curves increase rapidly during the initial loading cycles, which are typical for fatigue strain, and then flatten out. The predicted strains are generally in good agreement with the experimental values. As before, the model's predictions deviate relatively strongly from the experimental results for the NSM-strengthened beams because of the failure to account for the effect of the bars' positions.
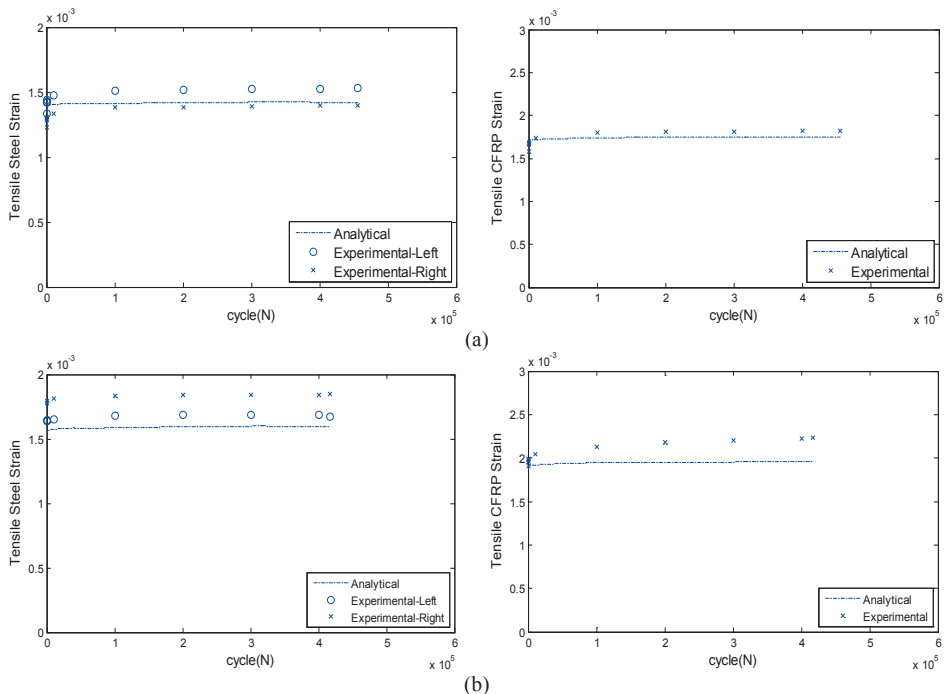
Fig. 7. Tensile strains of the mid-spain steel reinforcement and CFRP strain as a function of cycle number: (a) B1-PE1-F; (b) B6-PE2-F
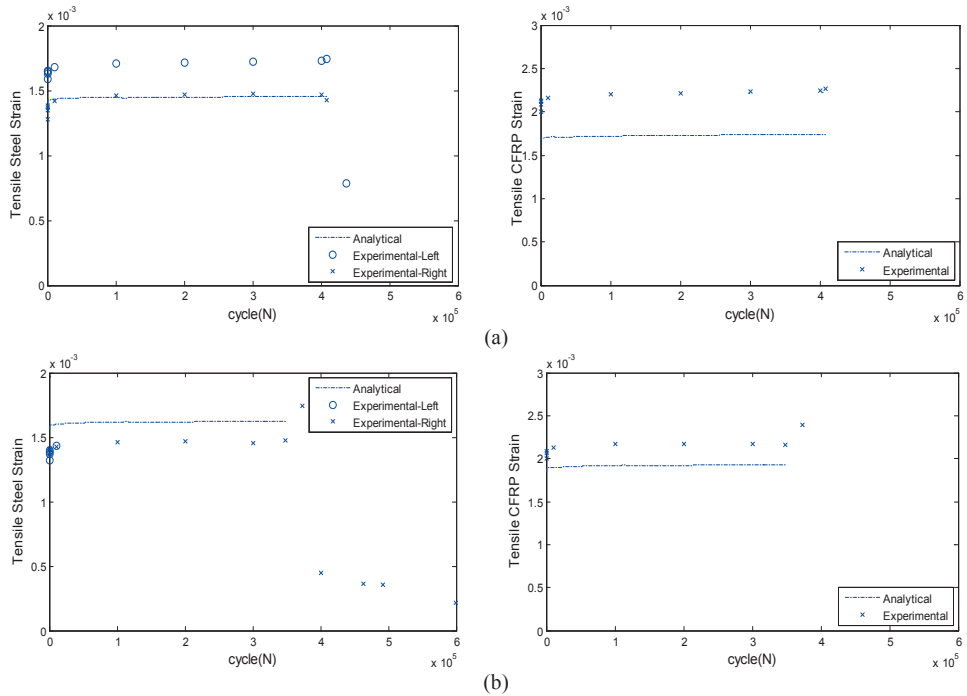
Fig. 8. Tensile strains of the mid-spain steel reinforcement and CFRP strain as a function of cycle number: (a) B3-NE1-F; (b) B8-NE2-F

Table 2 lists the number of load cycles prior to steel rupture for each of the tested beams. These experimental results were compared to the predicted fatigue life values generated by the model presented herein and previously reported models, assuming a steel stress range of 258 MPa (see Table 3). The result obtained using the Helgason and Hanson model provides the most conservative estimate of the beam's life, and is in reasonably good agreement with the experimental fatigue life values of the CFRP-strengthened beams. Conversely, the S-N model developed in this work predicts a much longer fatigue life than was achieved experimentally. This indicates a need to develop an accurate S-N model for strengthened beams under fatigue loads that accounts for the effects of parameters other than the steel stress range such as the presence or absence of shear strengthening, the number of tension steel bars, and the effect of the shear span length.

Table 2. Fatigue life values for the tested beams.

Beam	No. of cycles at 1st steel rupture
B1-PE1-F	456,213
B6-PE2-F	416,866
B3-NE1-F	408,094
B8-NE1-F	348,245

Table 3. Fatigue life values obtained with different S-N models presented in the literature.

	Estimated fatigue life
Strengthened beam model from this work (Eq.11)	801,555
RC beam model of Tilly and Moss [2]	600,000
RC beam model, Model Code [35]	353,986
Helgason and Hanson model for steel under direct tension in air [37]	342,336

Conclusion

An analytical model has been developed to predict the deflection and residual strain of CFRP-strengthened reinforced concrete beams under fatigue loading. The model is constructed using the lamellar approach and is based on the fatigue properties of the concrete and CFRP strengthening material. Its predictions are in good agreement with the results of experimental studies on CFRP-strengthened beams even though it does not consider the impact of different strengthening methods. Consequently, it cannot describe effects arising from the positioning of NSM bars within soffit beams. However, it can be used to study the evolution of stresses and strains during the fatigue lifetime of a strengthened reinforced beam and it is straightforward to determine the parameters of the model by performing static tests on the individual materials that comprise the beam of interest.

Steel fatigue life models are useful for predicting the number of cycles until failure for strengthened reinforced concrete beams because steel fracture is the primary failure mode in beams strengthened using CFRP. Results presented herein indicate that conservative estimates of a strengthened reinforced beam's fatigue life can be obtained using the Helgason and Hanson equation [37] or the equation presented in the 2010 fib Model Code. The S-N model developed in this work, which were based on experimental data taken from the literature, overestimated the fatigue life of the studied beams. This indicates that there is a need to develop a more accurate S-N model for strengthened beams under fatigue load that accounts for parameters other than just the steel stress range.

Acknowledgments

[1] Heffernan P, Erki M. Fatigue behavior of reinforced concrete beams strengthened with carbon fiber reinforced plastic laminates. J.Composite Constr. 2004;8(2):132-40.

[2] Barnes RA, Mays GC. Fatigue performance of concrete beams strengthened with CFRP plates. J.Composite Constr. 1999;3(2):63-72.

[3] Aidoo J, Harries KA, Petrou MF. Fatigue behavior of carbon fiber reinforced polymer-strengthened reinforced concrete bridge girders. J.Composite Constr. 2004;8(6):501-9.

[4] Quattlebaum JB, Harries KA, Petrou MF. Comparison of three flexural retrofit systems under monotonic and fatigue loads. J.Bridge Eng. 2005;10(6):731-40.

[5] Johansson U. Fatigue tests and analysis of reinforced concrete bridge deck models. Trita-BKN.Bulletin 2004;76:1-197.

[6] Zanuy C, Albajar L, De la Fuente P. Sectional analysis of concrete structures under fatigue loading. ACI Struct.J. 2009;106(5).

[7] Mahal M, Blanksvärd T, Täljsten B. Examination at a Material and Structural Level of the Fatigue Life of Beams Strengthened with Mineral or Epoxy Bonded FRPs: The State of the Art. Adv.Struct.Eng. 2013;16(7):1311-28.

[8] Brena SF, Benouaich MA, Kreger ME, Wood SL. Fatigue tests of reinforced concrete beams strengthened using carbon fiber-reinforced polymer composites. ACI Struct.J. 2005;102(2).

[9] Al-Hammoud R, Soudki K, Topper TH. Fatigue flexural behavior of corroded reinforced concrete beams repaired with CFRP sheets. J.Composite Constr. 2010;15(1):42-51.

[10] Lin R, Huang P, Zhao C, Guo X, Zheng X. Prediction of fatigue lives of RC beams strengthened with CFL under random loading. Acta Mechanica Solida Sinica 2008;21(4):359-63.

[11] Zheng SS, Wang B, Li L, Zhang L, Hou PJ. Fatigue-Cumulative Damage Model of RC Crane Girders Strengthened with FRP Strips. Key Eng Mat 2008;385:165-8.

[12] Yao G, Huang PY, Zhao C. Flexural fracture and fatigue behavior of RC beams strengthened with CFRP laminates under constant amplitude loading. Key Eng Mat 2006;306:1343-8.

[13] El-Tawil S, Ogunc C, Okeil A, Shahawy M. Static and fatigue analyses of RC beams strengthened with CFRP laminates. J.Composite Constr. 2001;5(4):258-67.

[14] Papakonstantinou CG, Balaguru PN, Petrou MF. Analysis of reinforced concrete beams strengthened with composites subjected to fatigue loading. ACI Special Publication 2002;206.

[15] Oudah F, El-Hacha R. Analytical fatigue prediction model of RC beams strengthened in flexure using prestressed FRP reinforcement. Eng.Struct. 2013;46:173-83.

[16] Tan KH, Saha MK. Glass FRP bonded RC beams under cyclic loading. International Journal of Concrete structures and materials 2007;1(1).

[17] Balaguru P, Shah S. A method of predicting crack widths and deflections for fatigue loading. ACI Special Publication 1982;75.

[18] Holmen JO. Fatigue of concrete by constant and variable amplitude loading. ACI Special Publication 1982;75.

[19] Ferrier E, Bigaud D, Clement J, Hamelin P. Fatigue-loading effect on RC beams strengthened with externally bonded FRP. Constr.Build.Mater. 2011;25(2):539-46.

[20] Mogami K, Hayashi T, Ando K, Ogura N. Elastic-plastic fatigue-crack growth and tearing-instability behavior under cyclic loads. Int.J.Pressure Vessels Piping 1990;44(1):85-97.

[21] Barsom JM, Rolfe ST. Fracture and fatigue control in structures: applications of fracture mechanics. : ASTM International; 1999.

[22] Curtis P. The fatigue behaviour of fibrous composite materials. The Journal of Strain Analysis for Engineering Design 1989;24(4):235-44.

[23] Warner R, Hulsbos C. Probable fatigue life of prestressed concrete beams. PCI J. 1966;11(2):16-39.

[24] Schütz D, Gerharz J. Fatigue strength of a fibre-reinforced material. Composites 1977;8(4):245-50.

[25] Fatigue behaviour of bonded FRP used for flexural retrofit. Proceedings of international symposium on bond behaviour of FRP in structures (BBFS 2005); 2005.

[26] Kim YJ, Heffernan PJ. Fatigue behavior of externally strengthened concrete beams with fiber-reinforced polymers: State of the art. J.Composite Constr. 2008;12(3):246-56.

[27] Dong Y, Ansari F, Karbhari VM. Fatigue performance of reinforced concrete beams with externally bonded CFRP reinforcement. Structure and Infrastructure Engineering 2011;7(3):229-41.

[28] Yu T, Li C, Lei J, Zhang H. Fatigue of concrete beams strengthened with glass-fiber composite under flexure. J.Composite Constr. 2010;15(4):557-64.

[29] Badawi MA. Monotonic and fatigue flexural behaviour of RC beams strengthened with prestressed NSM CFRP rods 2007.

[30] Noran Abdel Wahab. University of Waterloo; 2011.

[31] Gussenhoven R, Brena S. Fatigue behavior of reinforced concrete beams strengthened with different FRP laminate conFigurations. ACI Special Publication 2005;230.

[32] Study on fatigue behavior of RC beams strengthened with prestressed CFRP sheets. FRPRCS-8; 2007.

[33] Derkowski W. Fatigue life of reinforced concrete beams under bending strengthened with composite materials. Archives of Civil and Mechanical Engineering 2006;6(4):33-47.

[34] Harries KA, Aidoo J, Zorn A, Quattlebaum J. Deterioration of FRP-to-concrete bond under failure loading. Adv.Struct.Eng. 2006;9(6):779-89.

[35] Comité Euro-International du Beton. CEB/FIB Model Code 2010. London: Thomas Telford; 2010.

[36] Helagson T, Hanson J. Investigation of design factors affecting fatigue strength of reinforcing bars-statistical analysis. ACI Special Publication 1974;41.

[37] Zorn AV. Effect of adhesive stiffness and CFRP geometry on the behavior of externally bonded CFRP retrofit measures subject to fatigue loads 2006.

PAPER V

"A two-scale damage model for high-cycle fatigue at the fiber-reinforced polymer-concrete interface."

BY
Mohammed Mahal, Björn Täljsten and Thomas Blanksvärd

A two-scale damage model for high-cycle fatigue at the fiber-concrete interface

Mohammed S.Mohammed[*1,2], Björn Täljsten[1,3] and Thomas Blanksvärd[1]

[1]Department of Civil, Environmental and Natural resources engineering, Luleå University of Technology, Luleå, Sweden

[2]Department of Civil Engineering, Mosul University, Mosul, Iraq

[3]Sto Scandinavia AB, Sweden

Abstract. This paper presents a new two-scale damage model of the fiber-reinforced polymer (FRP)-concrete bond under high-cycle fatigue. The material behavior is modeled as elastic-plastic coupled with damage for the microscale analysis and as elastic for the mesoscale analysis. A new damage law for the interface joint is described. The two-scale damage model has been implemented as a material model for a three dimensional an eight-node interface element of zero thickness and used to simulate a double shear joint specimen under high cycle fatigue. The numerical calculations were performed with a full incremental cycle solution and a new cycle jump approach.

Keywords: Damage, High-cycle fatigue, Finite element, Bond behavior, Fiber-reinforced polymer (FRP), Concrete

1. Introduction

Repeated cyclic loading on reinforced concrete (RC) structures such as bridges can cause reduced service life and structure failure from fatigue even when the stress ranges applied to the structural components are very low. However, the use of fiber-reinforced polymer (FRP) composites to strengthen and increase the fatigue life (service life) of these structures is a promising technology, and this technique might be the optimal choice for consulting engineers. The bond between the FRP materials and the concrete must be durable to ensure that the strengthening system remains effective for its expected service life. Several test methods have been used to evaluate the bond behavior of externally bonded FRP composite sheets and plates under high- or low-cycle fatigue loading, including the single shear (single lap joint) test (Bizindavyi, Neale et al. 2003, Mazzotti, Savoia 2009), the double lap joint test (Ferrier, Bigaud et al. 2005, Yun, Wu et al. 2008), the pullout specimen method for measuring peeling stresses (Khan, Al-Gadhib et al. 2011), and the partially bonded beam test (Gheorghiu, Labossière et al. 2004). In the high-cycle fatigue test, the maximum applied fatigue load is lower than the limit of linearity (yield load of the joint), and the joint behavior is elastic. In contrast, the joint is in the non-linear phase in the low-cycle fatigue test. The behavior of the FRP-concrete bonded joints under high-cycle fatigue is classified into three phases, see Fig. 1. The damage in the first phase occurs mostly from microcracks that cause residual plastic strain with negligible stiffness degradation. In the second phase, macrocracks start to cause stiffness degradation, with keeping the ability of the joint to resist the applied load. Finally, debonding occurs (fracture process) from crack propagations that produce loss of both the stiffness and resistance capacity of the joint. The period of any phase and the possibility of their presence in the behavior of the joint is dependent on the maximum applied stresses as well as fatigue limit stress of the joints. Where, the first phase be prevalent of the joints behavior when the applied maximum stresses are a somewhat more than the fatigue limit stress.

---

[*]Corresponding author, Ph.D, E-mail: mohammed.salih@ltu.se
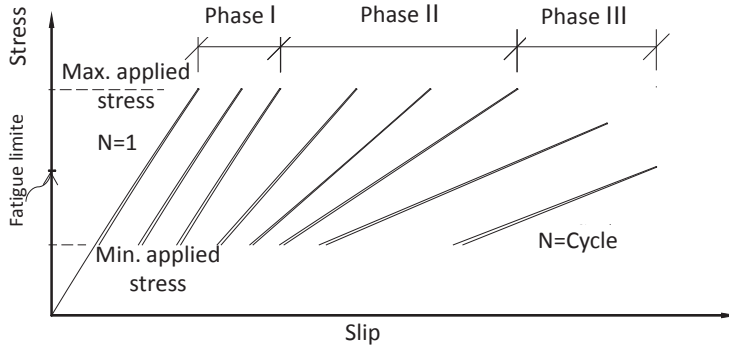
Fig. 1. Typical bond stress-slip relationship in FRP-concrete joints under high-cycle fatigue.

Few models have been developed for FRP-concrete interfaces under fatigue load, and most researchers analyzing FRP-strengthened RC beams subjected to fatigue load have simulated the FRP-concrete bond as a perfect bond (full composite action) (El-Tawil, Ogunc et al. 2001, Papakonstantinou, Balaguru et al. 2002, Al-Rousan, Issa 2011). The models described in the literature are mainly based on the fracture mechanism, which is unsuitable for simulating high-cycle fatigue, especially in the first phase. Loo et al. (2012) developed a model of the interface bond under fatigue load based on the degradation of the joint stiffness cycle, but this model did not produce good results when used to analyze the joint behavior with high-cycle fatigue. Daib et al. (2009) presented a model to assess the bonding fatigue behavior of the FRP-concrete interface. The model of the joint before the initiation of debonding and subsequent fatigue crack growth was based on the creep-fatigue interaction, which was represented by the degradation of the interfacial stiffness This is also not accurate for the first phase of high cycle fatigue.

In the present study, to get accurate results at the first phase of high cycle fatigue a two-scale model has been implemented for modeling FRP-concrete joints under high-cycle fatigue in the first phase when the stress level lower than the engineering yield stress. Plasticity coupled to a damage model for the microscale analysis and an elasticity model for the mesoscale analysis has been used. A double shear joint specimen under high-cycle fatigue using the three-dimensional finite element method (FEM) was modeled. After validating the model by comparison to experimental data, a parametric study was completed.

2. Damage constitutive equation

Damage to a material refers to gradual deterioration of mechanical strength from the development of microcracks and micro-cavities (Skrzypek, Ganczarski 1999). Most models of damage in a material introduce a damage variable (Lemaitre, Desmorat 2005). The damage variable is the ratio of the effective area or volume of the intersections of all microcracks or micro-cavities to the total undamaged area or volume. We designed the damage model according to this definition.

A suitable damage model for the joint interface represented by an interface element under fatigue load must allow for the different materials of the joint and must relate directly to the accumulated microplastic strain. In addition, the parameters must be easy to determine from static test. To meet these criteria, we need to describe the behavior of the joint under monotonic load. Fig. 2 shows the schematic of the general behavior of the FRP-concrete joint under static load constructed from an experiment (Täljsten 1997), where the stress is the applied average bond stress and slip represents the

slip of FRP with respect to the concrete block. The joint behavior has two stages, the elastic stage and the fracture stage. The fracture stage starts after the maximum load is reached, which means that the damage behavior of the bond occurs only during the elastic stage and thereby the first phase of fatigue joint behavior take place at entire this stage only. The fatigue behavior phases can be represented, schematically, with regard to static behavior in Fig. 2(b).To describe this damage behavior, we define the damage variable D_j for the 3-D joint as a function of the total strain (elastic and accumulated plastic strain) within the elastic stage as

$$D_j = (1 - \frac{\varepsilon_{j3}}{L_{e,j}})^{(\alpha - \frac{1}{\alpha})}, \tag{1}$$

where ε_{j3} is the current total strain (interface slip which has the dimension of length) in normal and shear directions(j), $L_{e,j}$ is the total length of the elastic stage obtained from static tests of FRP-concrete joints with different modes by this parameter the state of stress (mode I, mode II, mode III) is taken in the damage, and α is the damage exponent that determines the shape of the damage evolution curve and should be greater than one.
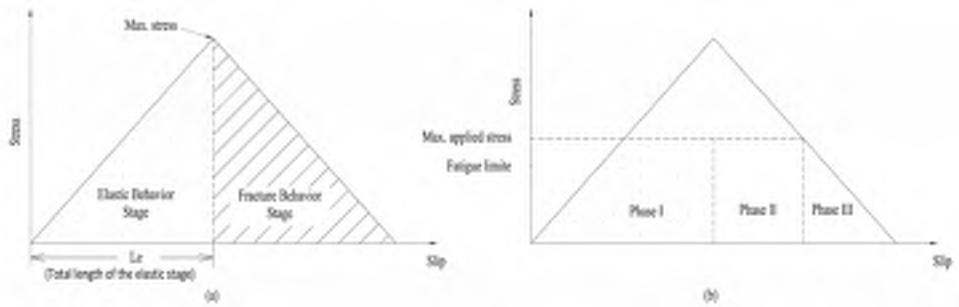
Fig. 2. Typical FRP-concrete joint behavior under static load (a).Static stages (b).fatigue phases in static stress-slip space.

3. Material models

In the FEM analysis, concrete and FRP are modeled at the mesoscale, the scale of the representative volume element. The behavior of material at this scale is linear elastic. The bond between the concrete and FRP, which is represented by the interface element, is treated with a two-scale damage model. The two scale model is considered as inclusion within in an elastic meso-matrix (Lemaitre, Sermage et al. 1999) as shown in Fig. 3 . This inclusion is modeled as elastic-plastic coupled with damage.

The general principles of a two scale damage model for FRP-concrete bond under high cycle fatigue are as follows:

-The behavior is considered as elastic at the mesoscale, the scale of representative volume element. Where, the material engineering yield stress being usually not reached in high cycle fatigue.

-The behavior at micoscale is elastic-perfectly plastic coupled with damage, the scale of micro-inclusion. Where, the weakness of the inclusion being represented by a yield stress at microscale taken equal to the fatigue limit of the joint.
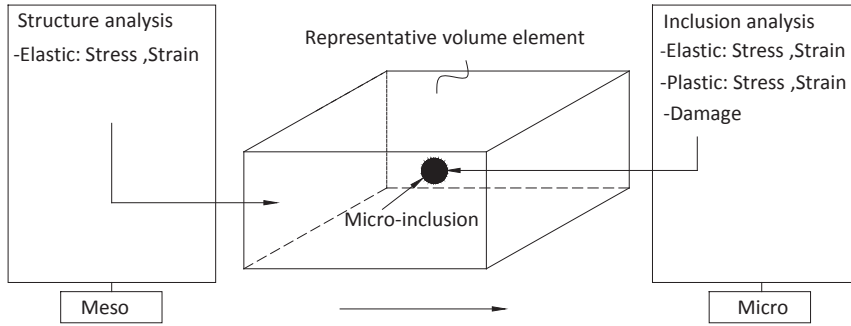
Fig.3. Two scale model

3.1. Elastic mesoscale model

The standard form of the linear elastic relationship between generalized stress (σ) and strain (ε) for the elements used in this paper is

$$\sigma = E\varepsilon^e, \tag{2}$$

where E is the elastic stiffness matrix for the interface element $\{K_n, K_s, K_t\}$ where n denotes the normal components and s and t denote the shear components. The stress and strain tensors have six components for the 3-D eight-node brick element and three components for the 3-D eight-node interface element. The full details of the constitutive equations of the eight-node brick element can be found in for example known finite element literature (Zienkiewicz, Taylor et al. 2005).

3.2. Plasticity and damage microscale model

Lemaitre et al. (1999) developed a micromechanical model of a weak micro-inclusion subjected to plasticity and damage embedded in an elastic meso-element for high-cycle fatigue. We used the principle this model, which is schematically described in Fig. 4, for the discontinuum interface element. The behavior is elastic-perfectly plastic with damage, and the plastic stress threshold is lower than the mesoscale yield stress and is equal to the fatigue limit. This means that there is no microplastic strain below the fatigue limit, and no damage occurs. The damage threshold limits the damage (the microcrack initiation).
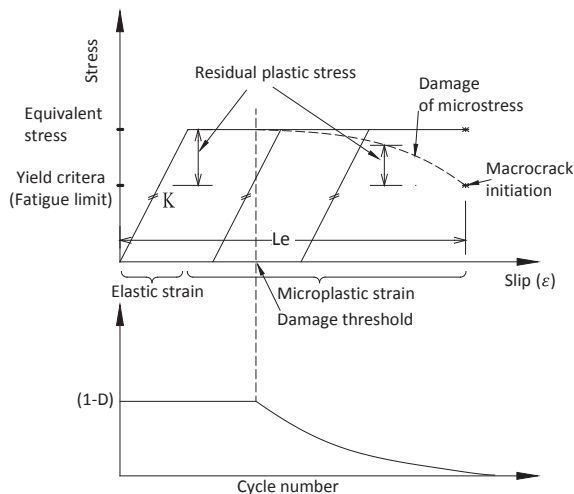
Fig. 4. Constitutive model for a FRP-concrete bond subjected to fatigue loading.

4

According to these assumptions, the total strain is divided into a microelastic ($\varepsilon_{j3}^{\mu e}$) part and a microplastic ($\varepsilon_{j3}^{\mu p}$) part (recall that μ-upper- script stands for variable at microscale):

$$\varepsilon_{j3}^{\mu} = \varepsilon_{j3}^{\mu e} + \varepsilon_{j3}^{\mu p}. \tag{3}$$

The microelastic strain is calculated at mesoscale, where the strain at the mesoscale is equal to the strain at the microscale, see Fig. 4. The microplastic strain rate is derived from the yield criterion function (Hashin 1980):

$$f^{\mu} = \frac{1}{(1-D)} \sqrt{\sigma^{\mu T} A \sigma^{\mu}} - 1 = 0, \tag{4}$$

where

$$\sigma^{\mu} = \begin{Bmatrix} \sigma_{33}^{\mu} \\ \tau_{13}^{\mu} \\ \tau_{23}^{\mu} \end{Bmatrix} \quad , A = \begin{bmatrix} \frac{1}{\sigma_{f33}^2} & 0 & 0 \\ 0 & \frac{1}{\tau_{f13}^2} & 0 \\ 0 & 0 & \frac{1}{\tau_{f23}^2} \end{bmatrix} \quad , 1 - D = D_j \quad , \sigma^{\mu T} = \left\{ \left| \sigma_{33}^{\mu} \right| \tau_{13}^{\mu} \tau_{23}^{\mu} \right\}$$

and σ_f and $\tau_{f_{j,3}}$ are the normal and shear fatigue stress limits of the joint.

By the normality rule, the microplastic strain is

$$\varepsilon_{ji}^{\cdot \mu p} = \frac{\partial f^{\mu}}{\partial \sigma^{\mu}} \dot{\lambda} = \frac{A \sigma^{\mu}}{g(\sigma^{\mu})} \frac{\dot{\lambda}}{(1-D)} \qquad \text{if} \qquad f^{\mu} = 0 \text{ and } \dot{f}^{\mu} = 0, \tag{5}$$

$$g(\sigma^{\mu}) = \sqrt{\sigma^{\mu T} A \sigma^{\mu}}, \tag{6}$$

where $\dot{\lambda}$ is the plastic multiplier derived from the accumulated plastic strain rate $(\dot{P})$ which must always be positive and increasing. The simplest combination of this kind which is dimensionally correct is defined in accordance with discontinuity consideration:

$$\dot{P} = \sqrt{(\dot{\varepsilon}_{ji}^{\mu P})^T \dot{\varepsilon}_{ji}^{\mu P}} = \frac{\dot{\lambda}}{(1-D)} \frac{\sqrt{\sigma^{\mu T} A^T A \sigma^{\mu}}}{g(\sigma^{\mu})}, \tag{7}$$

which can be arranged as

$$\frac{\dot{\lambda}}{(1-D)} = \dot{P} \frac{g(\sigma^{\mu})}{\sqrt{\sigma^{\mu T} A^T A \sigma^{\mu}}}. \tag{8}$$

The microscale stresses are related to the mesoscale stresses as follows:

$$\sigma^{\mu} = \sigma_{j3} \qquad \text{if} \qquad f^{\mu} < 0, \tag{9}$$

$$\sigma^{\mu} = \sigma_{j3} D_j \qquad \text{if} \qquad f^{\mu} \geq 0, \tag{10}$$

where

$$\sigma_{j3} = E(\varepsilon_{j3} - \varepsilon_{j3}^{\mu p}) \tag{11}$$

and $\qquad D_j = (1 - \frac{\varepsilon_{j3}^{\mu}}{L_{e,j}})^{(\alpha - \frac{1}{\alpha})}.$

5

4. 3-D FEM interface model

The eight-node zero thickness interface element shown in Fig. 5 is used to simulate the joint interface connecting the FRP laminate face with the concrete face. In the initial configuration, the two rectangle surfaces of the interface element are joined with no gaps. The surfaces separate when the adjacent solid elements deform.

Interface elements allow discontinuities in the displacement field and establish a direct relation between the tractions (t) and the relative displacements along the interface (Δu), which are given by

$$t = \{\tau_s \quad \tau_t \quad \sigma_n\} \tag{12}$$

$$\Delta u = \{\Delta u_s \quad \Delta u_t \quad \Delta u_n\} \tag{13}$$

Here, these quantities are conveniently defined as generalized stress vector σ and generalized strain vector ε, so that the same notation is adopted for continuum and discontinuous elements. The local nodal displacements for the top and bottom faces of the element are defined as

$$u_{top} = \{u_s^1 \, u_t^1 \, u_n^1 \ldots \ldots \ldots \ldots \ldots u_s^4 \, u_t^4 \, u_n^4\}^T, \; u_{bot} = \{u_s^5 \, u_t^5 \, u_n^5 \ldots \ldots \ldots \ldots \ldots u_s^8 \, u_t^8 \, u_n^8\}^T \tag{14}$$

where s and t represent the tangential directions and n represents the normal direction. The displacement jump between two paired nodes of u_{top} and u_{bot} can be written as (Bfer 1985)

$$\varepsilon_{local} = \begin{Bmatrix} \varepsilon_s \\ \varepsilon_t \\ \varepsilon_n \end{Bmatrix} = u_{top} - u_{bot}. \tag{15}$$

The displacement jumps in the local directions (normal and tangential to the contact surface) can be obtained from the global displacement jumps:

$$\varepsilon_{local} = \theta^T \varepsilon_{global}, \tag{16}$$

where

$$\varepsilon_{global} = \begin{Bmatrix} \varepsilon_x \\ \varepsilon_y \\ \varepsilon_z \end{Bmatrix} \quad \text{and} \quad \theta = [V_n, V_s, V_t].$$

The V_n, V_s, and V_t are the local normal coordinate and tangential coordinates vectors respectively The components of V_n, V_s, and V_t represent the direction cosines of the local coordinate system in the global coordinate system $(X_i, i = 1,2,3)$ and are obtained from

$$V_{\eta_i} = X_{i,\eta} \quad , \quad V_{\xi_i} = X_{i,\xi} \tag{17}$$

in the following:

$$V_n = \frac{V_{\xi_i} \, X \, V_{\eta_i}}{|V_{\xi_i} \, X \, V_{\eta_i}|} \quad , \quad V_s = \frac{V_{\xi_i}}{|V_{\xi_i}|} \; \text{and} \quad V_t = V_n X V_s. \tag{18}$$
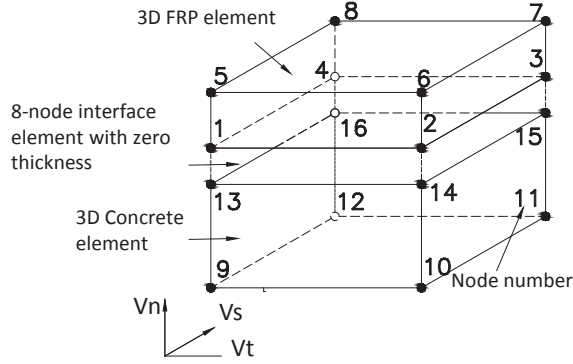
Fig. 5. Eight-node interface element.

5. Integration of the elastic-plastic damage equation

An incremental load procedure for each cycle is used to analyze the structure system under fatigue load as shown in Fig. 6. The method of integration is strain driven and consists of two steps: the calculation of trial elastic stress, also called the elastic predictor, and the return mapping to the yield surface, also called the plastic corrector. The solution must satisfy the yield function $f^\mu = 0$, which is solved locally by the Newton-Raphson iterative method. The derivation of the elastic predictor and plastic corrector is included in Appendix A.

The following algorithm is performed at each integration point at any time during the cycles:

1. Compute mesoscale elastic stress:

$$\sigma = E\varepsilon^e.$$

2. Compute trial elastic microstress:

$$\sigma^\mu = \sigma^e D.$$

3. Check for plastic behavior:

    If $f^\mu < 0$, the integration point is elastic. Update stress and strain.

    If $f^\mu \geq 0$, the integration point is plastic.

    For iterations $i = 0............$n,

    - Update cumulative plastic strain (P) by plastic corrector (CP):
      $$\Delta P^\mu_{i+1} = \Delta P^\mu_i + CP^\mu_{i+1},$$
    - Update stress (σ^μ) by elastic predictor ($C\sigma$):

      $$\Delta \sigma^\mu_{i+1} = \Delta \sigma^\mu_i + C\sigma_{i+1},$$

    until $f^\mu < Tolerance$.
4. Update microplastic strain and total strain and check and update the damage variables:

7

$$\varepsilon_{j3}^{\mu} = \varepsilon_{j3}^{\mu e} + \varepsilon_{j3}^{\mu p}$$

$$D_j = (1 - \frac{\varepsilon_{j3}^{\mu}}{L_{e,j}})^{(\alpha - \frac{1}{\alpha})} \quad \text{if} \quad P^{\mu} \geq P_{th}^{\mu},$$

$$D_j = 1 \qquad\qquad\qquad \text{if} \quad P^{\mu} < P_{th}^{\mu},$$

where P_{th}^{μ} is the damage threshold estimated as (Lemaitre 2001)

$$P_{th}^{\mu} = \varepsilon_u^{\mu} \left(\frac{\sigma_u - \sigma_f}{\sigma_{max} - \sigma_f} \right). \tag{19}$$

ε_u^{μ} and σ_u are ultimate static strain and stress, σ_f is the fatigue limit stress of FRP-concrete joint, and σ_{max} is the maximum stress at maximum cycle load applied on the joint.

5. Compute the equivalent nodal forces produced by residual plastic strain and reanalyze the structure to compute the equivalent nodal displacement and other variables.
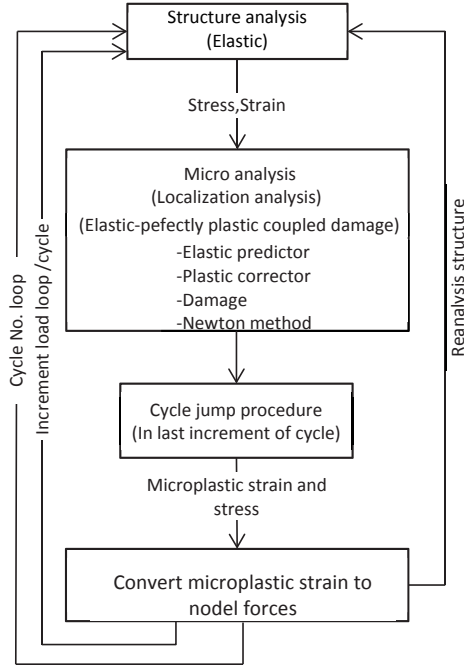
Fig.6. Numerical implementation

6. Cycle jump concept

The increment-by-increment calculation for each cycle of the elastic-plastic model is computationally expensive, and simulating fatigue behavior for a large number of cycles might take several days depending on the available computational resources. Therefore, we implemented a simple cycle jump strategy in the FEM model. Because the long-term response of the structure can be determined without modeling the details of each cycle, the computation can "jump" across a large number of cycles. A several authors have considered accelerated numerical simulations for cyclically loaded

structures. To save computations for a model subjected to cyclic loadings Kiewal et al. (2000) were extrapolated the internal variables (displacements, stresses and strains) over a certain number of cycles. For each material point in the model, a spline function is obtained based on the evolution equations of the internal variables. The variables are then extrapolated using the obtained spline functions. Based on this method, Wang et al. (2012) utilized a linear shape function for extrapolation. Bogard et al. (2008) developed an accelerated scheme where a cycle jump algorithm is incorporated. The internal variables are described as functions of time, and expressed in Taylor series up to second order. In this paper the cycle jump method is dependent on the nearly constant amount of residual stress or plastic strain present before the damage starts for each cycle at the integration point. The damage variable, strain, and stress at an integration point are computed for each cycle at maximum cycle load without the complete analysis of the structures during the cycle jump. Fig. 7 shows the schematic of an evolving strain for a structure subjected to cyclic loading during the analysis with using the cycle jump method. Should be noted that the finite element results in the figure it is not real, it is just to show finite element analysis stage. In jump steps eliminate the need of simulation each individual cycle and significantly reduce the time of analysis. The proposed method is based on conducting detailed finite element analysis for a set of cycles to establish the residual microplastic strain or stress in all integration points of structure, implementing the cycle jump method using the procedure listed below, and use the jumped variables as initial variables for additional finite element analysis simulation
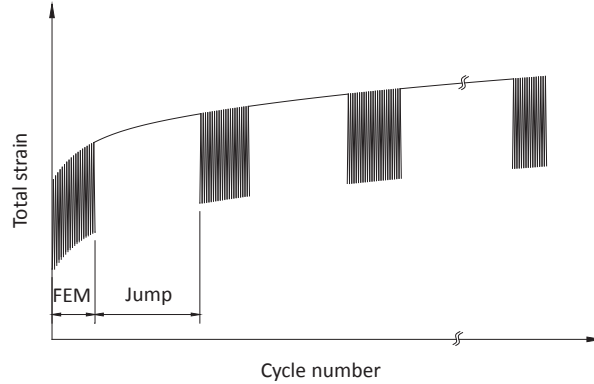
Fig. 7. A schematic of the cycle jump method.

The cycle jump method is implemented as follows.

$$\varepsilon_{cycle+1}^{\mu} = \varepsilon_{cycle}^{\mu} + \Delta\varepsilon^{\mu p} \tag{20}$$

$$\Delta\varepsilon^{\mu p} = D_{cycle+1} . \Delta\varepsilon_{G.P}^{\mu p} \tag{21}$$

Where, $\Delta\varepsilon_{G.P}^{\mu p}$ is the maximum residual microplastic strain at an integration point.

$$\sigma_{cycle+1}^{\mu} = D_{cycle+1} . \sigma \tag{22}$$

$$D_{cycle} = 1 \qquad\qquad\qquad \text{if} \qquad\qquad P^{\mu} < P_{th} \tag{23}$$

$$D_{cycle+1} = \left(1 - \frac{\varepsilon_{cycle}^{\mu}}{L_e}\right)^{\left(\alpha - \frac{1}{\alpha}\right)} \qquad\qquad \text{if} \qquad\qquad P^{\mu} > P_{th} \tag{24}$$

9

7. Model verification and parametric study

We computationally analyzed a double shear joint specimen under high-cycle fatigue without fracture (no stiffness degradation) using the bond slip model and compared these results to the corresponding experimental results from Yun et al. (2008) (test specimen F-EB-A in that paper). We also completed a parametric study to determine how the model parameters influence the fatigue behavior of the specimen. The material parameters used for the FRP-concrete joint are given in Table 1, and these were determined from the static test of the joint which was done by Yun et al. (2008). The dimensions, boundary conditions, and load conditions of the joint for the fatigue load case are shown in Fig. 8. We completed the computation for one fourth of the model due to symmetry. The fatigue load was distributed over an area of 25 mm × 200 mm, which is the size of the contact area between the FRP and concrete block when fully bonded.

Table 1. Material properties.

f_c $(N/mm^2)^*$	E_f $(GPa)^{**}$	K_n, K_s, K_t (N/mm^2)	τ_f (N/mm^2)	L_e (mm)	P_{th}	α
43.5	257	57.14	2.8	0.1	0.072	5.0

*Compressive concrete strength **Modulus of elasticity of FRP
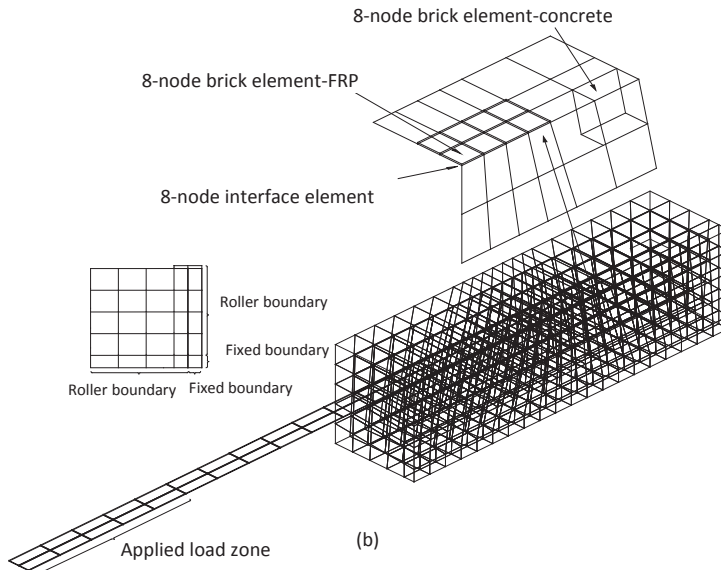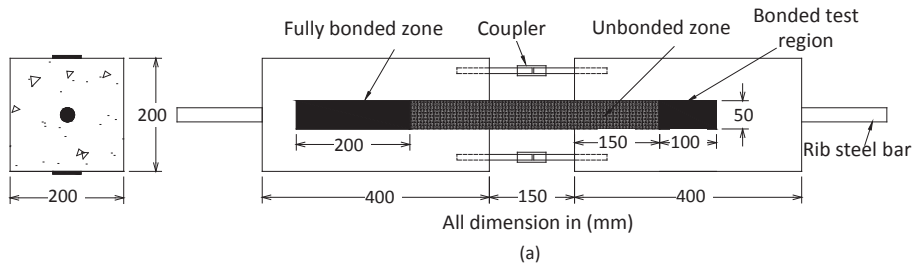
Fig. 8. (a) Dimensions of the double shear joint specimen tested by Yun et al. (2008). (b) Finite element mesh, boundary conditions, and load conditions for one fourth of the specimen.

Fig. 9 shows the FEM and experimental results for the loaded-end slip at each cycle number for the minimum and maximum cyclic loads. The computed loaded-end slip corresponds well with the experimental results. There is an 11% difference between the FEM and the experiment in the last cycle. 'This difference might have occurred because the damage of FRP plate was not accounted for in the model. Fig. 10 shows the load-slip relationship computed with the FEM, and Fig. 11 shows the slip computed at each cycle jump.
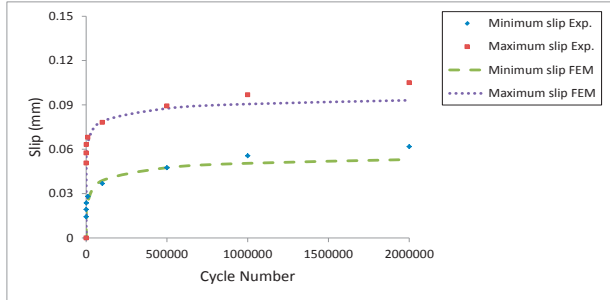
Fig. 9. Comparison between the experimental and numerical results.
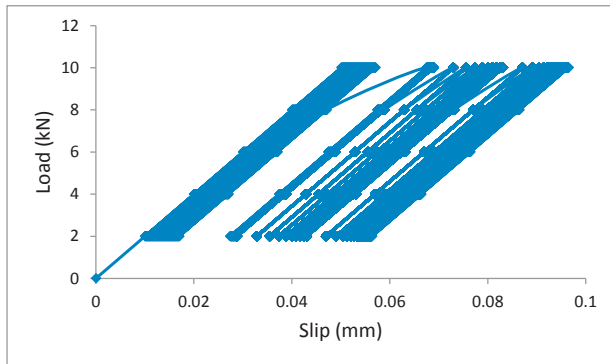
Fig. 10. Load-slip relationship computed with the FEM.
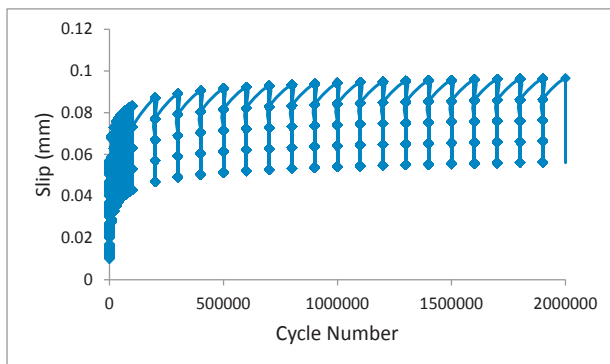
Fig. 11. Computed slip at each cycle number.

11

After verifying the FEM model, we determined the sensitivity of the model at maximum cycle load to the following parameters: the damage exponent (α), damage threshold strain (P_{th}), the length of the elastic zone (L_e), and the fatigue limit (τ_f). Each parameter was varied separately while the other parameters remained constant.

Fig. 12 shows the loaded-end slip versus the number of cycles for different values of α. As can be seen, the slip damage under fatigue loading increases as the damage exponent decreases. The low values of α result in a low initial damage rate of residual stress. This causes an increase in plastic strain that produces an increase in slip damage during the initial stage. We can conclude from this that the lower values of α are more suitable for materials with limited ductility.
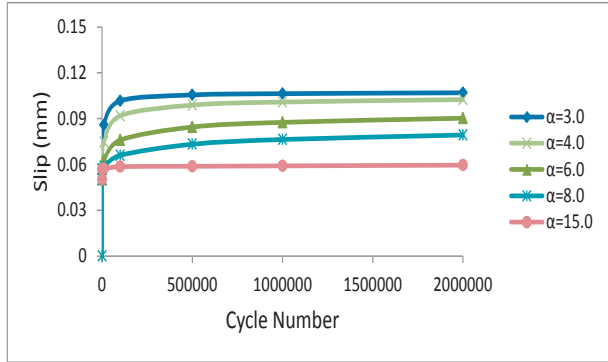
Fig. 12. Influence of the α parameter on the fatigue behavior of the joint.

Fig. 13 shows the effect of L_e on the joint behavior. It can be seen that the slip at the initial stage increases as L_e is increased. Increasing L_e delays the initiation of damage and reduces the damage rate. This increasing in slip is due to only the reduction in damage rate because the damage threshold and other parameters were fixed.
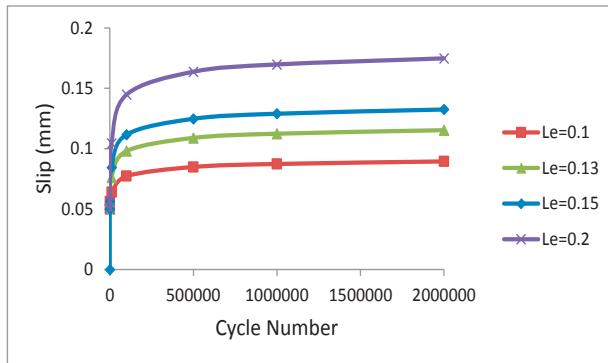
Fig. 13. Influence of L_e on the fatigue behavior of the joint.

Fig. 14 shows the loaded-end slip versus the number of cycles with a constant applied load for different values of τ_f. When τ_f is higher than the maximum applied stress($\tau_f = 3\ N/mm^2$), no plastic strain or damage occurs. However, reducing τ_f to below nominal applied stress increases the

plastic strain because of increased residual stress. The constant damage rate at very low τ_f it is due to the other parameters were held constant.
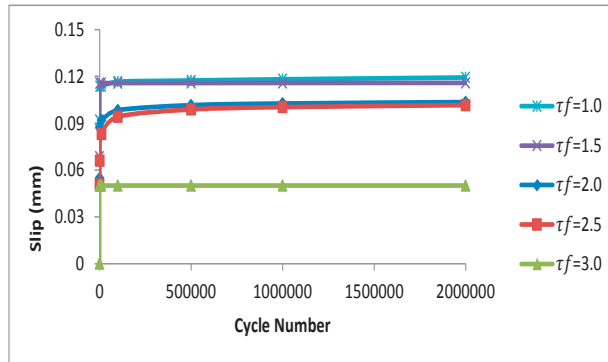
Fig. 14. Influence of τ_f on the fatigue behavior of the joint.

The effect of P_{th} on the fatigue behavior is shown in Fig. 15. Increasing P_{th} increases the period of microcrack nucleation and creates a large amount of plastic strain before the damage starts.
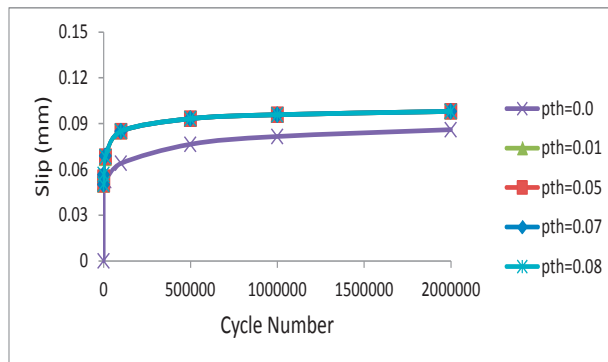
Fig. 15. Influence of P_{th} on the fatigue behavior of the joint.

Finally, the behavior of the damage propagation with cyclic loading with respect to the longitudinal displacement along the bond length zone in the middle of the FRP plate is shown in Fig. 16. We observed that the microcracks started at the loaded end and propagated toward the free end as the number of fatigue cycles increased. The reduction in curvature of the displacement line, especially after 10,000 cycles, indicates an insignificant dissipation of energy due to the small plastic deformation (microcracking) of the bond at the loaded end.
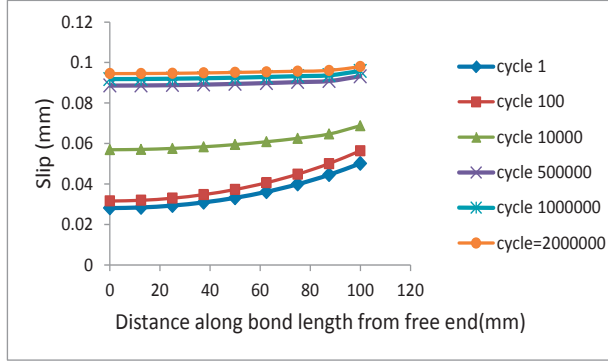
Fig. 16. Slip along bond length at maximum cycle load.

8. Conclusion

A damage model of the FRP-concrete interface bond under high-cycle fatigue has been developed. This model combines an elastic mesoscale model with an elastic-plastic coupled with damage microscale model. The advantage of this two-scale model for high-cycle fatigue damage is that the plasticity and damage occur at the microscale, and the stiffness degradation of the material at the mesoscale does not need to be modeled as it does in other models to get damage in the joint. The double shear joint specimen under high-cycle fatigue was modeled with the FEM program, and the computational results were compared to experimental data for verification. The model includes the full increment cycle procedure and the cycle jump procedure. The following list highlights the features of the model:

1. It is easy to identify the model parameters from the static test of FRP-concrete joints.
2. The model efficiently computes the damage to the FRP-concrete bond under high-cycle fatigue loading until the fracture stage is reached.
3. The cycle jump method produces accurate results.
4. Suitability of the procedure which was followed to link microscale and mesoscale in the analyses.

We determined the sensitivity of the model to different parameters. In conclusion, this method is useful for modeling different conditions of a joint under high-cycle fatigue.

Appendix A

In the following derivation, we used effective microstress ($\bar{\sigma} = \frac{\sigma^\mu}{(1-D)}$) for simplicity. To calculate the residual stresses that cause plastic strain for each increment in a cycle, the following equations must be satisfied:

$$h = \bar{\sigma} - K_s\left(\varepsilon_{ji} - \varepsilon_{ji,n}^P\right) + K_s\left(\frac{A\bar{\sigma}}{\sqrt{\bar{\sigma}^T A^T A\bar{\sigma}}}\right) \Delta \dot{P}, \tag{A.1}$$

$$h = \bar{\sigma} - K_s\left(\varepsilon_{ji} - \varepsilon_{ji,n}^P\right) + K_s S \Delta \dot{P}, \tag{A.2}$$

$$f = \sqrt{\bar{\sigma}^T A\bar{\sigma}} - 1 = 0, \tag{A.3}$$

and

$$D_j = (1 - \frac{\varepsilon_{j3}^\mu}{L_{e,j}})^{(\alpha - \frac{1}{\alpha})}$$
(A.4)

To solve this nonlinear problem, Newton iterative method for multiple variables was used:

$$f + \frac{\partial f}{\partial \bar{\sigma}} : C\bar{\sigma} + \frac{\partial f}{\partial \Delta P} : CP = 0,$$
(A.5)

$$h + \frac{\partial h}{\partial \bar{\sigma}} : C\bar{\sigma} + \frac{\partial h}{\partial \Delta P} : CP = 0.$$
(A.6)

Taking the derivatives of (A.3) with respect to $\bar{\sigma}$ and ΔP,

$$\frac{\partial f}{\partial \bar{\sigma}} = \frac{A\bar{\sigma}}{\sqrt{\bar{\sigma}^T A \bar{\sigma}}} = \frac{A\bar{\sigma}}{g(\bar{\sigma})} \quad , \quad \frac{\partial f}{\partial \Delta P} = 0,$$
(A.7)

and substituting (A.7) in (A.5) yields

$$C\bar{\sigma} = -\frac{g(\bar{\sigma})}{A\bar{\sigma}} : f.$$
(A.8)

The derivatives of (A.2) with respect to $\bar{\sigma}$ and ΔP are

$$\frac{\partial h}{\partial \bar{\sigma}} = \left[\mathrm{II} + K_S \frac{\partial S}{\partial \bar{\sigma}} \Delta \dot{P} \right] \quad , \quad \frac{\partial h}{\partial \Delta P} = K_S S,$$
(A.9)

and (A.6) can be rewritten with (A.9) as

$$h + \left[\mathrm{II} + K_S \frac{\partial S}{\partial \bar{\sigma}} \Delta \dot{P} \right] : C\bar{\sigma} + K_S S : CP = 0.$$
(A.10)

Substituting (A.8) in (A.10) yields

$$h - \left[\mathrm{II} + K_S \frac{\partial S}{\partial \bar{\sigma}} \Delta \dot{P} \right] \frac{g(\bar{\sigma})}{A\bar{\sigma}} : f + K_S S : CP = 0,$$
(A.11)

where
$$\mathrm{II} = \begin{bmatrix} 1 & 0 & 0 \\ 0 & 1 & 0 \\ 0 & 0 & 1 \end{bmatrix}.$$

(A.11) multiplied by S is

$$S : h - \left[S : \mathrm{II} + K_S S \frac{\partial S}{\partial \bar{\sigma}} : \Delta \dot{P} \right] \frac{g(\bar{\sigma})}{A\bar{\sigma}} : f + K_S S : S : CP = 0,$$
(A.12)

where

$$\frac{\partial S}{\partial \bar{\sigma}} = \frac{A}{\sqrt{\bar{\sigma}^T A^T A \bar{\sigma}}} - \frac{(A\bar{\sigma})(\bar{\sigma}^T A^T A)}{(\bar{\sigma}^T A^T A \bar{\sigma})^{3/2}}.$$

Because $\frac{\partial S}{\partial \bar{\sigma}} : S = 0$, $S : \mathrm{II} = S$ and $S : S = 1$, (A.12) can be rewritten as

$$S : h - \frac{A\bar{\sigma}}{\sqrt{\bar{\sigma}^T A^T A \bar{\sigma}}} \frac{g(\bar{\sigma})}{A\bar{\sigma}} : f + K_S : CP = 0.$$
(A.13)

CP can be written as

$$CP = \frac{\frac{g(\bar{\sigma})}{\sqrt{\bar{\sigma}^T A^T A \bar{\sigma}}} f - S : h}{K_S}.$$ (A.14)

By substituting (A.14) in (A.10), we get

$$C\bar{\sigma} = AC^{-1}\left(-h - S\left(\frac{g(\bar{\sigma})}{\sqrt{\bar{\sigma}^T A^T A \bar{\sigma}}} f - S : h\right)\right),$$ (A.15)

where $AC = \left[II + K_S \frac{\partial S}{\partial \bar{\sigma}} \Delta \dot{P}\right]$.

References

AL-ROUSAN, R. and ISSA, M., 2011. Fatigue performance of reinforced concrete beams strengthened with CFRP sheets. *Construction and Building Materials,* **25**(8), pp. 3520-3529.

BFER, G., 1985. An isoparametric joint/interface element for finite element analysis. *International Journal for Numerical Methods in Engineering,* **21**(4), pp. 585-600.

BIZINDAVYI, L., NEALE, K. and ERKI, M., 2003. Experimental investigation of bonded fiber reinforced polymer-concrete joints under cyclic loading. *Journal of Composites for Construction,* **7**(2), pp. 127-134.

BOGARD, F., LESTRIEZ, P. and GUO, Y., 2008. Numerical modeling of fatigue damage and fissure propagation under cyclic loadings. *International Journal of Damage Mechanics,* **17**(2), pp. 173-187.

DIAB, H., WU, Z. and IWASHITA, K., 2009. Theoretical solution for fatigue debonding growth and fatigue life prediction of FRP-concrete interfaces. *Advances in Structural Engineering,* **12**(6), pp. 781-792.

EL-TAWIL, S., OGUNC, C., OKEIL, A. and SHAHAWY, M., 2001. Static and fatigue analyses of RC beams strengthened with CFRP laminates. *Journal of Composites for Construction,* **5**(4), pp. 258-267.

FERRIER, E., BIGAUD, D., HAMELIN, P., BIZINDAVYI, L. and NEALE, K., 2005. Fatigue of CFRPs externally bonded to concrete. *Materials and Structures,* **38**(1), pp. 39-46.

GHEORGHIU, C., LABOSSIÈRE, P. and RAICHE, A., 2004. Environmental fatigue and static behavior of RC beams strengthened with carbon-fiber-reinforced polymer. *Journal of Composites for Construction,* **8**(3), pp. 211-218.

HASHIN, Z., 1980. Failure criteria for unidirectional fiber composites. *Journal of applied mechanics,* **47**(2), pp. 329-334.

KHAN, A., AL-GADHIB, A. and BALUCH, M., 2011. Experimental and Computational Modeling of Low Cycle Fatigue Damage of CFRP Strengthened Reinforced Concrete Beams. *International Journal of Damage Mechanics,* **20**(2), pp. 211-243.

KIEWEL, H., AKTAA, J. and MUNZ, D., 2000. Application of an extrapolation method in thermocyclic failure analysis. *Computer Methods in Applied Mechanics and Engineering,* **182**(1), pp. 55-71.

LEMAITRE, J., SERMAGE, J. and DESMORAT, R., 1999. A two scale damage concept applied to fatigue. *International Journal of Fracture,* **97**(1-4), pp. 67-81.

LEMAITRE, J., 2001. *Handbook of Materials Behavior Models, Three-Volume Set: Nonlinear Models and Properties.* Academic press.

LEMAITRE, J. and DESMORAT, R., 2005. *Engineering damage mechanics: ductile, creep, fatigue and brittle failures.* Springer.

LOO, K.Y.M., FOSTER, S.J. and SMITH, S.T., 2012. FE modeling of CFRP-repaired RC beams subjected to fatigue loading. *Journal of Composites for Construction,* **16**(5), pp. 572-580.

MAZZOTTI, C. and SAVOIA, M., 2009. FRP-concrete bond behaviour under cyclic debonding force. *Advances in Structural Engineering,* **12**(6), pp. 771-780.

PAPAKONSTANTINOU, C.G., BALAGURU, P.N. and PETROU, M.F., 2002. Analysis of reinforced concrete beams strengthened with composites subjected to fatigue loading. *ACI SPECIAL PUBLICATIONS,* **206**, pp. 41-60.

SKRZYPEK, J.J. and GANCZARSKI, A., 1999. *Modeling of material damage and failure of structures: theory and applications.* Springer.

TÄLJSTEN, B., 1997. Defining anchor lengths of steel and CFRP plates bonded to concrete. *International Journal of Adhesion and Adhesives,* **17**(4), pp. 319-327.

WANG, P., CUI, L., LYSCHIK, M., SCHOLZ, A., BERGER, C. and OECHSNER, M., 2012. A local extrapolation based calculation reduction method for the application of constitutive material models for creep fatigue assessment. *International Journal of Fatigue,* **44**, pp. 253-259.

YUN, Y., WU, Y. and TANG, W.C., 2008. Performance of FRP bonding systems under fatigue loading. *Engineering Structures,* **30**(11), pp. 3129-3140.

ZIENKIEWICZ, O., TAYLOR, R. and ZHU, J., 2005. *The finite element method: its basis and fundamentals. 2005.* Butterworth-Heinemann, Oxford.

PAPER VI

"FE Modelling of FRP-concrete Interface for Very High Cycle Fatigue Behavior"

BY
Mohammed Mahal, Thomas Blanksvärd and Björn Täljsten

FE Modeling of FRP-concrete Interface for Very High Cycle Fatigue Behavior

M. Mahal[1,2,a], T. Blanksvärd[1,b] and B. Täljsten[1,3,c]

[1]Department of Civil and Natural Resources, Luleå University of Technology, Luleå, Sweden

[2]Dep.of Civil Eng., Mosul University, Mosul, Iraq

[3]Sto Scandinavia AB, Sweden

[a]Mohammed.salih@ltu.se, [b]thomas.blanksvard@ltu.se, [c]bjorn.taljsten@ltu.se

Kewords: High cycle fatigue, Finite element method, Bonding, Damage

Abstract. The fatigue damage of FRP-concrete interface is a major problem in strengthened structures subjected to fatigue loading. The available FRP-concrete interface models published in the literature usually deal with fracture mechanism approach, which is unsuitable for high cycle fatigue damage. In this study, a constitutive micro model is developed for FRP-concrete interface for high cycle fatigue and incorporated into a three dimensional finite-element program. Numerical analysis of a double lap joint is carried out, and the results show that the proposed model is reasonably accurate.

Introduction

Externally bonded FRP plates and sheets have been widely accepted techniques for strengthening reinforced concrete bridges, which are subjected to repetitive live loads of low-stress level due to passing vehicles. The durability and the performance of the FRP-strengthened structures subjected to fatigue loading depend mainly on the bond between FRP and concrete [1]. To get a complete understanding of the bonding behavior, various experimental investigations on the behavior of bonded FRP-to-concrete joints include single lap joint test and double lap joint tests has been carried out. These investigations can be classified as two types. First, high cycle fatigue type to simulate traffic loads on bridges (e.g. [2]). In this type, the maximum effective equivalent stress in the first cycle (usually, average shear bond stress) is lower than the yield stress of the joint. Second, low cycle fatigue type (e.g. [3]) for seismic investigation purpose. But in this type, the maximum effective equivalent stress is above the yield stress of the joint. Not that much analytical and numerical works has been done to simulate the FRP-concrete interface bond for fatigue loading. Available models published in literature (e.g. [4, 5]) are based on the bonding fatigue fracture mechanism. These does not give accurate results for high cyclic fatigue due to the neglecting of the damage mechanism for the first stage of joint fatigue behavior.

This paper presents the model at microscale, which can describe the behavior of the FRP-to-concrete bonded interface subjected to very high cycle fatigue loading. This model is incorporated in the 3D FE model as a material model for 3D-8 node interface element with zero thickness.

Damage Behavior and Model

The experimental results from the review show that the fatigue failure of FRP/concrete bonded joints under high cyclic fatigue can be classified into three phases as shown in Fig.1(a). In the first phase the most damage occurs due to microcracks causing residual plastic strain and no or

negligible stiffness degradation. In the second phase, the macrocracks starts causing stiffness degradation with keeping the ability of the joint to resist the applied load. Finally, debonding occurs due to crack propagations producing loss of both, stiffness and resistance capacity of the joint. The long period of phase I and the possibility of their presence in the behavior are a function of the maximum and minimum applied stresses as well as fatigue limit stress of the joints. Where phase I be prevalent of the joint's behavior when the applied maximum stresses are a somewhat larger than the fatigue limit stress and the shape of the deformation curve is shown in Fig.1(b). Initially, a significant increase of damage is observed between the 10th cycle and the 100, 000th cycle then followed by an increase the damage slowly until the last cycle. The damage rate increase after the 100, 000th cycle is considerably lower than the initial rate [4].
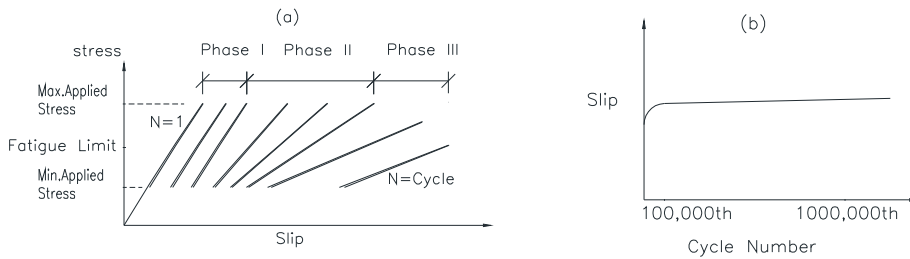
Fig.1 Typical high cycle fatigue curve : (a) Bond stress -slip curve of FRP-concrete joints (b) Slip curve during cycle loading.

The two scale damage model proposed by Lemaitre et.al [6] are used here for modeling the interfacial zone of the joint under phase I conditions. In this, the model assumes that the damage and plasticity occur at the microscale and have no influence on the elastic macroscopic behavior. For that, the fatigue limit stress is taken as the yield stress. This means that the stress over this value is causing plastic strain, and no damage happens below this value. The Constitutive model for FRP-concrete bond subjected to high cycle fatigue used in this study is schematically described in Fig.2. According to these assumptions, the following constitution equations at microscale (μ) can be written as follows:

- $\sigma_{i3}^{\mu} = K_i : \varepsilon_{i3}^{\mu e}$ (1)
- Effective stress $\tilde{\sigma}_{i3}^{\mu} = \sigma_{i3}^{\mu}/(1-D)$ (2)
- Yield criterion $f^{\mu} = \frac{1}{(1-D)}\left(\frac{(\tilde{\sigma}_{33}^{\mu})^2}{\sigma_f^2} + \frac{(\tilde{\sigma}_{13}^{\mu})^2}{\tau_{f13}^2} + \frac{(\tilde{\sigma}_{23}^{\mu})^2}{\tau_{f23}^2}\right) - 1 = 0.0$ (3)
- Elastin strain $\varepsilon_{i3}^{\mu e} = \varepsilon_{i3}^{\mu} - \varepsilon_{i3,N}^{\mu p} - \dot{\varepsilon}_{i3,in}^{\mu p}$ (4)
- Plastic multiplier rate $\dot{P} = \sqrt{\dot{\varepsilon}_{i3}^P . \dot{\varepsilon}_{i3}^P}$ (5)
- Plastic strain rate $\dot{\varepsilon}_{i3}^{\mu p} = \frac{\partial f^{\mu}}{\partial \sigma^{\mu}}\lambda$ (6)
- Damage evolution $D = 1 - \frac{\varepsilon_{i3}^{\mu}}{L_{e,i}}$ if $P^{\mu} > P_{th}$ (7)

Where, σ_f, τ_f are the fatigue limit obtained from fatigue life curve, where the fatigue strength of the joint is plotted against the number of cycles to failure. K_i are the normal and shear contact stiffness i is the directional index. α is the damage exponent that determines the shape of the damage

evolution curve. $L_{e,i}$ is the total elastic slip value take from static test, ε_{i3}^{μ} is the cumulative strain (interface slip) at an increment (in) within cycle (N) , P_{th} is the damage threshold.

Finite element implementation

The finite element analysis using the two scale damage model, described previously, is carried out with time integration of the constitutive equation. An incremental load procedure, with an iterative approach to the solution of equilibrium equations for each load increment within the cycle is used. After calculating the accumulated plastic strain and the effective stress, the values of the damage and the stresses (microscale stresses) are updated. In a degradation process involving high-cycle fatigue, an incremental approach and cycle-by-cycle analysis becomes computationally intractable. Therefore, a cycle jump strategy is implemented in the finite-element model [7].The Eight-node 3D interface element, shown in Fig.3, with proposed two scale damage model as a material model is used to model the slip between the FRP plate and concrete.
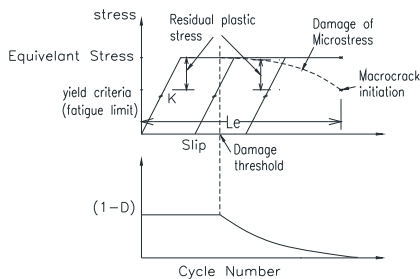
Fig.2 Constitutive model   Fig.3 Eight-node Interface element
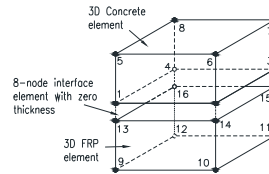
Validation Example

The proposed model is validated using a double-shear joint test specimen (F-EB-A) data by Yun et al. [2]. This experiment represents a high-cyclic fatigue test. A three-dimensional FE was carried out to simulate the experimental specimen as shown in Fig.4; only one-quarter of the specimen was modeled due to the symmetry in geometry and loading conditions. The three main components of the specimen are concrete block, FRP Plate and adhesive between the two. The concrete and FRP Plate are modeled using Eight-node solid brick element with linear-elastic material model. The concrete compressive strength was 43.5 MPa and the CFRP had an elastic modulus 257 GPa. The FRP-Concrete interface layer is represented by Eight-node interface element with zero thickness. From static bond test, $K_n = K_s = 57.14$ N/mm^3, while $\tau_f = 2.8$ N/mm^2 were selected as a maximum average applied shear stress depending on the definition of fatigue limit, and $L_e = 0.1$ mm. The damage threshold (P_{th})is assumed to be 0.07, where the micro damage started from the first applied maximum load in the first cycle. Damage exponent (α) is assumed to be 5.0, which take high value corresponds to a large number of microvoids existing between FRP and concrete that do not grow rapidly until macrocracks are formed. The relationship between the cyclic number and the loaded end slip for the minimum and maximum cyclic loads obtained numerically is compared in Fig.5 with the results registered experimentally and show a good agreement between the results. It should be noted that there is only 11 % the maximum difference in the last cycle result between FEM and experimental. More data are needed to find more accurate model parameters.
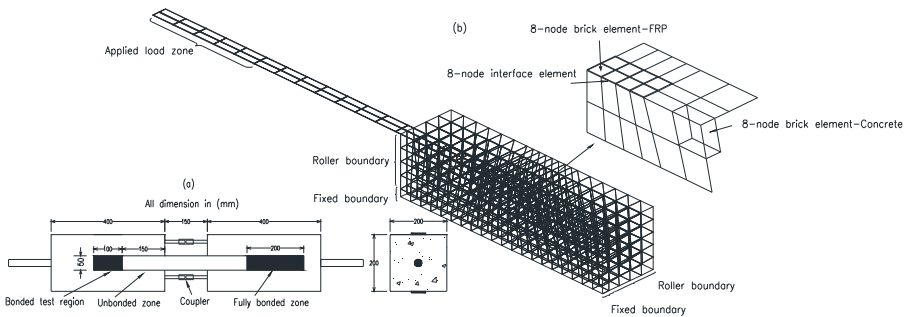
Fig.4 Double shear joint test of Yun et al. [2] (a) Specimen details (b) FE model of quarter of the specimen
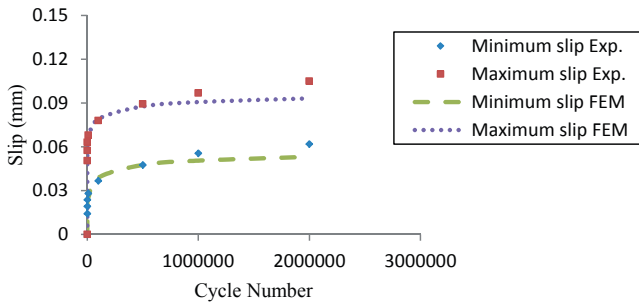
Fig.5 Comparison between experimental and numerical results

Summary

The proposed model, which is implemented into a 3D finite-element program, takes into account the elasticity, plasticity and damage at the microscale and is suitable for high cycle fatigue. It allows us to take the effect of microvoid growth along the FRP-concrete interface. The validity of the finite-element program has been checked by analyzing double shear joint test specimen under high cycle fatigue. The results from the numerical model compared well with the experimental data.

References

[1] K. A. Harries and J. Aidoo: J. Compos. Constr., Vol. 10, No. 1(2006), pp. 87–90.

[2] YC. Yun, YF .Wu and WC Tang: Eng. Struct.,Vol.30,No.11(2008),pp. 3129–40.

[3] H. Ko and Y. Sato: J. Compos. Constr., Vol.11,No.4(2007),pp. 419–426.

[4] H. M. Diab, Z.Wu, and K. Iwashita: Advances in Structural Engineering, Vol.12, No. 6,(2009), pp. 781–792.

[5]K.Y.M. Loo, S.J. Foster and S.T. Smith: J.Compos.Constr.,Vol.16,No.5 (2012),pp. 572-580.

[6] J.Lemaitre, J.P. Sermage and R.Desmorat: Int. J. Fracture,Vol.97 (1999),pp. 67-81.

[7] D. Cojocaru and A.M. Karlsson: Int. J. Fatigue, Vol.28, No.12 (2006),pp. 1677–89.

Doctoral and Licentiate Theses

Division of Structural Engineering

Luleå University of Technology

Doctoral theses

1980   Ulf Arne Girhammar: *Dynamic fail-safe behaviour of steel structures*. Doctoral Thesis 1980:060D. 309 pp.

1983   Kent Gylltoft: *Fracture mechanics models for fatigue in concrete structures*. Doctoral Thesis 1983:25D. 210 pp.

1985   Thomas Olofsson: *Mathematical modelling of jointed rock masses*. Doctoral Thesis 1985:42D. 143 pp. (In collaboration with the Division of Rock Mechanics).

1988   Lennart Fransson: *Thermal ice pressure on structures in ice covers*. Doctoral Thesis 1988:67D. 161 pp.

1989   Mats Emborg: *Thermal stresses in concrete structures at early ages*. Doctoral Thesis 1989:73D. 285 pp.

1993   Lars Stehn: *Tensile fracture of ice. Test methods and fracture mechanics analysis*. Doctoral Thesis 1993:129D, September 1993. 136 pp.

1994   Björn Täljsten: *Plate bonding. Strengthening of existing concrete structures with epoxy bonded plates of steel or fibre reinforced plastics*. Doctoral Thesis 1994:152D, August 1994. 283 pp.

1994   Jan-Erik Jonasson: *Modelling of temperature, moisture and stresses in young concrete*. Doctoral Thesis 1994:153D, August 1994. 227 pp.

1995   Ulf Ohlsson: *Fracture mechanics analysis of concrete structures*. Doctoral Thesis 1995:179D, December 1995. 98 pp.

1998   Keivan Noghabai: *Effect of tension softening on the performance of concrete structures*. Doctoral Thesis 1998:21, August 1998. 150 pp.

1999   Gustaf Westman: *Concrete creep and thermal stresses. New creep models and their effects on stress development*. Doctoral Thesis 1999:10, May 1999. 301 pp.

1999   Henrik Gabrielsson: *Ductility in high performance concrete structures. An experimental investigation and a theoretical study of prestressed hollow core slabs and prestressed cylindrical pole elements.* Doctoral Thesis 1999:15, May 1999. 283 pp.

2000   Patrik Groth: Fibre r*einforced concrete − Fracture mechanics methods applied on self-compacting concrete and energetically modified binders.* Doctoral Thesis 2000:04, January 2000. 214 pp. ISBN 978-91-85685-00-4.

2000   Hans Hedlund: *Hardening concrete. Measurements and evaluation of non-elastic deformation and associated restraint stresses.* Doctoral Thesis 2000:25, December 2000. 394 pp. ISBN 91-89580-00-1.

2003   Anders Carolin: *Carbon fibre reinforced polymers for strengthening of structural members.* Doctoral Thesis 2003:18, June 2003. 190 pp. ISBN 91-89580-04-4.

2003   Martin Nilsson: *Restraint factors and partial coefficients for crack risk analyses of early age concrete structures.* Doctoral Thesis 2003:19, June 2003. 170 pp. ISBN: 91-89580-05-2.

2003   Mårten Larson: *Thermal crack estimation in early age concrete − Models and methods for practical application.* Doctoral Thesis 2003:20, June 2003. 190 pp. ISBN 91-86580-06-0.

2005   Erik Nordström: *Durability of sprayed concrete. Steel fibre corrosion in cracks.* Doctoral Thesis 2005:02, January 2005. 151 pp. ISBN 978-91-85685-01-1.

2006   Rogier Jongeling: *A process model for work-flow management in construction. Combined use of location-based scheduling and 4D CAD.* Doctoral Thesis 2006:47, October 2006. 191 pp. ISBN 978-91-85685-02-8.

2006   Jonas Carlswärd: *Shrinkage cracking of steel fibre reinforced self compacting concrete overlays − Test methods and theoretical modelling.* Doctoral Thesis 2006:55, December 2006. 250 pp. ISBN 978-91-85685-04-2.

2006   Håkan Thun: *Assessment of fatigue resistance and strength in existing concrete structures.* Doctoral Thesis 2006:65, December 2006. 169 pp. ISBN 978-91-85685-03-5.

2007   Lundqvist Joakim: *Numerical analysis of concrete elements strengthened with carbon fiber reinforced polymers.* Doctoral Thesis 2007:07, March 2007. 50 pp. ISBN 978-91-85685-06-6.

2007   Arvid Hejll: *Civil structural health monitoring − Strategies, methods and applications.* Doctoral Thesis 2007:10, March 2007. 189 pp. ISBN 978-91-85685-08-0.

2007   Stefan Woksepp: *Virtual reality in construction: Tools, methods and processes.* Doctoral Thesis 2007:49, November 2007. 191 pp. ISBN 978-91-85685-09-7.

2007   Romuald Rwamamara: *Planning the healthy construction workplace through risk assessment and design methods.* Doctoral Thesis 2007:74, November 2007. 179 pp. ISBN 978-91-85685-11-0.

2008   Björnar Sand: *Nonlinear finite element simulations of ice forces on offshore structures.* Doctoral Thesis 2008:39, September 2008. 241 pp.

2008   Bengt Toolanen: *Lean contracting: relational contracting influenced by lean thinking.* Doctoral Thesis 2008:41, October 2008. 190 pp.

2008   Sofia Utsi: *Performance based concrete mix-design: Aggregate and micro mortar optimization applied on self-compacting concrete containing fly ash.* Doctoral Thesis 2008:49, November 2008. 190 pp.

2009   Markus Bergström: *Assessment of existing concrete bridges: Bending stiffness as a performance indicator*. Doctoral Thesis, March 2009. 241 pp. ISBN 978-91-86233-11-2.

2009   Tobias Larsson: *Fatigue assessment of riveted bridges*. Doctoral Thesis, March 2009. 165 pp. ISBN 978-91-86233-13-6.

2009   Thomas Blanksvärd: *Strengthening of concrete structures by the use of mineral based composites: System and design models for flexure and shear*. Doctoral Thesis, April 2009. 156 pp. ISBN 978-91-86233-23-5.

2011   Anders Bennitz: *Externally unbonded post-tensioned CFRP tendons − A system solution*. Doctoral Thesis, February 2011. 68 pp. ISBN 978-91-7439-206-7.

2011   Gabriel Sas: *FRP shear strengthening of reinforced concrete beams*. Doctoral Thesis, April 2011. 97 pp. ISBN 978-91-7439-239-5.

2011   Peter Simonsson: *Buildability of concrete structures: processes, methods and material*. Doctoral Thesis, April 2011. 64 pp. ISBN 978-91-7439-243-2.

2011   Stig Bernander: *Progressive landslides in long natural slopes. Formation, potential extension and configuration of finished slides in strain-softening soils*. Doctoral Thesis, May 2011, rev. August 2011 and April 2012. 250 pp. ISBN 978-91-7439-238-8. (In collaboration with the Division of Soil Mechanics and Foundation Engineering).

2012   Arto Puurula: *Load carrying capacity of a strengthened reinforced concrete bridge: non-linear finite element modeling of a test to failure. Assessment of train load capacity of a two span railway trough bridge in Örnsköldsvik strengthened with bars of carbon fibre reinforced polymers (CFRP)*. Doctoral Thesis, May 2012. 100 pp. ISBN 978-91-7439-433-7.

Licentiate theses

1984   Lennart Fransson: *Bärförmåga hos ett flytande istäcke. Beräkningsmodeller och experimentella studier av naturlig is och av is förstärkt med armering*. Licentiate Thesis 1984:012L. 137 pp. (In Swedish).

1985   Mats Emborg: *Temperature stresses in massive concrete structures. Viscoelastic models and laboratory tests*. Licentiate Thesis 1985:011L, May 1985. rev. November 1985. 163 pp.

1987   Christer Hjalmarsson: *Effektbehov i bostadshus. Experimentell bestämning av effektbehov i små- och flerbostadshus*. Licentiate Thesis 1987:009L, October 1987. 72 pp. (In Swedish).

1990   Björn Täljsten: *Förstärkning av betongkonstruktioner genom pålimning av stålplåtar*. Licentiate Thesis 1990:06L, May 1990. 205 pp. (In Swedish).

1990   Ulf Ohlsson: *Fracture mechanics studies of concrete structures*. Licentiate Thesis 1990:07L, May 1990. 66 pp.

1990   Lars Stehn: *Fracture toughness of sea ice. Development of a test system based on chevron notched specimens*. Licentiate Thesis 1990:11L, September 1990. 88 pp.

1992   Per Anders Daerga: *Some experimental fracture mechanics studies in mode I of concrete and wood*. Licentiate Thesis 1992:12L, April 1992, rev. June 1992. 81 pp.

1993   Henrik Gabrielsson: *Shear capacity of beams of reinforced high performance concrete*. Licentiate Thesis 1993:21L, May 1993. 109 pp.

1995   Keivan Noghabai: *Splitting of concrete in the anchoring zone of deformed bars. A fracture mechanics approach to bond*. Licentiate Thesis 1995:26L, May 1995. 123 pp.

1995   Gustaf Westman: *Thermal cracking in high performance concrete. Viscoelastic models and laboratory tests*. Licentiate Thesis 1995:27L, May 1995. 125 pp.

1995   Katarina Ekerfors: *Mognadsutveckling i ung betong. Temperaturkänslighet, hållfasthet och värmeutveckling*. Licentiate Thesis 1995:34L, October 1995. 137 pp. (In Swedish).

1996   Patrik Groth: *Cracking in concrete. Crack prevention with air-cooling and crack distribution with steel fibre reinforcement*. Licentiate Thesis 1996:37L, October 1996. 128 pp.

1996   Hans Hedlund: *Stresses in high performance concrete due to temperature and moisture variations at early ages*. Licentiate Thesis 1996:38L, October 1996. 240 pp.

2000   Mårten Larson: *Estimation of crack risk in early age concrete. Simplified methods for practical use*. Licentiate Thesis 2000:10, April 2000. 170 pp.

2000   Stig Bernander: *Progressive landslides in long natural slopes. Formation, potential extension and configuration of finished slides in strain-softening soils.*. Licentiate Thesis 2000:16, May 2000. 137 pp. (In collaboration with the Division of Soil Mechanics and Foundation Engineering).

2000   Martin Nilsson: *Thermal cracking of young concrete. Partial coefficients, restraint effects and influences of casting joints*. Licentiate Thesis 2000:27, October 2000. 267 pp.

2000   Erik Nordström: *Steel fibre corrosion in cracks. Durability of sprayed concrete*. Licentiate Thesis 2000:49, December 2000. 103 pp.

2001   Anders Carolin: *Strengthening of concrete structures with CFRP – Shear strengthening and full-scale applications*. Licentiate thesis 2001:01, June 2001. 120 pp. ISBN 91-89580-01-X.

2001   Håkan Thun: *Evaluation of concrete structures. Strength development and fatigue capacity*. Licentiate Thesis 2001:25, June 2001. 164 pp. ISBN 91-89580-08-2.

2002   Patrice Godonue: *Preliminary design and analysis of pedestrian FRP bridge deck*. Licentiate Thesis 2002:18. 203 pp.

2002   Jonas Carlswärd: *Steel fibre reinforced concrete toppings exposed to shrinkage and temperature deformations*. Licentiate Thesis 2002:33, August 2002. 112 pp.

2003   Sofia Utsi: *Self-compacting concrete – Properties of fresh and hardening concrete for civil engineering applications*. Licentiate Thesis 2003:19, June 2003. 185 pp.

2003   Anders Rönneblad: *Product models for concrete structures – Standards, applications and implementations*. Licentiate Thesis 2003:22, June 2003. 104 pp.

2003   Håkan Nordin: *Strengthening of concrete structures with pre-stressed CFRP*. Licentiate Thesis 2003:25, June 2003. 125 pp.

2004   Arto Puurula: *Assessment of prestressed concrete bridges loaded in combined shear, torsion and bending*. Licentiate Thesis 2004:43, November 2004. 212 pp.

2004   Arvid Hejll: *Structural health monitoring of bridges. Monitor, assess and retrofit*. Licentiate Thesis 2004:46, November 2004. 128 pp.

2005   Ola Enochsson: *CFRP strengthening of concrete slabs, with and without openings. Experiment, analysis, design and field application.* Licentiate Thesis 2005:87, November 2005. 154 pp.

2006   Markus Bergström: *Life cycle behaviour of concrete structures − Laboratory test and probabilistic evaluation.* Licentiate Thesis 2006:59, December 2006. 173 pp. ISBN 978-91-85685-05-9.

2007   Thomas Blanksvärd: *Strengthening of concrete structures by mineral based composites.* Licentiate Thesis 2007:15, March 2007. 300 pp. ISBN 978-91-85685-07-3.

2008   Peter Simonsson: *Industrial bridge construction with cast in place concrete: New production methods and lean construction philosophies.* Licentiate Thesis 2008:17, May 2008. 164 pp. ISBN 978-91-85685-12-7.

2008   Anders Stenlund: *Load carrying capacity of bridges: Three case studies of bridges in northern Sweden where probabilistic methods have been used to study effects of monitoring and strengthening.* Licentiate Thesis 2008:18, May 2008. 306 pp. ISBN 978-91-85685-13-4.

2008   Anders Bennitz: *Mechanical anchorage of prestressed CFRP tendons − Theory and tests.* Licentiate Thesis 2008:32, November 2008. 319 pp.

2008   Gabriel Sas: *FRP shear strengthening of RC beams and walls.* Licentiate Thesis 2008:39, December 2008. 107 pp.

2010   Tomas Sandström: *Durability of concrete hydropower structures when repaired with concrete overlays.* Licentiate Thesis, February 2010. 179 pp. ISBN 978-91-7439-074-2.

2013   Johan Larsson: *Mapping the concept of industrialized bridge construction: Potentials and obstacles.* Licentiate Thesis, January 2013. 66 pp. ISBN 978-91-7439-543-3.

2013   Jonny Nilimaa: *Upgrading concrete bridges: Post-tensioning for higher loads.* Licentiate Thesis, January 2013. 300 pp. ISBN 978-91-7439-546-4.

2013   Katalin Orosz: *Tensile behaviour of mineral-based composites.* Licentiate Thesis, May 2013. 92 pp. ISBN 978-91-7439-663-8.

2013   Peter Fjellström: *Measurement and modelling of young concrete properties.* Licentiate Thesis, May 2013. 121 pp. ISBN 978-91-7439-644-7.

2014   Majid Al-Gburi: *Restraint in structures with young concrete: Tools and estimations for practical use.* Licentiate Thesis, September 2014. 106 pp. ISBN 978-91-7439-977-6.

2014   Tarek Edress Saaed:Structural Identification of Civil Engineering Structures. Licentiate Thesis, November 2014. 136 pp. ISBN 978-91-7583-053-7.

2015   Niklas Bagge: Assessment of Concrete Bridges: Models and Tests for Refined Capacity Estimates. Licentiate Thesis, December 2014. 132 pp. ISBN 978-91-7583-163-3.